INTERACTIVE ROLES OF HYDROGEN PEROXIDE AND CALCIUM IN THE ENDOTHELIAL SIGNALING NETWORK THAT UNDERPINS THE EDHF PHENOMENON

A thesis submitted for the fulfilment of the degree of Doctor of Philosophy

Yiwen Li

Supervisors: Dr David H. Edwards and Professor Tudor M. Griffith

Cardiff University School of Medicine

Cardiff September 2012

DECLARATION

This work has not been submitted in substance for any other degree or award at this or any other university or place of learning, nor is being submitted concurrently in candidature for any degree or other award.

Signed …… (candidate)

Date ……

This thesis is being submitted in partial fulfilment of the requirements for the degree of PhD.

Signed …… (candidate)

Date ……

This thesis is the result of my own independent work/investigation, except where otherwise stated. Other sources are acknowledged by explicit references.

Signed …… (candidate)

Date ……

I hereby give consent for my thesis, if accepted, to be available for photocopying and for inter-library loan, and for the title and summary to be made available to outside organisations.

Signed …… (candidate)

Date ……

DEDICATION

To my parents and Jiadi

For all your love, support and encouragement

and

In memory of my supervisor Tudor

ACKNOWLEDGEMENTS

Thank you to Dr. David Edwards for being a fantastic supervisor over the past four years. Without him, this thesis would be impossible. He has given me endless encouragement and support when the hardest thing happened in my PhD. A special thank you must go to Prof. Tudor Griffith for his passion and faith for this work. I have great respect for him and I will continue to be inspired by the works he took and the words he said to me. I wish Tudor enjoys reading this thesis.

Thank you to Prof. Karl Swann for guiding me through the intricacies of fluorescence microscopy. His patience and guidance has been hugely appreciated.

Thank you to Dr. Sofia Fernandez-Rodriguez for being a great friend and colleague. She has given me so many useful discussions and helpful advice in both work and life over the years.

Thank you to everyone who has worked in office 3/08 for good humour and distracting me from writing this thesis. I've enjoyed having you guys around. Thank you to all members of WHRI, past and present. It's been an honour to work with you all.

Finally, thank you to my examiners Prof. Michael Randall and Dr. Sergey Smirnov for giving me a thoughtful and enjoyable viva, and I have learnt loads from our excellent discussion.

Summary

Endothelium-derived hydrogen peroxide (H_2O_2) has been suggested to function as a freely diffusible endothelium derived hyperpolarizing factor (EDHF). However, in the rabbit vasculature, it has been shown that the electrotonic spread of endothelial hyperpolarization via myoendothelial and homocellular smooth muscle gap junctions is essential for nitric oxide (NO)-prostanoid-independent arterial relaxation. Therefore, a series of interlinked experiments, both mechanical and imaging, have been undertaken to investigate the role of H_2O_2 in vascular control, focusing on the mechanisms through which H_2O_2 may regulate intracellular endothelial calcium (Ca^{2+}) homeostasis. These studies have shown that exogenous H_2O_2 does not directly mediate an EDHF-type response, but can potentiate electrotonically-mediated relaxations by facilitating the elevation of endothelial cell intracellular Ca^{2+} concentration ($[Ca^{2+}]_i$), thereby promoting the activation of hyperpolarizing endothelial Ca^{2+}-activated potassium channels (K_{Ca}). Mechanistically, this potentiating effect of H_2O_2 involves enhanced depletion of the ryanodine-sensitive endoplasmic reticulum Ca^{2+} store, through inhibition of sarcoplasmic-endoplasmic reticulum Ca^{2+}-ATPase (SERCA) activity, and therefore increased extracellular Ca^{2+} influx through store-operated Ca^{2+} entry. This effect of H_2O_2 is independent of the nature of the initiating stimulus, as it is observed with both the receptor-coupled agonist acetylcholine and the SERCA pump inhibitor cyclopiazonic acid. Paradoxically, however, H_2O_2 was also shown to exert inhibitory effects on NO-mediated endothelium-dependent relaxations. Additionally, arsenite was found to modulate vascular responses through the elevation of the endogenous endothelial-produced H_2O_2 that is secondary to the activation of NADPH oxidase. This thesis provides evidence that H_2O_2 is a physiological-important signalling molecule in endothelial Ca^{2+} homeostasis. The findings also give further insights into the mechanism underlying the compensatory role of the EDHF phenomenon to compromised NO-mediated response that are observed in diseased vessels.

Abbreviations

AA	arachidonic acid
AC	adenylate cyclase
ACh	acetylcholine
AM	acetoxymethyl
ANOVA	analysis of variance
ASIC	acid-sensitive cationic channels
ATP	adenosine triphosphate
A23187	calcium ionophore/calimycin
(4-Br-A23187)	(4-Bromo-calcium Ionophore A23187)
BPAECs	bovine pulmonary artery endothelial cells
Ca^{2+}	calcium ion
$[Ca^{2+}]_i$	intracellular calcium concentration
$[Ca^{2+}]_{ER}$	calcium concentration in the ER
$[Ca^{2+}]_m$	calcium concentration in the mitochondria
CaM	calmodulin
cAMP	cyclic adenosine monophosphate
CCE	capacitative Ca^{2+} entry
cGMP	cyclic guanosine monophosphate
COX	cyclooxygenase
CPA	cyclopiazonic acid
Cx	connexins
DAG	diacylglycerol
DCF	2',7'-dichlorodihydrofluorescein diacetate
DHE	dihydroethidium
dH_2O	deionised water
DMEM	Dulbecco's modified eagle medium
DMSO	dimethylsulfoxide
EC	endothelial cells
(p)EC_{50}	(negative log) half maximal effective concentration
EDH	endothelium-dependent hyperpolarization
EDHF	endothelium-derived hyperpolarizing factor
EDRF	endothelium-derived relaxing factor
EETs	epoxyeicosatrienoic acids
EGTA	ethylene glycol-bis(2-aminoethylether)-N,N,N',N'-tetraacetic acid
(*e*)NOS	(endothelial) nitric oxide synthase
(the) ER	endoplasmic reticulum
FAD^{++}	oxidised flavoproteins
FBS	fetal bovine serum
GA	glycyrrhizic acid
GJ	gap junctions

HAECs	human aorta endothelial cells
HCl	hydrochloride acid
$HO^{\bullet}$	hydroxyl radical
HPAECs	human pulmonary artery endothelial cells
HUVECs	human umbilical vein endothelial cells
H_2O_2	hydrogen peroxide
I_{ARC}	AA-regulated Ca^{2+} entry current
IbTX	iberiotoxin
I_{CRAC}	Ca^{2+} release activated Ca^{2+} channel current
$(p)IC_{50}$	(negative log) half maximal inhibitory concentration
indomethacin	1-(4-Chlorobenzoyl)-5-methoxy-2-methyl-3-indoleacetic acid
$InsP_3(R)$	inositol 1,4,5-triphsphate (receptor)
K_{ATP}	ATP-activated K^+ channel
$(S, I, B)K_{Ca}$	(small, intermediate, large-conductance) Ca^{2+}-activated K^+ channel
K_{ir}	inwardly rectifying potassium channels
K_V	voltage-gated K^+ channel
L-Arg	L-arginine
L-NAME	N^{ω}-nitro-L-arginine methyl ester
L-NNA	N^{G}-nitro-L-arginine
MAHMA NONOate	6-(2-Hydroxy-1-methyl-2-nitrosohydrazino)-N-methyl-1-hexanamine
mCU	mitochondrial Ca^{2+} uniporter
Mg^{2+}	magnesium ion
MLCK	myosin light-chain kinase
MLCP	myosin light-chain phosphatase
mNCE	mitochondrial Na^+-Ca^{2+} exchanger
Mn^{2+}	manganese ion
MnTMPyP	manganese(III)-tetrakis-(1-methyl-4-pyridyl)porphyrin
MTG	MitoTracker Green
NADPH	nicotinamide adenine dinucleotide phosphate oxidase
NCX	sodium-calcium exchanger
NO	nitric oxide
NOX	nicotinamide adenine dinucleotide phosphate oxidase
NSCC	non-selective cation channel
OH^-	hydroxyl radical
$ONOO^-$	peroxynitrite
Orai	Ca^{2+} channel protein
$O_2^{\bullet -}$	superoxide anion
PAEC	porcine aortic endothelial cells
PASMC	pulmonary arterial smooth muscle cells
PBS	phosphate buffered saline
PE	phenylephrine
PGE_2	prostaglandin E2
PGIS	prostacyclin synthase

PGI_2	prostacyclin
PIP_2	phosphatidylinositol 4,5-bisphosphate
PKA	protein kinase A
PKC	protein kinase C
PKG	protein kinase C
PLA_2	phospholipase A2
PLC	phospholipase
PMCA	plasma membrane Ca^{2+}-ATPase
P2X4	purinoceptors
RAECs	rat aorta endothelial cells
R_{max}	maximal response
ROS	reactive oxygen species
Ry(R)	ryanodine (receptor)
SEM	standard error of the mean
SERCA	sarcoplasmic-endoplasmic reticulum Ca^{2+}-ATPase
*s*GC	soluble guanylate cyclase
SMC	smooth muscle cells
SOC	store-operated Ca^{2+} channel
SOCE	store-operated Ca^{2+} entry
SOD	superoxide dismutase
SPCA	secretory pathway Ca^{2+}-ATPases
STIM1	stromal interacting molecule
TRAM(-34)	1-[(2-Chlorophenyl)diphenylmethyl]-1H-pyrazole
TRPC	transient receptor potential cation
VOCC	voltage-operated Ca^{2+} channels
WHO	World Health Organisation
XesC	xestospongin C

Contents

CHAPTER 1 ..... **1**

GENERAL INTRODUCTION **1**

1.1 THE CARDIOVASCULAR SYSTEM 1

1.1.1 WHO facts *1*

1.1.2 Cardiovascular diseases *2*

1.1.3 Structure and function of the blood vessels *2*

1.2 THE ENDOTHELIUM 3

1.2.1 Function of the endothelium *4*

1.2.1.1 Vascular relaxation 4

1.2.3 Prostanoids *5*

1.2.4 Nitric Oxide *7*

1.2.5 Endothelium-derived Hyperpolarising Phenomenon *9*

1.2.5.1 Gap Junctions 12

1.2.5.2 Calcium-activated potassium channels 14

1.3 REACTIVE OXYGEN SPECIES 17

1.3.1 Vascular effects of H_2O_2 ..... *17*

1.3.1.1 Vascular production and degradation of H_2O_2 18

1.3.1.2 Vasorelaxing effects of H_2O_2 18

1.3.1.3 Vasoconstriction effects of H_2O_2 20

1.3.1.4 H_2O_2 and the EDHF phenomenon 21

1.3.2 ROS in disease- arsenic toxicity *23*

1.4 CALCIUM HOMEOSTASIS IN ENDOTHELIAL CELLS 24

1.4.1 Intracellular Ca^{2+} stores in endothelial cells *25*

1.4.1.1 Endoplasmic reticulum store 25

1.4.1.2 Mitochondria store 26

1.4.1.3 Golgi store 27

1.4.2 Intracellular Ca^{2+} homeostasis in endothelial cells *28*

1.4.2.1 $InsP_3$ receptor 28

1.4.2.2 Ryanodine receptor 30

1.4.2.3 SERCA pump 31

1.4.2.4 PMCA pump 33

1.4.3 Ca^{2+} entry into endothelial cells *34*

1.4.3.1 Voltage-dependent Ca^{2+} channels 34

1.4.3.2 Store operated calcium entry (SOCE) 34

1.4.3.3 Non-selective cation channels 36

1.4.3.4 Non-capacitative calcium entry (NCCE) 36

1.5 GENERAL AIMS OF THESIS 37

CHAPTER 2 ..... **39**

MATERIALS AND METHODS **39**

2.1 ANIMALS 39
2.1.1 Isolated Tissues *39*
2.1.1.1 The aorta 39
2.1.1.2 The external iliac arteries 41
2.1.1.3 The aortic valve 42
2.1.2 Rabbit tissue dissection *42*
2.2 MECHANICAL STUDIES IN RABBIT TISSUE 43
2.2.1 Myograph *44*
2.2.1.1 Calibrating the myograph 44
2.2.1.2 Maintenance and cleaning 46
2.2.2 Experimental procedures 46
- First pre-incubation for 30 minutes: 46
- Second incubation for 30 minutes: 47
- Pre-contraction 48
- Cumulative concentration-response curves 48

2.2.3 Data collection *49*
2.3 IMAGING STUDIES IN RABBIT TISSUE PREPARATIONS 49
2.3.1 Imaging systems *49*
2.3.1.1 Confocal laser scanning microscope (CLSM) 49
2.3.1.2 Inverted fluorescence microscope system from Life Science Resources 51
2.3.1.3 Inverted epifluorescence microscope 51
2.3.2 Chemicals used for imaging studies *51*
2.3.3 Assessing dye responsiveness to calcium *52*
2.3.4 Loading of fluorescent indicators *53*
2.3.4.1 Dihydroethidium (DHE) for ROS detection 55
2.3.4.2 Fluo-4 for cytosolic calcium 56
2.3.4.3 Mag-fluo-4 for endoplasmic reticulum calcium 56
2.3.4.4 Rhod-2 for mitochondria calcium 57
2.3.4.5 MitoTracker Green for mitochondrial localization 57
2.3.4.6 Dual loading of Rhod-2 and MitoTracker Green 57
2.3.4.7 Fura-2 for cytosolic calcium and Manganese quench experiments 58
2.3.5 Excitation and emission wavelength *58*
2.3.6 Data recording of ROS imaging with DHE *59*
2.3.7 Data recording of Intracellular Ca^{2+} signal *59*
2.3.8 Data recording of manganese (Mn^{2+}) quench imaging *60*
2.4 CELL CULTURE 61
2.4.1 Cell line descriptions *61*
2.4.2 Tissue culture medium *61*
- Reagents used for the culture of EA.hy926 cells 61
- Freezing medium 62

2.4.3 Culturing EA.hy926 cells *62*
2.4.3.1 Subculturing Procedure (75 cm^2 flask) 62
2.4.3.2 Freezing Procedure 63
2.4.3.3 Thawing Procedure 64
2.4.3.4 Plating Procedure 64
2.5 IMAGING STUDIES WITH EA.HY926 CELLS 64
2.5.1 Loading of fluorescent indicators *64*
2.5.1.1 Mag-fluo-4 for endoplasmic reticulum calcium 64
2.5.1.2 Fluo-4 for cytosolic calcium 65
2.5.1.3 Rhod-2 for mitochondria calcium 65
2.5.1.4 MitoTracker Green for mitochondrial localization 65
2.5.1.5 Dual loading of Rhod-2 and MitoTracker Green 65
2.5.2 Data recording of Intracellular Ca^{2+} signal *66*
2.6 STATISTICAL ANALYSIS 66
2.7 HEALTH AND SAFETY 67
CHAPTER 3 68
MODULATION OF ENDOTHELIUM-DEPENDENT ARTERIAL RELAXATION BY EXOGENOUS HYDROGEN PEROXIDE 68
3.1 INTRODUCTION 68
3.1.1 Background *68*
3.1.2 Aim of this chapter *69*
3.2 MATERIALS AND METHODS 70
3.2.1 Mechanical Responses *70*
3.2.2 Data recording and Statistics *71*
3.3 RESULTS 72
3.3.1 Mechanisms contributing to ACh-evoked relaxations *72*
3.3.2 Effects of K_{Ca} channel inhibitors on tension in rabbit iliac artery. *72*
3.3.3 Effects of H_2O_2 on responses to CPA in the absence and presence of L-NAME/indomethacin in rabbit iliac arteries. *76*
3.3.4 Effects of H_2O_2 on responses to ACh in the absence and presence of L-NAME/indomethacin in rabbit iliac arteries. *76*
3.3.5 Effects of thimerosal on responses to CPA in the absence and presence of L-NAME/indomethacin in rabbit iliac arteries. *80*
3.3.6 Effects of thimerosal on responses to ACh in the absence and presence of L-NAME/indomethacin in rabbit iliac arteries. *80*
3.3.7 Effects of H_2O_2 on responses to MAHMA NONOate in rabbit iliac arteries. *80*
3.3.8 Effects of thimerosal on responses to MAHMA NONOate in rabbit iliac arteries. *84*
3.3.9 Relaxations to exogenous H_2O_2 and thimerosal in rabbit aorta *87*
3.3.10 Effects of H_2O_2 and thimerosal on responses to CPA in rabbit aorta. *87*
3.3.11 Effects of H_2O_2 and thimerosal on responses to ACh in rabbit aorta. *90*

3.3.12 Effects of H_2O_2 and thimerosal on responses to MAHMA NONOate in rabbit aorta. *92*
3.3.13 Effects of lower concentrations of H_2O_2 and thimerosal on responses to CPA in rabbit aorta. *94*
3.3.14 Effects of lower concentrations of H_2O_2 and thimerosal on responses to ACh in rabbit aorta. *94*
3.3.15 Effects of H_2O_2 and thimerosal on contraction induced by PE *97*
3.4 DISCUSSION 99
3.4.1 Current investigations *99*
3.4.2 Conclusions *105*
3.5 CHAPTER SUMMARY 105
CHAPTER 4 106
POTENTIATION OF THE EDHF PHENOMENON BY INORGANIC ARSENITE: ROLE OF HYDROGEN PEROXIDE 106
4.1 INTRODUCTION 106
4.1.1 Preliminary investigation of arsenite responses in rabbit iliac artery *107*
4.1.2 Aim of this chapter *108*
4.2 MATERIALS AND METHODS 108
4.2.1 Mechanical Responses *108*
4.2.2 Detection of superoxide/hydrogen peroxide *109*
4.2.3 Data recording and Statistics *109*
4.2.4 Reagents *110*
4.3 RESULTS 110
4.3.1 Effects of arsenite on NO-mediated aortic relaxation evoked by CPA *110*
4.3.2 Effects of arsenite on NO-mediated aortic relaxation evoked by ACh *110*
4.3.3 Effects of arsenite on contraction induced by PE *114*
4.3.4 Fluorescence imaging of ROS production *114*
4.4 DISCUSSION 117
4.4.1 Potentiating effects of arsenite on the EDHF phenomenon *117*
4.4.2 Differential effects of arsenite on EDHF-type and NO-mediated relaxations *119*
4.4.3 Conclusions and further studies *121*
4.5 CHAPTER SUMMARY 122
CHAPTER 5 123
APPLICATION OF FLUORESCENT PROBES FOR SENSING AND IMAGING CALCIUM SIGNAL – THE DYE RESPONSIVENESS TEST WITH HYDROGEN PEROXIDE 123
5.1 INTRODUCTION 123
5.1.1 The development of calcium indicators *123*
5.1.2 The probes applied in the studies described in this thesis *124*
5.1.2.1 Fluo-4 124
5.1.2.2 Mag-fluo-4 124

5.1.2.3 Rhod-2/MitoTracker Green 125
5.1.2.4 Fura-2 125
5.1.3 Aim of this chapter 126
5.2 MATERIALS AND METHODS 126
5.2.1 Accessing dye responsiveness 126
5.2.2 Imaging of rabbit aortic valve leaflets 126
5.2.3 Imaging of EA.hy926 cells 127
5.3 RESULTS 127
5.3.1 Effect of H_2O_2 on Fluo-4 responses to calcium 127
5.3.2 Effect of H_2O_2 on Mag-fluo-4 responses to calcium 127
5.3.3 Effect of H_2O_2 on Rhod-2 responses to calcium 127
5.3.4 Effect of H_2O_2 on Fura-2 responses to calcium 130
5.3.5 Confocal laser-scanning microscopy imaging using the intracellular Ca^{2+} indicators 134
5.4 DISCUSSION 139
5.5 CHAPTER SUMMARY 140
CHAPTER 6 141
INTERACTIVE ROLES OF HYDROGEN PEROXIDE AND CALCIUM IN THE ENDOTHELIAL SIGNALLING NETWORK THAT UNDERPINS THE EDHF PHENOMENON 141
6.1 INTRODUCTION 141
6.1.1 General backgrounds 141
6.1.2 Aim of this chapter 143
6.2 MATERIALS AND METHODS 143
6.2.1 Imaging studies with rabbit aortic valve 143
6.2.2 Imaging studies with EA.hy926 cells 144
6.2.3 Data recording and Statistics 144
6.3 RESULTS 144
6.3.1 Effect of H_2O_2 on CPA-evoked elevation of $[Ca^{2+}]_i$ in the rabbit aortic valve leaflets. 144
6.3.2 Effect of thimerosal on CPA-evoked elevation of $[Ca^{2+}]_i$ in the rabbit aortic valve leaflets. 147
6.3.3 Effect of H_2O_2 on CPA-evoked depletion of $[Ca^{2+}]_{ER}$ in the rabbit aortic valve leaflets. 147
6.3.4 Effect of thimerosal on CPA-evoked depletion of $[Ca^{2+}]_{ER}$ in the rabbit aortic valve leaflets. 147
6.3.5 Effect of H_2O_2 on ACh-evoked depletion of $[Ca^{2+}]_{ER}$ in the rabbit aortic valve leaflets. 150
6.3.6 Effect of H_2O_2 on Ca^{2+} re-entry by CPA in the rabbit aortic valve leaflets. 150
6.3.7 Effect of thimerosal on Ca^{2+} re-entry by CPA in the rabbit aortic valve leaflets. 150

6.3.8 Effect of CPA on non-selective divalent cation entry in the rabbit aortic valve leaflets. *154*
6.3.9 Effect of H_2O_2 and CPA on non-selective divalent cation entry in the rabbit aortic valve leaflets. *154*
6.3.10 Effect of thimerosal and CPA on non-selective divalent cation entry in the rabbit aortic valve leaflets. *154*
6.3.11 Effect of H_2O_2 and thimerosal on depletion and refilling of $[Ca^{2+}]_{ER}$ in the rabbit aortic valve leaflets. *158*
6.3.12 Effect of ryanodine on non-selective divalent cation entry and depletion/refilling of $[Ca^{2+}]_{ER}$ in the rabbit aortic valve leaflets. *160*
6.3.13 Effect of CPA, ACh and A-Br-23187 on $[Ca^{2+}]_m$ in the rabbit aortic valve leaflets. *160*
6.3.14 Effect of H_2O_2 and CPA on $[Ca^{2+}]_m$ in EA.hy926 cells. *163*
6.3.15 Effect of thimerosal on CPA-evoked elevation of $[Ca^{2+}]_m$ in EA.hy926 cells. *163*
6.3.16 Effect of H_2O_2 and CPA on $[Ca^{2+}]_{ER}$ in EA.hy926 cells. *163*
6.3.17 Effect of thimerosal on CPA-evoked depletion of $[Ca^{2+}]_{ER}$ in EA.hy926 cells. *163*
6.3.18 Effect of H_2O_2 and CPA on $[Ca^{2+}]_i$ in EA.hy926 cells. *168*
6.3.19 Effect of thimerosal on CPA-evoked elevation of $[Ca^{2+}]_i$ in EA.hy926cells. *168*
6.4 DISCUSSION 171
6.4.1 Current investigations *171*
6.4.2 Conclusions and further studies *177*
6.5 CHAPTER SUMMARY 177
CHAPTER 7 ..... **178**
SUMMARY AND DISCUSSION **178**
7.1 OVERVIEW 178
7.2 CONCLUDING REMARKS 187
APPENDIX **188**
LIMITATION AND POTENTIAL METHODS OF DIRECT IMAGING OF INTRACELLULAR HYDROGEN PEROXIDE CONCENTRATION **188**
A.1 INTRODUCTION 188
A.2 RESULTS AND DISCUSSION 188
A.2.1 DCF *188*
A.2.2 DHE *190*
A.2.3 Amplex Red *190*
A.2.4 PG1 and PC1 ..... *191*
A.2.5 HyPer *193*
A.2.6 CONCLUSIONS AND FURTHER STUDIES 195
LIST OF PUBLICATIONS **197**
AWARDS **197**
REFERENCES **198**

Chapter 1

General Introduction

1.1 THE CARDIOVASCULAR SYSTEM

The cardiovascular system, comprising of the heart and blood vessels, is the first organ system that is formed in an embryo (Levick, 2010). The key function of this system is to rapidly transport oxygen, nutrients, water and hormones around the body to the tissue, while at the same time, taking away the metabolic waste products such as carbon dioxide. The cardiovascular system also has other functions such as helping to regulate pH, temperature, salt and water balance in the body and protection of the body from diseases and bleeding through various blood cells, proteins and antibodies.

1.1.1 WHO facts

Diseases of the cardiovascular system are the biggest cause of death worldwide. 17.3 million people died from cardiovascular diseases in 2008, primarily coronary heart diseases and stroke, this represented 30% of all deaths in that year. More than 3 million of these deaths occurred in people below the age of 60, and men are more likely to develop cardiovascular diseases at an earlier age than women. The cardiovascular mortality rate ranges from 4% in high-income countries to 42% in low-income countries, leading to growing inequalities in the occurrence and outcome of cardiovascular diseases between countries and populations. It is estimated that 23.6 million people will die from cardiovascular diseases annually by 2030 (Mendis *et al.*, 2011; WHO, 2012).

1.1.2 Cardiovascular diseases

Cardiovascular diseases represent a group of disorders of the heart and blood vessels, WHO has defined them into six categories: coronary heart disease, cerebrovascular disease, peripheral arterial disease, rheumatic heart disease, congenital heart disease, and deep vein thrombosis/pulmonary embolism (WHO, 2012). Smoking, lack of exercise, excessive alcohol intake, unhealthy diets, obesity, hypertension, high cholesterol and diabetes are among the leading risk factors of cardiovascular diseases.

1.1.3 Structure and function of the blood vessels

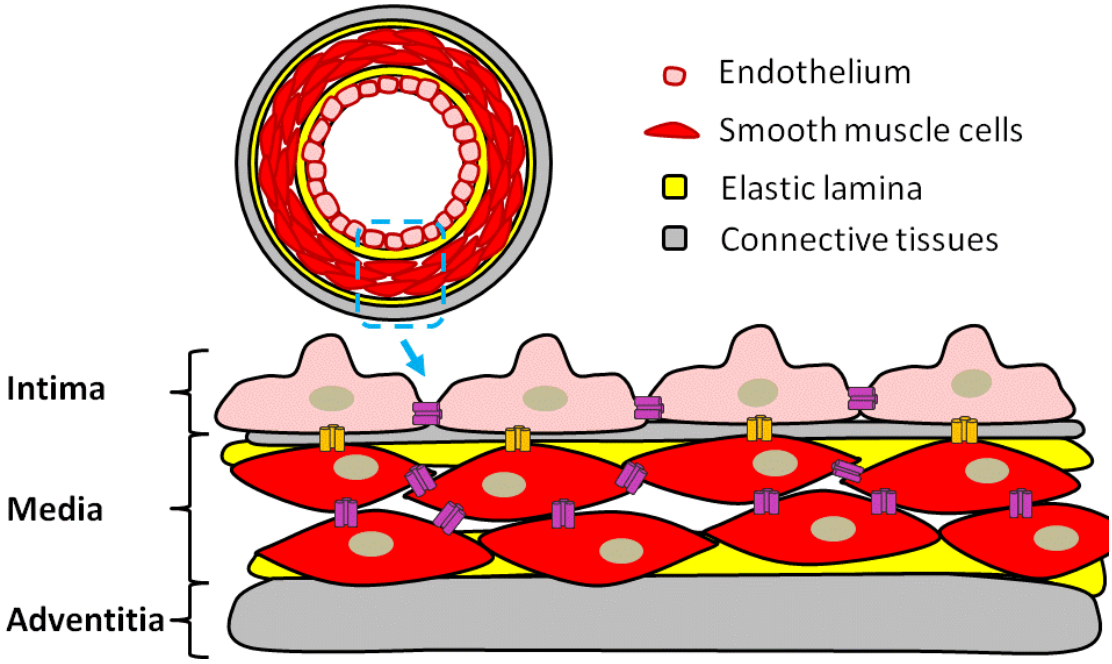

Figure 1.1 Schematic representation of the structure of the blood vessel wall.

The wall of all blood vessels, except capillaries, is made of three layers: (i) Tunica Intima: composing of endothelial cells that are in contact with the blood and are attached to the internal elastic lamina; (ii) Tunica Media: consists of spindle-shaped smooth muscle cells and (iii) Tunica Adventitia: made of collagenous connective tissues that contains nerve fibers and fibroblasts and sometimes, an external elastic

lamina (Levick, 2010) (Figure 1.1). The wall structure of each type of vessels is specially adapted to their function. Large arteries such as aorta and iliac arteries are called elastic arteries, they express high levels of elastin protein and collagen, have high extensibility, can expand by ~10% during each heart beat to accommodate the ejected blood and can recoil during diastole. Medium sized arteries such as femoral and coronary arteries are called conduit arteries, they have a thicker smooth muscle layer relative to the lumen diameter than in elastic arteries. These muscular arteries have low resistance conduits and their thick walls can prevent collapse at sharp bends like the knee joint. They normally comply with a rich autonomic nerve supply and can dilate or contract actively. They conduct the flow from the large elastic arteries to smaller resistance arterioles. The arterioles have high resistance due to the narrow lumen and they regulate local blood flow for capillary perfusion. The numerous capillaries are called exchange vessels, their wall comprises of a single layer of endothelial cells with no media or adventitia, they have a low resistance to flow and facilitate transfer of oxygen and nutrients to the tissue. Venous vessels have an intima, a thin media of smooth muscle cells and an adventitia, they offer a low resistance to flow and are called capacitance vessels because of their large number and size that contain about two-thirds of the circulating blood at any one moment. The total length of all arteries may exceed 60,000 miles in the human body (Levick, 2010).

1.2 THE ENDOTHELIUM

The term ‘endothelium’ was first used by the Swiss anatomist Wilhelm His in 1865 (Aird, 2007). The endothelium consists of a single layer of endothelial cells lining the luminal surface of the entire vasculature (veins, arteries and capillaries) and the lymphatic system. It may be considered to be one of the largest organs in the body, its total mass may exceed that of the liver and its surface area is over 4000 square metres in the human (Andonegui *et al.*, 2009). Endothelial cells are squamous epithelial cell that each cell is 0.2-0.3 μm thick, and has a flattened shape (Levick, 2010).

1.2.1 Function of the endothelium

Endothelial cells contribute to cardiovascular regulation in many ways. They (i) serve as a permeability barrier that modulates the exchange of oxygen, nutrients and metabolic products between plasma and interstitial fluid; (ii) regulate vascular haemostasis and platelet function by producing both antithrombotic and pro-clotting factors; (iii) secrete growth factors, hormones and cytokines; (iv) contribute to the formation and degradation of the extracellular matrix, therefore influencing vascular smooth muscle proliferation and angiogenesis and (v) modulate vascular tone (Widmaier *et al.*, 2004; Vanhoutte and Feletou, 2005).

1.2.1.1 Vascular relaxation

Resistance vessels and large arteries exhibit some degree of smooth muscle contraction called basal tone, which determines the diameter of the vessel (Levick, 2010). Basal tone is regulated by both extrinsic and intrinsic factors. Extrinsic factors such as sympathetic neuroeffectors (e.g. noradrenaline) and circulating hormones (e.g angiotension II) may preferentially increase vascular tone and cause vasoconstriction. Whereas intrinsic factors such as endothelial factors are responsible for local regulation and may either increase or decrease vascular tone. Indeed, a significant function of the endothelium is regulation of the vascular tone of underlying smooth muscle cells. The smooth muscle tone depends primarily on cytosolic/intracellular calcium concentration ($[Ca^{2+}]_i$) and Ca^{2+} sensitivity. To initiate contraction, Ca^{2+} binds to calmodulin to form Ca^{2+}-calmodulin complex, which activates myosin light-chain kinase (MLCK) that phosphorylates myosin to cause contraction. By contrast, if $[Ca^{2+}]_i$ decreased, constitutively active myosin light-chain phosphatase (MLCP) will dephosphorylate myosin to cause relaxation (Levick, 2010). Arterial endothelium expresses receptors to many vasoactive agents such as acetylcholine (ACh), upon stimulation by such an agonist, the endothelium produces a spectrum of vasodilators and vasoconstrictors, including prostacyclin (PGI_2), nitric oxide (NO), EDHF (endothelium-derived

hyperpolarizing factor) and endothelin. These endothelium-derived signalling molecules may diffuse directly into the underlying smooth muscle cells or through channels such as gap junctions. PGI_2, NO and EDHF all cause relaxation of the smooth muscles by decreasing $[Ca^{2+}]_i$.

1.2.3 Prostanoids

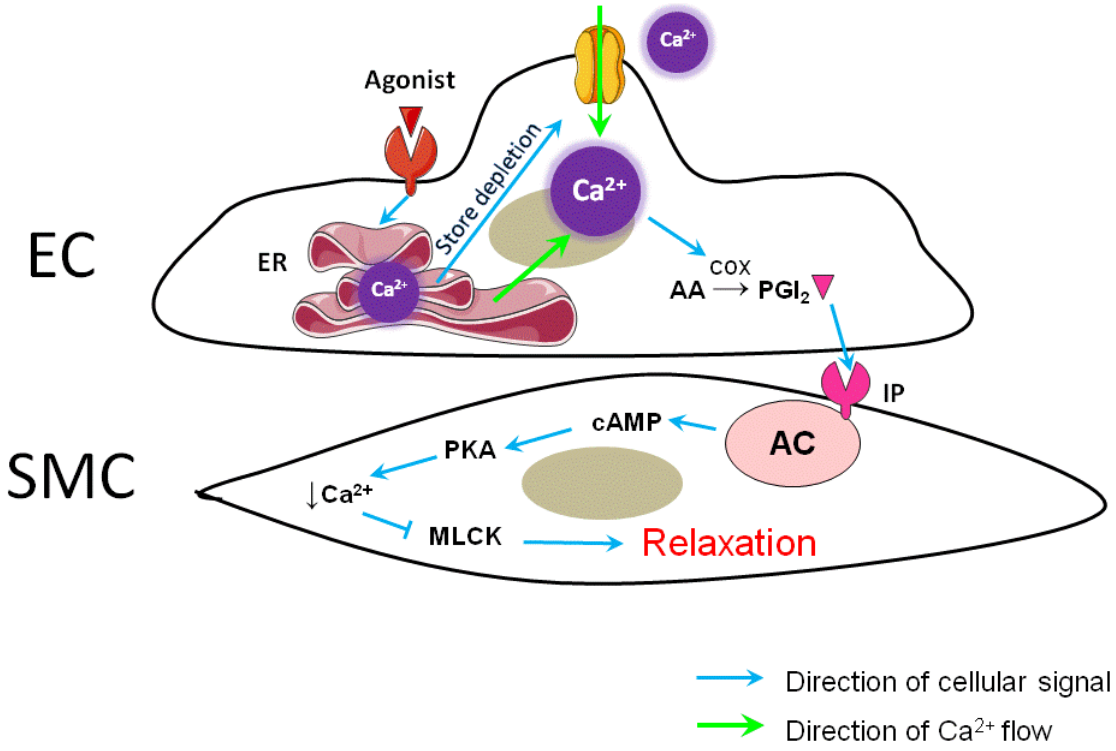

Figure 1.2 Schematic representations of the agonist-evoked production of PGI_2 and its downstream signaling pathway. The generation of PGI_2 is a calcium-dependent process that requires the presence of COX, which catalyses the conversion of arachidonic acid (AA) into PGI_2. The endothelium-derived PGI_2 binds to its adenylate cyclase (AC)-coupled receptor IP on the surface of the smooth muscle cells (SMC), leading to accumulation of cyclic adenosine monophosphate (cAMP). cAMP activates phosphorylating enzyme protein kinase A (PKA), resulting in the reduction of $[Ca^{2+}]_i$ and deactivation of myosin light chain kinase (MLCK), therefore relaxation. EC: endothelial cells, ER: endothelial reticulum.

PGI_2 is a potent vasodilator and inhibitor of platelet aggregation that is secreted from the endothelium (Moncada *et al.*, 1976; Moncada *et al.*, 1977). In endothelial cells, it is a major metabolite of the membrane–bound lipid arachidonic acid (AA). Its synthesis requires the presence of the cyclooxygenase enzyme COX. In healthy blood vessels,

COX-1 and COX-2 enzymes are expressed by both endothelial and vascular smooth muscle cells, COX-1 is the predominate and constitutive isoform for the generation of prostacyclin in endothelial cells (Egan and FitzGerald, 2006; Feletou, 2011a). The final step in PGI_2 synthesis also requires prostacyclin synthase (PGIS), a cytochrome P450 haemoprotein, which is expressed in both endothelial and vascular smooth muscle cells (Wu and Liou, 2005; Egan and FitzGerald, 2006; Tang and Vanhoutte, 2008).

To dilate the vessel, endothelium-derived PGI_2 binds to its G_s-protein coupled receptor (IP) on the vascular smooth muscle and transduces the signal through activation of adenylate cyclase, leading to the accumulation of the second messenger cyclic adenosine monophosphate (cAMP) and activation of phosphorylating enzyme protein kinase A (PKA). cAMP-PKA induces vascular relaxation through a number of downstream pathways including: (i) stimulation sarcoplasmic-endoplasmic reticulum Ca^{2+}-ATPase (SERCA) leads to sequestration of Ca^{2+} in the sarcoplasmic reticulum; (ii) stimulation of plasma membrane extrusion Ca^{2+}-ATPase (PMCA) leads to increased efflux of Ca^{2+}; (iii) stimulation of potassium (K^+) channels leads to inhibition of Ca^{2+} influx through voltage-operated Ca^{2+} channels (VOCC); and (iv) inhibition of MLCK leads to decreased Ca^{2+} sensitivity (Levick, 2010; Morgado *et al.*, 2012) (Figure 1.2). Genetic deletion or a mutated IP receptor leads to accelerated cardiovascular disease such as atherosclerosis (Kobayashi *et al.*, 2004), atherothrombosis (Arehart *et al.*, 2008) and reperfusion injury (Xiao *et al.*, 2001), whereas deletion of PGIS is associated with hypertension (Nakayama *et al.*, 2002).

PGI_2 may also evoke either hyperpolarization and depolarization in certain vascular beds (Feletou, 2011a). For example, in the guinea-pig carotid artery (Corriu *et al.*, 2001), guinea-pig coronary artery (Parkington *et al.*, 1993), guinea-pig aorta (Clapp *et al.*, 1998), porcine coronary artery (Edwards *et al.*, 2001) or rat tail artery smooth muscle cells (Schubert *et al.*, 1996), relaxation to PGI_2 or its analogue is associated with a hyperpolarization, possibly through PKA-dependent potassium channel

activation. However, in guinea-pig carotid artery (Corriu *et al.*, 2001), rabbit aorta (Borda *et al.*, 1983), rat aorta (Borda *et al.*, 1983; Williams *et al.*, 1994), bovine coronary artery (Schror and Verheggen, 1986) and human umbilical artery (Pomerantz *et al.*, 1978), depolarization or contractile responses to PGI_2 are often observed. However, it should be noted that in many blood vessels, the transient endothelium-dependent hyperpolarization following the addition of neurohumoral mediators is persistent after inhibition by a non-selective COX inhibitor indomethacin (Quignard *et al.*, 1999; Edwards *et al.*, 2001; Burnham *et al.*, 2006; Ng *et al.*, 2008) (See Section 1.2.5 below).

1.2.4 Nitric Oxide

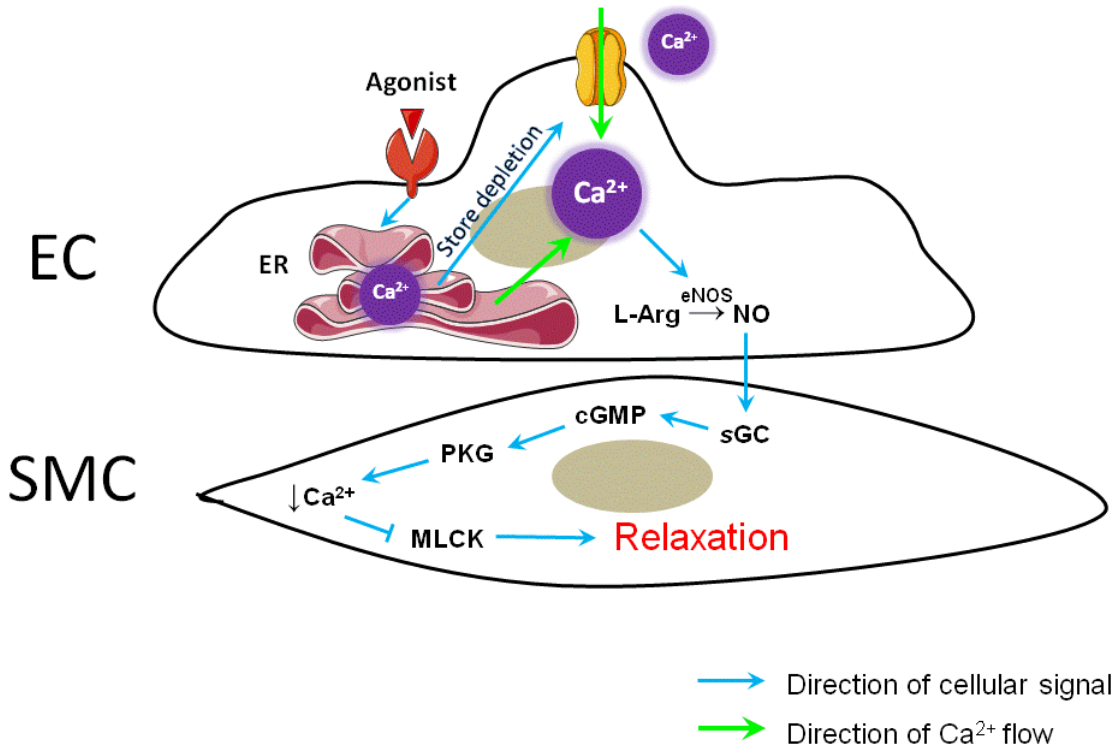

Figure 1.3 Schematic representations of the agonist-evoked production of NO in endothelial cells (EC) and its downstream signaling pathway. The generation of NO is a calcium-dependent process that requires the activation of eNOS, which catalyses the conversion of L-arginine (L-Arg) into NO and L-citrulline. The endothelium-derived NO activates the soluble guanylate cyclase in the smooth muscle cells (SMC), which increases cGMP levels and causes the activation of phosphorylating enzyme protein kinase G (PKG), resulting in the reduction of $[Ca^{2+}]_i$ and deactivation of myosin light chain kinase (MLCK), therefore relaxation. ER: endothelial reticulum, CaM: calmodulin.

The term endothelium-derived relaxing factor (EDRF) was first suggested by Furchgott and Zawadzki in 1980 (Furchgott and Zawadzki, 1980), who described the release of an unknown endothelial factor that relaxed isolated trips of rabbit aorta in response to ACh. Later research has showed that EDRF activated soluble guanylate cyclase (*s*GC) (Rapoport and Murad, 1983; Ignarro *et al.*, 1984), was synthesised and released from the endothelium continuously under basal conditions (Griffith *et al.*, 1984), has a half-life of only a few seconds (Griffith *et al.*, 1984; Rubanyi *et al.*, 1985), was scavenged by oxyhemoglobin (Martin *et al.*, 1985) and is inactivated by the superoxide anion (Rubanyi and Vanhoutte, 1986). Seven years after the first demonstration of existence of EDRF, the true identity of this EDRF was finally revealed to be NO (Ignarro *et al.*, 1987; Palmer *et al.*, 1987). Using analogues of L-arginine (L-Arg), these workers showed that NO production occurred through the L-arginine–NO-synthase (L-Arg–NOS) pathway (Ignarro *et al.*, 1987; Palmer *et al.*, 1987; Palmer *et al.*, 1988; Rees *et al.*, 1989).

Endothelial NOS (*e*NOS) is constitutively active and mainly localised in luminal membrane invaginations of endothelial cells called caveolae (Forstermann *et al.*, 1991; Garcia-Cardena *et al.*, 1996; Shaul *et al.*, 1996). NO contributes to vascular relaxation mainly through the activation of soluble guanylate cyclase (*s*GC), which produces cyclic guanosine monophosphate (*c*GMP). Elevation in cGMP levels leads to the activation of phosphorylating enzyme protein kinase G (PKG) (Pfeifer *et al.*, 1998). cGMP-PKG has similar actions as cAMP-PKA, it phosphorylates multiple targets such as (i) SERCA pump; (ii) PMCA pump; (iii) K^+ channels and (iv) MLCK, leading to decreased $[Ca^{2+}]_i$ and ultimately, the vascular relaxation (Levick, 2010) (Figure 1.3).

As NO is the most dominant endogenous vasodilator, its deficiency can lead to vasoconstriction in vascular beds and an increase in blood pressure. Indeed, reduced bioavailability of NO is observed in the endothelial dysfunction that is associated with atherosclerosis, hypertension, diabetes and other cardiovascular diseases

(Schachinger and Zeiher, 2000; Maxwell, 2002; Barbato and Tzeng, 2004). Genetic knockout mice that are deficient of eNOS (*e*NOS$^{-/-}$) are hypertensive (Huang *et al.*, 1995). Although the ACh response in large conductance vessels in these *e*NOS$^{-/-}$ mice is completely abolished (Brandes *et al.*, 2000), it should be noted that, in resistance vascular beds such as mesenteric artery, the ACh response is maintained and accompanied by a hyperpolarizing effect on the smooth muscle (Huang *et al.*, 2001; Scotland *et al.*, 2001). It has been reported that NO itself can induce hyperpolarization in guinea-pig coronary artery (Parkington *et al.*, 1993) and rat mesenteric artery (Garland and McPherson, 1992), possibly through direct action on a range of potassium channels (calcium-activated/K_{Ca}, voltage-dependent/K_v, ATP-sensitive/K_{ATP}), in either a cGMP-dependent or -independent manner (Murphy and Brayden, 1995b; Hohn *et al.*, 1996; Yuan *et al.*, 1996). However, it has became clear that hyperpolarization induced by exogenous NO is different to that induced by agonist such as ACh (Garland and McPherson, 1992; Plane *et al.*, 1995), and in some artery types, NO fails to evoke any membrane potential change at all (Zygmunt *et al.*, 1998).

1.2.5 Endothelium-derived Hyperpolarising Phenomenon

The endothelium can promote arterial relaxation through a mechanism, distinct from NO and prostanoids, in which hyperpolarization of this monolayer results in hyperpolarization of underlying vascular smooth muscle cells and closure of voltage-dependent L-type smooth muscle Ca^{2+} channels. This endothelium-derived hyperpolarizing phenomenon (EDH) has been demonstrated in a variety of vessel types, including rabbit mesenteric artery (Hutcheson *et al.*, 1999), rabbit iliac artery (Taylor *et al.*, 1998), guinea-pig carotid artery (Corriu *et al.*, 1996), rat mesenteric artery (Garland and McPherson, 1992; Randall *et al.*, 1996), rat coronary artery (Randall and Kendall, 1997) and human coronary artery (He, 1997). The EDH phenomenon is insensitive to *e*NOS/COX inhibition, is accountable for the dominant vasorelaxation in some smaller vessels and has been suggested to be a compensation mechanism for

reduced NO bioavailability (Busse *et al.*, 2002). Indeed, an inverse relationship between NO release and EDH phenomenon has been demonstrated in many artery types, including rabbit ear arteries (Berman *et al.*, 2002), rabbit carotid artery (Bauersachs *et al.*, 1996), porcine coronary artery (Bauersachs *et al.*, 1996) and rat isolated superior mesenteric arterial bed (McCulloch *et al.*, 1997).

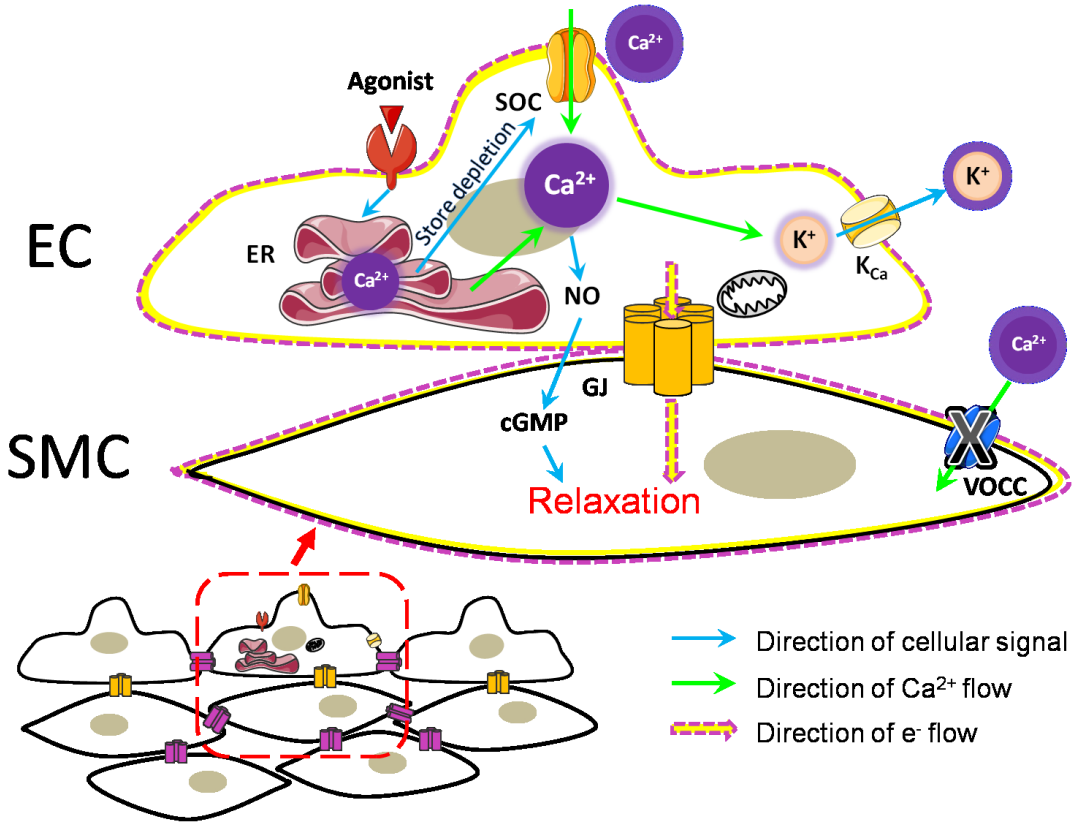

Figure 1.4 Schematic representations of the endothelium-derived hyperpolarizing factor (EDHF) signaling pathway. Depletion of the ER store by agonist stimulation leads to an increase in Ca^{2+} influx through store-operated channel (SOC), which in turn activates K_{Ca}, hyperpolarizing the endothelial cells (EC). This hyperpolarization propagates to the underlying smooth muscle cells (SMC) via myoendothelial gap junctions (GJ). VOCC: voltage-operated calcium channel.

Numerous candidates have been proposed to be an EDHF that is freely diffusible to the underlying smooth muscle cells, including NO itself, arachidonate metabolites such as epoxyeicosatrienoic acids (EETs) (Campbell *et al.*, 1996) and anandamide (Randall *et al.*, 1996), K^+ (Edwards *et al.*, 1998), hydrogen peroxide (Matoba *et al.*, 2000), C-type natriuretic peptide (Chauhan *et al.*, 2003), and hydrogen sulfide (Wang, 2009).

However, none could be considered to have emerged as a universal mediator of hyperpolarization-dependent relaxation. An alternative hypothesis is that electrical signaling via gap junctions plays a crucial role in the EDH phenomenon, indeed, in rabbit arteries, EDHF-type relaxations involve direct intercellular communication via myoendothelial and homocellular smooth muscle gap junctions that allow passive spread of endothelial hyperpolarization through the vessel wall (Chaytor *et al.*, 1998). This gap junction-dependent mechanism is now evident in many vessel types in many species including rabbit iliac artery (Taylor *et al.*, 1998; Griffith *et al.*, 2002; Chaytor *et al.*, 2005), rabbit mesenteric artery (Hutcheson *et al.*, 1999), rabbit ear artery (Taylor *et al.*, 2001; Berman *et al.*, 2002), rat mesenteric artery (Sandow *et al.*, 2002) and mouse mesenteric artery (Dora *et al.*, 2003).

EDH/EDHF-type relaxations can be evoked by either receptor-dependent or receptor-independent pathways. In the case of G protein-coupled agonists that stimulate relaxation, including ACh, bradykinin and substance P, two mechanisms contribute to the elevation in $[Ca^{2+}]_i$ necessary for endothelial K_{Ca} channel activation, namely (i) transient release of Ca^{2+} from the endoplasmic reticulum (ER) through the activation of phospholipase C (PLC), followed by the formation of inositol 1,4,5-trisphosphate ($InsP_3$), which binds to its receptor $InsP_3R$ on the store (Fleming *et al.*, 1996) and (ii) sustained influx of extracellular Ca^{2+} (also called capacitative calcium entry) via store-operated Ca^{2+} channels (SOCs) that are regulated by the resulting $InsP_3$-evoked depletion of the ER Ca^{2+} store (Pasyk *et al.*, 1995; Fukao *et al.*, 1997; Tomioka *et al.*, 2001). Additionally, store-operated Ca^{2+} influx and relaxation can also be triggered by inhibitors of the SERCA pump such as cyclopiazonic acid (CPA) and thapsigargin, which selectively block ER Ca^{2+} uptake thereby promoting direct ER depletion (Pasyk *et al.*, 1995). Agents such as Ca^{2+} ionophore A21387 will also evoke receptor-independent stimulation of EDH/EDHF-type relaxations (Petersson *et al.*, 1997;

Zygmunt *et al.*, 1998; Hutcheson *et al.*, 1999), possibly by depleting the ER Ca^{2+} store directly (Figure 1.4).

1.2.5.1 Gap Junctions

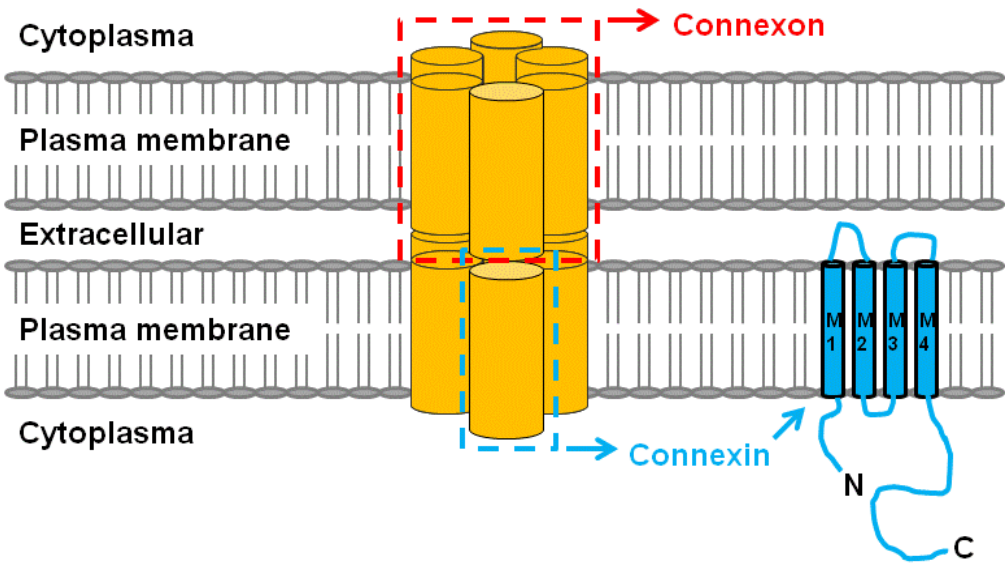

Figure 1.5 Schematic representations showing the structure of gap junction. Docking of two connexon from apposing cells results in the formation of an aqueous pore, that allows the transfer of ions and small molecules between coupled cells. Each connexon is formed by six connexins, and each connexin possesses four transmembrane domains (M1-4). N: N-terminal, C: C-terminal.

Gap junctions are formed by the linking of two hemichannels or connexons, one on each cell membrane of two adjacent cells. Each connexon is assembled from six subunit proteins called connexins (Cx), each connexin possessing four transmembrane segments (M1-4) (Griffith, 2004; Griffith *et al.*, 2004) (Figure 1.5). Four connexin subtypes have been demonstrated to be present in the vasculature depends on species and vessel type, Cx37, Cx40, Cx43 and Cx45, named after their molecular weights. Gap junctions may be homotypic, in which each connexon contains the same connexin subtype, or heterotypic, in which each connexon is formed by a different connexin subtype, or heteromeric, in which each connexon is constructed from a mixture of subtypes. The expression of connexins may vary depending on the species and vessel types, for example, Cx37 and Cx40 are often seen co-localized within

myoendothelial gap junctions (Haddock *et al.*, 2006) and are abundantly expressed in the endothelium of hamster (Hakim *et al.*, 2008) and mice (Looft-Wilson *et al.*, 2004), whereas Cx43 expression appears to decrease with vessel size in many species (Hong and Hill, 1998; Berman *et al.*, 2002; Looft-Wilson *et al.*, 2004; Matchkov *et al.*, 2006). The expression of these connexins is essential in maintaining cardiovascular function, as deficiency of Cx43 (display cardiac malformation) (Ya *et al.*, 1998), Cx45 (display defect in vessel development, impaired vessel maturation and cardiac malformation) (Kruger *et al.*, 2000), or simultaneous knockout of Cx40 and Cx37 (display abnormal vascular channels and distended vessels) (Simon and McWhorter, 2002, 2003) in genetically engineered mice are lethal.

Large numbers of individual gap junctions are organized as plaques at the point of cell-cell contact. Gap junction channels allow propagation of ions and signalling molecules <1 kDa in size such as Ca^{2+} ions and $InsP_3$, and electrical signals such as hyperpolarization from endothelial cells to the underlying smooth muscle cells (Griffith, 2004). In addition, there are reports that suggest substances such as $InsP_3$ and possibly Ca^{2+} ions can also diffuse into the endothelium from activated smooth muscle cells, thereby elevating the endothelial $[Ca^{2+}]_i$, promoting K_{Ca} activation and resulting in reduced contractile responses in the smooth muscles (Dora *et al.*, 1997; Dora *et al.*, 2000; Yashiro and Duling, 2000; Budel *et al.*, 2001). Evidence that direct endothelial-smooth muscle electrical coupling contributes to the EDHF phenomenon has been provided by studies with short peptides that block myoendothelial gap junctional communication by targeting specific connexin. Such short synthetic connexin-mimetic peptides possess sequences homologous with the conserved Gap 26 and 27 extracellular domains of Cxs 37, 40 and 43 (i.e. ^{37,40}Gap26, ^{43}Gap26, ^{37,43}Gap27 and ^{40}Gap27) (Griffith *et al.*, 2004). When administered individually or in combination, these peptides attenuate or abolish EDHF-type relaxations and subintimal smooth muscle hyperpolarizations evoked by ACh, ATP, UTP, substance P, bradykinin and CPA in a

range of arteries and veins from the rabbit (Chaytor *et al.*, 1998; Chaytor *et al.*, 1999; Dora *et al.*, 1999; Berman *et al.*, 2002; Chaytor *et al.*, 2003; Ujiie *et al.*, 2003; Chaytor *et al.*, 2005; Griffith *et al.*, 2005; Edwards *et al.*, 2007), rat (Edwards *et al.*, 1999; Doughty *et al.*, 2000; Chaytor *et al.*, 2001; Sandow *et al.*, 2002; Matchkov *et al.*, 2006; Sokoya *et al.*, 2006), pig (Edwards *et al.*, 2000), guinea-pig (Edwards *et al.*, 1999) and human arteries (Lang *et al.*, 2007). It should be noted that connexin-mimetic peptides do not depress the initiating endothelial hyperpolarization, and have no effect on the smooth muscle membrane potential (de Wit and Griffith, 2010), they act by modulating the gating of the gap junctional channels, without disturbing the structure of the plaques (Martin *et al.*, 2005). It has been reported that the EDHF phenomenon can also be inhibited by derivatives of glycyrrhizic acid (GA) that is found in the liquorice root *glycyrrhizia glabra*, including lipophilic 18α- and 18β-isoforms of GA and the water-soluble hemisuccinate derivative of 18β-GA carbenoxolone (Taylor *et al.*, 1998; Yamamoto *et al.*, 1998; Chaytor *et al.*, 2000; Doughty *et al.*, 2000).

1.2.5.2 Calcium-activated potassium channels

It is now generally accepted that the opening of endothelial K_{Ca} channels is the key initiating electrical event in the EDHF phenomenon (Busse *et al.*, 2002; Griffith, 2004; Sandow, 2004; Shimokawa and Matoba, 2004; Feletou, 2011b). There are three categories of K_{Ca}, the small conductance calcium-activated potassium channels subfamily (SK_{Ca}), the intermediate conductance calcium-activated potassium channels (IK_{Ca}) and the large conductance (BK_{Ca}) calcium-activated potassium channels. SK_{Ca} and IK_{Ca} channels are tetrameric complexes of four α-subunits, each subunit comprised of six-transmembrane domains (S1–S6), with intracellular N- and C-termini (Vergara *et al.*, 1998). BK_{Ca} channels are also tetrameric, which formed by four pore-forming α-subunits, each possessing seven transmembrane domains (S0–S6), an extracellular N-terminus and an intracellular C-terminus (Shen *et al.*, 1994; Wallner *et al.*, 1996; Meera *et al.*, 1997; Quirk and Reinhart, 2001). Each α-subunit is co-assembled with a

regulatory β-subunit, each displaying two transmembrane domains and intracellular N- and C-terminus (Orio *et al.*, 2002). S5 and S6 of α-subunit in SK_{Ca}, IK_{Ca} and BK_{Ca} channels are the pore-forming domain (Vergara *et al.*, 1998) (Figure 1.6).

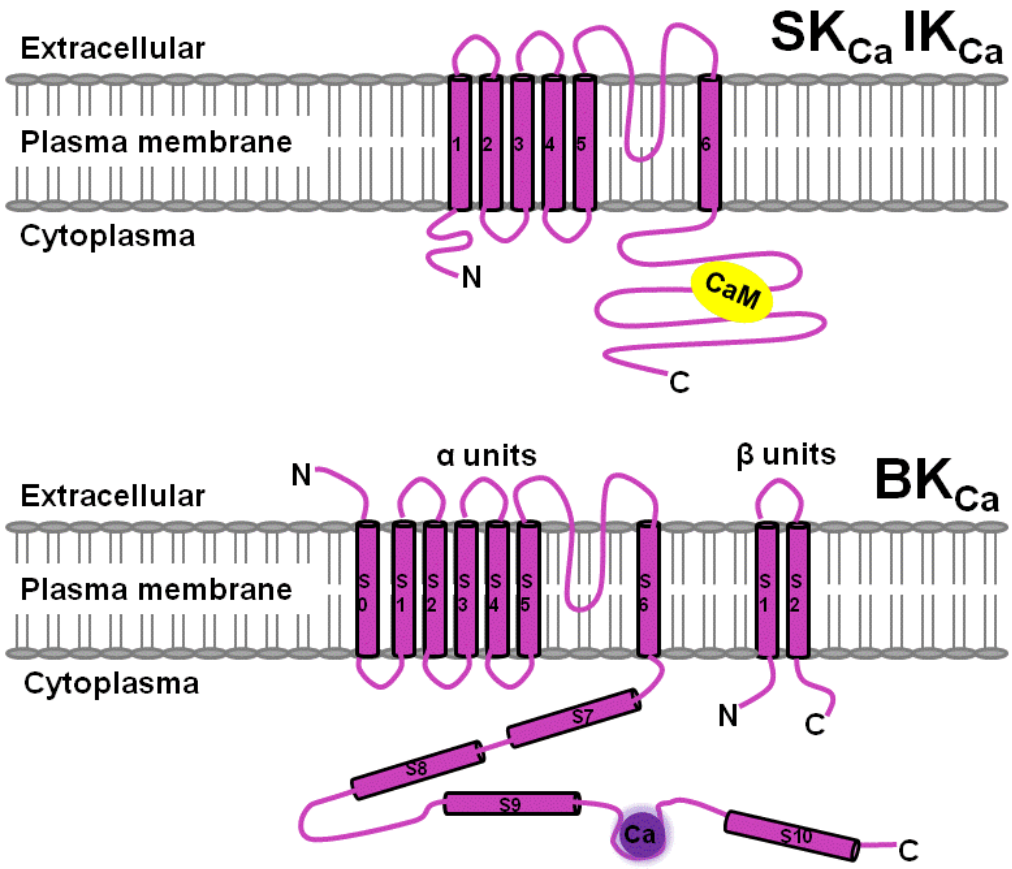

Figure 1.6 Schematic representations showing the structure of subunits that forming the K_{Ca} channels. Calmodulin (CaM) binds close to the phosphorylation site (shown as yellow circles) in SK_{Ca} and IK_{Ca}. The α-subunit of BK_{Ca} channels has 11 (S0-S10) hydrophobic domains, with S0-S6 located in the cytoplasmic membrane. Ca^{2+} binding sites in BK_{Ca} are depicted as purple circles. N: N-terminal, C: C-terminal.

SK_{Ca} and IK_{Ca} channels share many similarities: (i) they are voltage-independent, (ii) they do not contain a Ca^{2+}-binding domain, instead, each α-subunit in SK_{Ca} and IK_{Ca} channels are bound by calmodulin, a ubiquitous small Ca^{2+}-binding protein and regulated by Ca^{2+} indirectly (Xia *et al.*, 1998; Fanger *et al.*, 1999; Kong *et al.*, 2000; Zhang *et al.*, 2001), (iii) they are constitutively expressed in endothelial cells (Marchenko and Sage, 1996; Kohler *et al.*, 2000; Burnham *et al.*, 2002; Bychkov *et al.*,

2002; Feletou, 2011a). It is worth noting that, in endothelial cells, SK_{Ca} and IK_{Ca} channels are often localized at the sites of gap junctions. In the rat mesenteric artery, SK_{Ca} are distributed over the plasma membrane with preferential localization at sites of homocellular endothelial gap junctions and in caveolin-rich domains along with other components of the classical EDHF pathway such as close to the ER $InsP_3$ receptors (Lockwich *et al.*, 2000; Sandow *et al.*, 2006; Absi *et al.*, 2007; Dora *et al.*, 2008; Ledoux *et al.*, 2008). In contrast, IK_{Ca} are non-caveolar and are localized in proximity to myoendothelial gap junctions, and also close to sections of ER densely expressing $InsP_3$ receptors (Weston *et al.*, 2005; Sandow *et al.*, 2006; Absi *et al.*, 2007; Dora *et al.*, 2008; Ledoux *et al.*, 2008; Sandow *et al.*, 2009).

BK_{Ca} channels are both voltage and Ca^{2+}-regulated, unlike SK_{Ca} and IK_{Ca} channels they are not linked with calmodulin and their sensitivity to Ca^{2+} relies on the direct binding of Ca^{2+} to two high affinity Ca^{2+}-sensing regions in the C-terminus of the α-subunit, while the β-subunit modulates their Ca^{2+} sensitivity (Toro *et al.*, 1998; Schreiber *et al.*, 1999; Kohler *et al.*, 2000; Papassotiriou *et al.*, 2000; Xia *et al.*, 2002; Yusifov *et al.*, 2008). BK_{Ca} channels are mainly expressed in vascular smooth muscle cells, although some reports suggest that they are also located in the endothelium of some species, such as rat gracilis muscle arterioles (Ungvari *et al.*, 2002), porcine renal artery (Brakemeier *et al.*, 2003), rabbit ductus arteriosus (Thebaud *et al.*, 2002), and rat mesenteric artery (Hilgers *et al.*, 2006).

Selective pharmacological inhibition of SK_{Ca}, IK_{Ca} and BK_{Ca} channels has been shown to attenuate EDHF-type relaxations, for example, in rat mesenteric artery, EDHF is blocked by a combination of apamin (SK_{Ca}) and charybdotoxin (IK_{Ca} and BK_{Ca}) (Doughty *et al.*, 1999). And in rabbit iliac and renal artery, when administered individually or in combination, apamin, TRAM-34 (IK_{Ca}) and iberiotoxin (BK_{Ca}) attenuates EDHF-type responses to a different extent (Kagota *et al.*, 1999; Edwards *et al.*, 2008). Indeed, in some arteries, a specific inhibitor of one K_{Ca} channel type may be

individually ineffective, whereas used in combination substantial or complete inhibition of EDHF-type relaxations is usually achieved.

1.3 REACTIVE OXYGEN SPECIES

Reactive oxygen species (ROS), such as unstable free radical superoxide anion ($O_2^{\bullet -}$) and peroxynitrite ($ONOO^-$), or non-free radicals such as H_2O_2, are by-products of oxygen metabolism and have a crucial role in regulating cellular redox status. In the vascular system, ROS has been shown to be an important regulator in controlling endothelial function, vascular tone and vascular integrity. Vascular endothelium (Arroyo *et al.*, 1990; Kinnula *et al.*, 1991; Sundqvist, 1991; Heinzel *et al.*, 1992; Brandes *et al.*, 1997) and smooth muscle cells (Zafari *et al.*, 1998; Li and Fukagawa, 2010; Trebak *et al.*, 2010) generate significant amounts of ROS, either due to spontaneously metabolic processes or in response to receptor-dependent and receptor-independent stimulation. Under normal physiological conditions, the rate and magnitude of oxidant formation is usually balanced by the rate of oxidant elimination that is provided by activities of enzymes such as superoxide dismutase (SOD), catalase and glutathione peroxidase. However, oxidative stress results from an imbalance between prooxidants and antioxidants often lead to multiple pathological conditions including cardiovascular disease. Indeed, disturbed redox cellular status is linked with inflammation, angiogenesis, endothelial dysfunction, vascular contraction and arterial remodeling.

1.3.1 Vascular effects of H_2O_2

Historically, H_2O_2 was considered to be a damaging substance that is implicated in the pathological processes such as atherosclerosis and hypertension (Tate and Repine, 1983; Smith *et al.*, 1992; Halliwell, 1993). However, endothelium-derived H_2O_2 is now thought to participate in the physiological response to endothelium-dependent agonists and fluid shear stress (Matoba *et al.*, 2000; Matoba *et al.*, 2002; Liu *et al.*, 2006), and can compensate for the loss of NO bioavailability observed in experimental models of

hypertension and diabetes and in patients with arterial disease (Cosentino *et al.*, 1998; Karasu, 2000; Landmesser *et al.*, 2003; Phillips *et al.*, 2007; Larsen *et al.*, 2009).

1.3.1.1 Vascular production and degradation of H_2O_2

$O_2^{\bullet-}$ is formed from molecular oxygen and is a precursor for several ROS including H_2O_2. Vascular cells contain various $O_2^{\bullet-}$-producing oxidases including mitochondria, COX, nicotinamide adenine dinucleotide phosphate (NADPH) oxidases, xanthine oxidases, lipoxygenases and NOS. As a reducing agent (loss of electrons), $O_2^{\bullet-}$ rapidly inactivates NO to form $ONOO^-$. While as an oxidizing agent (gain of electrons), $O_2^{\bullet-}$ is degraded to H_2O_2 spontaneously or through SOD-dependent dismutation. Therefore, loss of NO will alter the balance and could lead to enhanced formation of H_2O_2 through increased $O_2^{\bullet-}$ availability. In addition, enzymes such as xanthine oxidase and glucose oxidase can directly produce H_2O_2 by donating two electrons to oxygen (Cai, 2005). H_2O_2 levels in vascular cells are regulated by the endogenous scavengers catalase and glutathione peroxidase, which degrade H_2O_2 into water and oxygen. H_2O_2 is also decomposed to hydroxyl radical ($HO^{\bullet}$) through a transition metals-dependent pathway known as Haber-Weiss/Fenton reaction.

1.3.1.2 Vasorelaxing effects of H_2O_2

Exogenous applied H_2O_2 itself can induce direct smooth muscle relaxation in many vessels including porcine coronary artery (Barlow and White, 1998; Hayabuchi *et al.*, 1998), rabbit mesenteric small artery (Fujimoto *et al.*, 2001), canine middle cerebral arteries (Iida and Katusic, 2000), human mesenteric artery (Matoba *et al.*, 2002) and human coronary arterioles (Sato *et al.*, 2003). The mechanism that underpins the vasodilatation effect of H_2O_2 is complex, with both endothelium-dependent and –independent components being reported. The endothelium-dependent vasorelaxing effect of H_2O_2 in rabbit aorta (Zembowicz *et al.*, 1993; Yang *et al.*, 1999a), canine basilar artery (Yang *et al.*, 1998a) and guinea-pig nasal mucosa vasculature (Hirai *et*

al., 2000) involves the NO-cGMP and cytochrome P450 metabolism pathways, that may also be related to an increase in endothelial $[Ca^{2+}]_i$. In porcine coronary arterioles, this endothelium-dependent effect of H_2O_2 was reported to involve the COX-prostaglandin E2 (PGE_2) pathway (Thengchaisri and Kuo, 2003). By contrast, the endothelium-independent vasorelaxing effect of H_2O_2 in bovine pulmonary arterial (Burke and Wolin, 1987), rabbit pulmonary arterial (Burke-Wolin *et al.*, 1991), rabbit mesenteric small artery (Fujimoto *et al.*, 2001), guinea-pig aorta (Fujimoto *et al.*, 2003) and human coronary arterioles (Sato *et al.*, 2003) may involve activation of sGC and accumulation of cGMP. Whereas in canine middle cerebral arteries, this endothelium-independent effect of H_2O_2 was shown to involve COX and cyclic AMP pathway (Iida and Katusic, 2000), and in porcine coronary artery, this endothelium-independent effect of H_2O_2 was found to involve phospholipase A2 (PLA_2) pathway (Barlow *et al.*, 2000).

In addition, H_2O_2 can directly cause hyperpolarizations of the vascular smooth muscle cells and therefore vasodilatation of the vessel by opening several K^+ channels, including K_{Ca} channels (Hayabuchi *et al.*, 1998; Barlow *et al.*, 2000; Matoba *et al.*, 2000; Brakemeier *et al.*, 2003), K_{ATP} channels (Wei and Kontos, 1990; Gao *et al.*, 2003; Hattori *et al.*, 2003), K_V channels (Gao *et al.*, 2003; Rogers *et al.*, 2006) and/or inwardly rectifying potassium channels (K_{ir}) (Bychkov *et al.*, 1999; Iida and Katusic, 2000). In endothelial cells, H_2O_2 has also been shown to modulate K^+ channel activity and thus the contractile activity of the underlying smooth muscle. In cultured endothelial cells of the human umbilical vein, H_2O_2 elicits both depolarization and hyperpolarization of the membrane potential, at low H_2O_2 concentrations (0.01-0.25 μM) inhibited K_{ir} channel activity, whereas higher H_2O_2 concentrations (1 mM) increased the K_{Ca} channel activity. (Bychkov *et al.*, 1999). It is worth noting that the oxidative state of amino acid residue suphydryl groups is known as to be the determinant factor in ion channel activity, therefore the ability of H_2O_2 to regulate the opening of these K^+ channels can be attributed to its oxidative modification of the suphydryl groups (Cai and Sauve, 1997).

1.3.1.3 Vasoconstriction effects of H_2O_2

H_2O_2 has been shown to cause vasoconstriction in a variety of vessels including rat aorta (Rodriguez-Martinez *et al.*, 1998; Sotnikova, 1998; Yang *et al.*, 1998b), rat pulmonary artery (Jin and Rhoades, 1997; Gao and Lee, 2001), rat superior mesenteric artery (Gao *et al.*, 2003), mouse aorta (Ardanaz *et al.*, 2008), mouse carotid artery (Ardanaz *et al.*, 2008), porcine pulmonary artery (Pelaez *et al.*, 2000b), canine basilar artery (Katusic *et al.*, 1993; Yang *et al.*, 1998a) and canine cerebral arterial (Yang *et al.*, 1999b). In addition, there is evidence that the contractile response induced by agonist stimulation such as angiotensin II may be mediated by endogenously produced H_2O_2 (Torrecillas *et al.*, 2001; Chin *et al.*, 2007). Indeed, in transgenic mice overexpressing catalase, the basal arterial pressure and H_2O_2 release from the mouse aorta were similar to those of wild-type mice. However, in the transgenic mice, the angiotensin II-induced pressor response is decreased and accompanied with a reduced H_2O_2 production in the arterial wall, indicating that endogenously produced H_2O_2 may contribute to the vasopressor responses evoked by angiotensin II (Yang *et al.*, 2003).

In arteries such as rat aorta and canine basilar artery, the mechanism involved in H_2O_2-evoked vasoconstriction is reported to be Ca^{2+}-dependent (Katusic *et al.*, 1993; Yang *et al.*, 1998a; Yang *et al.*, 1998b), as removal of extracellular Ca^{2+} and addition of voltage-dependent Ca^{2+} channel blocker verapamil resulted in a significant attenuation of the contractile responses to H_2O_2 in rat aorta. In addition, cyclooxygenase products, protein kinase C and products of protein tyrosine phosphorylation may play some role in H_2O_2-induced contractions, as administration of protein kinase C inhibitor staurosporine, treatment with inhibitor of protein tyrosine phosphorylation genistein and employment of COX inhibitor indomethacin also resulted in a significant reduction of the contractile responses to H_2O_2 in rat aorta (Yang *et al.*, 1998b). H_2O_2 has been reported to directly increase the $[Ca^{2+}]_i$ in smooth muscle cells via various Ca^{2+}

channels, including voltage-operated Ca^{2+} channel (Tabet *et al.*, 2004), SERCA pumps (Grover and Samson, 1997), ryanodine receptor (Favero *et al.*, 1995) and $InsP_3$ receptors (Wada and Okabe, 1997). Furthermore, there is evidence that H_2O_2 can impair endothelium-dependent vasodilatations, possibly through prevention of eNOS-NO generation (Andreozzi *et al.*, 2004; Loot *et al.*, 2009), inhibition of the vasodilator EETs via cytochrome P450 epoxygenase (Larsen *et al.*, 2008) and attenuation of NO-dependent activation of BK_{Ca} (Brakemeier *et al.*, 2003) and IK_{Ca} (Cai and Sauve, 1997). It should be noted that, in some artery types such as rat and rabbit pulmonary arteries, H_2O_2 can also induce constriction via Ca^{2+}-independent and endothelium-independent pathways (Rhoades *et al.*, 1990; Sheehan *et al.*, 1993; Pelaez *et al.*, 2000a; Pelaez *et al.*, 2000b). In these arteries, the constriction evoked by H_2O_2 was persistent after endothelium removal and/or incubation in Ca^{2+} free solution, although the underlying mechanism is not fully identified.

In arteries such as rat mesenteric artery, the response to H_2O_2 was found to be concentration-dependent. Low concentrations of H_2O_2 (10-100 μM) evoked only contraction, while higher concentrations of H_2O_2 (0.3-1 mM) caused a biphasic response, where a transient contraction was first observed followed by a relaxation response. This transient contraction is likely to be mediated through AA metabolite thromboxane A2 (TXA_2) pathway as inhibitors of PLA_2 significantly attenuated this contractile response (Gao *et al.*, 2003). The biphasic effect of H_2O_2 was also reported in other artery types such as porcine cerebral artery (Leffler *et al.*, 1990), retinal vasculature of newborn and adult pigs (Abran *et al.*, 1995), microvascular lung pericytes (Kerkar *et al.*, 2001), and rat gracilis skeletal muscle arterioles (Cseko *et al.*, 2004).

1.3.1.4 H_2O_2 and the EDHF phenomenon

In 2000, Matoba and colleagues gave the first evidence that suggested H_2O_2 derived from eNOS acts as an EDHF (Matoba *et al.*, 2000). In small mesenteric arteries from

eNOS-knockout ($eNOS^{-/-}$) mice, the ACh-induced relaxation and hyperpolarization, resistant to NOS inhibition with L-NNA and COX inhibition with indomethacin, are sensitive to catalase, a specific inhibitor of H_2O_2, and when inactivated at its peroxide-binding site by aminotriazole, catalase lost its inhibitory effect on this EDHF-type relaxation. Exogenous applied H_2O_2 is able to evoke similar relaxation and hyperpolarization in endothelium-denuded arteries of $eNOS^{-/-}$ mice and H_2O_2/ACh-evoked relaxation were both inhibited by K_{Ca} blocker apamin plus charybdotoxin. It has been reported in this study that multiple pathways are involved in endogenous production of H_2O_2, however, it seems that eNOS appears to be the dominant source of H_2O_2 in mouse mesenteric arteries, because these $eNOS^{-/-}$ mice have shown markedly reduced levels of ACh-induced H_2O_2 production. It is worth mentioning that the gap junction inhibitor 18β-GA had no significant inhibitory effect on the EDHF-type relaxation in mouse small mesenteric arteries (Matoba *et al.*, 2000).

Further investigations have revealed that in more artery types such as porcine pial artery (Lacza *et al.*, 2002), canine coronary artery (Yada *et al.*, 2003), porcine coronary artery (Matoba and Shimokawa, 2003), human mesenteric artery (Matoba *et al.*, 2002) and human coronary artery (Miura *et al.*, 2003; Liu *et al.*, 2011), H_2O_2 was also reported to relax the adjacent smooth muscle cells by acting as a freely diffusible EDHF. These conclusions were reached because in these arteries: (i) the NO and prostanoids-independent relaxation is sensitive to catalase; (ii) agonist-evoked EDHF-type relaxation is associated with catalase-sensitive endothelial production of H_2O_2 and (iii) this relaxation is linked with vascular K_{Ca} channel activation, a key initiating electrical event in the EDH phenomenon.

By contrast, in other artery types including rat coronary artery (Fulton *et al.*, 1997), human radial artery (Hamilton *et al.*, 2001), canine coronary artery (Tanaka *et al.*, 2003), guinea-pig carotid artery (Gluais *et al.*, 2005), rabbit iliac-femoral artery (Chaytor *et al.*, 2003), rabbit mesenteric artery (Itoh *et al.*, 2003), and also in results with porcine

coronary artery (Pomposiello *et al.*, 1999) and human mesenteric artery (Chadha *et al.*, 2011) that conflict with those reported in the previous paragraph, H_2O_2 cannot be considered as the EDHF, because EDHF-type relaxation in these arteries are: (i) not sensitive to catalase; (ii) H_2O_2 does not cause hyperpolarization of the vascular smooth muscle cells, or (iii) the relaxing effect of H_2O_2 is not associated with the opening of K_{Ca} channels.

In addition, exogenous applied H_2O_2 or substances that promote H_2O_2 formation can promote depletion of the ER Ca^{2+} store and amplify increases in $[Ca^{2+}]_i$ evoked by pharmacological stimulation of the endothelium (Hu *et al.*, 2000). The synergistic elevation of $[Ca^{2+}]_i$ with H_2O_2 and agents that deplete the ER store can enhance the opening of K_{Ca} thereby allowing H_2O_2 to potentiate "EDHF-type" relaxations that are mediated by the spread of endothelial hyperpolarization into the arterial media via myoendothelial and homocellular smooth muscle gap junctions (Edwards *et al.*, 2008; Garry *et al.*, 2009).

1.3.2 ROS in disease- arsenic toxicity

High levels of arsenic are present in drinking water in some parts of the USA, Mexico, Chile, Argentina, Peru, Hungary, Bangladesh, India, Thailand, China and Australia, and constitute a major public health epidemic that affects more than 140 million people (Freeman, 2009; Hall *et al.*, 2009). In the cardiovascular system, exposure to arsenic accelerates the development of atherosclerosis and predisposes to hypertension and peripheral microvascular abnormalities such as Blackfoot Disease (Balakumar and Kaur, 2009; States *et al.*, 2009). Underlying mechanisms have been suggested to involve increased oxidant stress, because exposure of endothelial cells to arsenite at concentrations within the range found in contaminated drinking water (0.3-15 μM) causes excess production of the $O_2^{\bullet-}$ by nicotinamide adenine dinucleotide phosphate (NADPH) oxidase (Barchowsky *et al.*, 1999; Smith *et al.*, 2001; Qian *et al.*, 2005; Straub *et al.*, 2008). While $O_2^{\bullet-}$ may contribute to vascular dysfunction through a rapid

interaction with NO (Lassegue and Griendling, 2010), dismutation by SOD also generates H_2O_2, and the production of both ROS increases within minutes of exposing endothelial cells to low concentrations of arsenite (5 μM) (Barchowsky *et al.*, 1999; Smith *et al.*, 2001; Tsai *et al.*, 2001). The oxidative stress resulting from arsenic toxicity may therefore alter endothelium-dependent responses not only as a result of decreased NO bioavailability but also through a increased H_2O_2 production.

1.4 CALCIUM HOMEOSTASIS IN ENDOTHELIAL CELLS

Calcium is recognised as the most important messenger in a variety of cells including vascular cells and contraction of smooth muscle cells is directly regulated by changes in free cytosolic calcium concentration ($[Ca^{2+}]_i$). In endothelial cells, the elevation in $[Ca^{2+}]_i$ is the initial response to hormonal/chemical transmitter stimulation such as angiotensin II and to the changes in physical parameters such as shear stress (Tran and Watanabe, 2006) that leads to the production of NO from endothelial *e*NOS that is greatly dependent on the calcium-calmodulin complex (Knowles *et al.*, 1989; Bredt and Snyder, 1990). In the events leading to the EDHF phenomenon, the opening of endothelial K_{Ca} is the key initiating electrical stimuli that leads to the hyperpolarizing effects.

Elevation of $[Ca^{2+}]_i$ in the endothelial cells in response to receptor activation or other stimuli such as shear stress are often biphasic, with an initial phase of Ca^{2+} release from intracellular stores such as the ER, followed by sustained extracellular Ca^{2+} influx. For example, elevation of intracellular Ca^{2+} by ACh is achieved in two stages: (i) Ca^{2+} release from the ER that involves $InsP_3$ and (ii) depletion of ER stores initiates Ca^{2+} influx through store-operated Ca^{2+} entry (SOCE) (Pasyk *et al.*, 1995; Fukao *et al.*, 1997; Tomioka *et al.*, 2001).

1.4.1 Intracellular Ca^{2+} stores in endothelial cells

1.4.1.1 Endoplasmic reticulum store

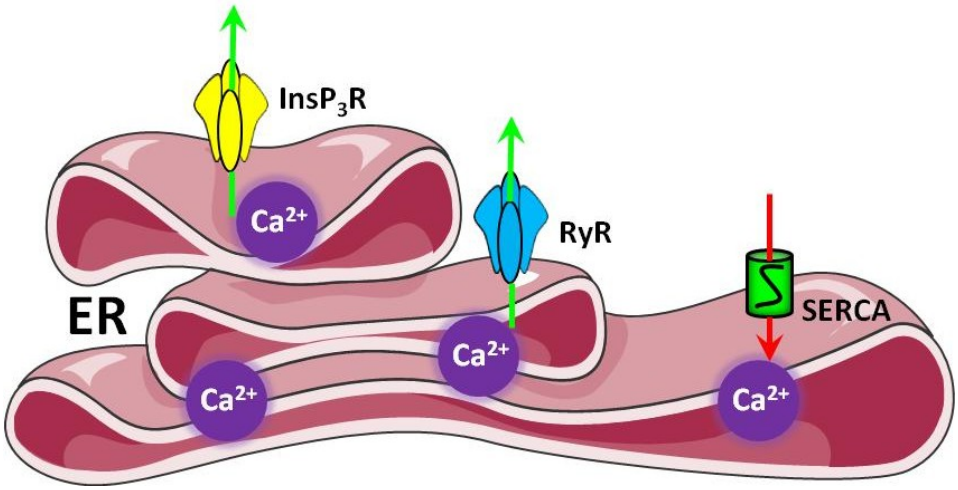

Figure 1.7 Schematic representations showing the Ca^{2+} channels on the surface of the ER. $InsP_3R$: $InsP_3$ receptors, RyR: ryanodine receptors.

The ER extends like a net through the entire cytoplasm and is responsible for the biosynthesis of the protein and lipid components of most of the cell's organelles such as the ER itself, the Golgi apparatus and the plasma membrane. The ER functions as the most important Ca^{2+} store, and accumulates Ca^{2+} via SERCA pumps and releases it into the cytosol through $InsP_3$ and ryanodine receptors (Figure 1.7). The ER contains a large number of Ca^{2+}-binding proteins such as GRP94, BiP (GRP78), RP 60 and calreticulin, each of these molecules is able to sequester as many as 30 Ca^{2+} ions (Tran and Watanabe, 2006). When the ER is loaded, the concentration of Ca^{2+} in the ER ($[Ca^{2+}]_{ER}$) is at least 100 μM, and some reports suggest it might be between 400-800 μM (Pinton *et al.*, 1998; Alonso *et al.*, 1999). In endothelial cells, the ER accounts for ~75% of the total intracellular Ca^{2+} reserve (Wood and Gillespie, 1998).

1.4.1.2 Mitochondria store

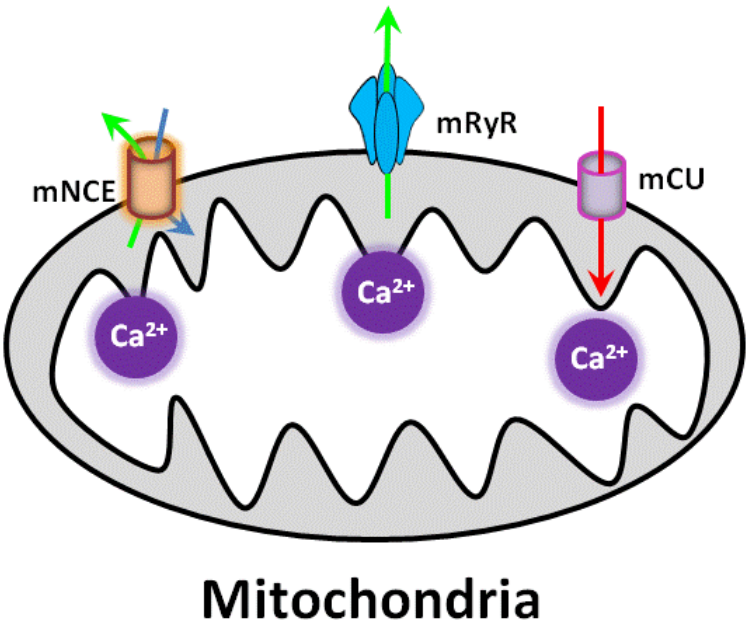

Figure 1.8 Schematic representations showing the Ca^{2+} channels on the surface of the mitochondria. mNCE: mitochondrial Na^{+}-Ca^{2+} exchanger, mCU: mitochondrial Ca^{2+} uniporter.

Mitochondria are the primary energy producers of the cell, that they combine oxygen with glucose to form adenosine triphosphate (ATP), a process known as oxidative phosphorylation. Additionally, mitochondria are also important store of intracellular Ca^{2+} in endothelial cells, accounting for ~25% of the total intracellular Ca^{2+} reserve (Wood and Gillespie, 1998). Mitochondria Ca^{2+} uptake becomes apparent when the $[Ca^{2+}]_i$ is over 1 μM and the primary driving force for Ca^{2+} entry into the mitochondria is the negative charged inner mitochondria membrane. Mitochondria express a Ca^{2+} uniporter that is responsible for Ca^{2+} uptake. Ca^{2+} release occurs via the Na^{+}-Ca^{2+} exchanger. There is evidence that a mitochondria-located ryanodine receptor may also exist in cardiomyocytes and neurons (Beutner *et al.*, 2001; Beutner *et al.*, 2005) (Figure 1.8).

The dynamic role of mitochondria in physiological Ca^{2+} signalling is reflected by their close proximity to the ER $InsP_3$ receptors and the plasma membrane, a spatial relationship that allows them to function in concert with the ER to sequester/release

cytosolic Ca^{2+} and supply the immediate ATP requirement for the removal of Ca^{2+} from the cytosol by the SERCA pump and PMCA (Malli *et al.*, 2003; Camello-Almaraz *et al.*, 2006; Zhang and Gutterman, 2007). It has been shown that $InsP_3$-mediated Ca^{2+} release is very efficient at elevating mitochondria Ca^{2+} concentration ($[Ca^{2+}]_m$) (Rizzuto *et al.*, 1993a; Rizzuto *et al.*, 1998). Each mitochondrial Ca^{2+} uptake site faces multiple $InsP_3$ receptors, activation of these receptors by $InsP_3$ and the subsequent release of Ca^{2+} appear to be required for optimal activation of mitochondrial Ca^{2+} uptake (Csordas *et al.*, 1999). In addition, cross-talk between the ER and mitochondria is found to be important in ER Ca^{2+} refilling, which is depended on the presence of extracellular Ca^{2+} as the source and SERCA pump activity. In the presence of an $InsP_3$-generating agonist, ER Ca^{2+} refilling was prevented by the inhibition of trans-mitochondrial Ca^{2+} flux, either through a mNCE blocker CGP 37157, or by mitochondrial depolarization using a mixture of oligomycin and antimycin A (Malli *et al.*, 2005).

1.4.1.3 Golgi store

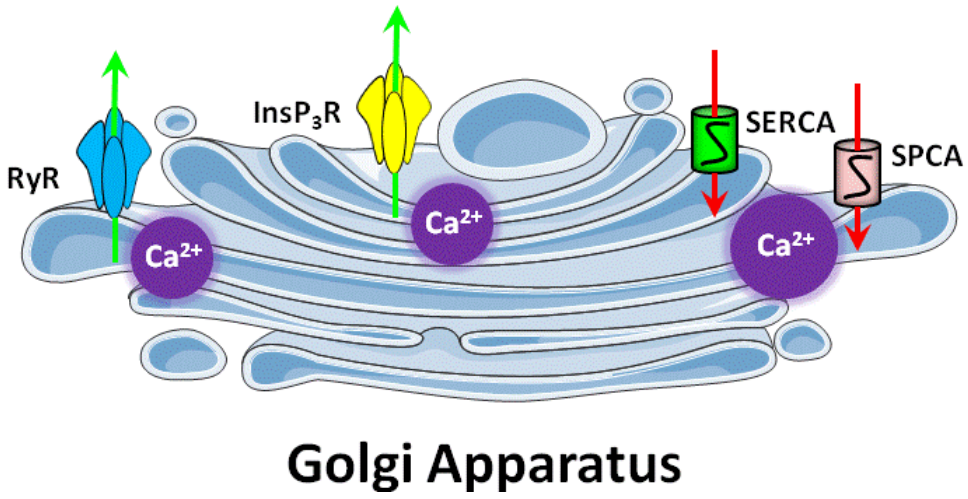

Figure 1.9 Schematic representations showing the Ca^{2+} channels on the surface of the Golgi apparatus. RyR: ryanodine receptors, $InsP_3R$: $InsP_3$ receptors.

The golgi apparatus is known to be important in intracellular sorting, trafficking and targeting of proteins, in the last two decades, more reports suggest that it also

represents an important intracellular Ca^{2+} store, which can store up to ~5% of the total intracellular Ca^{2+} reserve ($[Ca^{2+}]_{Golgi}$ ~300 μM) and more resistance to Ca^{2+} depletion than other organelles (Chandra *et al.*, 1991; Pinton *et al.*, 1998). Golgi apparatus has been shown to express a number of receptors, including $InsP_3$ receptors (Yoshimoto *et al.*, 1990; Gerasimenko *et al.*, 1996; Petersen, 1996; Pinton *et al.*, 1998; Surroca and Wolff, 2000) and ryanodine receptors (Cifuentes *et al.*, 2001), through which it releases the Ca^{2+} into the cytosol. Uptake of Ca^{2+} in the golgi apparatus is dependent on the activity of SERCA pumps and the secretory pathway Ca^{2+}-ATPases (SPCAs) (Figure 1.9). Furthermore, golgi apparatus has been shown to act in concert with the ER to elevate cytosolic Ca^{2+} in response to agonist stimulation though different kinetics (Missiaen *et al.*, 2004). In freshly isolated live pancreatic acinar cells, the golgi apparatus and mitochondria structures form very close and stable contacts and their co-localization help to support a Ca^{2+} gradients across the golgi apparatus (Dolman *et al.*, 2005).

1.4.2 Intracellular Ca^{2+} homeostasis in endothelial cells

1.4.2.1 $InsP_3$ receptor

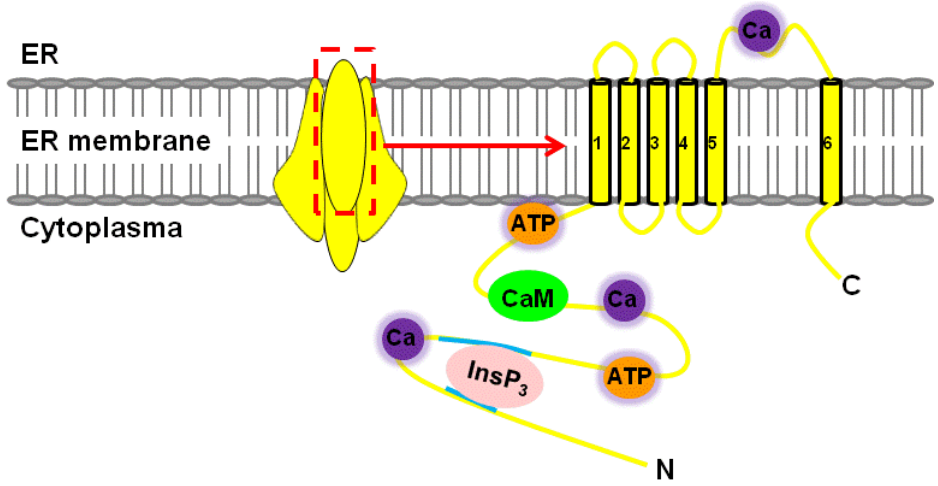

Figure 1.10 Schematic representations showing the structure of subunits that forming the tetrameric $InsP_3$ channels. $InsP_3$ binding site are illustrated as blue lines. Ca^{2+} binding sites are depicted as purple circles, ATP-binding sites are shown as orange circles, and phosphorylation sites are shown as green circles. Calmodulin (CaM) binds close to one of the phosphorylation sites. N: N-terminal, C: C-terminal.

Three types of $InsP_3$ receptors isoforms (types 1, 2 and 3) are known to exist in human and other animal cells (Yamada *et al.*, 1994; Yamamoto-Hino *et al.*, 1994). They are 60-80% homologous in amino acid sequences (Foskett *et al.*, 2007). In mammals, at least one isoform of the $InsP_3$ receptors is expressed in each type of cells, and many cells express all three isoforms (Furuichi *et al.*, 1993; De Smedt *et al.*, 1994; Fujino *et al.*, 1995). $InsP_3$ receptor channels are tetramers comprised of four subunits, each containing 2,700 residues with a molecule mass of ~310 kDa (Foskett *et al.*, 2007). The structure of $InsP_3$ receptors is divided into three functional domains: the N-terminal ligand-binding domain which comprises ~85% of the protein mass, the modulatory/coupling domain, and the C-terminal transmembrane/channel-forming domain (Furuichi *et al.*, 1989; Furuichi *et al.*, 1994) (Figure 1.10).

The $InsP_3$ receptors allow the release of Ca^{2+} ions into the cytoplasm in response to $InsP_3$ produced by diverse stimuli. For example, binding of ACh to its receptor on the endothelial cell surface leads to the activation of phospholipase C (PLC), which hydrolysis the phosphatidylinositol 4,5-bisphosphate (PIP_2), a phospholipid that is located in the plasma membrane, to $InsP_3$ (Streb *et al.*, 1983). $InsP_3$ binds to the $InsP_3$ receptor on the surface of the ER, opens the $InsP_3$ receptors and Ca^{2+} ions are released into the cytoplasm from the ER. The $InsP_3$ receptor is also modulated by $[Ca^{2+}]_i$, high $[Ca^{2+}]_i$ is inhibitory to $InsP_3$ receptors activity (Foskett *et al.*, 2007). It should be noted that, the expression of $InsP_3$ receptors is not restricted to the ER, other organelles such as the Golgi apparatus and secretory vesicles may also function as $InsP_3$-sensitive Ca^{2+} stores (Vermassen *et al.*, 2004).

1.4.2.2 Ryanodine receptor

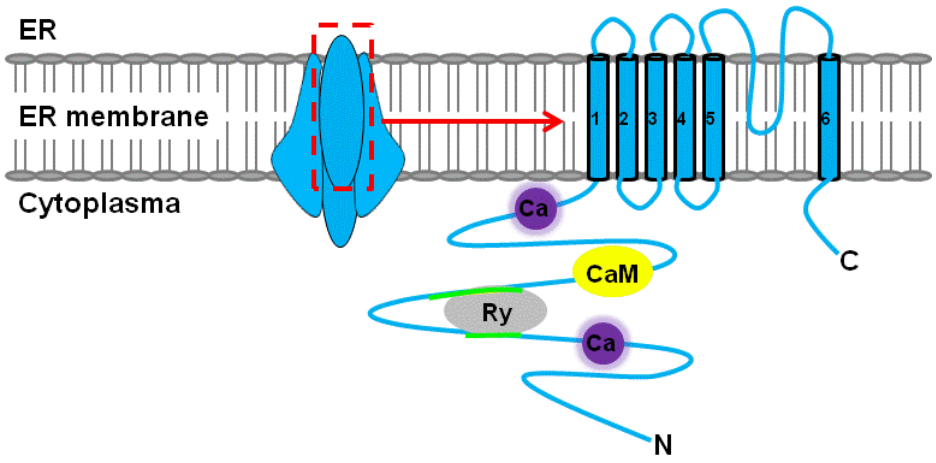

Figure 1.11 Schematic representations showing the structure of subunits that forming the tetrameric ryanodine channels. Ryanodine binding site are illustrated as green lines. Ca^{2+} binding sites are depicted as purple circles. Phosphorylation sites are shown as yellow circles. Calmodulin (CaM) binds close to one of the phosphorylation sites. N: N-terminal, C: C-terminal.

RyRs are a family of Ca^{2+} releasing channels, that are the largest ion channels currently known and form a homotetrameric assemblies measuring approximately 2.3 MDa (565 kD/subunit) (Kimlicka and Van Petegem, 2011) (Figure 1.11). RyRs share a significant sequence homology with the $InsP_3$ receptors, with highest homology occurring at the sequence forming the channel's pore (Mignery *et al.*, 1989; Zhao *et al.*, 1999). In mammals, three isoforms (RyR1, RyR2 and RyR3) have been identified and they exhibit subtype-specific expression patterns in tissues. The RyR1 isoform is primarily expressed in skeletal muscles (Takeshima *et al.*, 1989; Zorzato *et al.*, 1990), but also expressed at low levels in cardiac muscle, smooth muscle (Neylon *et al.*, 1995), stomach, kidney and many other tissues (Lanner *et al.*, 2010). The RyR2 isoform is the predominant form of RyR in cardiac muscle (Nakai *et al.*, 1990; Otsu *et al.*, 1990), but also expressed at high low levels in cerebellum and cerebral cortex (Lai *et al.*, 1992; Nakanishi *et al.*, 1992), and low levels in stomach, kidney and many other tissues (Lanner *et al.*, 2010). The RyR3 isoform is mainly expressed in brain (Hakamata *et al.*, 1992; Lai *et al.*, 1992).

The expression of RyRs has been found in porcine endocardium and thoracic aorta endothelial cells (Lesh *et al.*, 1993), and these RyRs exhibit a high homology with the cardiac isoform RyR2. The functional role of RyRs in endothelial cells was evident in cultured endothelial cells from rat aorta (RAECs), human aorta (HAECs), human umbilical vein (HUVECs) and bovine pulmonary artery (BPAECs), because ryanodine significantly reduced bradykinin-induced Ca^{2+} release (Ziegelstein *et al.*, 1994). In freshly isolated endothelial cell from rabbit aorta, ryanodine was able to slowly deplete the ACh-sensitive store, thus indicating the presence of functional ryanodine receptors in these native endothelial cells (Wang *et al.*, 1995). In addition, a number of co-factors such as Ca^{2+}, magnesium (Mg^{2+}) and ATP are important small molecule regulators of RyRs (Fill and Copello, 2002; Liang *et al.*, 2004). Mg^{2+} and ATP modulate RyRs in the cytoplasm, whereas Ca^{2+} regulates RyRs both in the cytoplasm and in the lumen of SR/ER (Lanner *et al.*, 2010). Ca^{2+} has direct effects on RyRs and also regulates RyRs via calmodulin, which calmodulin also regulates the RyRs by direct binding (Lanner *et al.*, 2010).

1.4.2.3 SERCA pump

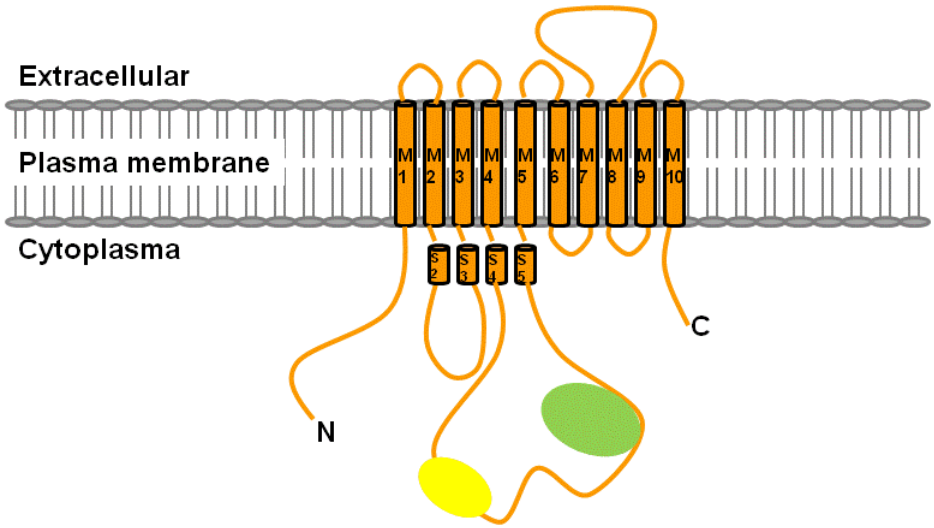

Figure 1.12 Schematic representations showing the structure of SERCA pump. Phosphorylation sites are shown as yellow circles. Nucleotide binding domain is shown as green circles. N: N-terminal, C: C-terminal.

SERCA is an ATP-dependent Ca^{2+} pump located in the ER/SR membrane that is responsible for the sequestration of cytosolic Ca^{2+}. It is a single polypeptide with a molecular mass of 110 kDa (Periasamy and Kalyanasundaram, 2007). The bulk of the protein consists of a cytoplasmic globular headpiece structure (S2-S5) and 10 membrane-spanning segments (M1–M10). The large globular cytoplasmic part is composed of three domains: (i) the β-strand domain, between M2 and M3; (ii) the phosphorylation domain, attached to M4 at one end and to the nucleotide binding domain at the other and (iii) the nucleotide binding domain runs into a hinge domain that is attached to M5 (Figure 1.12). In vertebrates, there are three distinct genes encoding SERCA (SERCA1, 2 and 3), producing more than 10 isoforms (Periasamy and Kalyanasundaram, 2007). The SERCA1 encoding SERCA1a and SERCA1b are expressed in fast-twitch skeletal muscle (Brandl *et al.*, 1986; Brandl *et al.*, 1987). The SERCA2 is also alternatively spliced to encode SERCA2a and SERCA2b. SERCA2a is expressed predominately in cardiac and slow-twitch skeletal muscle (MacLennan *et al.*, 1985; Zarain-Herzberg *et al.*, 1990), while SERCA2b is expressed in all tissues at low levels including smooth muscle (Gunteski-Hamblin *et al.*, 1988; Lytton and MacLennan, 1988; de la Bastie *et al.*, 1990). The SERCA3 is known to encode for six isoforms in human (Periasamy and Kalyanasundaram, 2007) and its isoforms are expressed mainly in non-muscle tissues (Burk *et al.*, 1989; Wuytack *et al.*, 1994).

Endothelial cells express two isoforms of SERCA (SERCA2b and SERCA3), and they are found to be co-expressed (Anger *et al.*, 1993). The SERCA2b isoform is known to be the predominate isoform that responsible for sequestration of cytosolic Ca^{2+}, however, SERCA3 deficient mice have impaired ACh-induced endothelium-dependent relaxation and intracellular Ca^{2+} signalling (Liu *et al.*, 1997), suggesting that SERCA3 also plays a critical role in regulating endothelial cell Ca^{2+} signalling. It should be noted that depletion of the ER Ca^{2+} stores by inhibiting the SERCA pump with compounds such as CPA is not associated with increases in $InsP_3$ production, this therefore

provides an alternative approach to investigate intracellular Ca^{2+} signalling in contrast to receptor-dependent stimulation (Tran and Watanabe, 2006).

1.4.2.4 PMCA pump

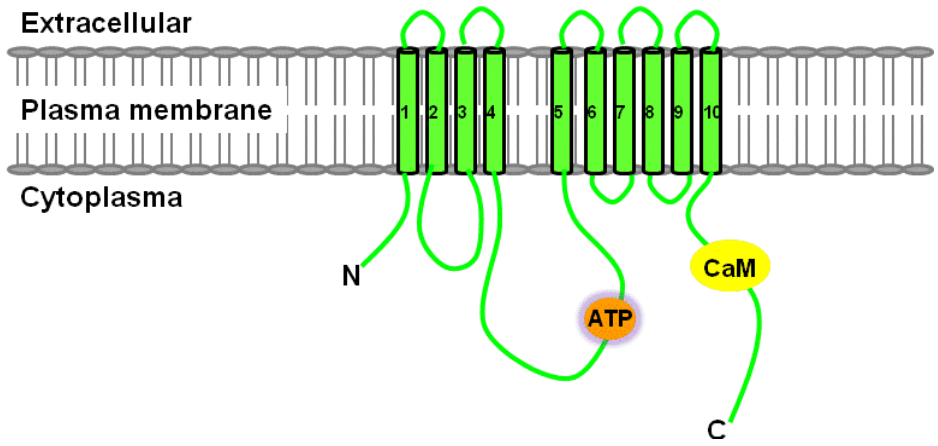

Figure 1.13 Schematic representations showing the structure of the PMCA. ATP-binding sites are shown as orange circles. Phosphorylation sites are shown as yellow circles. Calmodulin (CaM) binds close to one of the phosphorylation sites. N: N-terminal, C: C-terminal.

PMCAs are ATP-consuming calmodulin-dependent pumps that eject Ca^{2+} into the extracellular space against a concentration gradient (Carafoli *et al.*, 1990). There are four isoforms of PMCA (PMCA1-4, 134 kD) that have been described in humans, they share a similar structure consisted of 10 transmembrane domains and four intracellular regions: (i) the N-terminal region of low sequence similarity between isoforms; (ii) a loop between transmembrane domains 2 and 3 that forms the channel's Ca^{2+} pore; (iii) a large loop between transmembrane domains 4 and 5 that forms the ATP-binding site and (iv) the C-terminal region that contains the calmodulin binding domain (Cartwright *et al.*, 2011) (Figure 1.13). Calmodulin is an essential regulator of PMCAs activity, binding of it leads to an inhibitory effect on the pump (Falchetto *et al.*, 1992). PMCA1 and PMCA4 are widely expressed in most cell types (Stauffer *et al.*, 1993; Stauffer *et al.*, 1995), while PMCA2 is predominantly expressed in brain (Stahl *et al.*, 1992), mammary glands (Reinhardt *et al.*, 2000) and inner ear cilia (Ficarella *et al.*, 2007), and

PMCA3 is expressed in brain (Greeb and Shull, 1989; Brown *et al.*, 1996), skeletal muscle (Greeb and Shull, 1989; Stauffer *et al.*, 1993) and pancreatic islet cells (Kamagate *et al.*, 2000). Endothelial cells have been found to express the PMCA1 isoform (Szewczyk *et al.*, 2007; Szewczyk *et al.*, 2010). Genetic overexpression of PMCA1a in rat aortic endothelial cells is associated with altered expression of other Ca^{2+} regulating components, such that expression and activity of the SERCA pump and $InsP_3$ were both down-regulated, and the rate of $InsP_3$-mediated Ca^{2+} release in permeable cells was decreased without affecting the affinity of the channel for $InsP_3$ (Liu *et al.*, 1996). Inhibition of PMCA1 with the selective inhibitor caloxin 1b3 increased cytosolic Ca^{2+} concentration in endothelial cells (Szewczyk *et al.*, 2010). Oxidant regulation of PMCA has been shown in pancreatic acinar cells, as high concentrations of H_2O_2 (0.1-1 mM) have been shown to inactivate the PMCA (Bruce and Elliott, 2007).

1.4.3 Ca^{2+} entry into endothelial cells

1.4.3.1 Voltage-dependent Ca^{2+} channels

Endothelial expression of both L-type and T-type voltage-dependent Ca^{2+} channels has been described in bovine endothelial cell (Bossu *et al.*, 1989; Bossu *et al.*, 1992a; Bossu *et al.*, 1992b; Vinet and Vargas, 1999). However, due to the non-excitable nature of the endothelial cells, these voltage-dependent channels are considered to be not functional important (Himmel *et al.*, 1993). Indeed, inhibition of these channels with blockers such as diltiazem and verapamil did not affect agonist-induced Ca^{2+} entry in freshly isolated endothelial cells (Luckhoff and Busse, 1990; Yamamoto *et al.*, 1995).

1.4.3.2 Store operated calcium entry (SOCE)

The rise in $[Ca^{2+}]_i$ brought about by agonist stimulation (ACh) or store depletion (CPA) is achieved in two stages: (i) a small and transient rise reflecting the release of Ca^{2+} from intracellular ER stores and (ii) a large and sustained Ca^{2+} increase that requires Ca^{2+} entry from extracellular space. In endothelial cells, it has been suggested that this

sustained Ca^{2+} entry is most commonly mediated by capacitative Ca^{2+} entry (CCE), or SOCE (Tran and Watanabe, 2006), a model first proposed by Putney (Putney, 1986, 1990), explaining the mechanism for intracellular Ca^{2+} store refilling, a phenomenon observed earlier (Brading and Sneddon, 1980; Casteels and Droogmans, 1981). SOC channels (SOCC) are Ca^{2+}-permeable channels in the plasma membrane that open following depletion of intracellular ER Ca^{2+} stores, the best characterized SOCC is the so-called Ca^{2+} release activated Ca^{2+} channel (CRAC) (Hoth and Penner, 1992), which is highly selective to Ca^{2+}. The CRAC current (I_{CRAC}) has been described in endothelial cells (Fasolato and Nilius, 1998; Fierro *et al.*, 2000).

The SOCE pathway requires two components: the Ca^{2+} sensor protein named stromal interacting molecule (STIM) (Liou *et al.*, 2005; Roos *et al.*, 2005) and the Ca^{2+} channel protein Orai (Prakriya *et al.*, 2006; Yeromin *et al.*, 2006). Orai has been found to be the pore forming subunit of I_{CRAC} (Prakriya *et al.*, 2006). There is evidence that various endothelial cells from different vascular bed express vascular specific STIM1 and Orai1 protein isoforms and display SOCE and I_{CRAC} (Abdullaev *et al.*, 2008). The STIM1 proteins are localized throughout the membrane of the ER with the N-terminal region containing the calcium-binding motif inside the ER, while the cytosolic C-terminal region contains the amino acid sequence involved in the protein–protein interaction and activation of Orai1 (Hewavitharana *et al.*, 2007; Penna *et al.*, 2008). Store depletion causes the Ca^{2+} sensor STIM1 on the ER membrane to oligomerize and translocate to regions of the ER situated close to the plasma membrane. Orai1 channels on the plasma membrane also move to the same region and are activated by STIM1 oligomers through direct interaction of C-terminal region of STIM1 to the C- and N-terminal region of Orai1 (DeHaven *et al.*, 2007; Hewavitharana *et al.*, 2007; Penna *et al.*, 2008).

1.4.3.3 Non-selective cation channels

Non-selective cation channels (NSCCs) are widely expressed in endothelial cells, they are voltage-independent, poorly discriminating between cations and permeable to both monovalent and divalent cations. NSCCs are a heterogeneous family of channels that include transient receptor potential cation (TRPC) channels, calcium activated non-selective channels, hyperpolarization activated cation currents, acid-sensitive cationic channels (ASIC) and many more. NSCCs have been shown to activate in a number of ways: (i) binding of an agonist to its receptor, such as thrombin, bradykinin (Colden-Stanfield *et al.*, 1990), serotonin (Brauneis *et al.*, 1992), histamine (Groschner *et al.*, 1994), ATP (Popp and Gogelein, 1992) and endothelin-1. Using TRPC channels as an example, after binding of an agonist to its G_q-protein coupled receptor, the activation of PLC leads to the formation of $InsP_3$ and diacylglycerol (DAG), DAG activates TRPC channels resulting in receptor-operated Ca^{2+} entry (Dietrich *et al.*, 2010); (ii) depletion of intracellular Ca^{2+} stores by direct inhibition of SERCA pumps (by CPA or thapsigargin) as well as $InsP_3$ applied intracellularly (Gericke *et al.*, 1993; Zhang *et al.*, 1994). It has been reported that in a patch-clamp study, CPA concentration-dependently activates a NSCC in human umbilical vein endothelial cells, possibly through its action on Ca^{2+} stores depletion and the subsequent stimulation on Ca^{2+} influx (Zhang *et al.*, 1994), and (iii) by shear stress. Although the mechanisms by which shear stress elevates $[Ca^{2+}]_i$ in endothelial cells are still unclear, it has been reported that in human pulmonary artery endothelial cells (HPAEC), shear stress can induce activation of purinoceptors P2X4 through endogenously released ATP and this channel may be responsible for the shear stress-dependent Ca^{2+} influx (Yamamoto *et al.*, 2000; Yamamoto and Ando, 2004).

1.4.3.4 Non-capacitative calcium entry (NCCE)

In addition to CCE, an alternative non-store-operated or non-capacitative Ca^{2+} entry (NCCE) mode also exists in events such as Ca^{2+} oscillations and agonist-activated Ca^{2+}

entry (Shuttleworth, 1996; Shuttleworth and Thompson, 1996; Mathias *et al.*, 1997; Zhu *et al.*, 1998). The evidence that AA is responsible for this NCCE is given by the facts that (i) low concentrations of exogenous AA (3-8 μM) induces Ca^{2+} entry without any detectable depletion of intracellular Ca^{2+} stores; (ii) agonist stimulation leads to the production and release of AA that is independent of $InsP_3$; (iii) pharmacological inhibition of agonist-induced generation of AA attenuates NCCE without effect on CCE and (iv) the specific action of AA on Ca^{2+} entry is unaffected by inhibition of the enzymes responsible for the metabolism of AA (Shuttleworth, 1996; Shuttleworth and Thompson, 1998). An AA-regulated Ca^{2+} entry current (I_{ARC}) has been observed in many cell types including endothelial cells (Mottola *et al.*, 2005; Leung *et al.*, 2006). The reciprocal regulation of CCE and NCCE was demonstrated by the findings that at low agonist concentrations, NCCE was the main Ca^{2+} entry mechanism, whereas at high agonist concentrations, CCE attenuated NCCE (Shuttleworth *et al.*, 2004). Furthermore, in A7r5 vascular smooth muscle cells, AA formed in response to agonist vasopressin stimulates eNOS and NO produced by eNOS have been shown to mediate this reciprocal regulation between CCE and NCCE. In detail, NO directly stimulates Ca^{2+} entry through NCCE and, via protein kinase G, it inhibits CCE (Moneer *et al.*, 2003).

1.5 GENERAL AIMS OF THESIS

The aim of this thesis is to provide a clearer understanding of the mechanisms underlying how H_2O_2 contributes to the EDH phenomenon and the role that H_2O_2 plays in the regulation of endothelial Ca^{2+} homeostasis. This idea is based on evidence that in an artery where the EDH phenomenon is gap junction-dependent (i) H_2O_2 potentiates relaxation and endothelial Ca^{2+} mobilization, rather than acts as a freely diffusible EDHF, and (ii) that potentiation is inhibited by inhibitors of mitochondrial H_2O_2 production. Clarification of the pathways involved, and their modulation by NO, will therefore provide major new insights into the role of direct intercellular vascular

signalling in disease states characterized by increased oxidative stress. Given the complex effects of H_2O_2 on endothelial Ca^{2+} homeostasis, it is difficult to predict dominant interactions at this stage, so that the intention is to focus on key pathways, such as the possible central positive feedback loop linking H_2O_2, the $InsP_3R$, the SERCA and $[Ca^{2+}]_i$.

Four types of preparations will be used in this study, in which the rabbit iliac artery has both EDHF and NO-mediated responses, whereas aorta dominantly expresses NO-mediated response, thus provides possible comparison between the two mechanisms. For the ease of selective Ca^{2+}-sensitive dye loading, rabbit aortic valve leaflets were used in this study. In addition to the practicality of studying the intact endothelium, studying Ca^{2+} signaling in this preparation is likely to be relevant to physiology and clinical medicine for a number of reasons: (i) valves are exposed to intermittent turbulent blood flow that can provoke platelet adhesion and lesion formation; (ii) valvular endothelium is easily damaged during catheterization and is a frequent target for streptococcal infections and (iii) endothelium-derived relaxing factor secretion exerts a protective effect that is regulated by fluctuations in endothelial Ca^{2+} concentration (Li and van Breemen, 1996). Human endothelial cellline EA.hy926 was also chosen in this study for comparison between intact/cultured and rabbit/human endothelial cells.

Chapter 2

Materials and Methods

This chapter details the materials and methods used for all experimental work described in this thesis. Subsequent chapters will provide a brief outline of the methods used together with any specific details of the protocols.

2.1 ANIMALS

Male New Zealand White (NZW) rabbits (2-2.5 kg) were used in the studies described in this thesis. Rabbits were maintained under conventional animal housing conditions following a 12 hour light-dark cycle and at an ambient room temperature of 16-20 °C and humidity of 55%±10%. Animals received food and drinking water *ad libitum*. The welfare of the animals was carried out by experienced technicians.

2.1.1 Isolated Tissues

2.1.1.1 The aorta

As shown in Figure 2.1, the descending aorta, the largest artery in the body, is divided into thoracic and abdominal regions. The thoracic aorta lies between the aortic arch and the diaphragm. The abdominal aorta passes through the diaphragm, crossing it via the aortic hiatus and ends with its division into left and right common iliac arteries. For the experiments described in this thesis, the rabbit descending aorta was dissected between the aortic arch and the diaphragm. The isolated thoracic aorta was approximately 40 mm in length and 5 mm in diameter.

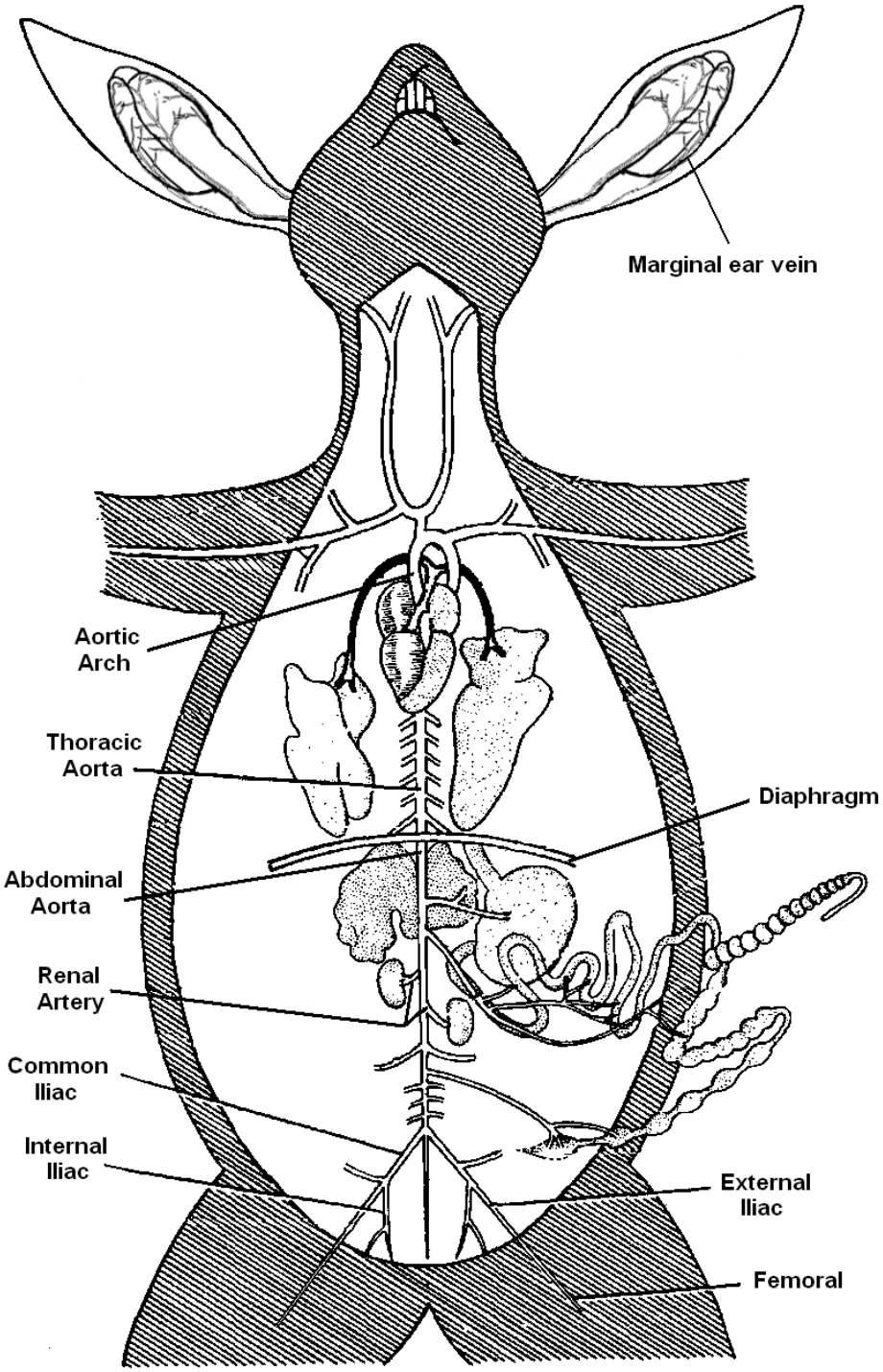

Figure 2.1 Arterial system of the rabbit (ventral view). The heart of the rabbit provides a double circuit. The right atrium and ventricle constitute the pulmonary heart, which transport the circulated blood to the lungs for oxygenation. The left halves form the systemic heart, where the oxygenated blood is pumped by the left ventricle to be circulated to all parts of the body.

Picture adapted from http://www.tutornext.com/arterial-system-rabbit/8962

2.1.1.2 The external iliac arteries

As shown in Figure 2.1, the left and right common iliac arteries further divide into an external and internal iliac artery. The internal iliac artery descends into the pelvic cavity whereas the external iliac artery continues beneath the inguinal ligament and becomes the femoral artery in the leg. In the rabbits used for the experiments described in this thesis, the diameter of the external iliac artery was approximately 1 mm, and the length was approximately 30 mm.

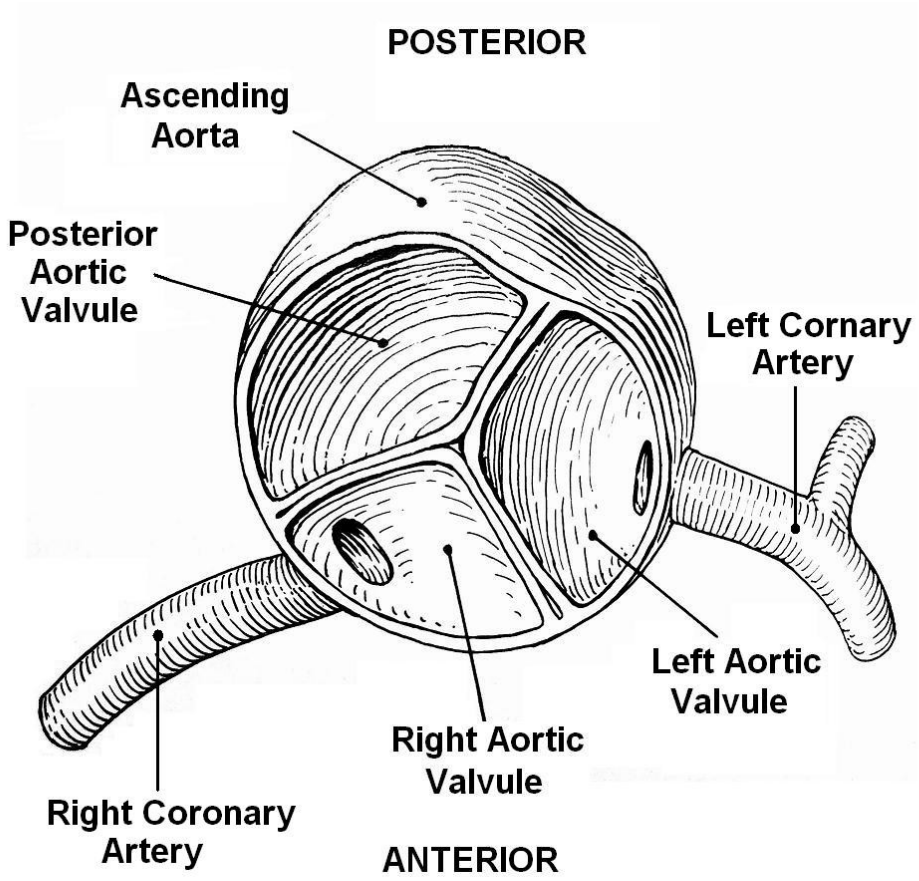

Figure 2.2 The rabbit aortic valve. Similar to humans, the rabbit aortic valve is tricuspid (it has three valve leaflets). It opens during the ventricular systole as the pressure in the left ventricle rises above the pressure in the aorta, therefore allowing blood to flow from the left ventricle into the aorta. Conversely, when the ventricular systole ends, the rapidly drop in pressure in the left ventricle forces the aortic valve to close.

Picture adapted from (Hall-Craggs and Abeloff, 1995)

2.1.1.3 The aortic valve

The aortic valve is situated at the opening between the left ventricle of the heart and the aorta. It has three leaflets attached by its convex margin to the artery wall as shown in Figure 2.2. Only the free-floating part of the leaflet was dissected out for imaging studies. Aortic valve leaflets have been shown to be composed primarily of endothelial lining cells on a matrix of collagen and elastic fibres (Cooper *et al.*, 1966). Studies with canine cardiac valves have revealed that there is a continuous basal release of vasodilatory prostanoids and endothelium-derived relaxing factor from the valvular endothelium, which can be further stimulated with ACh and SOD, and inhibited by indomethacin and haemoglobin (Ku *et al.*, 1990).

2.1.2 Rabbit tissue dissection

Male New Zealand White (NZW) rabbits were killed with sodium pentobarbitone (Euthatal, 150 mg/kg; i.v.) injected to the marginal ear vein (Figure 2.1) and inspected for nervous reflexes (corneal reflex of the eye and withdrawal reflex of the toes) according to University guidelines that observe strict compliance to UK Home Office regulations and the Guide for the Care and Use of Laboratory Animals issued by the US National Institutes of Health (NIH Publication No. 85-23, revised 1996).

The aorta, the iliac arteries and surrounding tissue, and the heart containing the valves were carefully dissected and placed in ice cold Holman's buffer of the following composition: NaCl (120 mM), KCl (5 mM), NaH_2PO_4 (1.3 mM), $NaHCO_3$ (25 mM), Glucose (11 mM), Sucrose (10 mM), $CaCl_2$ (2.5 mM), pH 7.4. The buffer was prepared in deionised water (dH_2O) on the day of experiments and was kept at room temperature gassed with 95% O_2 and 5% CO_2. All chemicals used for the buffer were obtained from Fisher Scientific, UK.

2.2 MECHANICAL STUDIES IN RABBIT TISSUE

The rabbit iliac arteries and the aorta were carefully dissected free of adipose and connective tissue in oxygenated Holman's buffer at room temperature. The arteries were cut into rings of 2-3 mm wide and where required, denuded of their endothelium by gentle abrasion with a wooden stick. Rings were then mounted on a myograph.

Figure 2.3 Myograph units. The myograph model 610M consists of 4 individual units, made of aluminium. The 10ml stainless steel chamber is located in the centre of each unit. There are two paired tissue supports pins in the middle of each chamber. Gassing pipes are on the side of each unit. Heating control and calibration procedures are in the myograph interface.

Picture and information taken from http://www.dmt.dk

2.2.1 Myograph

In-vitro mechanical studies of rabbit iliac (~1 mm in diameter) and aorta ring preparations (~5mm in diameter) were performed using a 4-channel multi myograph unit (model 610M) from Danish Myo Technology, Aarhus, Denmark (DMT) (Figure 2.3). This multi myograph is based on the small artery isometric wire myograph introduced in 1976 by Professor M. J. Mulvany and Professor W. Halpern (Mulvany and Halpern, 1976). A pair of supports pins was positioned in each chamber, one pin was attached to the force transducer and the other one was attached to a micropositioner. Each chamber can hold a maximum volume of 10 ml of solution and has heating control and individual gas inflow.

2.2.1.1 Calibrating the myograph

The force calibration kit was used for calibrating the force transducer. It consists of a 2 g weight, bridge and T-balance. The myograph was turned on and heated up to 37 °C for 20 mins with 8 ml of deionised water in each chamber. The bridge/T-balance was placed on myograph as illustrated in Figure 2.4. The tip of T-balance was placed as close as possible to the pin on the transducer side of the myograph, without touching it. In the calibration menu on the Myo-Interface, the force transducer 1 was selected first and when the relative force reading in the display was stable, the 2 g weight was carefully placed on the pan. This 2 g weight pushed the tip of the T-balance against the mounted support pin, and the force produced this way was transferred through the force transducer to the myograph. This process aimed to mimic the stretch created by the contraction of a mounted ring preparation. When the relative force reading was stable, the calibration was selected to finish and an output around 9.81 mN should be seen on the display. The same steps were repeated for force transducers 2, 3 and 4. The calibration procedure was performed on a weekly basis to ensure the accuracy of the recording.

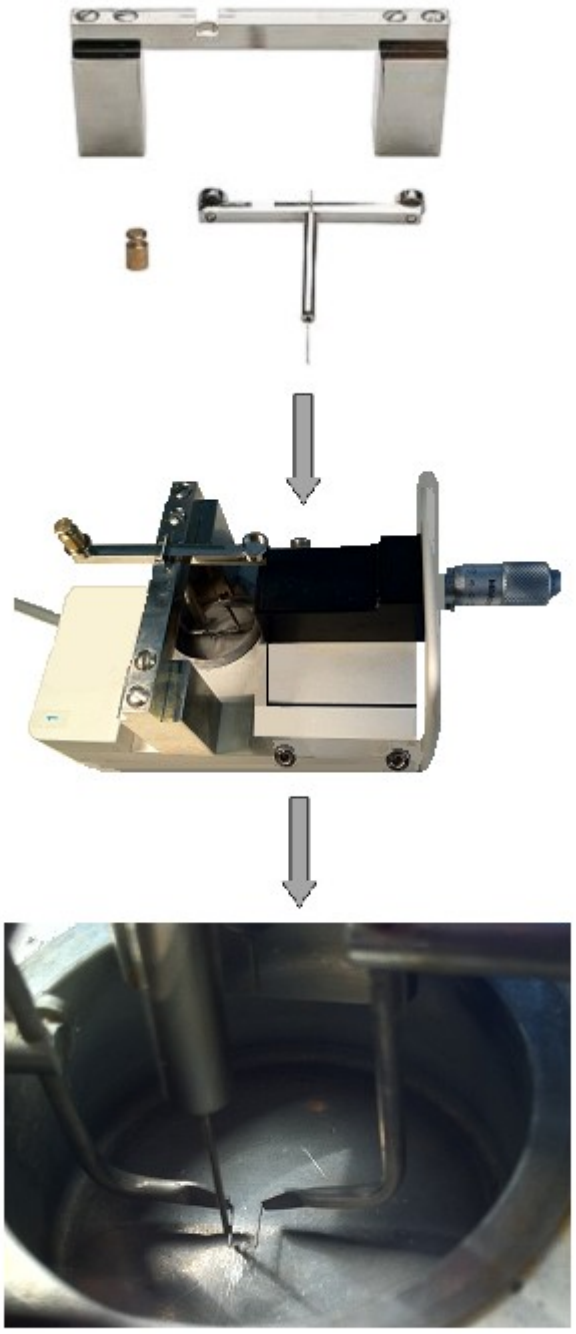

Figure 2.4 Myograph calibration units. The force calibration kit consists of a bridge, a T-balance and a 2 g weight. Bridge is designed to sit on top of the chamber. It has a groove that will fit the T-balance. The 2g weight goes in the pan that located on each side of the T-balance.

Picture and information taken from http://www.dmt.dk

2.2.1.2 Maintenance and cleaning

The chambers and surrounding surface of the myograph unit were cleaned with 0.8M hydrochloride acid (HCl) and then washed thoroughly with deionised water before and after each experiment to remove residual chemicals and calcium deposits.

2.2.2 Experimental procedures

Iliac artery or aortic rings were mounted in a myograph containing 8ml oxygenated (95% O_2, 5% CO_2) Holman's buffer at 37˚C, and repeatedly adjusted to maintain a resting tension of 2 mN (optimal resting tension for this tissue, Prof. TM Griffith personal communication) during a 1h equilibration period. Some preparations were incubated with N^{ω}-nitro-L-arginine methyl ester (L-NAME, 300 μM) and/or 1-(4-Chlorobenzoyl)-5-methoxy-2-methyl-3-indoleacetic acid (indomethacin, 10 μM) for 30 min as indicated (see below). These concentrations of the blockers were previously shown to give complete inhibition on rabbit artery in this laboratory [Prof. TM Griffith personal communication (Taylor *et al.*, 1998)]. Vessel rings were subsequently pre-incubated for further 30 minutes with the drugs of interest when required. In all experiments tone was induced by phenylephrine (PE) at 1 μM, this concentration was previously shown to give sub-maximum constriction in rabbit artery in this laboratory [Prof. TM Griffith personal communication (Taylor *et al.*, 1998)]. To obtain the cumulative concentration-response curves, the response to a given concentration of the drug was allowed to reach a plateau before addition of the next concentration. A brief description of the drugs and concentrations employed for the mechanical experiment is described below. More detailed information will be described in subsequent chapters.

- ***First pre-incubation for 30 minutes:***
    - **L-NAME** (Sigma, UK): L-NAME is an analogue of L-arginine and is commonly used as a potent competitive inhibitor of nitric oxide synthases type 1, type 2, and type 3 (NOS_1/nNOS, NOS_2/iNOS, and

NOS_3/eNOS) (Furfine *et al.*, 1997). Stock solutions of 100 mM were freshly made in Holman's buffer on the day of the experiment and were kept on ice at all times. Final bath concentration of 300 μM was used in all experiments.

- **Indomethacin** (Sigma, UK): Indomethacin is a non-selective competitive inhibitor of cyclooxygenase isoenzymes COX-1 and COX-2. It works by blocking the arachidonate binding sites. COX-1 and COX-2 catalyze the conversion of arachidonic acid to prostaglandin. 10 mM stock solutions were freshly prepared in absolute ethanol and were kept at room temperature. Further dilutions were made in Holman's buffer to give a final bath concentration of 10 μM.

➢ *Second incubation for 30 minutes:*

- **Hydrogen Peroxide (H_2O_2)** (Sigma, UK): H_2O_2 is the simplest peroxide that is naturally produced in organisms as a by-product of oxidative metabolism. It is a potent oxidizing agent and is considered as one of the reactive oxygen species. Stock concentration of 100 mM was freshly made in Holman's buffer and was kept on ice at all times. 30 or 100 μM final bath concentrations were used in experiments.

- **Thimerosal** (Sigma, UK): Thimerosal is an organic mercury sulfhydryl compound. It exhibits a strong thiol oxidant effect and is known to sensitize the $InsP_3$ receptors. Stock solutions of thimerosal were freshly prepared in dH_2O to a concentration of 10 mM and were kept on ice at all times. The final bath concentration used in experiments was 1 or 10 μM.

- **Sodium (meta) arsenite (arsenite)** (Sigma, UK): Sodium arsenite ($NaAsO_2$) is a sodium salt of inorganic compound arsenous acid

(H_3AsO). 100 mM stock arsenite were made freshly in dH_2O and were kept on ice. In the experiments described in this thesis, 100 µM final bath concentrations were applied.

- ***Pre-contraction***
  - **PE** (Sigma, UK): PE is a selective α-adrenergic receptor agonist. Stock solutions of concentration 1 mM were freshly made in Holman's buffer and were kept at room temperature. Final bath concentration of 1 µM was used in the studies described in this thesis.

- ***Cumulative concentration-response curves***
  - **CPA** (Ascent, UK): CPA is a specific inhibitor of SERCA pump. Stock solutions of CPA were prepared in dimethylsulfoxide (DMSO) at a concentration of 100 mM and were stored at -20˚C. Further dilutions were made in Holman's buffer and were kept on ice at all times. Bath concentrations between 10 nM to 100 µM were applied to give cumulative concentration-response curves.
  - **ACh** (Sigma, UK): ACh acts through a G protein-coupled receptor (M_3 muscarinic receptors), which is linked to a heterotrimeric GTP-binding protein Gq that can activate PLC to produce $InsP_3$ that binds to $InsP_3$ receptors on intracellular stores to stimulate the release of Ca^{2+}. 10 mM stock solutions of ACh were freshly made in dH_2O and were kept on ice. Further dilutions were prepared in Holman's buffer and were kept on ice at all times. 1 nM to 10 µM final bath concentration was added cumulatively for the concentration-response curves.
  - **MAHMA NONOate** (Sigma, UK): MAHMA NONOate is an exogenous nitric oxide (NO) donor, which spontaneously generates NO in a pH

dependent manner, with a half-life of 1 minute at 37°C and 3 minutes at 22-25°C (pH 7.4) to liberate 2 moles of NO per mole of parent compound. 100 mM stock solutions of MAHMA NONOate were made in 10mM NaOH and were stored at -20˚C, because MAHMA NONOate exhibits high stability at high pH. Further dilutions in Holman's buffer were prepared ≤1 hour prior to use due to its short life and were kept on ice, in the dark at all times. 1 nM to 30 μM of bath concentration was added cumulatively for the concentration-response curves.

2.2.3 Data collection

The data from the mechanical experiments were recorded using Myodaq software and analysed by Myodata software (DMT, Denmark). Tension values were read and collected manually at baseline and after addition of each drug. The percentage of relaxation/constriction was calculated with Microsoft Excel software and further analysed using Graphpad Prism 4 software.

2.3 IMAGING STUDIES IN RABBIT TISSUE PREPARATIONS

2.3.1 Imaging systems

For the imaging studies described in this thesis, the following microscope systems were used.

2.3.1.1 Confocal laser scanning microscope (CLSM)

Leica Confocal laser scanning microscope (CLSM) model SP5 was used for imaging studies. This system is equipped with a DMI 6000 inverted microscope. The emitted light from the sample is passed through a pinhole that prevents the out of focus light from being detected by the scan head (Figure 2.5). The electrical signal was recorded by the computer equipped with Leica Application Suite Advanced Fluorescence (LAS AF) software.

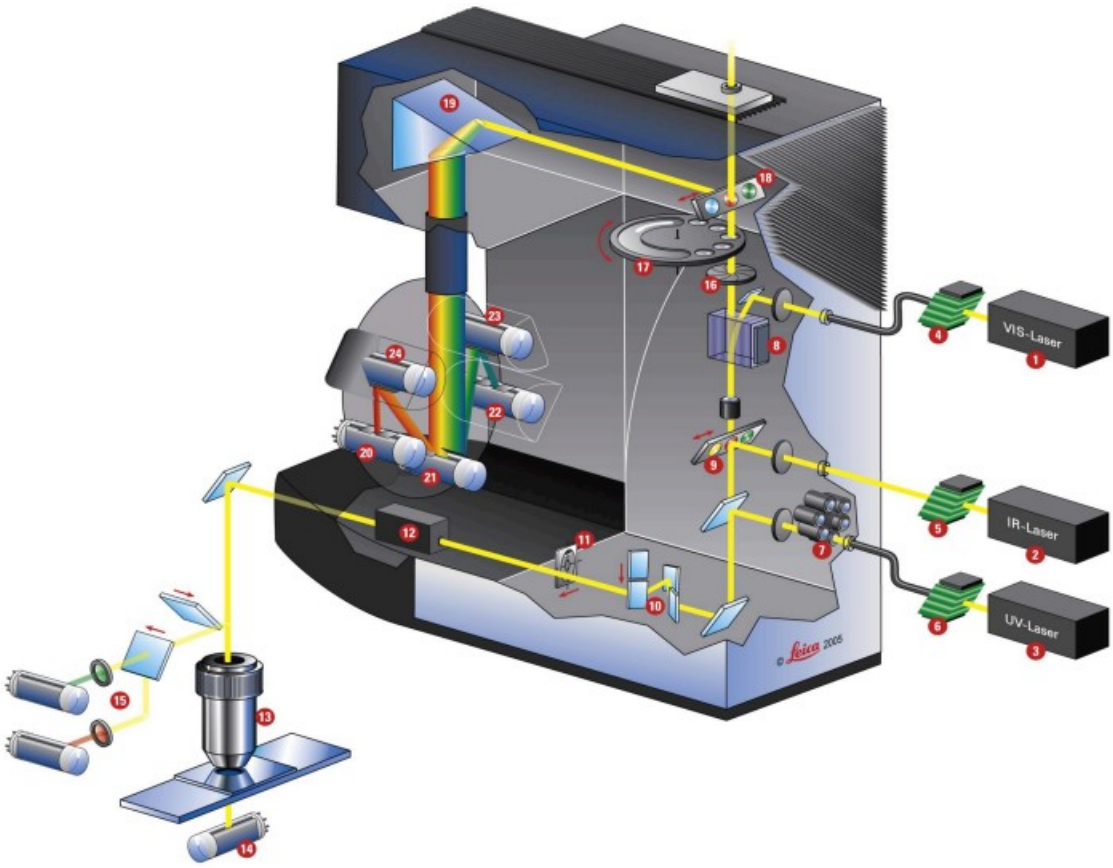

① Visible range lasers (up to 5)
② IR laser
③ UV laser
④ Visible range AOTF
⑤ IR EOM
⑥ UV AOTF
⑦ UV optics imaging
⑧ AOBS
Acousto Optical Beam Splitter
⑨ Multi Function Port (MFP)
⑩ Tandem Scanner
⑪ Calibration target
⑫ Field rotation optics
⑬ Objective lens
⑭ Transmitted light dedector
⑮ Reflected light NDD
⑯ Confocal detection pinhole
⑰ Filter- and polarizer wheel
⑱ X1-emission port
⑲ Spectrophotometer prism
⑳ PMT channel 1
㉑ PMT channel 2
㉒ PMT channel 3
㉓ PMT channel 4 (optional FLIM)
㉔ PMT channel 5 (optional FLIM)

Figure 2.5 Outline of the Leica SP5 system. The unique features in Leica TCS SP5 are Acousto-Optical Tunable Filter (AOTF), Acousto Optical Beam Splitter (AOBS®) and Spectrophotometer Detector (SP-Detector).

Image taken from www.zmb.uzh.ch/resources/download/CLSM.pdf

2.3.1.2 Inverted fluorescence microscope system from Life Science Resources

Imaging experiments for ratiometric measurement of Fura-2 were carried out on a Zeiss Axiovert S100 inverted microscope attached to a cooled CCD camera (Astrocam Model TE3/A/S). Excitation light was provided by a 75-W integral xenon lamp (Life Science Resources, Cambridge, UK). Excitation wavelengths were controlled with a computer-driven Spectramaster imaging system and data were recorded using Merlin software, version 2.0 (Life Science Resources).

2.3.1.3 Inverted epifluorescence microscope

Manganese quench experiments, using Fura-2, were performed with an inverted epifluorescence microscope (Nikon eclipse T*i*-U) equipped with excitation/emission/shutter wheels (Sutter Lambda 10-3 controller) and a CCD camera (Photomertics CoolSNAP HQ^2). The light source was from OptoLED Lite (CAIRN Research) and the software used for recording was InVivo (MediaCybernetics).

2.3.2 Chemicals used for imaging studies

A brief description of the drugs and concentrations employed for the imaging studies is listed in Table 2.1. More detailed information will be given in subsequent chapters.

DRUG	CONCENTRATIONS USED	STOCK	MANUFACTURER
N_{ω}-Nitro-L-arginine methyl ester hydrochloride —(L-NAME)	300 µM in buffer	100 mM in buffer	Sigma, UK
1-(4-Chlorobenzoyl)-5-methoxy-2-methyl-3-indoleacetic acid —(Indomethacin/Indo)	10 µM in buffer	10 mM in absolute ethanol	Sigma, UK
Sodium (meta)arsenite —(Arsenite)	100 µM in buffer	100 mM in dH_2O	Sigma, UK
Acetovanillone —(Apocynin)	100 µM in buffer	100 mM in absolute ethanol	Sigma, UK
TPEN	100 µM in buffer	10 mM in DMSO	Tocris, UK
Ethylene glycol-bis(2-aminoethylether)-N,N,N',N'-tetraacetic acid —(EGTA)	20 mM in buffer	0.3 M in dH_2O	Sigma, UK
Cyclopiazonic Acid —(CPA)	10 nM to 100 µM in buffer	100 mM in DMSO	Ascent, UK
Acetylcholine chloride —(ACh)	1 nM to 10 µM in buffer	10 mM in dH_2O	Sigma, UK
4-Bromo Calcium Ionophore (4-Br-A23187)	1 and 3 µM in buffer	10mM in DMSO	Sigma, UK
Hydrogen Peroxide —(H_2O_2)	100 µM in buffer	100 mM in buffer	Sigma, UK
Thimerosal	10 µM in buffer	10 mM in dH_2O	Sigma, UK
Xestospongin C —(Xes C)	10 µM in buffer	5 mM in DMSO	Enzo, UK
Ryanodine	100 µM in buffer	100 mM in absolute ethanol	Ascent, UK

Table 2.1 Summary of drugs used for imaging studies

2.3.3 Assessing dye responsiveness to calcium

All the fluorescence probes used for the detection of intracellular calcium were obtained from Invitrogen, UK. The following protocols for assessing dye responsiveness to calcium were as suggested by Invitrogen.

The acetoxymethyl (AM) ester-linked dyes (Fluo-4, Mag-fluo-4, Rhod-2 and Fura-2) were dissolved in 50 µl of DMSO, an equal volume of methanol and 25 µl of 2M KOH (dissolved in dH_2O) was then added to de-esterify the probe (hydrolysis of AM esters is

essential for a full Ca^{2+}-sensitive fluorescence response). If the probe was not fully dissolved, more methanol were added. The amount of methanol required at this stage was different for each probe, more details are given in Table 2.2. The mixtures were allowed to stand for 1 hour in the dark before the pH was adjusted to 7 with HCl.

In the dye responsiveness test, samples of interests (with or without H_2O_2) were prepared in dH_2O or buffers and 100 µl of each sample were mixed with 5 µl of each fluorescence probe in a 96-well plate and incubated in the dark at room temperature for 0-60 minutes. Fluorescence intensities were read using a Fluostar optima spectrophotometer (BMG Labtech) and recorded in Fluostar software. Details of the excitation/emission wavelength are listed in Table 2.3. Data of intensities were further analysed with Excel/Graphpad Prism 4 software.

2.3.4 Loading of fluorescent indicators

All the fluorescents indicators used for the studies described in this thesis are listed in Table 2.4. The concentration and time used to load each indicator was that found previously to be the optimum condition in rabbit aortic valve leaflets (Dr DH Edwards personal communication). After loading the fluorescent indicators, the rabbit aortic valves leaflets were pinned into a 35mm glass bottomed culture dishes (MatTek Corporation, Figure 2.6) to allow imaging with conventional and confocal microscopes. To reduce photobleaching, all the loading procedures with rabbit preparations were performed in a dark room and were kept in a light tight box between transfers.

	DMSO	METHANOL	2M KOH	1M HCL	STOCK CONCENTRATION	WELL CONCENTRATION
Fluo-4	50 µl	175 µl	25 µl	29 µl	$1.6x10^{-4}$ µM	8 µM
Mag-Fluo-4	50 µl	100 µl	25 µl	28 µl	$3x10^{-4}$ µM	15 µM
Rhod-2	50 µl	150 µl	25 µl	30 µl	$1.7x10^{-4}$ µM	8.5 µM
Fura-2	50 µl	50 µl	25 µl	30 µl	$3.2x10^{-4}$ µM	16 µM

Table 2.2 Details of the composition and concentrations used for each fluorescence probe in the responsiveness test.

	EXCITATION	EMISSION COLLECTION
Fluo-4	484nm	520-P nm bandpass filter
Mag-Fluo-4	484nm	520-P nm bandpass filter
Rhod-2	544nm	590nm bandpass filter
Fura-2	340-10nm/355nm/380-10nm	520-P nm bandpass filter

Table 2.3 Details of the excitation and emission wavelengths used for fluorescence probes.

DRUG	CONCENTRATIONS USED	STOCK	MANUFACTURER
DHE	5 µM in buffer/DMEM	5 mM in dH_2O	Sigma, UK
Fluo-4	2 µM in buffer/DMEM	5 mM in DMSO	Invitrogen, UK
Mag-Fluo-4	2 µM in buffer/DMEM	5 mM in DMSO	Invitrogen, UK
Rhod-2	1 µM or 5 µM in buffer/DMEM	1 mM in DMSO	Invitrogen, UK
MitoTracker Green	0.1 µM buffer/DMEM	5 mM in DMSO	Invitrogen, UK
Fura-2	5 µM in buffer/DMEM	5 mM in DMSO	Invitrogen, UK

Table 2.4 Fluorescence probes used for imaging studies.

Figure 2.6 Dishes with pins used for imaging of rabbit aortic valve leaflets in confocal microscopy. The 35mm glass bottomed culture dish was glued with 3 pairs of pins, which holds the valve leaflets against the glass.

2.3.4.1 Dihydroethidium (DHE) for ROS detection

Rabbit aortic valve leaflets and endothelium-denuded rings of iliac artery and aorta (2-3mm wide) were placed in oxygenated Holman's Buffer containing L-NAME (300 μM) and indomethacin (10 μM). These preparations were then incubated with arsenite (100 μM) and/or apocynin (100 μM) for 60 minutes at 37°C. DHE (5 μM) was then added to act as a fluorescent indicator of ROS generated in response to the arsenite/apocynin treatment for 30 minutes. This protocol was designed to match the total exposure of rings preincubated with 100 μM arsenite for 30 min in mechanical experiments in which it took a further ~60 min to construct full concentration-relaxation curves. The

preparations were then briefly washed three times with phosphate buffered saline (PBS), followed by 90 minutes fixation in 4% paraformaldehyde. Valve leaflets were immediately mounted on glass slides with FluorSave (Calbiochem, UK). Artery preparations were covered with cryo-embedding media OCT (Agar Scientific, UK) and stored in liquid nitrogen. Prior to sectioning, the frozen artery block was transferred to a cryotome cryostat (-20°C) and the temperature of the frozen artery block was allowed to equilibrate to the temperature of the cryostat. Artery slices 10 µm thick, were sectioned and mounted on glass slides with FluorSave.

2.3.4.2 Fluo-4 for cytosolic calcium

To assess the $[Ca^{2+}]_i$ in the endothelial cells, the aortic valve leaflets from the rabbit heart were placed in Holman's buffer gassed with 95% O_2 and 5% CO_2. The valves were then incubated with the Ca^{2+} indicator Fluo-4 (2 µM) in oxygenated Holman's buffer at room temperature for 2 hours followed by a wash with indicator-free buffer for 5 minutes. Each valve leaflet was incubated with L-NAME (300 µM) and/or indomethacin (10 µM) in indicator-free Holman's buffer for 30 minutes before the experiment protocol. In some cases, the valves were incubated for the 30 minutes period with calcium free Holman's buffer of the following composition: NaCl (120 mM), KCl (5 mM), NaH_2PO_4 (1.3 mM), $NaHCO_3$ (25 mM), Glucose (11 mM), Sucrose (10 mM), EGTA (0.2 mM, except where indicated), pH 7.4. Buffer solutions were freshly prepared in dH_2O and were kept oxygenated at room temperature. All chemicals used for the buffers were obtained from Fisher Scientific, UK.

2.3.4.3 Mag-fluo-4 for endoplasmic reticulum calcium

To assess the $[Ca^{2+}]_{ER}$ in the endothelial cells, the aortic valve leaflets from the rabbit heart were placed in Holman's buffer gassed with 95% O_2 and 5% CO_2. The valves then were incubated with the low-affinity Ca^{2+} indicator Mag-fluo-4 (2 µM) in oxygenated Holman's buffer at room temperature for 60 minutes. After loading of the

dye, the valves were washed for 30 minutes with oxygenated indicator-free buffer at 37°C, followed by a further 60 minutes wash at room temperature to allow the Mag-fluo-4 located in the cell cytosol to be taken up into the ER. L-NAME (300 μM) and/or indomethacin (10 μM) were added to the valve leaflets and incubated for 30 minutes before starting the experiment. In some cases, the valves were incubated for the 30 minutes with calcium free Holman's buffer.

2.3.4.4 Rhod-2 for mitochondria calcium

To assess the $[Ca^{2+}]_m$ in the endothelial cells, aortic valve leaflets from the rabbit heart were placed in Holman's buffer gassed with 95% O_2 and 5% CO_2. The valves were then incubated with the Ca^{2+} indicator Rhod-2 AM (5 μM) in oxygenated Holman's buffer at 37°C for 30 minutes, followed by 30 minutes washing with indicator-free Holman's buffer to allow for de-esterification at room temperature. Each valve leaflet was then incubated with L-NAME (300 μM) and/or indomethacin (10 μM) in indicator-free Holman's buffer for 30 minutes before the experiment.

2.3.4.5 MitoTracker Green for mitochondrial localization

To assess the cellular localization of the mitochondria, valve leaflets were incubated with MitoTracker Green FM (0.1 μM) in oxygenated Holman's buffer at 37°C for 30 minutes, followed by a brief wash with indicator-free Holman's buffer before imaging.

2.3.4.6 Dual loading of Rhod-2 and MitoTracker Green

Valve leaflets were incubated with MitoTracker Green FM (0.1 μM) in oxygenated Holman's buffer at 37°C for 20 minutes, followed by washing with indicator-free buffer. The valves were then incubated with the Rhod-2 AM (5 μM) in oxygenated Holman's buffer at 37°C for 30 minutes, followed by 30 minutes washing with indicator free Holman's buffer to allow de-esterification at room temperature. Each valve leaflet was

incubated with L-NAME (300 μM) and/or indomethacin (10 μM) for 30 minutes in indicator-free Holman's buffer before use.

2.3.4.7 Fura-2 for cytosolic calcium and Manganese quench experiments

To assess $[Ca^{2+}]_i$ in endothelial cells, aortic valve leaflets from the rabbit heart were placed in oxygenated Holman's buffer and incubated with the Ca^{2+} indicator Fura-2 (5μM) at room temperature for 2 hours. After loading the dye, the valves were briefly washed with indicator-free buffer. From this stage, due to the fact that manganese precipitates out in Homan's buffer, the valves used for the quench experiments were washed with HEPES buffer of the following composition: HEPES (10 mM), NaCl (140 mM), KCl (5 mM), Glucose (10 mM), $CaCl_2$ (1 mM), pH adjusted to 7.4. HEPES buffer was freshly prepared in dH_2O and were kept at room temperature. All chemicals used for this buffer were obtained from Fisher Scientific, UK, except for HEPES (Sigma, UK). L-NAME (300 μM) and/or indomethacin (10 μM) were added in indicator-free Holman's/HEPES buffer 30 minutes prior to the experiments.

2.3.5 Excitation and emission wavelength

The excitation wavelength and the collection range for emission wavelength were optimized individually for each probe, according to the manufacturer's guideline. Details of the wavelength of excitation and emission for each probe are listed in Table 2.5.

	Excitation	Emission collection
DHE	514nm Argon	560-650nm
Fluo-4	488nm Argon	500-550nm
Mag-Fluo-4	488nm Argon	500-550nm
Rhod-2	514nm Argon	580-650nm
MitoTracker Green	488nm Argon	500-540nm
Dual staining with Rhod-2 and MitoTracker Green	488nm Argon	500-540nm green / 580-650nm red
Fura-2	340nm/355nm/380nm	520nm-550nm bandpass filter

Table 2.5 Excitation and emission wavelength used for fluorescent dyes and probes.

2.3.6 Data recording of ROS imaging with DHE

Experiments with DHE were performed using a Leica SP5 confocal microscope with an oil immersion 63X objective (Leica HCX PL APO 63X/1.40-0.60 OIL CS), images were acquired at 1024x1024 pixel resolution. Ten individual cells and 4 areas of background as described in Section 2.3.6 were selected from each valve leaflet for each experiment. Recordings of their intensities were analysed in Excel/Graphpad Prism 4 softwares.

2.3.7 Data recording of Intracellular Ca^{2+} signal

Experiments with Mag-fluo-4 ($[Ca^{2+}]_{ER}$), Fluo-4 ($[Ca^{2+}]_i$), Rhod-2 ($[Ca^{2+}]_m$) and MitoTracker Green (mitochondria localization) were performed using a Leica SP5 confocal microscope and visualised using a dry 20X objective (Leica HC PL FLUOTAR 20X/0.50). Image serials (xyt) were acquired every 10 seconds at 512x512 pixel resolution. High definition pictures were taken with an oil immersion, 100X objective

(Leica HCX PL APO 100X/1.40-0.70 OIL CS) at 1024x1024 pixel resolution. Ten individual cells from each experiment were selected for analysis and 4 areas of a similar size to the cells were used for background. Signal intensities were recorded with LAS AF software and analysed in Excel/Graphpad Prism 4 software.

Imaging experiments with Fura-2 ($[Ca^{2+}]_i$) were performed using an 40X oil immersion objective (Zeiss FLUAR 40X/1.30 OIL) with the Life Science Resources system as described in Section 2.3.1. The preparations were excited alternately at 340/380 nm and emission was selected by using a 510 nm long pass filter. Images were acquired at 2s intervals with an exposure time of 100 ms at each wavelength. Due to the low resolution image of the camera, an area giving fluorescence signal was selected for analysis and an area of no fluorescence signal was used for background. Fluorescence intensity was recorded and data were analysed in Excel/Graphpad Prism 4 software.

All experiments were performed in oxygenated Holman's buffer (with and without calcium as indicated).

2.3.8 Data recording of manganese (Mn^{2+}) quench imaging

Mn^{2+} quench experiments in aortic valve preparations loaded with Fura-2 were imaged with an inverted epifluorescence microscope and a 20X dry objective (Nikon PL APO 20X/0.75). The preparations were excited at 355/380 nm, and a series of images was acquired at 10 second intervals. Due to the low resolution image of the camera, an area giving fluorescence signal was selected for analysis and an area of no fluorescence signal was used for background. Fluorescence intensity was recorded and data were analysed in Excel/Graphpad Prism 4 software.

2.4 CELL CULTURE

2.4.1 Cell line descriptions

The EA.hy926 cell line, is a permanent human cell line that expresses highly differentiated functions that are characteristic of human vascular endothelium, such as expression of factor VIII-related antigen and cytoplasmic distribution of Weibel-Palade bodies. The cell line was originally obtained by fusing primary human umbilical vein cells (HUVEC) with a clone of A549/8 (human lung adenocarcinoma epithelial cell line) (Edgell *et al.*, 1983; Edgell *et al.*, 1990). Cells were obtained from the American Type Culture Collection (Manassas, VA, USA) (ATCC® Catalog No. CRL-2922™).

- Organism: *Homo sapiens* (human)
- Tissue: somatic human umbilical vein endothelial cells
- Doubling Time: approximately 31 hours
- Morphology: endothelial
- Growth Properties: adherent

2.4.2 Tissue culture medium

All growth medium, reagents and materials employed for cell culture were purchased from Gibco/Invitrogen, UK, except 0.9% w/v Sodium Chloride (NaCl) (Fresenius Kabi, UK), sterile culture flasks (Greiner, UK), sterile filling tubes (Uhs/Kwills, UK), sterile pipettes (Nunc/Fisher and Alpha laboratories, UK), sterile syringes (BD Plastipak, UK), and glass bottomed culture dishes (35mm petri dish; 14mm microwell; 0.085-0.13 mm coverglass) (MatTek, USA).

➢ *Reagents used for the culture of EA.hy926 cells*

- Complete Growth Medium
    - Dulbecco's Modified Eagle Medium (DMEM).

        - with 580mg/L L-Glutamine, 4500 mg/L D-Glucose, 110 mg/L Sodium Pyruvate
    - Supplemented with
        - 10% Heat Inactivated FBS (Fetal Bovine Serum; Origin: South America).
        - 100U/mL penicillin, 100ug/mL streptomycin and 0.292mg/mL L-glutamine.
- 0.05% Trypsin-Ethylenediaminetetraacetic acid (EDTA) (1x).
- Saline solution, NaCl 0.9% (w/v).

➢ ***Freezing medium***

Cryo.s™ Cryogenic Storage Vials (1ml) were purchased from Greiner, UK. Sterile DMSO was obtained from Sigma, UK.

- The freezing medium for EA.hy926 cells
    - 95% complete growth medium
    - 5% DMSO

2.4.3 Culturing EA.hy926 cells

The EA.hy926 cells were maintained in complete growth medium (Section 2.4.2). The cells were given fresh medium every 3 days and cells were passaged on a weekly basis. Flasks containing the cells were kept in a cell incubator at 37°C with a 5% CO_2 in air atmosphere.

All the following procedures were performed inside a tissue culture Class II hood decontaminated with 70% ethanol. Personal protection equipments including specialised lab coat and gloves were worn at all times.

2.4.3.1 Subculturing Procedure (75 cm² flask)

Cells were sub-cultured as soon as they reached confluence (i.e. ~1x10^5cells/ml). The complete growth medium and trypsin were warmed to 37°C before the passaging.

EA.hy926 are adherent cells therefore the spent cell culture medium was removed from the flask and discarded. The cells were briefly washed twice with saline solution (10 ml) to remove all traces of serum, which inhibits trypsin. Trypsin-EDTA solution (5 ml) was added and the flask was kept at 37°C for 5-10 minutes to facilitate detachment. Cells were viewed under a Nikon inverted microscope to make sure the cell layer was fully detached and that the cells were dispersed and floating. The side of the flasks was gently tapped to release any remaining attached cells. Complete growth medium (10 ml) was then added to the flask to neutralise the trypsin-EDTA. Cell suspension (100 µl) was placed in a haemocytometer for cell counting; the remainder was transferred to a centrifuge tube and spun at 1200 rpm for 3 minutes. The supernatant was discarded and the cells were re-suspended in fresh complete growth medium (20 ml) to give a concentration of approximately $5x10^3$ cells/ml. The culture flask was then transferred to the cell incubator and maintained at 37°C in a 5% CO_2 in air atmosphere.

2.4.3.2 Freezing Procedure

Cryogenic preservation (storage below -100°C) of cell cultures was performed to maintain backup cells and for long term storage when required. The recommended concentration for freezing EA.hy926 cells was $5x10^5$cells/ml. Twenty-four hours before freezing, the culture medium was renewed and cells should be approximately 80% confluence.

Cells were counted and centrifuged as described in Section 2.4.3.1. The cell pellet was resuspended in ice cold freezing medium at the appropriate dilution (i.e. $5x10^5$ cells/ml). The final cell suspension was placed into a cryogenic vial and immediately placed on ice before transfer to a -20°C freezer for 1 hour. The vials were then placed in a -80°C freezer overnight and then transferred to liquid nitrogen for long term storage.

2.4.3.3 Thawing Procedure

The vial containing the EA.hy926 cells was rapidly thawed by gentle agitation in a 37°C water bath for 1-2 minutes. As soon as contents were thawed, the vial was removed from the water bath and decontaminated by spraying with 70% ethanol. The contents were transferred to a centrifuge tube containing pre-warmed (37°C) complete growth medium and spun at 1200 rpm for 3 minutes. The cell pellet was resuspended in further pre-warmed complete growth medium and transferred into a culture flask. The flask was then placed in the incubator at 37°C and 5% CO_2 in air.

2.4.3.4 Plating Procedure

The density of the cells was calculated with the aid of a haemocytometer and cells were centrifuged as described in Section 2.4.3.1. The supernatant was discarded and cells were re-suspended in fresh complete growth medium to give $1.5x10^5$ cell/ml. Cells (2 ml) were seeded into each of the 35mm glass bottomed culture dishes and transferred to the cell incubator for 24 hours prior to use.

2.5 IMAGING STUDIES WITH EA.HY926 CELLS

2.5.1 Loading of fluorescent indicators

Twenty four hours prior to the experiment, fresh complete DMEM culture medium was given to the cells. All the loading procedures with EA.hy926 cells were performed in a dark room to avoid photobleaching. Between transfers, all dishes were kept in a light tight box.

2.5.1.1 Mag-fluo-4 for endoplasmic reticulum calcium

Cells were incubated with the low-affinity Ca^{2+} indicator Mag-fluo-4 (2 μM) in DMEM at 37°C (in a cell incubator) for 30 minutes. After loading of the dye, the cells were washed with oxygenated indicator-free Holman's buffer for a further 40 minutes at room

temperature. Each dish of cells was incubated with L-NAME (300 μM) and/or indomethacin (10 μM) in oxygenated Holman's buffer for 30 minutes before the experiment.

2.5.1.2 Fluo-4 for cytosolic calcium

Cells were incubated with the Ca^{2+} indicator Fluo-4 (2 μM) in DMEM at 37°C for 45 minutes in a cell incubator. After dye loading, the cells were briefly washed with indicator-free Holman's buffer before the 30 minutes incubation with L-NAME (300 μM) and/or indomethacin (10 μM) in oxygenated Holman's at room temperature prior to the experiment.

2.5.1.3 Rhod-2 for mitochondria calcium

Cells were incubated with the Ca^{2+} indicator Rhod-2 AM (1 μM) in DMEM at 37°C for 30 minutes in a cell incubator. After loading of the dye, the cells were washed with oxygenated indicator-free Holman's buffer for 30 minutes to allow de-esterification at room temperature. Each dish of cells was incubated with L-NAME (300 μM) and/or indomethacin (10 μM) in oxygenated Holman's buffer for 30 minutes before the experiment.

2.5.1.4 MitoTracker Green for mitochondrial localization

Cells were incubated with the MitoTracker Green FM (0.1 μM) in DMEM at 37°C for 20 minutes in a cell incubator, and followed by washing with oxygenated indicator-free Holman's buffer at room temperature.

2.5.1.5 Dual loading of Rhod-2 and MitoTracker Green

Cells were incubated with the MitoTracker Green FM (0.1 μM) in DMEM at 37°C for 20 minutes in a cell incubator, followed by a brief wash with indicator-free DMEM. Cells were then incubated with Rhod-2 AM (5 μM) in DMEM at 37°C for a further 30 minutes, followed by 30 minutes of washing with indicator free Holman's buffer at room

temperature to allow de-esterification of the dye. L-NAME (300 μM) and/or indomethacin (10 μM) was added to each dish of cells in oxygenated indicator-free Holman's buffer for 30 minutes prior to the experiment.

2.5.2 Data recording of Intracellular Ca^{2+} signal

A Leica SP5 confocal microscope was used for experiments with EA.hy926 cells. Fluorescence imaging of Mag-fluo-4 ($[Ca^{2+}]_{ER}$), Fluo-4 ($[Ca^{2+}]_i$), Rhod-2 ($[Ca^{2+}]_m$) and MitoTracker Green (mitochondria localization) were visualised using a dry 20X objective (Leica HC PL FLUOTAR 20X/0.50) and image serials (xyt) were acquired every 10 seconds at 512x512 pixel resolution. High definition pictures were taken with an oil immersion, 100X objective (Leica HCX PL APO 100X/1.40-0.70 OIL CS), at 1024x1024 pixel resolution.

All cell experiments were performed in oxygenated Holman's buffer. Ten individual cells and 4 areas of background as described in Section 2.3.6 were selected from each dish for each experiment. Fluorescence intensities were recorded with LAS AF software and analysed in Excel/Graphpad Prism 4 softwares.

2.6 STATISTICAL ANALYSIS

For mechanical experiments, the maximal percentage reversal of phenylephrine-induced constriction (R_{max}) by CPA, ACh or MAHMA NONOate was determined for each experiment. The concentrations of ACh or MAHMA NONOate giving the half maximal response (EC_{50}) were obtained from the concentration-response curve fitted to a sigmoidal logistic equation (Y=BOTTOM+(TOP-BOTTOM)*X^H/(EC50^H+X^H)) using GraphPad Prism. Relaxation of CPA was often preceded by small increases in tension which can be attributed to an effect of CPA on smooth muscle Ca^{2+} stores (Chaytor *et al.*, 2005), the concentration giving 50% reversal of whole constrictor response (IC_{50}) was therefore determined graphically for each experiment. R_{max}, pEC_{50}

or pIC_{50} (negative log molar EC_{50} or IC_{50}) values were calculated as mean±standard error of mean (mean±SEM).

For imaging studies, the fluorescence intensities were recorded and stored as arbitrary unit (A.U.) in spreadsheets and plotted in graphical form using GraphPad Prism 4 software. Data obtained from conventional microscopes (see Section 2.3.1) were analysed as background-corrected F355 (F/F_0, see explanation below), F340/380 or F355/F380 ratios. Data obtained from confocal microscopy to track the effects of interventions on Mag-fluo-4 ($[Ca^{2+}]_{ER}$), Fluo-4 ($[Ca^{2+}]_i$) or Rhod-2 ($[Ca^{2+}]_m$) fluorescence were analysed as fluorescence normalized to its value at the beginning of each experiment (F/F_0).

Significance between two groups was calculated using paired or un-paired Student's t-test as appropriate (two tail P value) assuming that the data are sampled from two populations with the same variance. Statistical comparisons between more than two groups were calculated using analysis of variance (ANOVA) followed by an appropriate post-hoc tests. $p<0.05$ was considered significant; n denotes the number of animals in each group.

2.7 HEALTH AND SAFETY

Personal protective equipment including laboratory coat, masks, gloves and headwear was used when performing laboratory work in accordance with COSHH regulations and local college regulations. Reagents were handled and stored as recommended by manufacturer's safety guidelines. All GMO work was carried out in accordance with GMSC guidelines and all tissue culture waste was disinfected before disposal.

Chapter 3

Modulation of Endothelium-dependent Arterial Relaxation by Exogenous Hydrogen Peroxide

3.1 INTRODUCTION

3.1.1 Background

It has been suggested that H_2O_2 functions as a freely diffusible EDHF in some artery types. This is because agonist-induced EDHF-type responses in these vessels are catalase-sensitive and exogenous/endogenous H_2O_2 evokes relaxation/hyperpolarization of the smooth muscle by activating K_{Ca} (Matoba *et al.*, 2000; Matoba *et al.*, 2003; Shimokawa and Matoba, 2004; Shimokawa and Morikawa, 2005; Liu *et al.*, 2011). However, in the rabbit iliac artery, a vessel modulated by both NO and EDHF, H_2O_2 cannot be considered as a transferable EDHF as the maximal smooth muscle hyperpolarization evoked by exogenous applied H_2O_2 is much smaller than that associated with the authentic "EDH phenomenon" (e.g. ~20 mV for 3 μM ACh; ~5 mV for 300 μM H_2O_2) and H_2O_2-evoked relaxation may be insensitive to a spectrum of K^+ channel inhibitors (Chaytor *et al.*, 2003). It was shown that H_2O_2 can potentiate CPA-evoked EDHF-type relaxation in this vessel (Edwards *et al.*, 2008), probably through enhanced Ca^{2+} release from the ER in the endothelium (Hu *et al.*, 1998; Zheng and Shen, 2005). It has been confirmed the ability of H_2O_2 to potentiate the

mobilization of Ca^{2+}, by CPA in rabbit aortic valve endothelium (Edwards *et al.*, 2008). However, the effects of H_2O_2 on NO-dependent relaxation remain to be investigated.

Depressed NO bioavailability is often observed in the vascular dysfunction that occurs in disease states such as diabetes, hypertension, heart failure and ischemia/reperfusion injury, conditions in which a compensational role for the "EDH phenomenon" has been proposed (McCulloch *et al.*, 1997; Katz and Krum, 2001; Wigg *et al.*, 2001; Katusic, 2002; Marrelli, 2002). It has been shown that NO depresses endothelial-dependent hyperpolarization in the rabbit iliac artery (Griffith *et al.*, 2005), and that the relative magnitudes of NO- and gap junction-dependent relaxation are inversely related in rabbit arteries of different sizes (Berman *et al.*, 2002). In endothelial cells, NO and/or its second messenger cGMP have been reported to decrease $[Ca^{2+}]_i$ by activating the SERCA pump (Dedkova and Blatter, 2002; Adachi *et al.*, 2004) and inhibiting SOCE (Kwan *et al.*, 2000; Dedkova and Blatter, 2002). However, it has also been reported that NO may increase endothelial Ca^{2+} influx by activating TRP channels (Yoshida *et al.*, 2006). Since NO can rapidly scavenge the H_2O_2 precursor $O_2^{\bullet-}$, the potentiating effect of H_2O_2 on EDHF-type relaxation in the rabbit iliac artery suggests that in disease states where NO bioavailability is decreased, the contribution of H_2O_2 to the EDHF phenomenon might be more prominent and then play a "compensatory" role. On the other hand, NO production by the Ca^{2+}-dependent enzyme eNOS may be increased by H_2O_2 through enhanced Ca^{2+} mobilization from the ER. Indeed, there is evidence that H_2O_2 acutely stimulates NO release in rabbit arteries (Zembowicz *et al.*, 1993; Yang *et al.*, 1998a).

3.1.2 Aim of this chapter

The work in this chapter was designed to investigate the mechanical effects that exogenous applied H_2O_2 has upon the rabbit vasculature in either EDHF-type or NO-mediated responses. In the rabbit iliac artery, the EDHF-type relaxations evoked by CPA and ACh can be suppressed either by pharmacological blockade of K_{Ca} channels

or gap junctional communication and maximal EDHF-type relaxation evoked by CPA and ACh are both depressed by exogenous applied catalase (Hutcheson *et al.*, 1999; Chaytor *et al.*, 2001; Edwards *et al.*, 2008). It has been shown that CPA depletes the ER store by inhibition of the SERCA pump, whereas ACh works through an $InsP_3$-dependent way, therefore, these two agents that have distinct mechanisms to induce vascular relaxation will be used to evaluate the effects of H_2O_2 in the rabbit arteries.

It has been shown previously, in rabbit iliac artery, that H_2O_2 and its thiol oxidant mimic thimerosal potentiate CPA evoked EDHF-type responses possibly through sensitization of the $InsP_3$ receptors (Edwards *et al.*, 2008). To test whether this effect of H_2O_2 is a universal phenomenon, a series of experiments were performed: (i) CPA (receptor independent agent) responses were compared with those induced by ACh (receptor dependent agent) in the absence or presence of L-NAME/indomethacin (NO-mediated and EDHF-type correspondingly); (ii) exogenous NO-mediated responses were examined with a NO donor MAHMA NONOate and (iii) since there is evidence that the relative magnitudes of NO- and gap junction-dependent relaxation are inversely related in rabbit arteries of different sizes (Berman *et al.*, 2002), the effect of H_2O_2 and thimerosal were also studied in the rabbit aorta.

3.2 MATERIALS AND METHODS

3.2.1 Mechanical Responses

Male NZW rabbits were killed and arterial preparations were dissected and mounted in a myograph as described in Section 2.1 and 2.2. Rings of iliac artery and aorta were maintained at a resting tension of 2 mN during a 1h equilibration period in oxygenated Holman's buffer at 37˚C. The buffer was replaced, and any subsequent alterations in baseline tension due to stress relaxation were corrected.

Iliac ring preparations were incubated in the presence or absence of indomethacin (10 μM) and L-NAME (300 μM) for 30 minutes as required. Aorta ring preparations were all incubated in the presence of indomethacin (10 μM) for 30 minutes and as required, some were also incubated with L-NAME (300 μM). In some studies, the rings were denuded of their endothelium by gentle abrasion and those rings were incubated in the presence of indomethacin (10 μM) and L-NAME (300 μM) for 30 minutes. Agents under study were added for a further 30 minutes, before tone was induced by phenylephrine (1 μM) and relaxation evoked by CPA, ACh or MAHMA NONOate. Cumulative concentration-response curves were constructed under control conditions and in the presence of the selective K_{Ca} channel blocker apamin (1 μM), TRAM-34 (TRAM, 10 μM) and iberiotoxin (IbTX, 100 nM) in combinations or alone as required. These concentrations of the blockers are known to inhibit the corresponding K_{Ca} channel fully as previously published in this type of vessel (Edwards *et al.*, 2008). Some rings were incubated with H_2O_2 (30 or 100 μM) or thimerosal (1 or 10 μM) for 30 minutes before constriction.

3.2.2 Data recording and Statistics

Details of data analysis were described in Section 2.2.3. In mechanical experiments the R_{max} by CPA, ACh or MAHMA NONOate and IC_{50} (in the case of CPA in iliac arteries, as explained in Section 2.6) or EC_{50} (in the case of ACh and MAHMA NONOate) were determined for each experiment. R_{max}, pIC_{50} and pEC_{50} values were calculated as mean±SEM and compared by the Student's t-test (2 groups), one-way ANOVA followed by Bonferroni post-hoc tests (3 or more groups) or two-way ANOVA (whole datasets). Details of statistical analyses used for each figure were indicated in figures descriptions.

3.3 RESULTS

3.3.1 Mechanisms contributing to ACh-evoked relaxations

In endothelium-intact iliac rings constricted by 1 μM phenylephrine (PE), maximal EDHF-type relaxations (in the presence of L-NAME/indomethacin) evoked by ACh were equivalent to 72.5±3.5% of the constrictor response to PE (R_{max}) with a pEC_{50} of 6.80±0.06 (n=15; Table 3.1). EDHF-type relaxations evoked by ACh were attenuated by K_{Ca} channel blockade in a channel-type selective manner. Apamin alone gave minimal depression in terms of R_{max}, but the rings exhibited a progressive decrease in R_{max} in the presence of TRAM-34, IbTX, the double combination Apamin+TRAM-34 and the triple combination Apamin+TRAM-34+IbTX. There was no significant difference between pEC_{50} values for those experimental groups where relaxation >50% (n=5-9; Figure 3.1; Table 3.1).

3.3.2 Effects of K_{Ca} channel inhibitors on tension in rabbit iliac artery.

In endothelium-intact rings in the presence of L-NAME/indomethacin or endothelium-denuded rings, apamin and TRAM-34 alone or in combination did not affect basal tone. In endothelium-intact rings in the presence of L-NAME/indomethacin, IbTX and apamin+TRAM+IbTX increased basal tone to an equivalent extent (both $p<0.001$), though there is a significant difference between the force developed by IbTX and the apamin+TRAM+IbTX combination ($p<0.05$). In rings constricted by PE, force development was only increased to a significant extent by apamin+TRAM+IbTX but not by IbTX or apamin+TRAM. In endothelium-denuded rings, basal tone was again increased to a significant extent by IbTX and apamin+TRAM+IbTX (both $p<0.001$) with no significant difference between these two groups, whereas in rings constricted by phenylephrine, none of the combinations of inhibitors had any effect on tone (Figure 3.2; Table 3.2, data pooled from corresponding experiments).

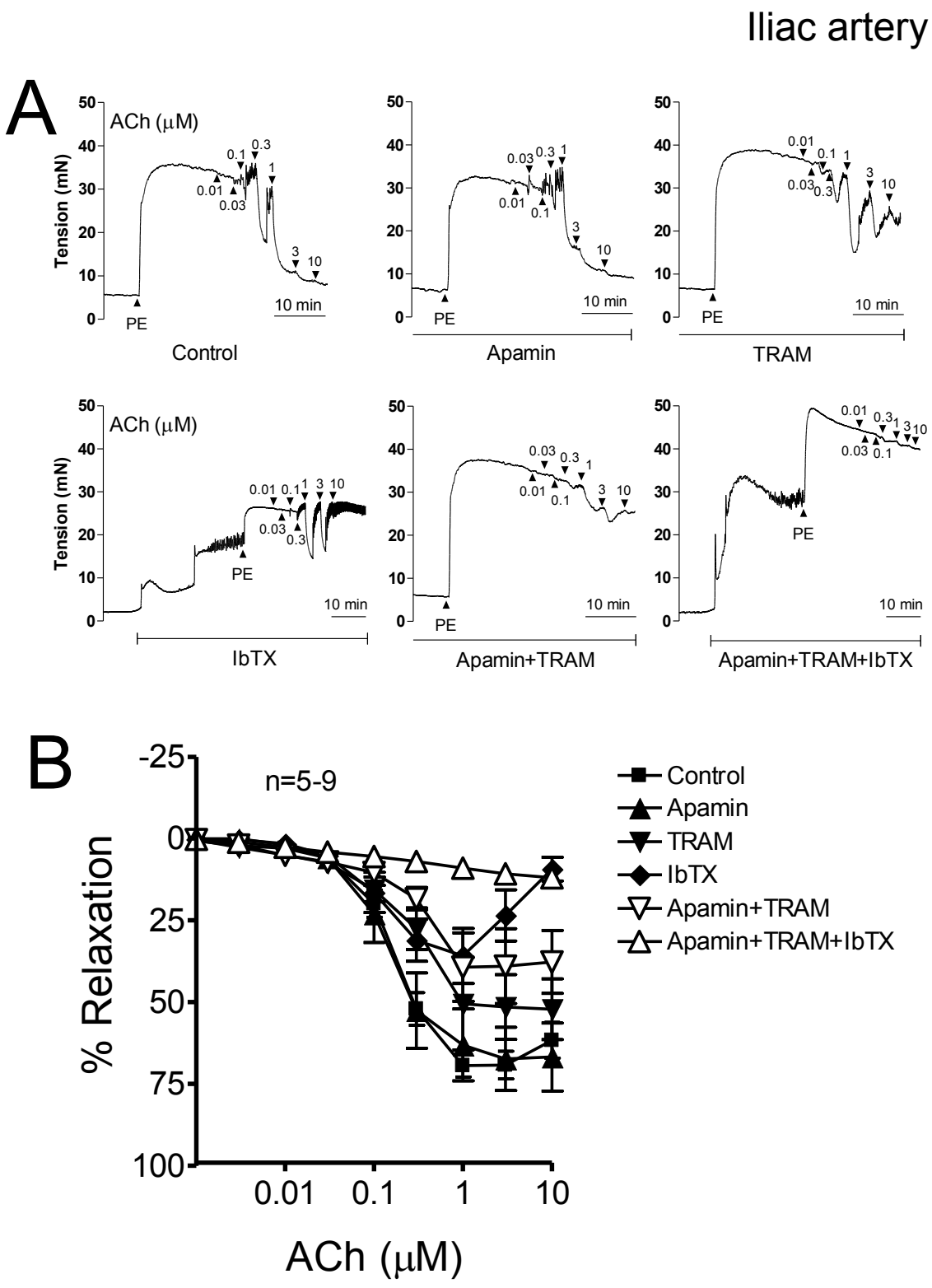

Figure 3.1 Inhibition of ACh-evoked relaxation by K_{Ca} channel blockers IbTX (100nM), TRAM-34 (100μM) and apamin (1μM), individually and in combinations. Representative graphs were shown in (A) and summary graph was shown in (B). All experiments were performed in presence of L-NAME (300μM) and indomethacin (10μM). n denotes the number of animals studied.

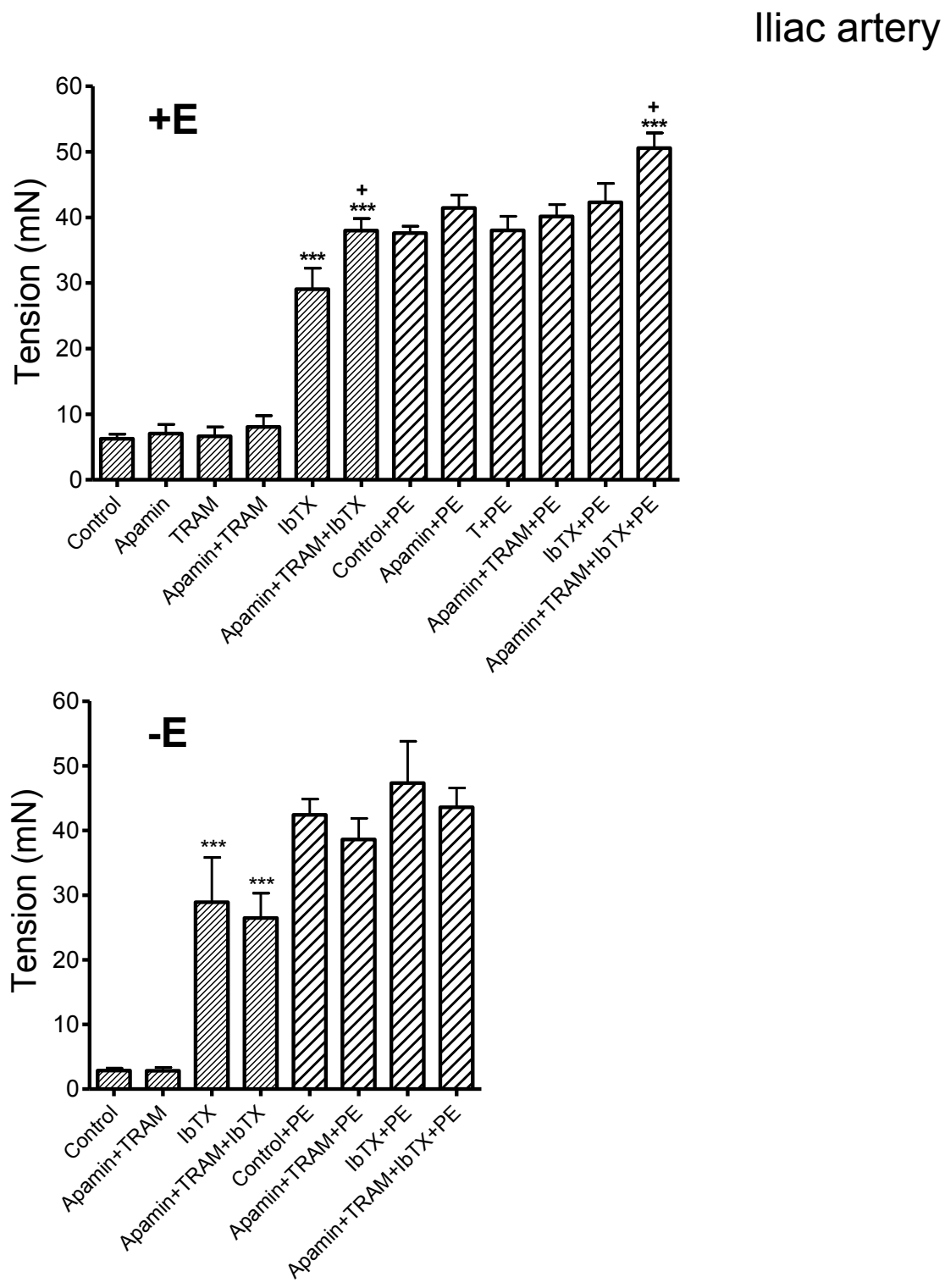

Figure 3.2 Effect of apamin, TRAM-34 and IbTX on basal tone and the contractile response to phenylephrine (PE) in rings with (+E) and without (-E) intact endothelium. All experiments were performed in presence of L-NAME/indomethacin. The basal tone and contractile response was measured at the peak point of the corresponding curve. *** denote $p<0.001$ compared with control; and the $^{+}$ denote $p<0.05$ compared with IbTX alone in one-way ANOVA.

Rabbit iliac artery			
Intervention	**n**	**pEC_{50}**	**R_{max}%**
L-NAME+Indo	15	6.80±0.06	72.5±3.5
L-NAME+Indo+apamin 1 μM	5	6.91±0.20	69.8±8.5
L-NAME+Indo+TRAM 100 μM	5	6.57±0.25	63.2±10.9
L-NAME+Indo+IbTX 100 nM	9	Relaxation<50%	43.8±7.7 *
L-NAME+Indo+Apamin+TRAM	5	Relaxation<50%	44.8±11.3 *
L-NAME+Indo+Apamin+TRAM+IbTX	6	Relaxation<50%	12.1±1.0 **

Table 3.1 Effects of K_{Ca} channel blockers on endothelium-intact arterial relaxations evoked by ACh in the presence of L-NAME and indomethacin. Potency (negative logEC_{50}) and maximal responses (R_{max}) are given as mean±SEM. * and ** denote p<0.05 and 0.01 compared with control in one-way ANOVA. n denotes the number of animals studied.

Rabbit iliac artery			
Intervention	***n***	***30mins pre-incubation***	***Addition of PE***
Endothelium intact		**Unit mN**	
L-NAME+Indo	72	6.26±0.69	37.6±1.0
L-NAME+Indo+apamin	12	7.05±1.39	41.5±2.0
L-NAME+Indo+TRAM	19	6.64±1.44	38.0±2.1
L-NAME+Indo+apamin+TRAM	22	8.08±1.70	40.2±1.8
L-NAME+Indo+IbTX	24	29.05±3.22***	42.3±2.9
L-NAME+Indo+apamin+TRAM+IbTX	40	38.01±1.83***,+	50.6±2.3***,+
Endothelium denuded		**Unit mN**	
L-NAME+Indo	12	2.88±0.36	42.4±2.4
L-NAME+Indo+apamin+TRAM	6	2.85±0.51	38.6±3.3
L-NAME+Indo+IbTX	6	28.90±6.91***	47.3±6.5
L-NAME+Indo+apamin+TRAM+IbTX	12	26.47±3.83***	43.6±3.0

Table 3.2 Effects of K_{Ca} channels blockers on tension in rabbit iliac arteries in the presence of L-NAME and indomethacin. Data given as mean±sem. *** denote p<0.001 compared with control; and the $^{+}$ denote p<0.05 compared with IbTX alone in one-way ANOVA.

3.3.3 Effects of H_2O_2 on responses to CPA in the absence and presence of L-NAME/indomethacin in rabbit iliac arteries.

In control iliac rings (endothelium-intact iliac rings in the absence of L-NAME/indomethacin), the additional contribution of NO to CPA-evoked relaxations was evidenced by pIC_{50} values of ~5.1, and increases in R_{max} to ~95% from ~85% compared to the corresponding EDHF-type concentration-relaxation curves (n=14; Table 3.3; control data pooled). In the absence of L-NAME/indomethacin, pre-incubation with 100 μM H_2O_2 for 30 minutes had no significant difference in pIC_{50} and R_{max} compared to control (n=7; Figure 3.3A; Table 3.3). In the presence of L-NAME/indomethacin, pre-incubation with 100 μM H_2O_2 for 30 minutes caused a significant potentiation on responses evoked by CPA, such that pIC_{50} increased from 4.67±0.05 to 5.36±0.23 (p<0.05; n=5) without alteration in overall R_{max} (Figure 3.3B; Table 3.3).

3.3.4 Effects of H_2O_2 on responses to ACh in the absence and presence of L-NAME/indomethacin in rabbit iliac arteries.

In control iliac rings, the additional contribution of NO to ACh-evoked relaxations was evidenced by pEC_{50} values of ~7.1, and increases in R_{max} to ~90% from ~80% compared to the corresponding EDHF-type concentration-relaxation curves (n=17; Table 3.4; control data pooled). In the absent of L-NAME/indomethacin, ACh-evoked responses was not affected by the addition of 100 μM H_2O_2 for 30 minutes (Figure 3.4A) and therefore no significant difference in neither pEC_{50} nor R_{max} (n=11; Table 3.4). In the presence of L-NAME/indomethacin, pre-incubation with 100 μM H_2O_2 for 30 minutes caused a significant potentiation on responses evoked by ACh, and pEC_{50} was increased from 6.51±0.05 to 7.53±0.10 (p<0.001; n=5) without alteration in overall R_{max} (Figure 3.4B; Table 3.4).

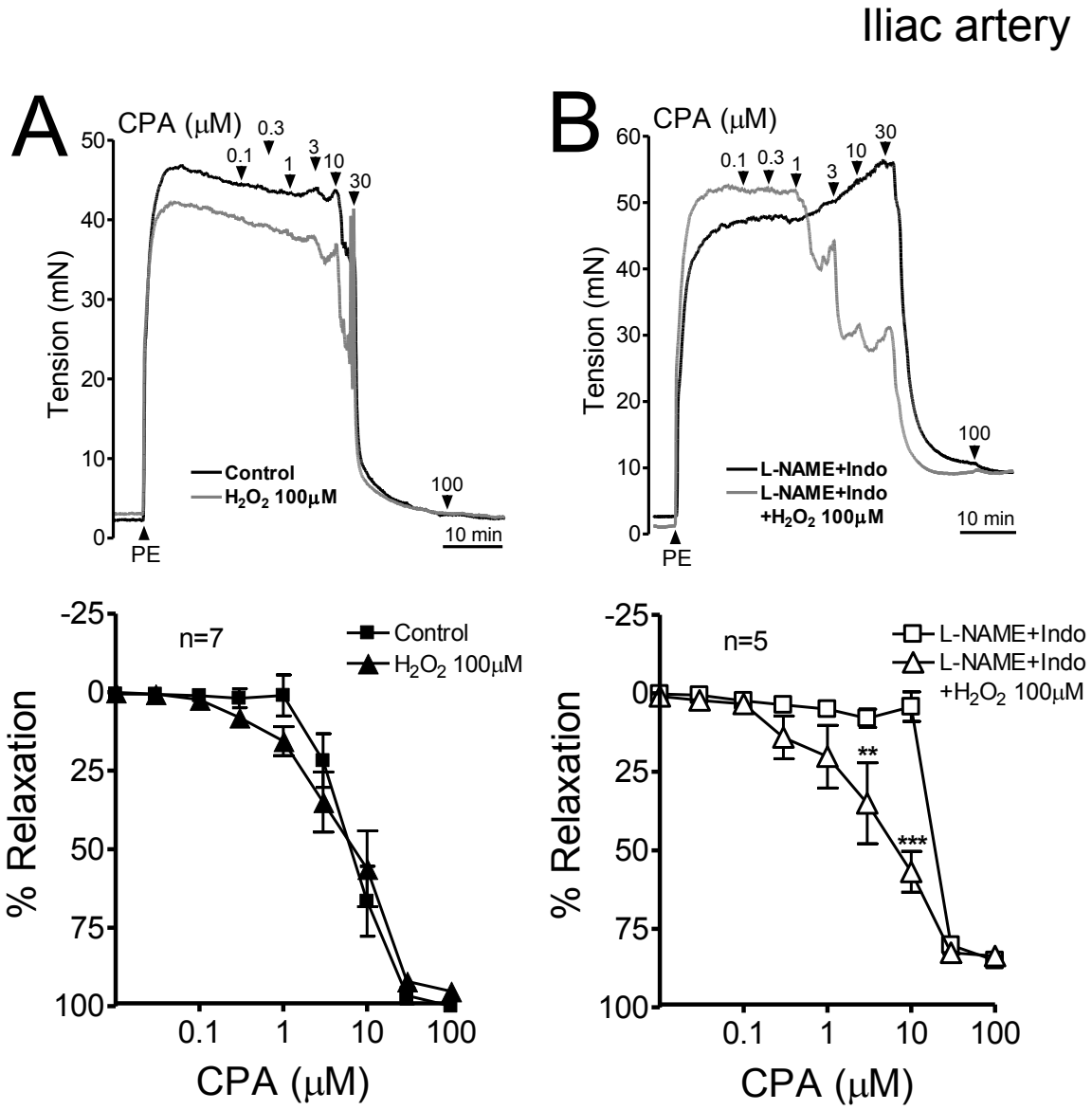

Figure 3.3 Effects of 100 μM H_2O_2 on relaxations evoked by CPA in endothelium-intact rabbit iliac rings. (A) In the absence of L-NAME and indomethacin, 100 μM H_2O_2 had no effect on responses to CPA. (B) In the presence of L-NAME and indomethacin, 100 μM H_2O_2 significantly potentiated CPA-evoked relaxation. ** and *** denote 0.01 and 0.001 compared with corresponding control in two-way ANOVA. n denotes the number of animals studied.

Iliac artery

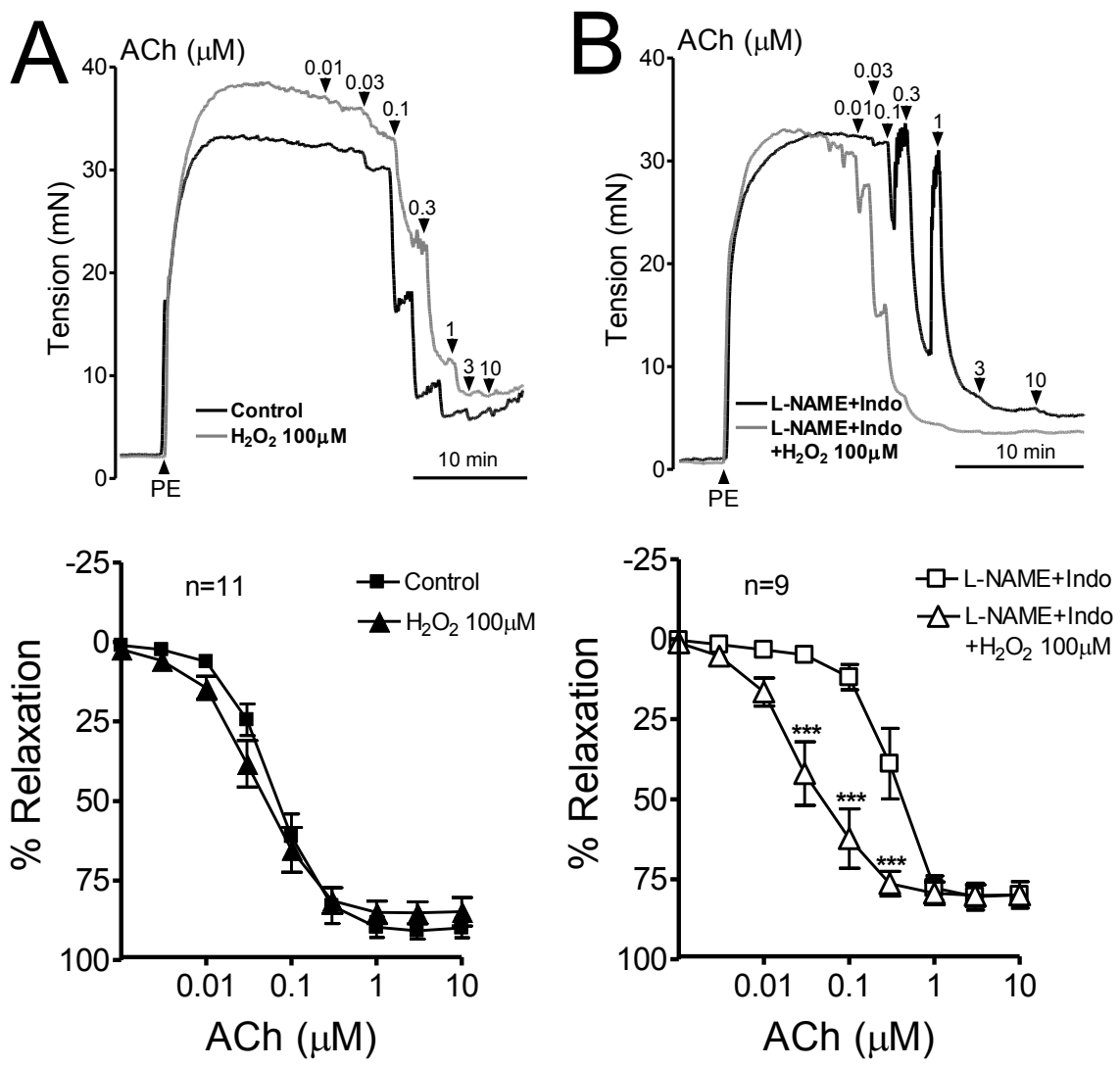

Figure 3.4 Effects of 100 μM H_2O_2 on relaxations evoked by ACh in endothelium-intact rabbit iliac rings. (A) In the absence of L-NAME and indomethacin, 100 μM H_2O_2 had no effect on responses to ACh. (B) In the presence of L-NAME and indomethacin, 100 μM H_2O_2 significantly potentiated ACh-evoked relaxation. *** denote 0.001 compared with corresponding control in two-way ANOVA. n denotes the number of animals studied.

Rabbit iliac artery			
Intervention	**N**	**pIC_{50}**	**R_{max}%**
30 minutes H_2O_2 incubation			
Control	7	5.19±0.09	98.5±0.7
H_2O_2 100 µM	7	5.26±0.15	95.3±1.5
L-NAME+Indo	5	4.67±0.05	85.1±2.7
L-NAME+Indo+H_2O_2 100 µM	5	5.36±0.23 *	83.7±2.8
30 minutes thimerosal incubation			
Control	7	5.11±0.07	96.7±0.9
Thimerosal 10 µM	7	6.12±0.16 ***	95.7±1.6
L-NAME+Indo	5	4.78±0.08	86.2±2.5
L-NAME+Indo+thimerosal 10 µM	5	5.95±0.17 **	83.6±2.1

Table 3.3 Effects of 100 µM H_2O_2 and 10 µM thimerosal on endothelium-intact arterial relaxations evoked by CPA. Potency (negative logIC_{50}) and maximal responses (R_{max}) are given as mean±SEM. *, ** and *** denote p<0.05, 0.01 and 0.001 compared with corresponding control in one-way ANOVA. n denotes the number of animals studied.

Rabbit iliac artery			
Intervention	**n**	**pEC_{50}**	**R_{max}%**
30 minutes H_2O_2 incubation			
Control	11	7.21±0.05	92.7±2.0
H_2O_2 100 µM	11	7.42±0.07	91.8±2.9
L-NAME+Indo	5	6.51±0.05	80.9±4.3
L-NAME+Indo+H_2O_2 100 µM	5	7.53±0.10 ***	81.6±2.4
30 minutes thimerosal incubation			
Control	6	7.06±0.04	92.7±2.0
Thimerosal 10 µM	6	7.49±0.04 *	91.6±2.4
L-NAME+Indo	4	6.53±0.05	78.7±2.4
L-NAME+Indo+thimerosal 10 µM	4	6.87±0.06 *	77.9±0.5

Table 3.4 Effects of 100 µM H_2O_2 and 10 µM thimerosal on endothelium-intact arterial relaxations evoked by ACh. Potency (negative logEC_{50}) and maximal responses (R_{max}) are given as mean±SEM. * and *** denote p<0.05 and 0.001 compared with corresponding control in one-way ANOVA. n denotes the number of animals studied.

3.3.5 Effects of thimerosal on responses to CPA in the absence and presence of L-NAME/indomethacin in rabbit iliac arteries.

In endothelium-intact iliac rings in the absence or presence of L-NAME/indomethacin, pre-incubation with 10 μM thimerosal for 30 minutes caused a significant potentiation on responses evoked by CPA without change in R_{max} (n=7 and 5 respectively; Figure 3.5; Table 3.3). The pIC_{50} was increased from 5.11±0.07 to 6.12±0.16 (p<0.001; n=7) for CPA responses and from 4.78±0.08 to 5.95±0.17 (p<0.01; n=5) for EDHF-type responses alone (Table 3.3).

3.3.6 Effects of thimerosal on responses to ACh in the absence and presence of L-NAME/indomethacin in rabbit iliac arteries.

In endothelium-intact iliac rings in the absence or presence of L-NAME/indomethacin, pre-incubation with 10 μM thimerosal for 30 minutes caused a significant potentiation on responses evoked by ACh without any alteration in R_{max} (Figure 3.6; Table 3.4). The pEC_{50} was increased from 7.06±0.04 to 7.49±0.04 (p<0.05; n=6) for ACh responses and from 6.53±0.05 to 6.87±0.06 (p<0.05; n=4) for EDHF-type responses alone (Table 3.4).

3.3.7 Effects of H_2O_2 on responses to MAHMA NONOate in rabbit iliac arteries.

In endothelium-intact iliac rings in the absence or presence of L-NAME/indomethacin, responses evoked by MAHMA NONOate was unaffected by 30 minutes incubation with 100 μM H_2O_2, with no significant change in pEC_{50} and R_{max} was observed (n=8; Figure 3.7; Table 3.5). In endothelium-denuded rings, H_2O_2 did not exert a significant effect when relaxation was induced by MAHMA NONOate compared to control, again , no significant change in pEC_{50} and R_{max} was observed (n=10; Figure 3.7; Table 3.5).

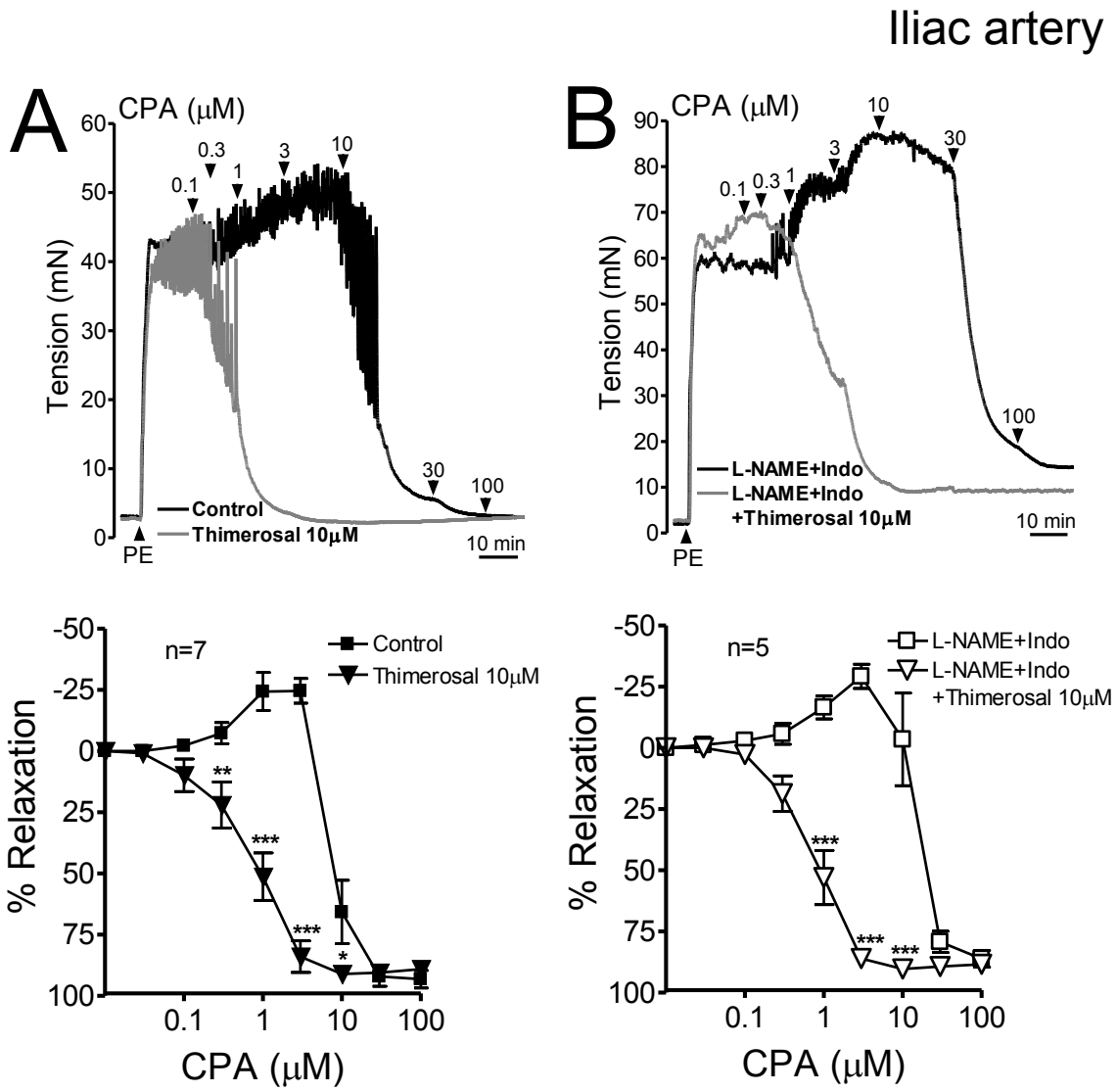

Figure 3.5 Effects of 10 μM thimerosal on relaxations evoked by CPA in endothelium-intact rabbit iliac rings. (A) In the absence of L-NAME and indomethacin, 10 μM thimerosal significantly potentiated responses to CPA. (B) In the presence of L-NAME and indomethacin, 10 μM thimerosal significantly potentiated CPA-evoked relaxation. *, ** and *** denote $p<0.05$, 0.01 and 0.001 compared with corresponding control in two-way ANOVA. n denotes the number of animals studied.

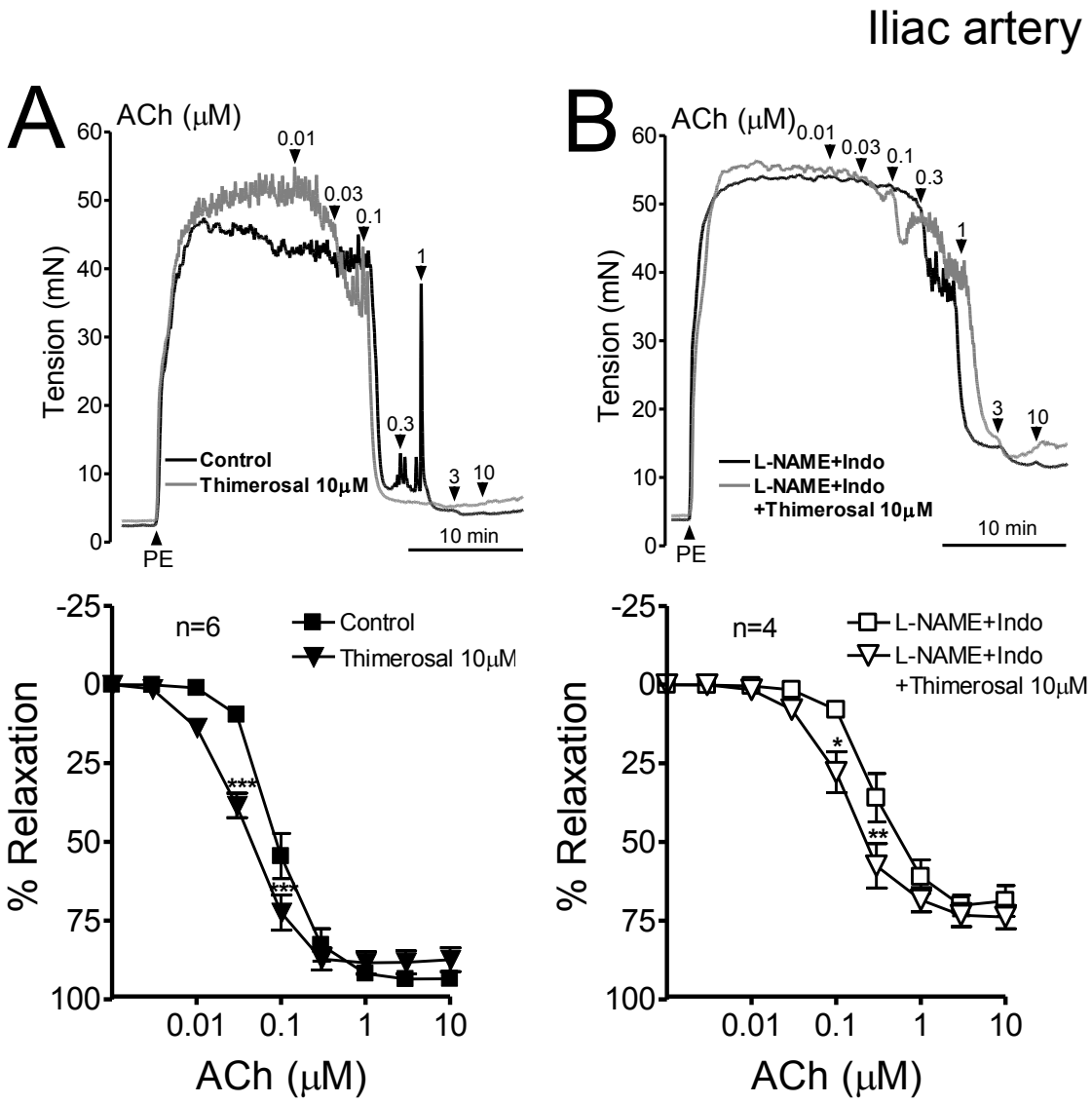

Figure 3.6 Effects of 10 μM thimerosal on relaxations evoked by ACh in endothelium-intact rabbit iliac rings. (A) In the absence of L-NAME and indomethacin, 10 μM thimerosal significantly potentiated responses to ACh. (B) In the presence of L-NAME and indomethacin, 10 μM thimerosal significantly potentiated ACh-evoked relaxation.*, ** and *** denote p<0.05, 0.01 and 0.001 compared with corresponding control in two-way ANOVA. n denotes the number of animals studied.

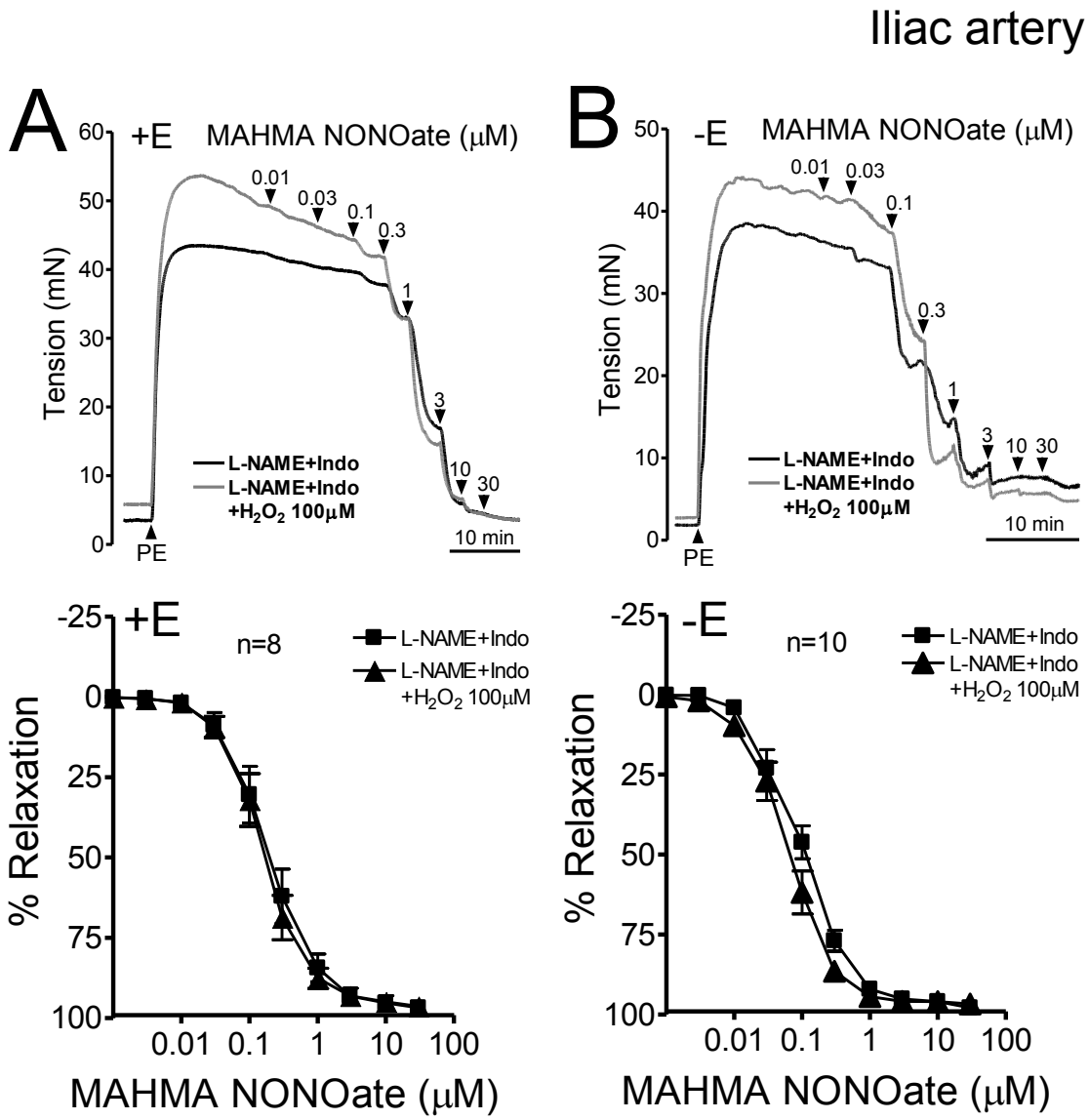

Figure 3.7 Concentration-response curves showing that pre-incubation with 100 μM H_2O_2 for 30 minutes did not affect (A) endothelium-dependent or (B) endothelium-denuded rabbit iliac ring relaxations evoked by MAHMA NONOate in the presence of L-NAME and indomethacin. n denotes the number of animals studied.

Rabbit iliac artery			
Intervention	**n**	**pEC_{50}**	**R_{max}%**
30 minutes H_2O_2 incubation			
L-NAME+Indo	8	6.73±0.06	96.3±2.9
L-NAME+Indo+H_2O_2 100 µM	8	6.80±0.05	95.3±2.2
Denuded Control	10	7.01±0.05	97.8±1.9
Denuded+H_2O_2 100 µM	10	7.20±0.05	96.8±1.9
30 minutes thimerosal incubation			
L-NAME+Indo	6	6.71±0.05	98.0±2.5
L-NAME+Indo+thimerosal 10 µM	6	6.11±0.06 *	95.9±4.0
Denuded Control	6	6.87±0.05	98.1±2.6
Denuded+thimerosal 10 µM	6	6.23±0.03 *	88.1±1.4 **
L-NAME+Indo	5	6.35±0.07	99.9±4.1
L-NAME+Indo+thimerosal 1 µM	5	6.57±0.08	102.7±5.3
Denuded Control	5	6.37±0.07	99.8±4.1
Denuded+thimerosal 1 µM	5	6.58±0.08	101.6±4.8

Table 3.5 Concentration-dependent effects of H_2O_2 and thimerosal on endothelium-intact arterial relaxations evoked by MAHMA NONOate. Potency (negative logEC_{50}) and maximal responses (R_{max}) are given as means±SEM. * and ** denote p<0.05 and 0.01 compared with corresponding control in Student's t-test. n denotes the number of animals studied.

3.3.8 Effects of thimerosal on responses to MAHMA NONOate in rabbit iliac arteries.

In endothelium-intact iliac rings in the presence of L-NAME/indomethacin and in endothelium-denuded rings, pre-incubation with 10 µM thimerosal for 30 minutes induced a significant potentiation on responses evoked by MAHMA NONOate. The pEC_{50} decreased from 6.71±0.05 to 6.11±0.06 (p<0.05; n=6) for endothelium-intact rings without change in R_{max} and pEC_{50} decreased from 6.87±0.05 to 6.23±0.03 (p<0.05; n=6) for denuded rings with a significant decrease in R_{max} from 98.1±2.6% to 88.1±1.4% (p<0.01; n=6; Figure 3.8; Table 3.5). However, this attenuation on relaxation was rescued when the concentration of thimerosal used decreased from 10 µM to 1 µM. Pre-incubation with 1 µM thimerosal for 30 minutes has no effect on relaxations evoked by MAHMA NONOate in endothelium-intact and -denuded iliac rings in terms of pEC_{50} and R_{max} (n=5 for each; Figure 3.9; Table 3.5).

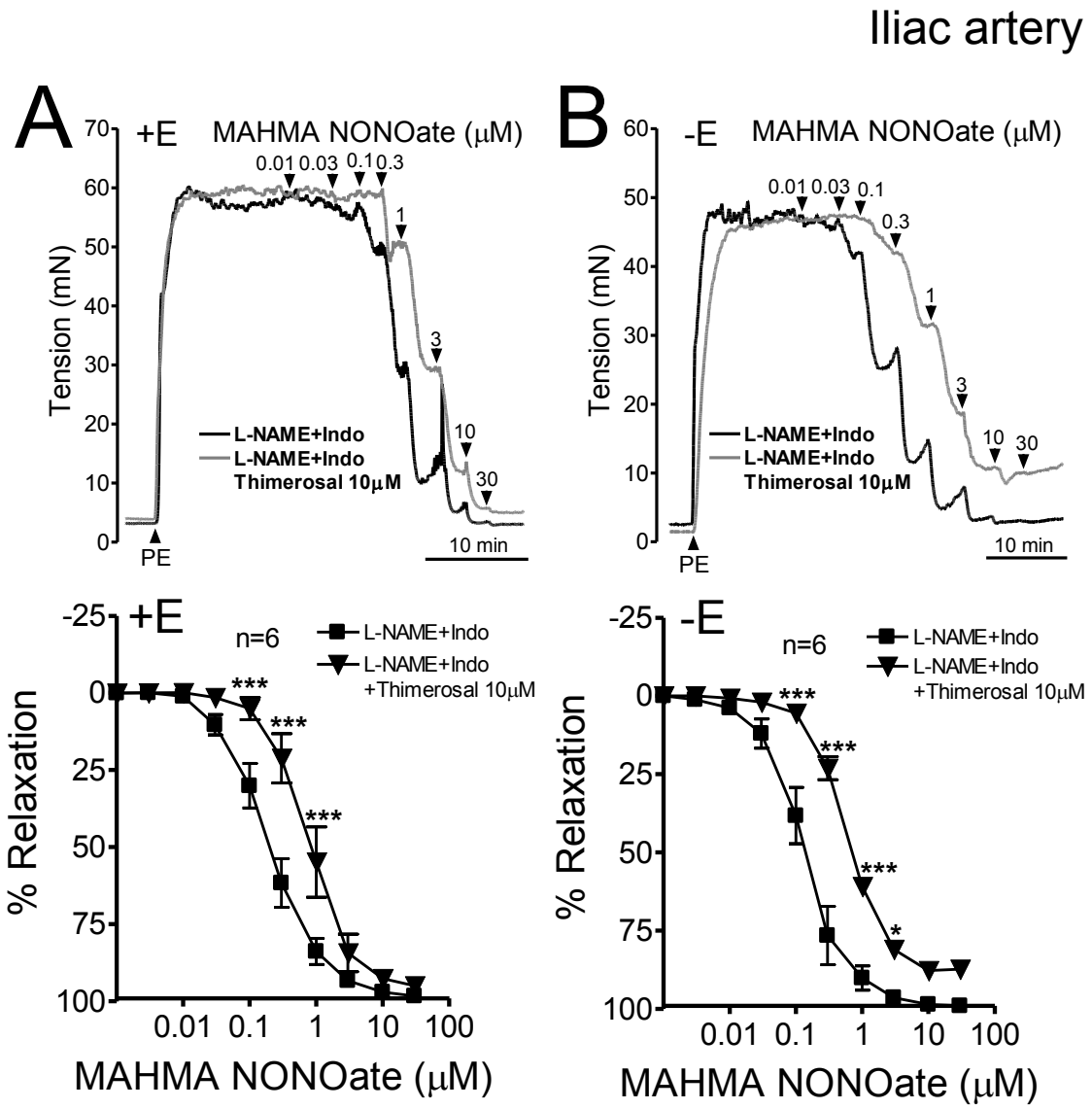

Figure 3.8 Concentration-response curves showing that pre-incubation with 10 μM thimerosal for 30 minutes attenuated both (A) endothelium-dependent and (B) endothelium-denuded rabbit iliac ring relaxations evoked by MAHMA NONOate in the presence of L-NAME and indomethacin. *and *** denote $p<0.05$ and 0.001 compared with corresponding control in two-way ANOVA. n denotes the number of animals studied.

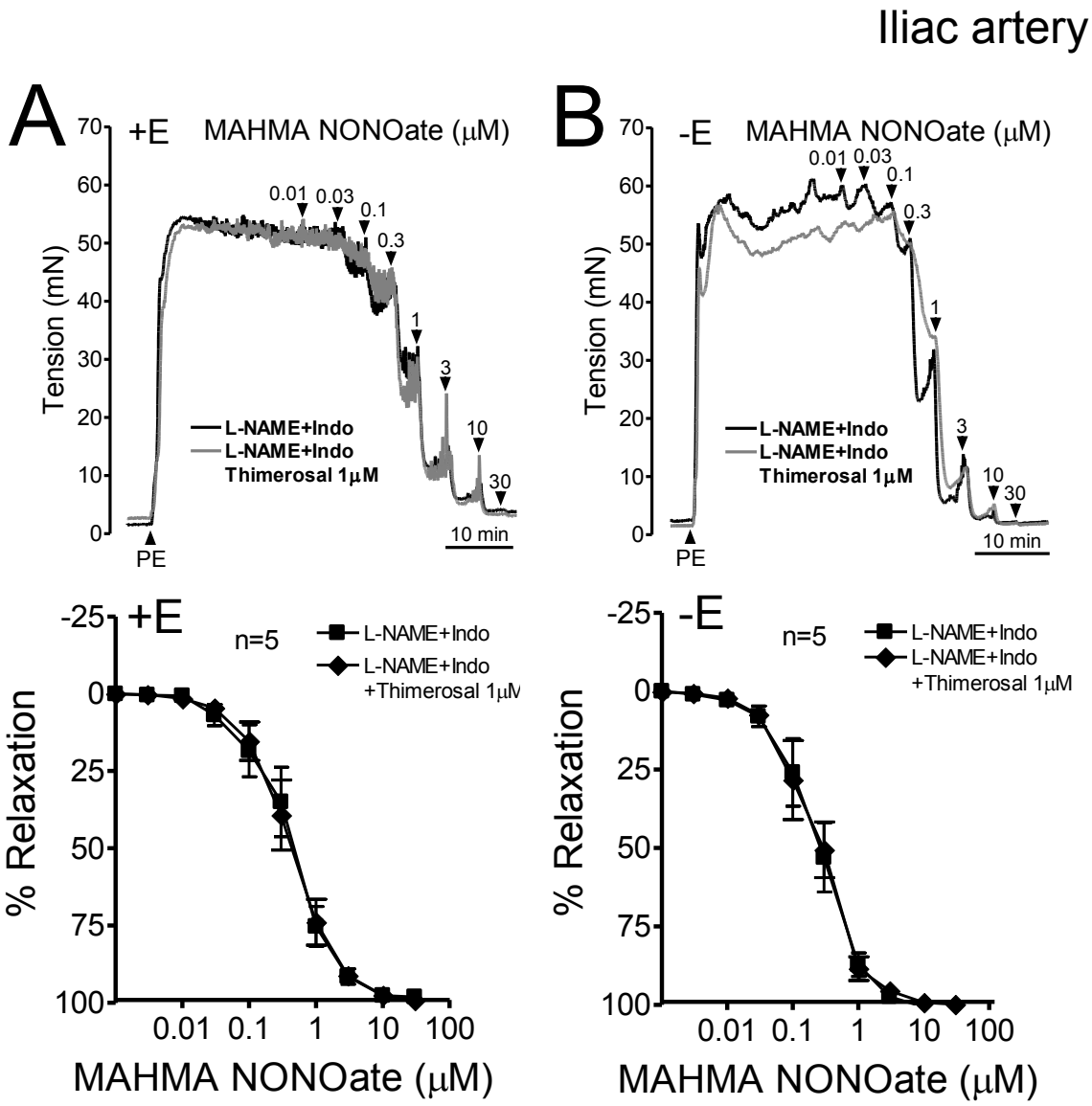

Figure 3.9 Concentration-response curves showing that pre-incubation with 1 μM thimerosal for 30 minutes did not affect (A) endothelium-dependent or (B) endothelium-denuded rabbit iliac ring relaxations evoked or by MAHMA NONOate in the presence of L-NAME and indomethacin. n denotes the number of animals studied.

3.3.9 Relaxations to exogenous H_2O_2 and thimerosal in rabbit aorta

In endothelium-intact and -denuded aortic rings in the absence or presence of L-NAME/indomethacin, relaxations evoked by exogenous H_2O_2 were evident at concentrations ≥ 100 μM (n=5; Figure 3.10A). In comparison, thimerosal did not itself evoke relaxation at concentrations ≤ 100 μM in endothelium-denuded rings or in endothelium-intact rings in the presence of L-NAME/indomethacin. However, in control rings, at concentrations ≥ 3 μM, thimerosal induced a triphasic response consisting of an endothelium-dependent relaxation superimposed on a biphasic direct smooth muscle response in which constriction preceded relaxation (n=5; Figure 3.10B). This thimerosal-induced endothelium-dependent relaxation was peaked ~50% at 10 μM. No pEC_{50} or R_{max} can be calculated.

3.3.10 Effects of H_2O_2 and thimerosal on responses to CPA in rabbit aorta.

In control aortic rings (endothelium-intact aortic rings in the absence of L-NAME/indomethacin), maximal relaxations evoked by CPA were equivalent to ~70% (n=20; Table 3.6; control data pooled) of PE-induced tone and were mediated by NO because no significant EDHF-type component was evident in the presence of L-NAME/indomethacin (p<0.001; n=5; Table 3.6). In the absence of L-NAME/indomethacin, pre-incubation with 100 μM H_2O_2 for 30 minutes caused significant inhibition on the relaxation evoked by CPA (Figure 3.11A), thus that the pIC_{50} was not affected but R_{max} was decreased from 72.9±2.5% to 59.1±1.8% (p<0.01; n=10 and 5 respectively; Table 3.6). Pre-incubation with 10 μM thimerosal for 30 minutes also caused significant inhibition on the relaxation evoked by CPA (Figure 3.11B), the R_{max} was decreased from 71.4±3.0% to 30.2±2.2% (p<0.001; n=10 and 5 respectively; Table 3.6). NO pIC_{50} can be calculated.

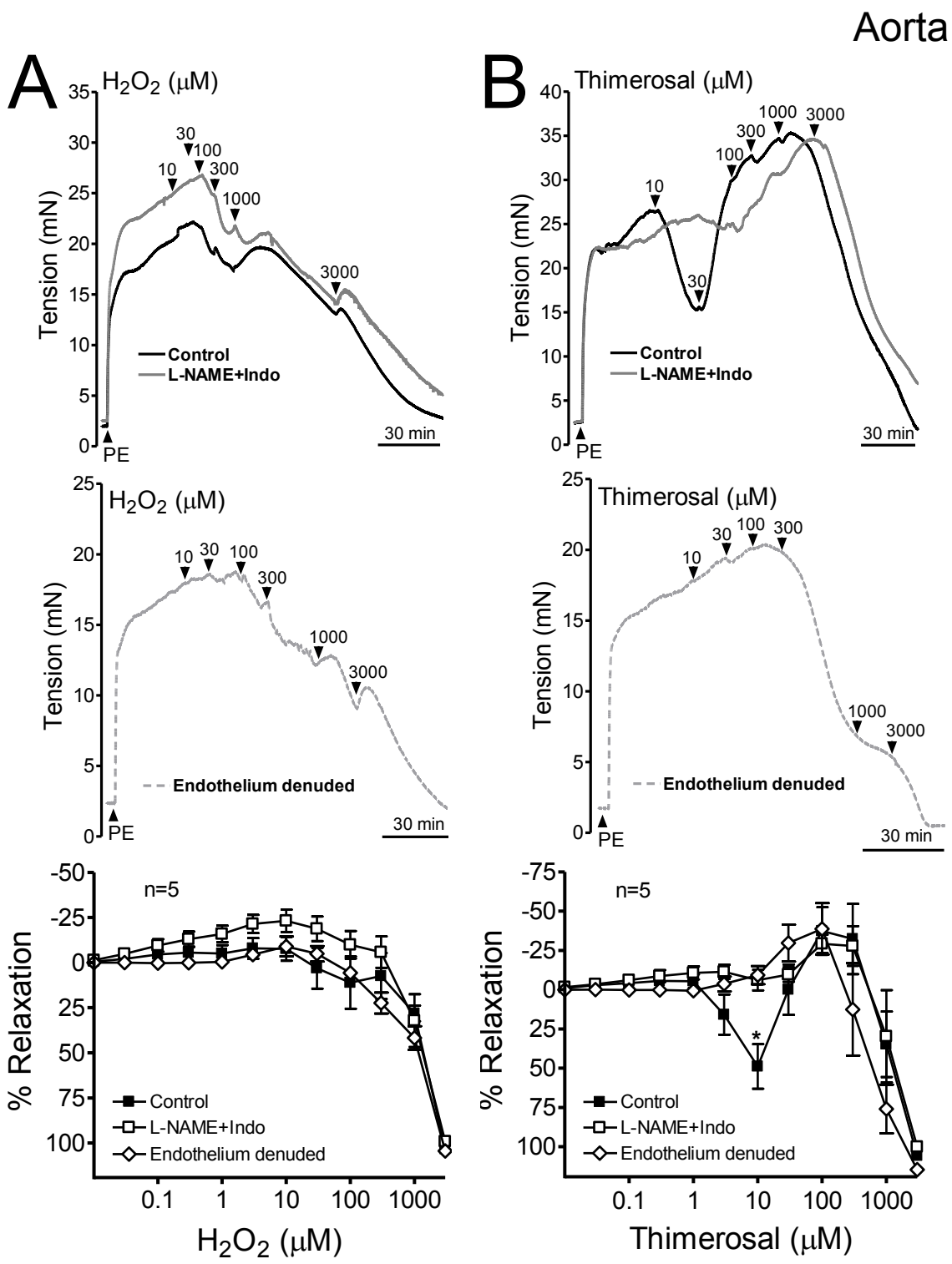

Figure 3.10 Cumulative Dose-response Curves to (A) H_2O_2 and (B) thimerosal in rabbit aortic rings in the presence of indomethacin. (A) 0-100 μM H_2O_2 has minimal effect on aorta regardless of the presence or absence of endothelium. (B) 10 μM thimerosal caused approximately 50% relaxation in control rings with intact endothelium. * denote $p<0.05$ compared with corresponding control in two-way ANOVA. n denotes the number of animals studied.

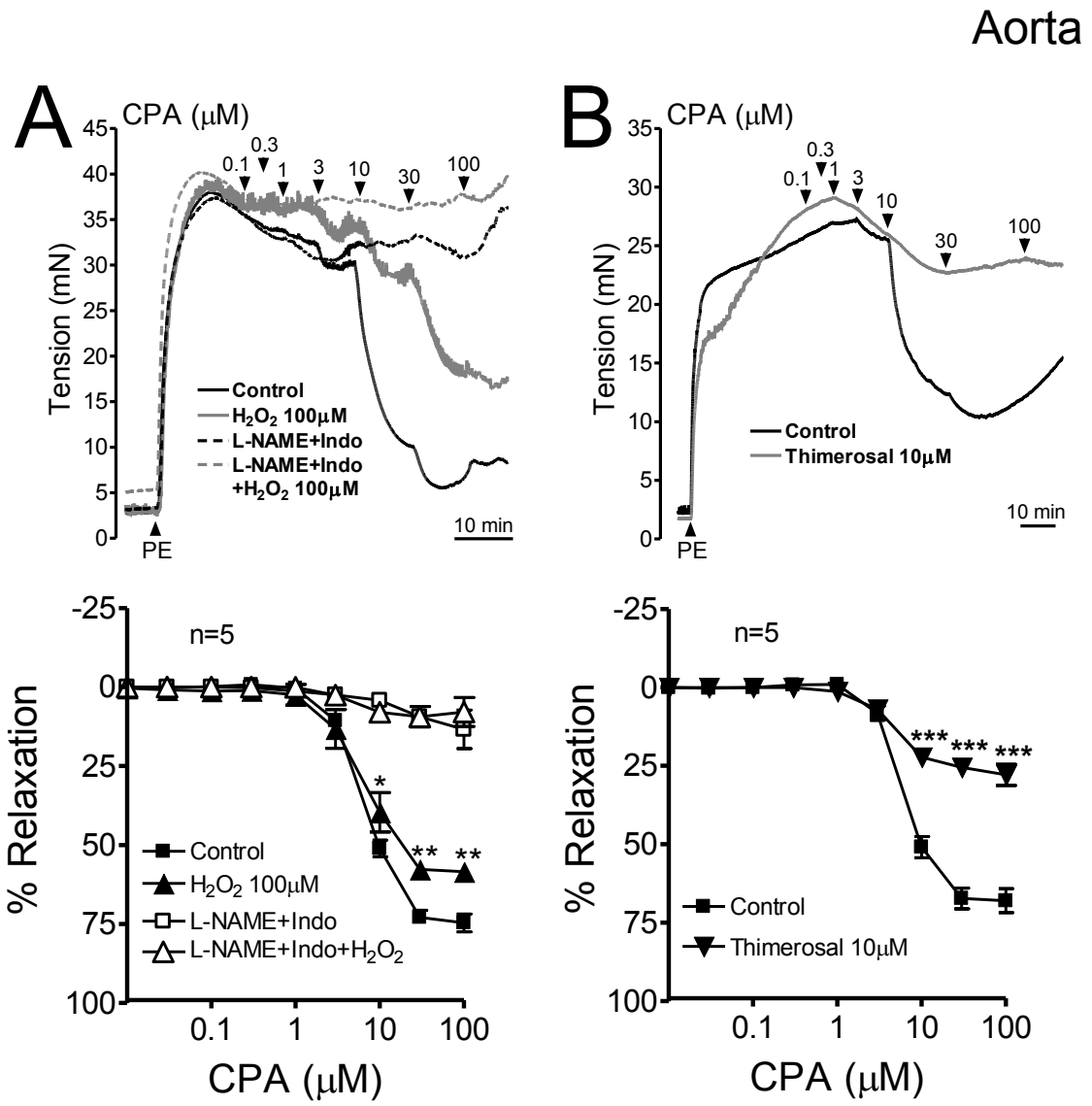

Figure 3.11 In rabbit aorta, pre-incubation with L-NAME and indomethacin attenuated relaxation to CPA. In the presence of indomethacin, CPA evoked concentration-response curves were significantly inhibited with 30 minutes pre-incubation by either (A) 100 μM H_2O_2 or (B) 10 μM thimerosal. *, ** and *** denote p<0.05, 0.01 and 0.001 compared with corresponding control in two-way ANOVA. n denotes the number of animals studied.

Rabbit aorta			
Intervention	**n**	**pIC_{50}**	**R_{max}%**
30 minutes H_2O_2 incubation			
Control	10	5.15±0.02	72.9±2.5
H_2O_2 30 μM	5	5.21±0.05	70.3±5.5
H_2O_2 100 μM	5	5.18±0.06	59.1±1.8 **
L-NAME+Indo	5	Relaxation<50%	16.8±4.6 ***
L-NAME+Indo+H_2O_2 100 μM	5	Relaxation<50%	9.8±1.9 ***
30 minutes thimerosal incubation			
Control	10	5.19±0.03	71.4±3.0
Thimerosal 1 μM	5	6.06±0.17 *	75.0±6.9
Thimerosal 10 μM	5	Relaxation<50%	30.2±2.2 ***

Table 3.6 Concentration-dependent effects of H_2O_2 and thimerosal on endothelium-intact arterial relaxations evoked by CPA. Potency (negative logIC_{50}) and maximal responses (R_{max}) are given as mean±SEM. *, ** and *** denote p<0.05, 0.01 and 0.001 compared with corresponding control in Student's t-test or one-way ANOVA. n denotes the number of animals studied.

3.3.11 Effects of H_2O_2 and thimerosal on responses to ACh in rabbit aorta.

In control aortic rings, maximal relaxations evoked by ACh were equivalent to ~70% (n=20; Table 3.7; control data pooled) of PE-induced tone and were mediated by NO because no significant EDHF-type component was evident in the presence of L-NAME/indomethacin (p<0.001; n=5; Table 3.7). In the absence of L-NAME/indomethacin, pre-incubation with 100 μM H_2O_2 for 30 minutes caused significant inhibition on the relaxation evoked by ACh (Figure 3.12A), thus that the pEC_{50} was not affected but R_{max} was decreased from 73.9±1.4% to 57.9±2.8% (p<0.01; n=10 and 5 respectively; Table 3.7). Pre-incubation with 10 μM thimerosal for 30 minutes also caused significant inhibition on the relaxation evoked by ACh (Figure 3.12B)., the R_{max} was decreased from 72.6±1.3 to 30.0±4.7% (p<0.001; n=10 and 5 respectively; Table 3.7). No pIC_{50} can be calculated.

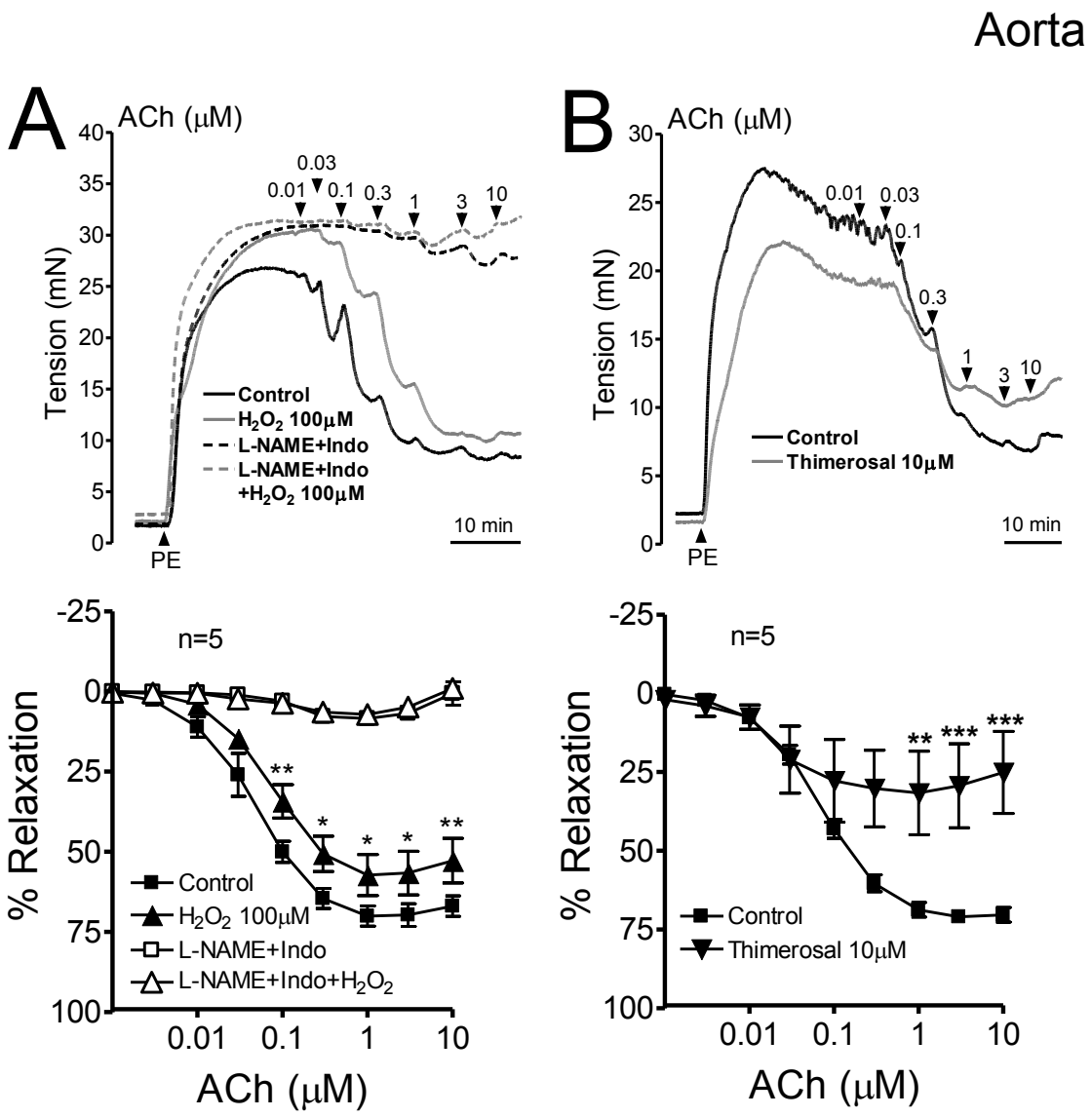

Figure 3.12 In rabbit aorta, pre-incubation with L-NAME and indomethacin attenuated relaxation to ACh. In the presence of indomethacin, ACh evoked concentration-response curves were significantly inhibited with 30 minutes pre-incubation by either (A) 100 μM H_2O_2 or (B) 10 μM thimerosal. *, ** and *** denote p<0.05, 0.01 and 0.001 compared with corresponding control in two-way ANOVA. n denotes the number of animals studied.

Rabbit aorta			
Intervention	**n**	**pEC_{50}**	**R_{max}%**
30 minutes H_2O_2 incubation			
Control	10	7.28±0.05	73.9±1.4
H_2O_2 30 μM	5	6.97±0.08	73.5±2.9
H_2O_2 100 μM	5	7.20±0.13	57.9±2.8 **
L-NAME+Indo	5	Relaxation<50%	5.9±1.0 ***
L-NAME+Indo+H_2O_2 100 μM	5	Relaxation<50%	0.3±1.4 ***
30 minutes thimerosal incubation			
Control	10	7.16±0.05	72.6±1.3
Thimerosal 1 μM	5	7.46±0.10 **	76.6±2.3
Thimerosal 10 μM	5	Relaxation<50%	30.0±4.7 ***
Denuded rings 30mins mhama	**n**	**pEC_{50}**	**R_{max}%**
Denuded Control	6	7.31±0.05	99.5±3.0
Denuded+H_2O_2 100 μM	6	7.21±0.06	98.1±2.5
Denuded+thimerosal 10 μM	6	6.82±0.08 ***	82.1±3.0 **

Table 3.7 Concentration-dependent effects of 30 minutes incubation with H_2O_2 and thimerosal on endothelium-intact arterial relaxations evoked by ACh and endothelium-denuded arterial relaxations evoked by MAHMA NONOate. Potency (negative logEC_{50}) and maximal responses (R_{max}) are given as mean±SEM. ** and *** denote p<0.01 and 0.001 compared with corresponding control in Student's t-test or one-way ANOVA. n denotes the number of animals studied.

3.3.12 Effects of H_2O_2 and thimerosal on responses to MAHMA NONOate in rabbit aorta.

In endothelium-denuded aortic rings, concentration-relaxation curves evoked by MAHMA NONOate were unaffected by pre-incubation with 100 μM H_2O_2 for 30 minutes (n=6; Figure 3.13). However, pre-incubation with 10 μM thimerosal for 30 minutes caused a significant inhibition on the relaxation evoked by MAHMA NONOate, such that pEC_{50} decreased from 7.31±0.05 to 6.82±0.08 (p<0.001; n=6) with R_{max} decreased from 99.5±3.0% to 82.1±3.0% (p<0.01; n=6; Figure 3.13; Table 3.7).

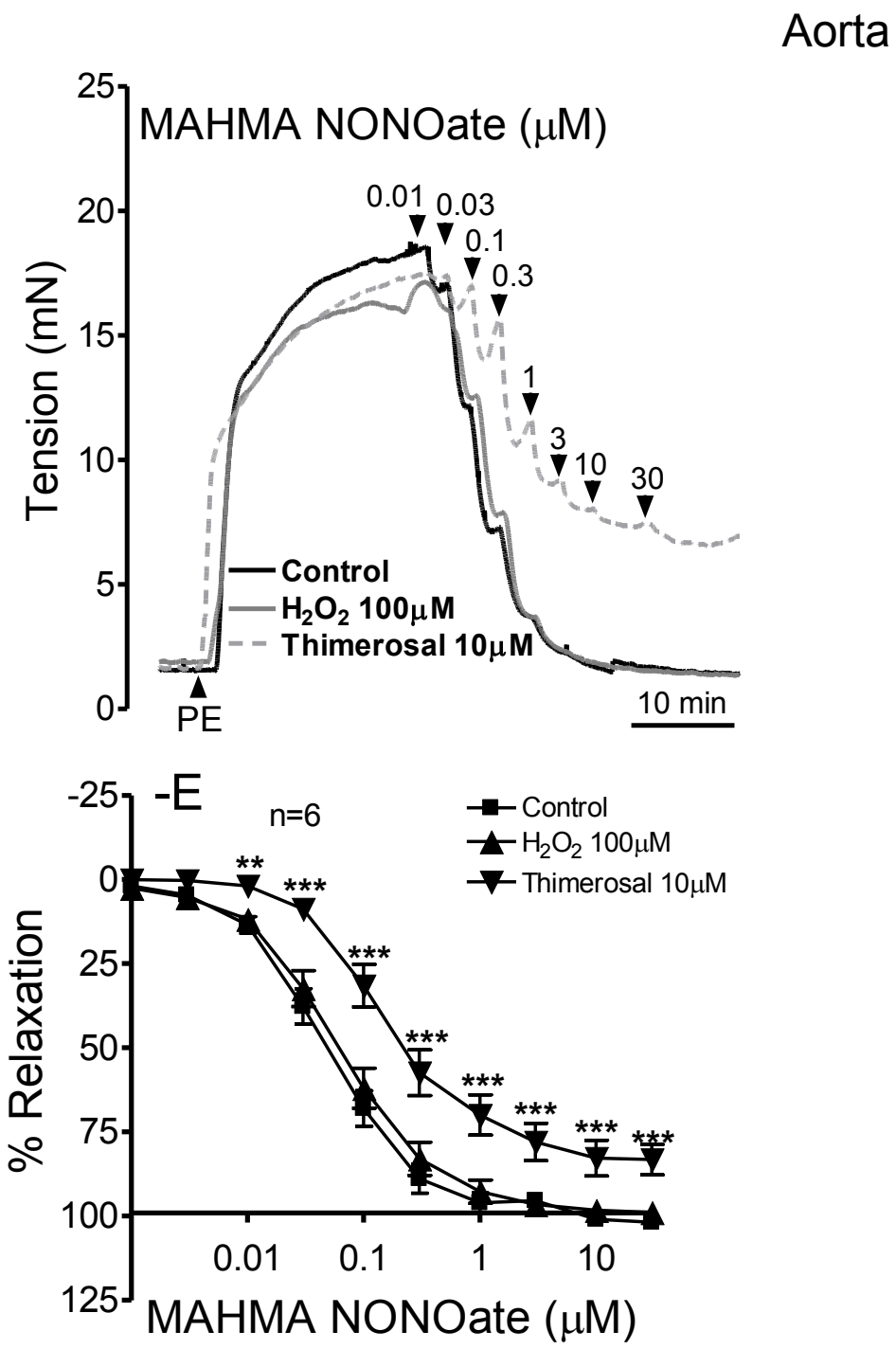

Figure 3.13 Effects of 100 μM H_2O_2 and 10 μM thimerosal in endothelium-denuded rabbit aortic rings in the presence of L-NAME and indomethacin. No difference was found on MAHMA NONOate-evoked relaxations in rings pre-incubated with 100 μM H_2O_2, however, a significant inhibition in the concentration-relaxation curves was observed with 10 μM thimerosal pre-incubation. ** and *** denote p<0.01 and 0.001 compared with corresponding control in two-way ANOVA. n denotes the number of animals studied.

3.3.13 Effects of lower concentrations of H_2O_2 and thimerosal on responses to CPA in rabbit aorta.

In control aortic rings, pre-incubation with 30 μM H_2O_2 for 30 minutes had no significant effect on responses evoked by CPA in terms of pEC_{50} and R_{max} (n=5; Figure 3.14A; Table 3.6). Pre-incubation with 1 μM thimerosal for 30 minutes caused a significant potentiation on responses evoked by CPA with a significant increase in pIC_{50} from 5.19±0.03 to 6.06±0.17 (p<0.05, n=10 and 5 respectively) without change in R_{max} (Figure 3.14B; Table 3.6).

3.3.14 Effects of lower concentrations of H_2O_2 and thimerosal on responses to ACh in rabbit aorta.

In control aortic rings, pre-incubation with 100 μM H_2O_2 for 30 minutes had no significant effect on responses evoked by ACh in terms of pEC_{50} and R_{max} (n=5; Figure 3.15A; Table 3.7). Pre-incubation with 1 μM thimerosal for 30 minutes caused a significant potentiation on responses evoked by ACh with a significant increase in pEC_{50} from 7.16±0.05 to 7.46±0.10 (p<0.01; n=10 and 5 respectively) without change in R_{max} (Figure 3.15B; Table 3.7).

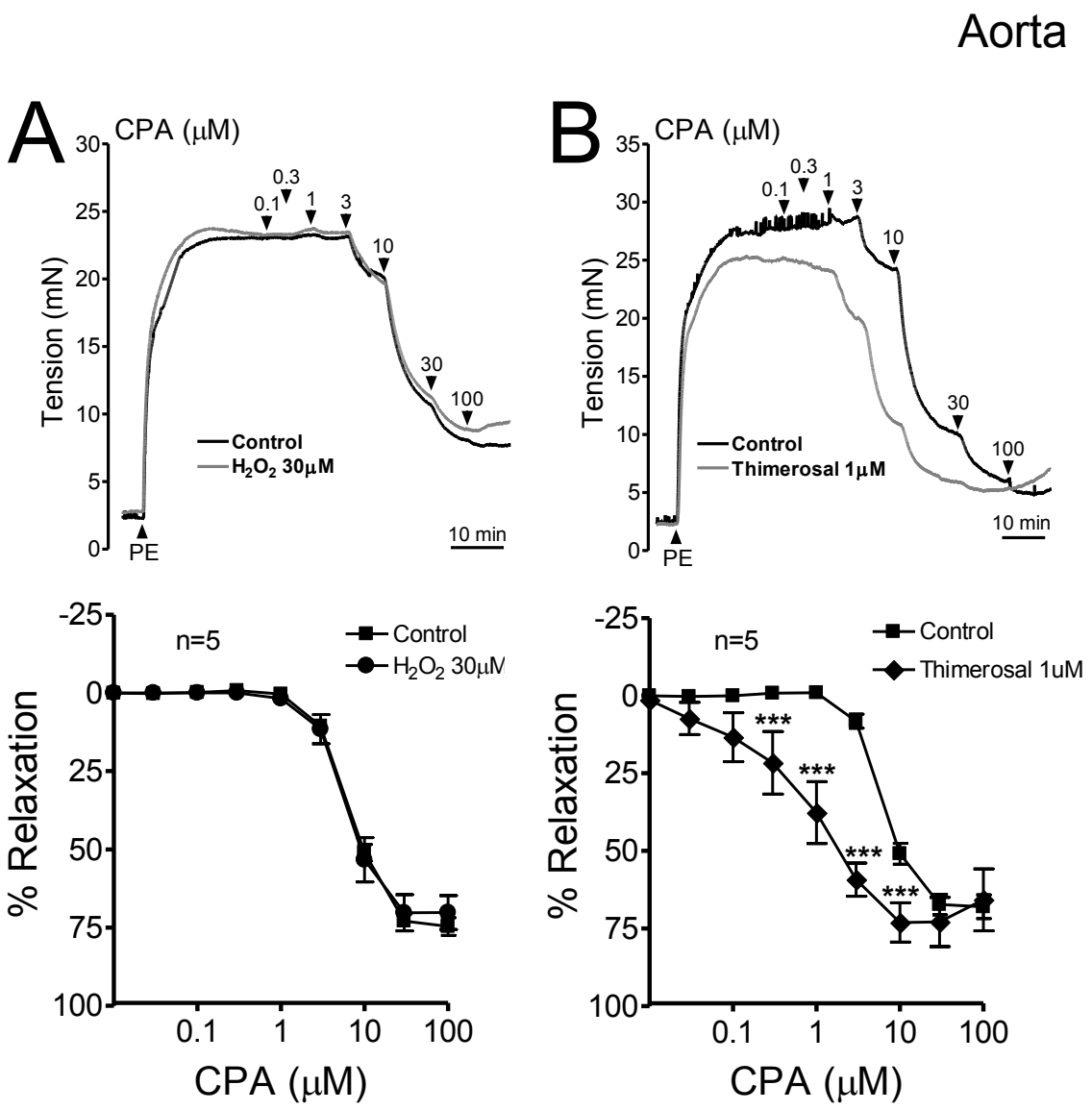

Figure 3.14 In rabbit aorta, in the presence of indomethacin, CPA evoked concentration-response curves were not affected with 30 minutes pre-incubation by (A) 30 μM H_2O_2, but were significantly inhibited by (B) 1 μM thimerosal. Representative graphs were shown on top. *** denote $p<0.001$ compared with corresponding control in two-way ANOVA. n denotes the number of animals studied.

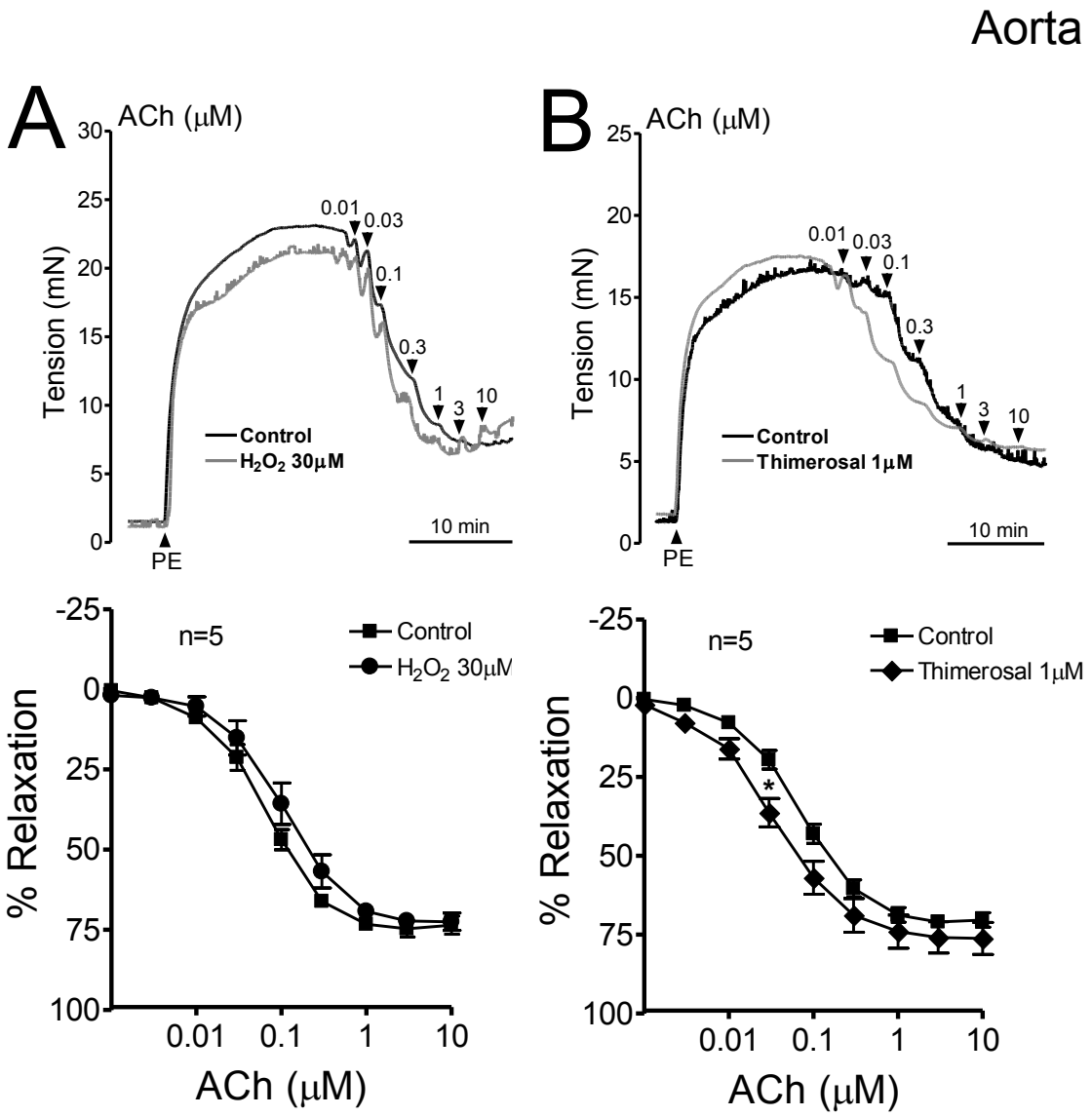

Figure 3.15 In rabbit aorta, in the presence of indomethacin, ACh evoked concentration-response curves were not affected by 30 minutes pre-incubation with (A) 30 μM H_2O_2, but were significantly inhibited by (B) 1 μM thimerosal. * denote $p<0.05$ compared with corresponding control in two-way ANOVA. n denotes the number of animals studied.

3.3.15 Effects of H_2O_2 and thimerosal on contraction induced by PE

In control iliac rings, the magnitude of the constrictor response to 1 μM PE was unaffected by pre-incubation with 100 μM H_2O_2 or 10 μM thimerosal for 30 minutes. PE-induced constriction was not altered by incubation with L-NAME/indomethacin and was not changed by pre-incubation with 100 μM H_2O_2, 1 μM or 10 μM thimerosal in L-NAME/indomethacin treated iliac rings. In iliac rings that carefully denuded of their endothelium, the PE-induced constriction matched the level observed in control rings, and this constriction was not affected by pre-incubations with 100 μM H_2O_2, 1 μM or 10 μM thimerosal for 30 minutes (Table 3.8, data pooled from all experiments).

Rabbit iliac artery		
Intervention	**n**	**PE-induced tone (mN)**
Control	31	48.5±1.2
L-NAME+Indo	38	48.7±1.4
Denuded Control	21	49.5±2.7
30 minutes H_2O_2 incubation		
H_2O_2 100 μM	20	45.9±1.8
L-NAME+Indo+H_2O_2 100 μM	18	48.6±2.0
Denuded+H_2O_2 100 μM	10	47.8±4.3
30 minutes thimerosal incubation		
Thimerosal 10 μM	13	48.9±2.5
L-NAME+Indo+thimerosal 1 μM	5	48.6±2.5
L-NAME+Indo+thimerosal 10 μM	15	50.5±2.1
Denuded+thimerosal 1 μM	5	48.6±5.7
Denuded+thimerosal 10 μM	6	49.2±4.0

Table 3.8 Effect of L-NAME/indomethacin, H_2O_2 and thimerosal on arterial tone induced by PE in endothelium-intact and endothelium-denuded rabbit iliac rings. There was no significant difference between PE-induced tone in rings compared with time-matched preparations incubated for the same periods without or without these treatments. Data given as mean±SEM. n denotes the number of animals studied. Data pooled from Figure 3.3 to Figure 3.9.

In aortic rings, the magnitude of the contraction to 1 μM PE was unaffected by pre-incubation with L-NAME/indomethacin (although the relaxations were minimal), by endothelium removal or by pre-incubation with 100 μM H_2O_2, 1 μM or 10 μM thimerosal (Table 3.9, data pooled from all experiments).

Rabbit aorta		
Intervention	**n**	**PE-induced tone (mN)**
Control	40	23.1±0.6
L-NAME+Indo	10	24.3±1.2
Denuded Control	6	22.4±1.9
30 minutes H_2O_2 incubation		
H_2O_2 30 μM	10	23.7±1.7
H_2O_2 100 μM	10	22.4±0.9
Denuded+H_2O_2 100 μM	6	22.5±2.4
30 minutes thimerosal incubation		
Thimerosal 1 μM	10	22.2±1.3
Thimerosal 10 μM	10	22.7±1.5
Denuded+thimerosal 10 μM	6	22.3±1.4

Table 3.9 Effect of L-NAME/indomethacin, H_2O_2 and thimerosal on arterial tone induced by PE in endothelium-intact and endothelium-denuded rabbit aorta. There was no significant difference between PE-induced tone in rings compared with time-matched preparations incubated for the same periods without or without these treatments. Data given as mean±SEM. n denotes the number of animals studied. Data pooled from Figure 3.11 to Figure 3.15.

3.4 DISCUSSION

3.4.1 Current investigations

To summarize the main findings of the current chapter: (i) Vascular K_{Ca} channels participate in an interactive manner in the EDHF phenomenon in the rabbit iliac artery; (ii) H_2O_2 can amplify EDHF-type relaxations evoked by ACh in the rabbit iliac artery, confirming previous findings with CPA; (iii) H_2O_2 had no effect on relaxations mediated by NO in response to CPA or ACh, (i.e.) in the absence of L-NAME/indomethacin, or to the NO donor MAHMA NONOate in the rabbit iliac artery; (iv) Relaxations to CPA and ACh in the rabbit aorta were sensitive to L-NAME therefore mediated exclusively by NO, and (v) H_2O_2 exerted a concentration-dependent inhibitory effect on NO-dependent relaxations evoked by CPA and ACh in the rabbit aorta through an as yet unknown action on endothelial cells.

Incubation of rabbit iliac artery with selective inhibitors of vascular K_{Ca} channel blockers, namely apamin (SK_{Ca}), TRAM-34 (IK_{Ca}) and IbTX (BK_{Ca}), provided evidence that all three channel subtypes contribute to the EDHF-type response in the rabbit iliac artery. In the EDHF-type relaxations evoked by ACh, minimal inhibition was apparent with apamin or TRAM-34 alone, whereas IbTX or the double combination (apamin+TRAM) caused ~30% reduction to the maximal relaxant response and further reduction to ~90% was achieved with all three inhibitors present. Similar observations have been reported with CPA-evoked relaxations in the presence of L-NAME/indomethacin (Edwards *et al.*, 2008), thus the results in this chapter confirm the generality of the findings in this artery type between receptor-dependent and –independent stimulation. It should be noted that the expression of SK_{Ca}, IK_{Ca} and BK_{Ca}, in native arterial endothelium exhibits both species and vessel heterogeneity (Rusko *et al.*, 1992; Murphy and Brayden, 1995a; Crane *et al.*, 2003; Hilgers *et al.*, 2006), and that the relative functional importance of these different subtypes may also vary according to the prevailing level of arterial

activation. In rat mesenteric artery, only SK_{Ca} attributes to ACh-induced endothelium-dependent hyperpolarization, whereas IK_{Ca} has a role during the ACh-mediated repolarization phase observed after depolarization (Crane *et al.*, 2003).

IbTX elicited a significant smooth muscle contractile response when applied under baseline conditions, indicating that smooth muscle BK_{Ca} channels are tonically active in the rabbit iliac artery. Further evidence for synergistic endothelial SK_{Ca}, IK_{Ca} and BK_{Ca} channel activity in the rabbit iliac artery was provided by observations that in endothelium-intact rings, the tone elicited by IbTX was enhanced by the triple apamin+TRAM+IbTX combination, but not by Apamin and TRAM alone or in combination. This was also true for conditions with phenylephrine-induced contraction. By contrast, apamin+TRAM+IbTX did not enhance IbTX-induced contraction in endothelium-denuded rings suggested that the effect of the combined inhibitors was an endothelium-dependent component. In 3rd order rat mesenteric arteries, modulation of phenylephrine-induced contraction by the endothelium has previously been attributed to diffusion of Ca^{2+} ions and/or $InsP_3$ from smooth muscle via myoendothelial gap junctions, with the resulting elevation in endothelial $[Ca^{2+}]_i$ stimulating SK_{Ca} activity, and that contraction could be selectively enhanced by apamin (Dora *et al.*, 2000). Furthermore, in theory, conducted hyperpolarizations and diffusible EDHFs will both mediate relaxation by closing the L-type VOCCs that are necessary to sustain smooth muscle Ca^{2+} influx and contraction. However, in the case of agents, such as a diffusible EDHF that activate smooth muscle BK_{Ca} channels, IbTX will always block relaxation, whereas a conducted hyperpolarizing signal will progressively reduce the open state probability of BK_{Ca} channels and reduce the sensitivity to IbTX. As in the rabbit iliac artery, iberiotoxin also induced direct smooth muscle constriction, and in theory an associated depolarization could be transmitted via myoendothelial gap junctions and attenuate endothelial hyperpolarization. In practice this mechanism does not seem to

be universal, since IbTX fails to modulate EDHF-type relaxations in the rat small mesenteric artery (Hilgers *et al.*, 2006).

It was previously shown that there is a potentiating effect of H_2O_2, and its thiol oxidant mimic thimerosal, on EDHF-type responses (Edwards *et al.*, 2008). As there is a common pathway for NO production and the EDHF response, namely a rise in endothelial $[Ca^{2+}]_i$, these two functions of the endothelium were examined. Investigation into the modulation of endothelium-dependent arterial relaxations by exogenous H_2O_2 in the iliac artery revealed different effects between NO-mediated and EDHF-type relaxations. In the absence of L-NAME/indomethacin, 100 μM H_2O_2 had no effect on relaxations to CPA, whereas the EDHF-type component, isolated by the addition of L-NAME/indomethacin, was increased. Similar results were obtained in rings where relaxations were induced by ACh. In the presence of L-NAME/indomethacin, 100 μM H_2O_2 potentiated the relaxations to ACh. These findings demonstrated that the effect of H_2O_2 on receptor-independent CPA-evoked responses and receptor-dependent ACh-evoked responses are universal.

By contrast, CPA-evoked relaxations were potentiated in iliac rings pre-incubated with 10 μM thimerosal both in the absence or presence of L-NAME/indomethacin. Further experiments showed that this potentiation effect also occurred with ACh-evoked relaxations both in the absence or presence of L-NAME/indomethacin. In the rabbit superior mesenteric artery, a lower concentration of thimerosal (300 nM) was previously reported to amplify EDHF-mediated relaxations evoked by ACh and the Ca^{2+} ionophore A23187, which also acts through a receptor-independent mechanism (Hutcheson *et al.*, 1999). These findings suggested the possibility of a common target in the endothelium for H_2O_2 and thimerosal, to which the latter is more potent. It should be noted that 100 μM H_2O_2 may only corresponds to 1-15 μM intracellular H_2O_2, since glutathione peroxidase, catalase and other mechanisms together limit cytosolic $[H_2O_2]$ to 1-15% of that applied extracellularly (Schroder and Eaton, 2008). Indeed, EDHF-

type relaxations induced by ACh and CPA were not affected by lower concentrations of H_2O_2 (≤ 30 μM) in rabbit iliac artery (Garry *et al.*, 2009).

To test whether the difference between the effect of H_2O_2 and thimerosal on the endothelial-mediated NO relaxation in iliac artery is due to the interaction of H_2O_2 with NO directly, experiments were carried out where relaxations were induced with the NO donor MAHMA NONOate. In endothelium-intact rings in the presence of L-NAME/indomethacin and in rings denuded of their endothelium, incubation with 100 μM H_2O_2 had no effects on MAHMA NONOate-evoked relaxations, and therefore its effects in iliac artery could not be attributed to interaction with NO directly. In contrast, pre-incubation with 10 μM thimerosal induced a small but significant inhibition on relaxations evoked by MAHMA NONOate. This inhibition was endothelium-independent, but concentration-dependent, as experiments repeated with 1 μM thimerosal showed no such attenuation effect.

To study the effect of H_2O_2 on endogenous NO-mediated responses and to eliminate the complexity of having simultaneous NO-dependent and EDHF-type responses as seen in the iliac artery, where EDHF may compensate for the loss of NO, studies with H_2O_2 and thimerosal were performed in rabbit aortic rings, a preparation in which there is a minimal EDHF-type response. Exogenous H_2O_2 at concentrations ≤ 100 μM did not relax the aortic rings, but higher concentrations evoked an NO-independent, endothelium-independent relaxation, which was not affected by the absence or presence of eNOS inhibitor L-NAME and/or prostaglandin synthesis inhibitors indomethacin, as reported in other type of vessels (Mian and Martin, 1995; Wheal *et al.*, 2012). However, when thimerosal was added to aortic rings, it induced concentration-dependent relaxations between 3 μM and 10 μM, but only in endothelium-intact rings, as suggested by earlier reports (Forstermann *et al.*, 1986a). For comparison, in rabbit iliac artery, endothelium independent relaxations were also observed with exogenous applied H_2O_2 at concentrations ≥ 100 μM (Edwards *et al.*, 2008), which is consistent

with earlier reports that H_2O_2 is not an EDHF in this type of vessel (Chaytor *et al.*, 2003). Thimerosal itself evoked EDHF-type responses at concentrations ≥ 30 μM in the rabbit iliac artery, although this relaxation was preceded by a constrictive effect on the smooth muscle (Edwards *et al.*, 2008).

The combination of L-NAME and indomethacin failed to unmask a residual EDHF-type response to CPA or ACh in the rabbit aorta as expected. “Paradoxically”, in this vessel, the exclusively NO-dependent relaxations were attenuated with exogenous H_2O_2 at 100 μM and thimerosal at 10 μM. To determine whether this attenuation was due to a direct effect on the smooth muscle, experiments were performed in denuded rings with exogenous NO generated by MAHMA NONOate. Pre-incubation with 100 μM H_2O_2 was shown to have no effect on MAHMA NONOate-evoked relaxations in denuded aortic rings, thus suggesting that the inhibitory effects of H_2O_2 were at the level of the endothelial cell. However, 10 μM thimerosal attenuated relaxations to exogenously applied NO, consistent with those seen in preparations with endogenously NO-mediated responses. Decreasing the concentration of H_2O_2 to 30 μM was without inhibitory effect on CPA and ACh induced relaxations seen with 100 μM H_2O_2. Decreasing the concentration of thimerosal to 1 μM abolished the attenuation seen with 10 μM thimerosal, in fact, caused a significant potentiation of both CPA and ACh induced relaxations. Therefore, the results suggested that the attenuation observed with 10 μM thimerosal was likely due to its constrictive effect on the smooth muscle cells. As well as the ability to sensitize the $InsP_3$ receptor, sulfhydryl reagents thimerosal is reported to stimulate endothelial NO synthesis (Beny, 1990), and to inhibit the acylcoenzyme A:lysolecithin acyltransferase by interacting with thiol group of the enzymes thereby elevate free arachidonic acid levels within the cell (Irvine, 1982; Forstermann *et al.*, 1986b). The present findings suggested that these actions were likely to be involved in the potentiation of endothelium-dependent relaxation of this compound at its sub-threshold concentration of 1 μM. It was also noticed that pre-

incubation with L-NAME (300 μM) and indomethacin (10 μM), H_2O_2 (30 and 100 μM), thimerosal (1 and 10 μM) or denudation of the endothelium was without effect on basal tone or the contractile response to phenylephrine in rabbit iliac artery and aorta.

Increased levels of H_2O_2 production and impaired endothelial-derived NO bioactivity are often seen in vascular diseases characterized by dysfunctional endothelium but the role of this increase in H_2O_2 is unclear. There is conflicting evidence suggesting that H_2O_2 either, enhances endogenous NO generation by increasing the expression of eNOS (Drummond *et al.*, 2000) or that it impairs NO production in response to receptor-dependent and receptor-independent agonists such as bradykinin, adenosine diphosphate and the calcium ionophore A23187, by inactivation of oxidant-sensitive eNOS cofactors (Jaimes *et al.*, 2001). It has been reported that free radical scavengers and iron chelators can reverse the H_2O_2-induced impairment of NO bioactivity in PAEC (Thomas *et al.*, 2006). However, the extracellular iron chelator deferoxamine (1mM), the intracellular iron chelator deferiprone (1mM) or the catalase inhibitor aminotriazole (50mM) was unable to reverse the inhibitory effects of H_2O_2 on NO-mediated response in the rabbit aorta, thus suggesting that generation of $OH^{\cdot}$ through the Fenton reaction is not the primary cause of H_2O_2 toxicity in this vessel (Prof. TM Griffith personal communication).

In addition, it has previously been shown that relaxations to ACh are depressed by ~10% in the presence of exogenous catalase (an enzyme that catalyses the decomposition of H_2O_2), whereas responses to CPA are suppressed by ~30% (Chaytor *et al.*, 2003; Edwards *et al.*, 2008). Although it was not tested in the present study, evidence that endogenously-generated H_2O_2 amplifies electrotonic hyperpolarization-mediated relaxation evoked by CPA and ACh in rabbit iliac artery (Edwards *et al.*, 2008; Garry *et al.*, 2009), and by endocannabinoids in rat small mesenteric arteries (Wheal *et al.*, 2012) is reported.

3.4.2 Conclusions

The current study extends the previous findings with CPA, by showing that exogenous H_2O_2 potentiates receptor dependent EDHF-type responses evoked by the G-protein coupled receptor agonist ACh. Both CPA and ACh evoke EDHF-type responses through the elevation of endothelial $[Ca^{2+}]_i$, therefore the present findings give further evidence that H_2O_2 is likely to potentiate the EDHF-type responses by facilitating an increase in $[Ca^{2+}]_i$ (Edwards *et al.*, 2008). The results presented in this chapter also demonstrated that in large arteries, H_2O_2 might partially impair NO-dependent relaxations by directly interacting with the endogenous generation of NO.

3.5 CHAPTER SUMMARY

1. In the rabbit iliac artery, vascular K_{Ca} channels participate in an interactive manner in the EDHF phenomenon.
2. In the rabbit iliac artery, H_2O_2 can amplify EDHF-type relaxations evoked by various modes of stimulation.
3. H_2O_2 exerts inhibitory effects on NO-mediated endothelium-dependent relaxations.

Chapter 4

Potentiation of the EDHF Phenomenon by Inorganic Arsenite: Role of Hydrogen Peroxide

4.1 INTRODUCTION

Environmental exposure to arsenic induces an accelerated development of cardiovascular abnormalities such as atherosclerosis, hypertension and blackfoot diseases (Balakumar and Kaur, 2009; States *et al.*, 2009). This physiological effect of arsenite in the cardiovascular system has been linked with excessive production of $O_2^{\bullet-}$ by NADPH oxidase (Barchowsky *et al.*, 1999; Smith *et al.*, 2001; Qian *et al.*, 2005; Straub *et al.*, 2008). $O_2^{\bullet-}$ itself induces limited signalling and its effect is mostly local because it only has a half-life of a few seconds and due to its negative charge, it does not readily cross membranes. But in general it contributes to vascular dysfunction through a rapid interaction with NO to form $ONOO^-$, and through a dismutation to H_2O_2 in the presence of SOD (Lassegue and Griendling, 2010):

$$O_2^{\cdot-} + \mathrm{NO} \rightarrow \mathrm{ONOO^-} + \mathrm{H^+}$$

$$2O_2^{\cdot-} + 2H^+ \xrightarrow{\mathrm{SOD}} \mathrm{H_2O_2} + \mathrm{O_2}$$

Indeed, H_2O_2 apparently is of much greater importance for signalling. In the previous chapter it was noted that exogenous applied H_2O_2 can promote EDHF-type relaxations of rabbit iliac arteries. Endogenous H_2O_2 has recently been suggested to play a role in the mediation of EDHF-type relaxant responses to endocannabinoid mediators in rat

mesenteric arteries (Wheal *et al.*, 2012). There is now evidence, from this laboratory, that sodium arsenite ($NaAsO_2/As^{III}$) enhances EDHF-type relaxations evoked by CPA and ACh in the presence of L-NAME/indomethacin, probably through the generation of endogenous H_2O_2 from endothelium. The study carried out in the current chapter was a further investigation to these findings. It should be noted that absorbed arsenate (As^V) from environmental exposure is fairly rapidly reduced in blood to As^{III}, which is intrinsically more toxic (Vahter, 2002).

4.1.1 Preliminary investigation of arsenite responses in rabbit iliac artery

In a study from this laboratory (Dr. DH Edwards personal communication) and results presented in the thesis of Dr. DC Ellinsworth in 2010 (Ellinsworth, 2010), the effects of arsenite on endothelial function were compared in the presence and absence of endogenous NO production in rabbit iliac arteries. Preliminary data have shown that EDHF-type relaxations evoked by CPA and ACh were unaffected by exposure to 30 μM arsenite for 30 minutes, whereas exposure to 100 μM arsenite for 30 minutes caused a potentiation in sensitivity to both agents. In control rings, relaxations to CPA and ACh were unaffected by incubation with 100 μM arsenite for 30 minutes but the magnitude of the constrictor response to 1 μM PE was reduced by ~15% (p<0.01).

The functional role of H_2O_2 was investigated with catalase and a manganese-based SOD/catalase mimetic MnTMPyP. The role of NADPH oxidase was investigated with apocynin, which blocks the assembly of specific forms of this enzyme, and is known to prevent the generation of $O_2^{\bullet-}$ and H_2O_2 in cultured endothelial cells treated with arsenite (Barchowsky *et al.*, 1999; Touyz, 2008). To investigate the mechanisms responsible for the selective potentiation of relaxations elicited in the presence of L-NAME/indomethacin, rings were preincubated with 2000 Units/ml catalase, 100 μM MnTMPyP or 100 μM apocynin. None of these agents alone significantly affected pIC_{50}

and R_{max} values for relaxation in the absence of arsenite, whereas the enhancement of relaxation observed following exposure to 100 μM arsenite for 30 minutes was fully prevented in each case.

4.1.2 Aim of this chapter

The aim of the current chapter was to further investigate how inorganic As^{III} affects EDHF-type and NO-mediated relaxations via the generation of $O_2^{\bullet-}$ and H_2O_2 with the aid of the ROS-sensitive probe DHE (Zielonka and Kalyanaraman, 2010). To achieve this: (i) endothelium-dependent relaxations of aortic rings were studied with receptor-dependent agonist ACh and receptor-independent agent CPA. In rabbit iliac arteries such relaxations consist of dual NO-mediated and EDHF-type gap junction-dependent components (Mulvany and Halpern, 1976; Griffith *et al.*, 2004; Chaytor *et al.*, 2005; Griffith *et al.*, 2005), whereas in the aorta the EDHF-type component is negligible, thus allowing separation of the two mechanism of relaxation (Ruiz *et al.*, 1997; Fernandez-Rodriguez *et al.*, 2009), and (ii) ROS production in the different layers of the arterial wall and in the endothelial cells on the surface of the aortic valves was compared in the presence or absence of arsenite/apocynin (NADPH oxidases inhibitor).

4.2 MATERIALS AND METHODS

4.2.1 Mechanical Responses

Aorta was obtained from male NZW rabbits as described in Section 2.1 and 2.2. Rings of aorta 2-3 mm wide were mounted in a myograph containing oxygenated Holman's buffer at 37°C and maintained at a resting tension of 2 mN over a 60 minutes equilibration period, with frequent readjustments in baseline tension to correct for stress relaxation. Aortic rings were then incubated with indomethacin (10 μM) for 30 minutes. To evaluate EDHF-type responses, preparations were incubated for 30 minutes with L-NAME (300 μM) in addition to indomethacin. Arsenite (100 μM) was

then added for 30 minutes prior to constriction with PE (1 μM). Once constrictor responses had reached a stable plateau, relaxation was studied by constructing cumulative concentration-response curves to CPA or ACh in the continued presence of arsenite. These full concentration-relaxation curves were generally completed within ~60 minutes so that total cumulative exposure to arsenite was ~90 minutes using this protocol. (Preliminary experiments had demonstrated that lower concentrations of arsenite [10 μM and 30 μM] did not affect relaxation under these experimental conditions.)

4.2.2 Detection of superoxide/hydrogen peroxide

Detailed staining and imaging procedures were described in Section 2.3.4 and 2.3.7 of Chapter 2. This protocol was designed to match the total exposure time of rabbit aortic rings to 100 μM arsenite in the mechanical experiments (90 minutes). It should be noted that oxidation of DHE can generate two products, ethidium and 2-hydroxyethidium, which possess overlapping emission spectra and whose fluorescence is enhanced by binding to DNA (Zielonka and Kalyanaraman, 2010). Although H_2O_2 does not oxidize DHE directly and the formation of 2-hydroxyethidium is specific for $O_2^{\bullet-}$, H_2O_2 may promote the formation of ethidium in the presence of peroxidase activity or haem proteins so that increased fluorescence in DHE-loaded vascular smooth muscle/ endothelial cells may reflect production of both $O_2^{\bullet-}$ and H_2O_2 (Fernandes *et al.*, 2007; Ray *et al.*, 2011). All imaging data presented were acquired in the presence of L-NAME in order to avoid potentially confounding effects of NO which has been reported to promote the formation of ethidium in the presence of molecular oxygen (Zielonka and Kalyanaraman, 2010).

4.2.3 Data recording and Statistics

Details of data recording were described in Section 2.2.3 and Section 2.3.7. In mechanical experiments the R_{max} by CPA or ACh and IC_{50} (in the case of CPA in iliac

arteries, as explained in Section 2.6) or EC_{50} (in the case of ACh) were calculated for each experiment. Details of statistical analyses used for each figure were indicated in figures descriptions.

4.2.4 Reagents

Chemical reagents were purchased from Sigma-Aldrich (UK), except CPA (Ascent Scientific), and were dissolved in Holman's buffer, except apocynin and indomethacin (absolute ethanol), and CPA and DHE (DMSO).

4.3 RESULTS

4.3.1 Effects of arsenite on NO-mediated aortic relaxation evoked by CPA

In control aortic rings (endothelium-intact rings in the absence of L-NAME/indomethacin), maximal relaxations evoked by CPA were equivalent to 82.4±1.7% of PE-induced tone and were mediated by NO because no significant EDHF-type component was evident in the presence of L-NAME/indomethacin (Figure 4.1; Table 3.6). R_{max} and pIC_{50} values for concentration-relaxation curves constructed for CPA were unaffected by pre-incubation with 100 μM arsenite for 30 minutes (Table 4.1).

4.3.2 Effects of arsenite on NO-mediated aortic relaxation evoked by ACh

In control aortic rings, maximal relaxations evoked by ACh were equivalent to 63.0±1.2% of PE-induced tone and were mediated by NO because no significant EDHF-type component was evident in the presence of L-NAME/indomethacin (Figure 4.2; Table 3.7). R_{max} and pEC_{50} values for concentration-relaxation curves constructed for ACh were unaffected by pre-incubation with 100 μM arsenite for 30 minutes (Table 4.1).

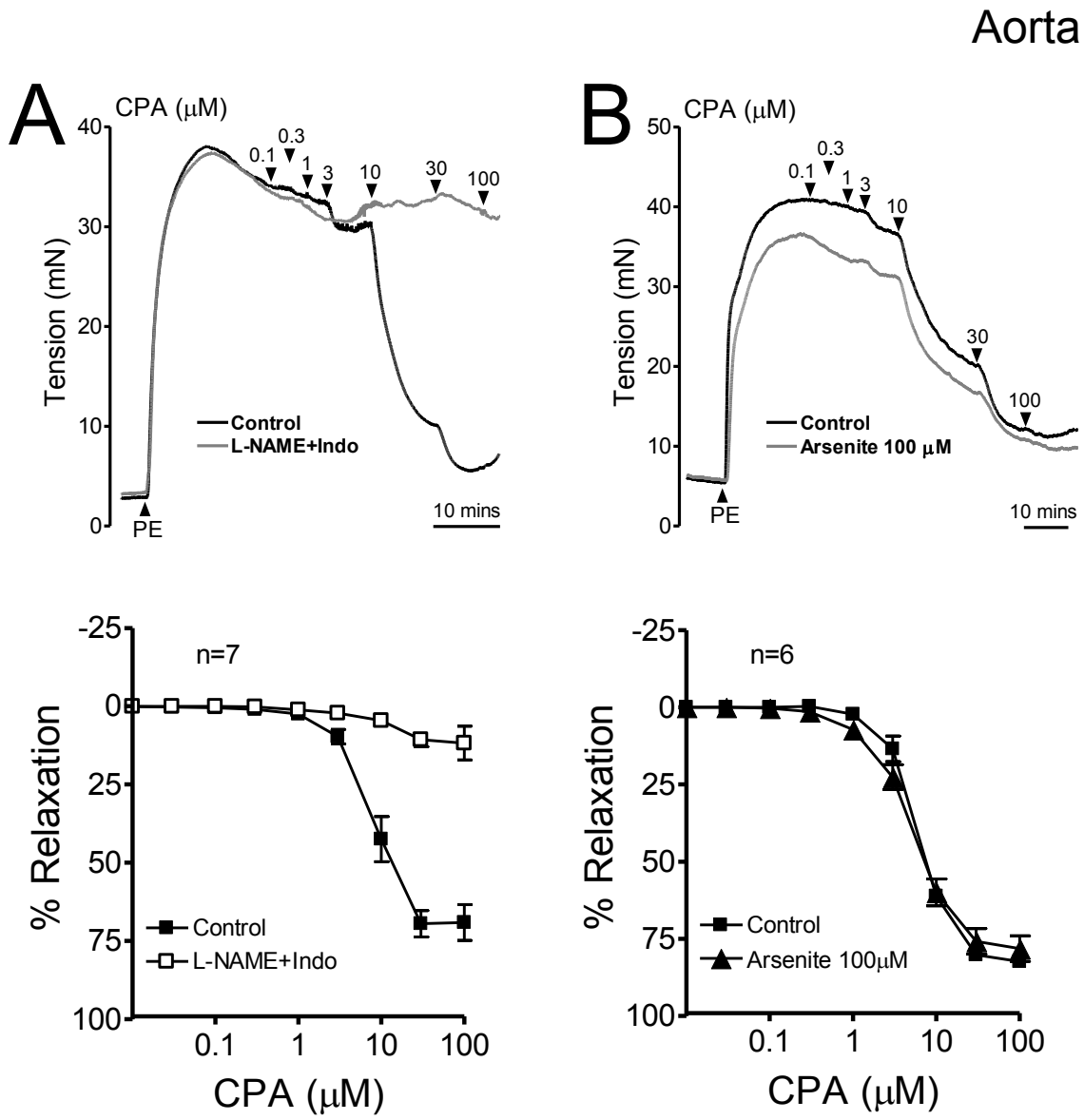

Figure 4.1 Effects of arsenite on CPA-evoked relaxation in aortic rings with intact endothelium. (A) EDHF-type relaxations in the presence of L-NAME and indomethacin were <5% of induced tone so that endothelium-dependent relaxation in this vessel can be attributed to NO. (B) Concentration-relaxation curves for CPA constructed in the absence of L-NAME were unaffected by exposure to 100 μM arsenite for 30 minutes. n denotes the number of animals studied.

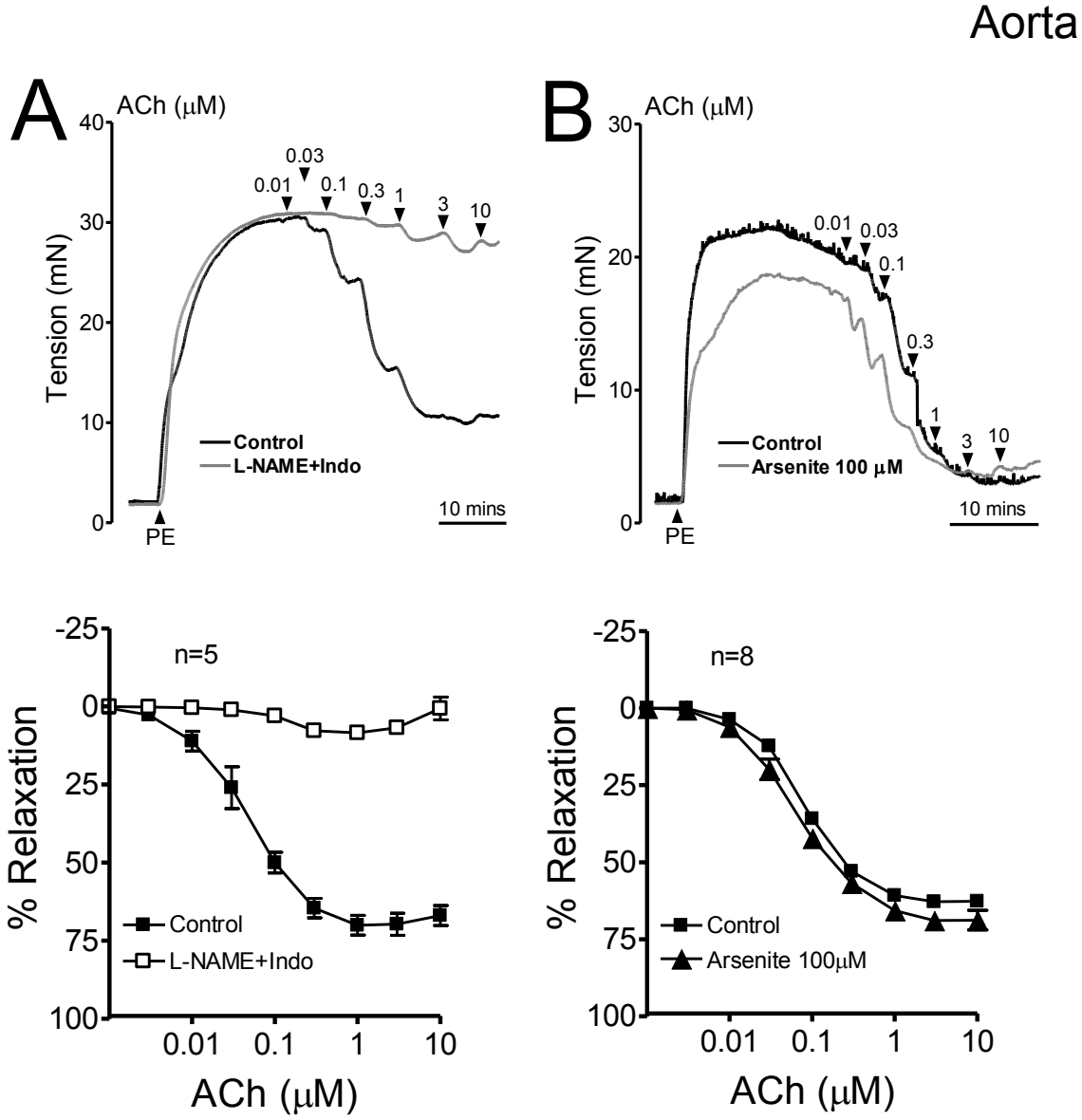

Figure 4.2 Effects of arsenite on ACh-evoked relaxation in aortic rings with intact endothelium. (A) EDHF-type relaxations in the presence of L-NAME and indomethacin were <5% of induced tone so that endothelium-dependent relaxation in this vessel can be attributed to NO. (B) Concentration-relaxation curves for ACh constructed in the absence of L-NAME were unaffected by exposure to 100 μM arsenite for 30 minutes. n denotes the number of animals studied.

Rabbit aorta			
Intervention	**N**	**pIC_{50}**	**R_{max} %**
CPA-evoked relaxations			
Control	6	4.73±0.24	82.4±1.7
Arsenite	6	5.00±0.12	78.1±4.1
ACh-evoked relaxations	**N**	**pEC_{50}**	**R_{max} %**
Control	8	7.09±0.03	63.0±1.2
Arsenite	8	7.19±0.07	69.5±2.5

Table 4.1 Effects of 100 μM arsenite for 30 minutes on endothelium-dependent relaxations to CPA and ACh in the rabbit aorta in the presence of indomethacin. Potency (negative logIC_{50} or logEC_{50}) and maximal responses (R_{max}) are given as mean±SEM. n denotes the number of animals studied.

Rabbit aorta		
Intervention	**N**	**PE-induced tone (mN)**
Control	14	27.0±1.6
Arsenite	14	22.9±1.3**

Table 4.2 Effect of 100 μM arsenite for 30 minutes on endothelium-intact rabbit aorta tone induced by PE. There was ~15% difference between PE-induced tone in rings compared with time-matched preparations incubated for the same periods without or without arsenite treatments. Data given as means±SEM. ** denote $p<0.01$ compared with corresponding control in Student's t-test. n denotes the number of animals studied.

4.3.3 Effects of arsenite on contraction induced by PE

In control aortic rings, the magnitude of the constrictor response to 1 μM PE was reduced by ~15% following exposure to 100 μM arsenite for 30 minutes (from 27.0±1.6 mN to 22.9±1.3 mN; data pooled from all experiments; $p<0.01$; n=14; Table 4.2).

4.3.4 Fluorescence imaging of ROS production

Exposure to 100 μM arsenite for 90 minutes significantly enhanced endothelial nuclear fluorescence in the rabbit aortic valve leaflets loaded with DHE in the presence of L-NAME/indomethacin, an effect that was fully prevented by pre-incubation with 100 μM apocynin (Figure 4.3). Exposure to 100 μM arsenite for 90 minutes did not increase fluorescence in either the media or adventitia of endothelium-denuded rabbit iliac arteries and aortic rings loaded with DHE (Figure 4.4).

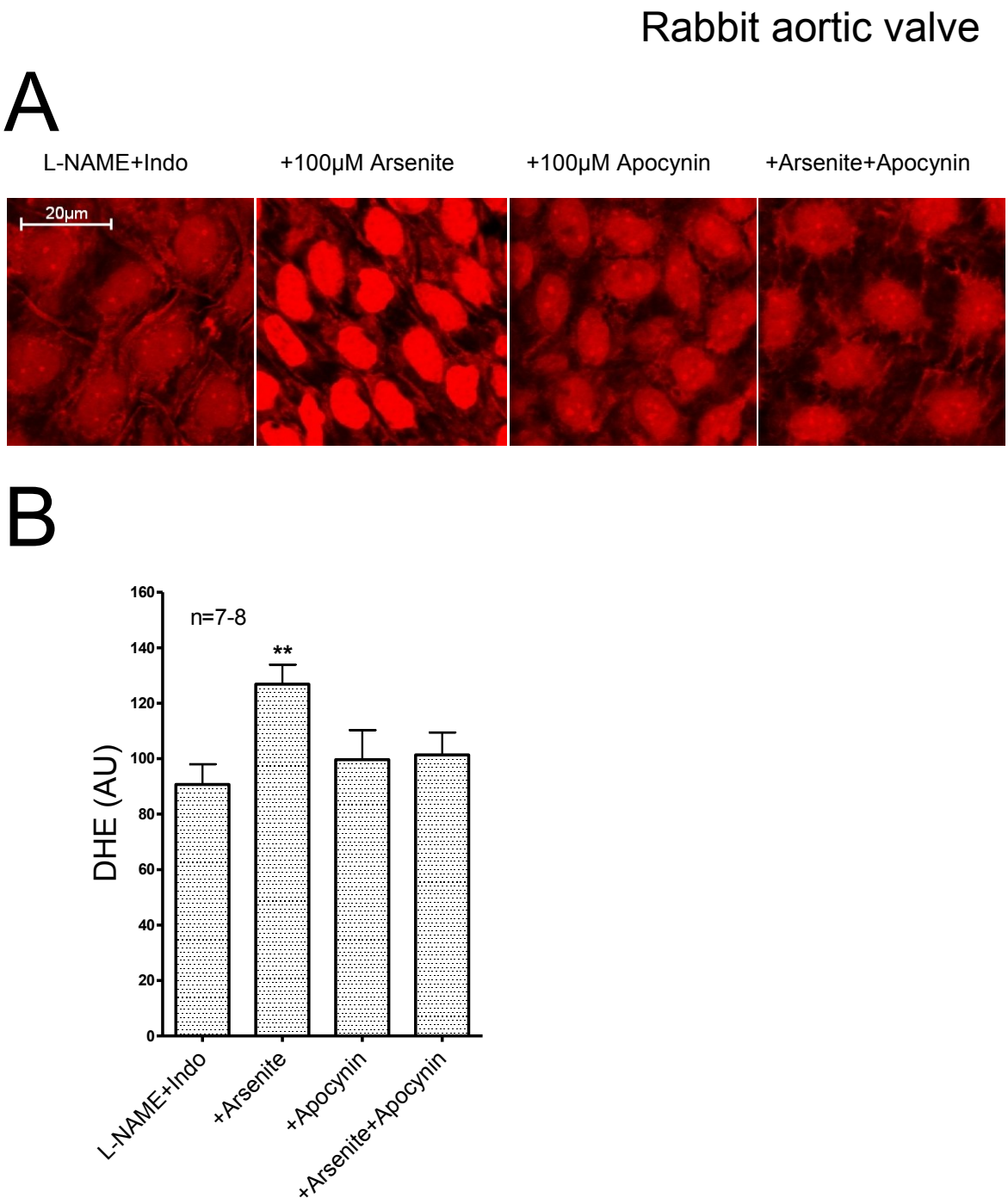

Figure 4.3 Endothelial ROS production in rabbit isolated aortic valve leaflets loaded with DHE in the presence of L-NAME and indomethacin. (A) Nuclear fluorescence increased following exposure to 100 μM arsenite for 90 minutes, but was unaffected by apocynin or arsenite in combination with apocynin. (B) Bar graphs confirming statistical significance. * denotes $p<0.05$ compared with corresponding control in one-way ANOVA. n denotes the number of animals studied. AU stands for arbitrary unit.

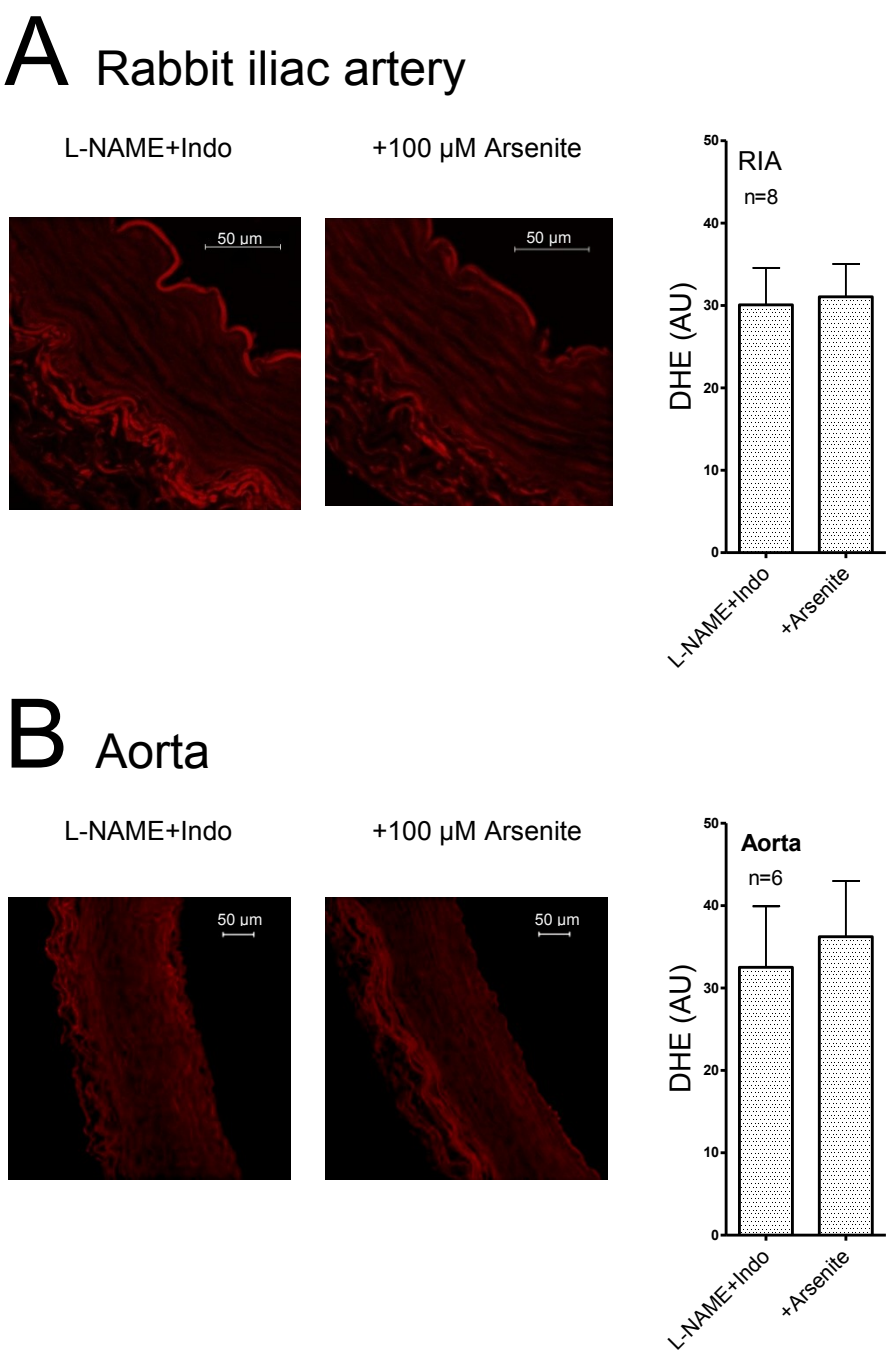

Figure 4.4 Fluorescence studies of endothelium-denuded rabbit iliac arteries and aortic rings loaded with DHE in the presence of L-NAME and indomethacin. (A,B) Images and bar graphs showing that neither artery type exhibited evidence of excess ROS production in the media of the vessel wall following exposure to 100 µM arsenite for 90 minutes. The adventitia of both vessels exhibited autofluorescence, but its appearance was unaltered by exposure to arsenite. Scalebars identify the vessel lumen. n denotes the number of animals studied. AU stands for arbitrary unit.

4.4 DISCUSSION

Arsenite has been shown to potentiate EDHF-type but not NO-mediated relaxations in the rabbit iliac artery by stimulating endothelial NADPH oxidase activity and thereby promoting the formation of H_2O_2 from $O_2^{\bullet-}$. The present chapter has extended the previous evidence and provided new insights into the mechanisms through which short-term exposure to inorganic arsenic can modulate endothelial function in the rabbit vasculature by generating H_2O_2 in the endothelium.

4.4.1 Potentiating effects of arsenite on the EDHF phenomenon

Summarising the results obtained previously from this group and the results from this chapter, the following findings may be described: (i) EDHF-type relaxations evoked by the SERCA inhibitor CPA in rabbit iliac artery rings was amplified by arsenite in a concentration-dependent manner, with potentiation being evidenced following exposure to 100 μM, but not 30 μM arsenite for 30 minutes; (ii) the central role for endogenously-generated H_2O_2 was confirmed in experiments where arsenite-mediated potentiation was prevented by catalase and the catalase/SOD mimetic MnTMPyP; (iii) The enhanced relaxation by 100 μM arsenite was prevented with the NADPH oxidase inhibitor apocynin, which also abolished the arsenite-induced increases in endothelial fluorescence in the rabbit aortic valve leaflets loaded with the ROS sensitive probe DHE, and (iv) EDHF-type relaxations to ACh were enhanced by arsenite, although this effect was less prominent than those obtained with CPA.

Taken together, these findings indicate that excess $O_2^{\bullet-}$ generated by the activation of endothelial NADPH oxidase by arsenite can serve as a source of H_2O_2 that modulates the EDHF phenomenon. Previous analyses have demonstrated that exogenous H_2O_2 (either authentic or generated by the oxidation of ascorbic acid or tetrahydrobiopterin) synergistically enhances depletion of the ER Ca^{2+} store by CPA and amplifies electrotonically conducted relaxations by promoting endothelial K_{Ca} channel opening (Edwards *et al.*, 2008; Garry *et al.*, 2009). The present study extends these

observations by demonstrating that endogenously generated H_2O_2 can enhance the biological role of the EDHF phenomenon under conditions of increased oxidative stress. The observation that is consistent with previous reports that exogenous H_2O_2 amplifies EDHF-type relaxations to ACh at a higher threshold (30 μM H_2O_2) compared with CPA (10 μM H_2O_2) (Garry *et al.*, 2009).

NADPH oxidase (Nox) enzymes are important sources of $O_2^{\bullet-}$, a precursor of reactive oxygen species and their family consists of 7 catalytic homologues. Currently four members have been identified in the vasculature: Nox1, Nox2, Nox4, and Nox5 (Lassegue and Griendling, 2010). These enzymes catalyzes the generation of $O_2^{\bullet-}$ from oxygen and NADPH:

$$\mathrm{NADPH} + 2\mathrm{O}_2 \rightarrow \mathrm{NADP}^+ + \mathrm{H}^+ + 2\mathrm{O}_2^{\bullet-}$$

The classical phagocytic Nox comprises a membrane-bound flavocytochrome b_{558} component and a number of cytosolic regulatory subunits ($p47^{phox}$, $p67^{phox}$, $p40^{phox}$ and the small GTPase(s) Rac1 or Rac2, phox stands for phagocyte oxidase) that are required for the activation of the enzyme. The heterodimeric b_{558} itself is constructed from a catalytic subunit Nox and a $p22^{phox}$ subunit (except for Nox5) (Babior *et al.*, 2002; Ray and Shah, 2005; Lassegue and Griendling, 2010). Upon Nox activation, the cytosolic regulatory subunits are translocated to the cell membrane where they associate with the b_{558} in a cascade that can be interrupted by apocynin at the level of $p47^{phox}$ (Stefanska and Pawliczak, 2008; Touyz, 2008). There is evidence that exposure to low level of arsenite increases the overall Nox catalytic activity of membrane fractions from cultured intact porcine aortic endothelial cells (PAEC) by twofold within 1 h, whereas treatment of isolated endothelial membranes is without effect (Smith *et al.*, 2001). More specifically, it has been reported the cytosolic subunits ($p47^{phox}$, $p67^{phox}$ and Rac1) and the membrane-bound $gp91^{phox}$ (the Nox2-based oxidase protein complexes) are required for arsenite to stimulate endothelial $O_2^{\bullet-}$ production (Smith *et al.*, 2001; Qian *et al.*, 2005; Straub *et al.*, 2008). It should be noted that in unstimulated cultured endothelial cells, the Nox-2-based oxidase can be

detected in a perinuclear distribution where it exists as a preassembled intracellular complex associated with the cytoskeleton, rather than being plasma membrane-bound as in neutrophils (Li and Shah, 2002). Therefore, it can be suggested that these Nox-2-based oxidases might contribute to the intracellular $O_2^{\bullet-}$ production directly (Ray and Shah, 2005).

In large arteries, Nox2 and Nox4 are the dominant subtypes found in the endothelium, whereas the Nox1 and Nox4 are found in smooth muscle (Brandes and Schroder, 2008; Lassegue and Griendling, 2010). Endothelial cells show a high expression of Nox4, markedly exceeding that of other Nox proteins (Ago *et al.*, 2004). In contrast to Nox2, the Nox4 homologue, of which four splice variants have been identified (Nox4B, NoxC, Nox4D and Nox4E) (Montezano *et al.*, 2011), has a number of differences: (i) it is the only constitutively active NADPH oxidase (Brandes and Schroder, 2008); (ii) it localizes to the endoplasmic/sarcoplasmic reticulum (Chen *et al.*, 2008); (iii) it generates H_2O_2 in preference to $O_2^{\bullet-}$ *in vitro* and *in vivo* (Dikalov *et al.*, 2008; Ray *et al.*, 2011) and (iv) its catalytic activity depends on Nox4/$p22^{phox}$; this lack of $p47^{phox}$ component from the structure makes Nox4 insensitive to apocynin. The present findings therefore imply that the Nox4-based oxidase does not contribute to the potentiating effects of arsenite on EDHF-type relaxations in the rabbit iliac arteries, as these were fully blocked by apocynin. It has been suggested that apocynin might act as an antioxidant rather than an inhibitor of NADPH oxidase in HEK-293 cells. But in cell free assays using DHE to quantify $O_2^{\bullet-}$ accumulation, antioxidant effects of apocynin were detected only at 1 mM and were absent at the 100 μM concentration employed in the present study (Heumuller *et al.*, 2008).

4.4.2 Differential effects of arsenite on EDHF-type and NO-mediated relaxations

Since NO can rapidly scavenge the $O_2^{\bullet-}$ to form $ONOO^-$, activation of endothelial NADPH oxidase by arsenite should in theory impair NO-mediated arterial relaxations.

Evidence of tissue protein nitrosation, presumably by peroxynitrite, has been detected from the endothelial cells taken from mice that have been exposed to drinking water with sodium arsenite (Straub *et al.*, 2008). In the present chapter, despite the fact that relaxations evoked by CPA and ACh in rabbit aorta were mediated exclusively by NO and that elevated fluorescence of DHE (i.e. increased ROS production) were seen with arsenite treatment in the rabbit aortic valve endothelium, no differences were observed in aortic relaxations evoked by CPA and ACh in the presence or absence of arsenite. In addition, as suggested by the work from this laboratory described in the introduction of this chapter, while arsenite potentiated EDHF-type relaxations evoked by CPA or ACh in the rabbit iliac arteries, no evidence of potentiation was observed in the absence of L-NAME/indomethacin. Taken together, these observations suggest (i) the rate of formation of $O_2^{\bullet-}$ induced by arsenite may be substantially slower than the flux of NO generated by CPA or ACh in rabbit endothelial cells, and (ii) the availability of $O_2^{\bullet-}$ to form H_2O_2 by dismutation may be limited by the presence of NO, thereby compromising the ability of arsenite to potentiate any co-existent EDHF-type component of relaxation.

Indeed, there was no evidence of increased ROS generation by arsenite in the media of the vessel wall in both the rabbit iliac arteries and aorta, regardless of elevated ROS production detected by the endothelium of the rabbit aortic valve. This further explained the inability of arsenite to impair NO-mediated relaxations. This finding is supported by other studies where, despite the significantly increased endothelial $O_2^{\bullet-}$ production in transgenic mice with targeted endothelial overexpression of Nox2, the endothelium-dependent and -independent relaxations to ACh or nitroprusside were not different compared to wild-type mice (Bendall *et al.*, 2007). Whereas in endothelium-targeted Nox4 overexpression transgenic mice, significantly greater ACh- or histamine-induced vasodilatation was observed in comparison with the wild-type, resulting from increased H_2O_2 (but not $O_2^{\bullet-}$) production and H_2O_2-induced hyperpolarization without altering NO bioavailability (Ray *et al.*, 2011). By contrast, angiotensin II treatment is often associated with a depressed NO-mediated endothelium-dependent relaxation and it is

well-documented that in angiotensin II induced hypertension, a global increase in ROS production by Nox protein is often observed, of which the smooth muscle-specific Nox1-based oxidase and the endothelial Nox2-based oxidase are apparent to play a role (Lassegue *et al.*, 2001; Touyz, 2008; Lassegue and Griendling, 2010; Takac *et al.*, 2012). In addition, there is evidence that angiotensin II may also stimulate ROS generation through vascular adventitial cells (Pagano *et al.*, 1997), whereas in the present study, no evidence for excess arsenite-induced adventitial DHE fluorescence was observed.

4.4.3 Conclusions and further studies

In this chapter of the thesis, the complex effects of short-term inorganic arsenic exposure have been identified on EDHF-type and NO-mediated arterial relaxations. Arsenite was found to potentiate EDHF-type responses through the elevation of the endogenous endothelial-produced H_2O_2 that is secondary to the activation of NADPH oxidase. And selective increase in endothelial $O_2^{\bullet-}$ production appeared to be insufficient to impair smooth muscle relaxations induced by endothelium-derived NO.

To correlate with the present *in vitro* observations, further *in vivo* studies are needed to test the long term vascular effects of arsenic ingestion, preferably at levels found in contaminated drinking water. Because there is evidence that arsenic *in vivo* can convert to more toxic metabolites such as monomethylarsonous acid that may result in direct inhibition of eNOS (Vahter, 2002; Lee *et al.*, 2003; Sumi *et al.*, 2005), more work is required to clarify these conflicting reports. In addition, given the fact that arsenic trioxide is now widely used in the treatment of haematological conditions such as acute promyelocytic leukaemia (Jing *et al.*, 1999), possible iatrogenic effects of trivalent arsenic on vascular function also remain to be investigated.

4.5 CHAPTER SUMMARY

1. Arsenite has minimal effect on NO-mediated responses.
2. Arsenite potentiates EDHF-type responses through the elevation of the endogenous endothelial-produced H_2O_2 that is secondary to the activation of NADPH oxidase.
3. Selective increase in endothelial $O_2^{\bullet -}$ production appeared to be insufficient to impair smooth muscle relaxations induced by endothelium-derived NO.

Chapter 5

Application of Fluorescent Probes for Sensing and Imaging Calcium Signal – The Dye Responsiveness Test with Hydrogen Peroxide

5.1 INTRODUCTION

5.1.1 The development of calcium indicators

It is accepted that calcium is the most important second messenger in many types of cells including vascular smooth muscle and endothelial cells. The elevation of free $[Ca^{2+}]_i$ is the key event for both NO and EDHF induced vessel relaxations. However, it was not until 1979, the development of the fluorescent Ca^{2+}-specific indicators started by Roger Y. Tsien in Cambridge (Tsien, 1980) . Those early indicators such as BAPTA and Quin2 were designed based on the structure of the Ca^{2+} chelator EGTA (Meldolesi, 2004). To make them membrane-permeant to allow imaging of the live cells, an AM group was attached to their chemical structure (Tsien, 1981). Masking of the carboxylic residues with AM ester groups results in an uncharged molecule that can permeate cell membranes and accumulate progressively within the cytosol. Once inside the cell, these AM groups are cleaved off by nonspecific esterases, resulting in a charged membrane-impermeant form that remains trapped within the cytosolic compartment of the cell (Tsien, 1981; Meldolesi, 2004). Nowadays, these AM ester derivatives and their analogous acetate groups of fluorescent Ca^{2+} indicators have made a major

contribution to advances in the understanding of the role of calcium in cellular regulation.

5.1.2 The probes applied in the studies described in this thesis

To identify the calcium signalling pathway inside the endothelial cells upon treatment with H_2O_2, a number of well-validated fluorescent probes, in their cell-permeant AM form, were used for the studies described in this thesis.

5.1.2.1 Fluo-4

Fluo-4 is an analogue of Fluo-3 that was originally developed by Tsien and his colleagues (Minta *et al.*, 1989). It is a high affinity Ca^{2+} indicator and has a dissociation constant (K_d) value of ~345 nM. Compared to Fluo-3, Fluo-4 has a greater fluorescence excitation at 488 nm and therefore higher signal levels for applications such as confocal laser-scanning microscopy (Johnson and Spence, 2010). Intracellular Ca^{2+} measurements using Fluo-4 have been previously tested with rabbit aortic valve in this group (Fernandez-Rodriguez *et al.*, 2009).

5.1.2.2 Mag-fluo-4

Mag-fluo-4 is an analog of Fluo-4 with a low Ca^{2+}-binding affinity (K_d value of ~22 μM for Ca^{2+}), making it suitable for detecting high Ca^{2+} concentrations in the 1 μM to 1 mM range such as those found in the ER (Johnson and Spence, 2010). To obtain differential loading into the ER as required in the present studies, the cells were incubated with the probe initially at 37 °C and then washed with indicator-free solution at room temperature to allow the cytosolically located Mag-fluo-4 to enter the ER (see Section 2.5.1, Chapter 2 for details). This loading method was previously developed and verified by others in the ER of isolated mouse pancreatic acinar cells and in the SR of isolated rat uterine smooth muscle cells (Park *et al.*, 2000; Shmigol *et al.*, 2001). In earlier studies presented in this group (Edwards *et al.*, 2008), this probe was used as a $[Ca^{2+}]_{ER}$ indicator in rabbit aortic valve.

5.1.2.3 Rhod-2/MitoTracker Green

Rhod-2 is a Ca^{2+} indicator that has a K_d value of ~570 nM. The dye has characteristics that make it possible to detect Ca^{2+} concentrations inside mitochondria as required in the present study: (i) it has a long-wavelength that is higher than the autofluorescence wavelength of oxidised flavoproteins (FAD^{++}) of mitochondria redox state (Dumollard *et al.*, 2004) (Prof. K Swann personal communication) and (ii) it has a net positive charge that can promote its sequestration into mitochondria via membrane potential-driven uptake (Johnson and Spence, 2010).

To verify that the Rhod-2 fluorescence distribution pattern is characteristic of mitochondria, MitoTracker Green (MTG) was loaded along with Rhod-2. The cell-permeant labelling reagent MTG can passively diffuse across the plasma membrane and accumulate in active mitochondria as it contains a mildly thiol-reactive chloromethyl moiety, which covalently reacts with accessible thiol groups on peptides in active mitochondria matrix (Poot *et al.*, 1996; Presley *et al.*, 2003; Johnson and Spence, 2010). It should be noted that MTG is relatively insensitive to H_2O_2 (Pendergrass *et al.*, 2004).

5.1.2.4 Fura-2

Fura-2 (K_d value of ~0.14 μM for Ca^{2+}) was first designed by Tsien and his colleagues in 1985 (Grynkiewicz *et al.*, 1985). Unlike the other Ca^{2+} indicators described above, it is used as a ratiometric dye, as such it is excited at two different wavelengths and the ratio of resulting emissions, at a single wavelength, is calculated. Ratiometric measurements can minimize distortions in data caused by events such as variations in probe loading and retention, unequal cell thickness in mixed populations, photobleaching and instrumental factors (Hanson and Hanson, 2008; Johnson and Spence, 2010). 340/380 nm excitation ratio of Fura-2 allows accurate measurements of the intracellular Ca^{2+} concentration, whereas 355nm excitation is at the Ca^{2+} insensitive isobestic point, which is used for quantify the Ca^{2+} entry through non-selective cation

channels by quenching of Fura-2 with Mn^{2+} (Prof. K Swann personal communication). Intracellular Ca^{2+} measurements with Fura-2 were previously reported in rabbit aortic valve (Edwards *et al.*, 2008).

5.1.3 Aim of this chapter

The aim of the present chapter is: (i) to test the responsiveness of each fluorescent probe to low level and high level of calcium, and to check whether H_2O_2, a strong oxidative agent, has any ability to interfere with their Ca^{2+} detection. The responsiveness test will be performed in a spectrophotometer compatible multi-well plate for parallel screening, and (ii) each probe will be loaded into rabbit aortic valve leaflets and EA.hy926 cells according to manufacturer guidelines. After loading, the fluorescence distribution and intensity will be compared.

5.2 MATERIALS AND METHODS

5.2.1 Accessing dye responsiveness

As described in Section 2.3.3, the AM dyes Fluo-4, Mag-fluo-4, Rhod-2 and Fura-2 were first hydrolysed to remove the AM group and the responses of the individual dyes to high-calcium buffer (HEPES buffer and/or Holman's buffer), low-calcium buffer (Ca^{2+}-free HEPES buffer and/or Ca^{2+}-free Holman's buffer), in the absence or presence of H_2O_2 (100 µM or 1mM) were examined in a cell free system. The fluorescence intensity of each sample was recorded at 0 minutes, 5 minutes, 20 minutes, 30 minutes and 60 minutes. All samples were prepared at room temperature. The wavelengths used for the spectrophotometer were listed in Table 2.3.

5.2.2 Imaging of rabbit aortic valve leaflets

Fluorescent dyes Fluo-4, Mag-fluo-4, Rhod-2 and MTG were loaded into the aortic valve as described in Section 2.3.4. Fluorescence images at high definition (Leica HCX PL APO 100X/1.40-0.70 OIL CS objective) and normal experimental definition (Leica HC PL FLUOTAR 20X/0.50 objective) were obtained as described in Section 2.3.6.

Valve leaflets were incubated in Holman's buffer for Mag-fluo-4 and Rhod-2/MitoTracker Green imaging, and in Ca^{2+}-free Holman's buffer for Fluo-4 imaging.

5.2.3 Imaging of EA.hy926 cells

Fluorescent dyes (Fluo-4, Mag-fluo-4, Rhod-2 and MTG) were loaded into the EA.hy926 cells as described in Section 2.5.1. Fluorescence images at high definition (Leica HCX PL APO 100X/1.40-0.70 OIL CS objective) and normal experimental definition (Leica HC PL FLUOTAR 20X/0.50 objective) were taken as described in Section 2.5.2. Cells were incubated in Holman's buffer for Mag-fluo-4 and Rhod-2/MitoTracker Green imaging, and in Ca^{2+}-free Holman's buffer for Fluo-4 imaging.

5.3 RESULTS

5.3.1 Effect of H_2O_2 on Fluo-4 responses to calcium

H_2O_2 100 μM or 1 mM did not affect Fluo-4 fluorescence in Holman's buffer or Ca^{2+}-free Holman's buffer over a 60 minutes period. The average fluorescence intensity was approximately 18000 A.U. in Holman's buffer and was approximately 11000 A.U. in Ca^{2+}-free Holman's buffer (Figure 5.1).

5.3.2 Effect of H_2O_2 on Mag-fluo-4 responses to calcium

Over a 60 minutes period, H_2O_2 100 μM or 1 mM had no effect on Mag-fluo-4 fluorescence in Holman's buffer ($CaCl_2$ 2.5 mM) or in Ca^{2+}-free Holman's buffer (without addition of $CaCl_2$). The average fluorescence intensity was approximately 60000 A.U. in Holman's buffer and was approximately 5000 A.U. in Ca^{2+}-free Holman's buffer (Figure 5.2).

5.3.3 Effect of H_2O_2 on Rhod-2 responses to calcium

Over a 60 minutes period, H_2O_2 100 μM or 1 mM had no effect on Rhod-2 fluorescence in Holman's buffer or in Ca^{2+}-free Holman's buffer. The average fluorescence intensity

was approximately 9000 A.U. in Holman's buffer and was approximately 5000 A.U. in Ca^{2+}-free Holman's buffer (Figure 5.3).

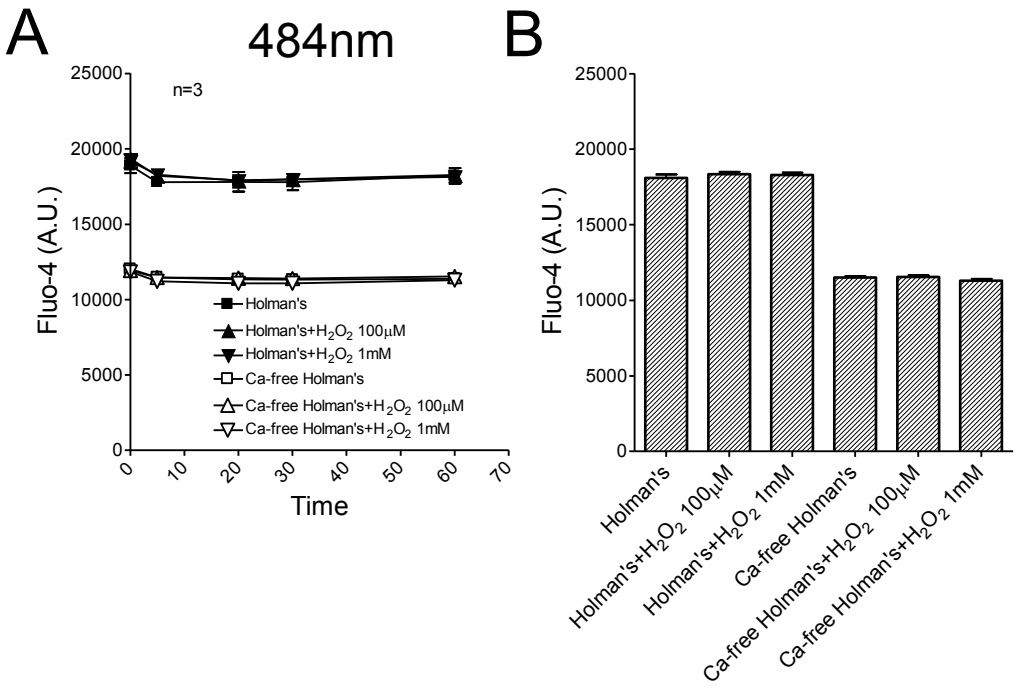

Figure 5.1 Effect of H_2O_2 on dye responsiveness test for Fluo-4 at 484nm. 100 μM and 1 mM H_2O_2 has no effect on Fluo-4 fluorescence over a 60 minutes period for (A) Holmans and Ca^{2+}-free Holmans buffer and (B) Bar graph of all data regardless of time confirmed this result. n denotes the number of tests examined. AU stands for arbitrary units.

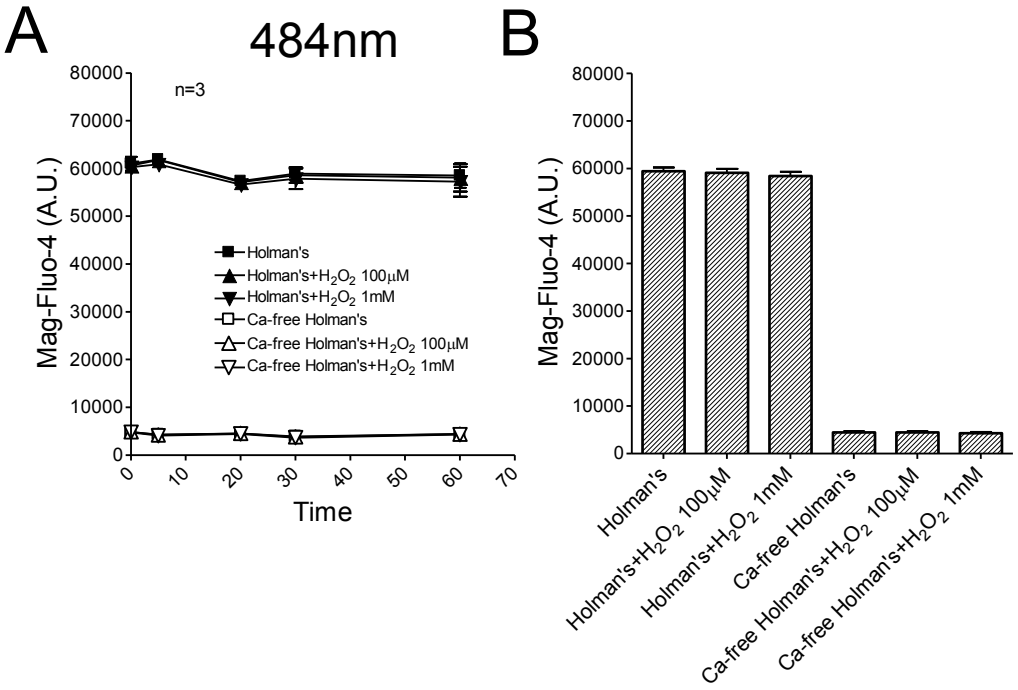

Figure 5.2 Effect of H_2O_2 on dye responsiveness test for Mag-fluo-4 at 484nm. 100 μM and 1 mM H_2O_2 has no effect on Mag-fluo-4 fluorescence over a 60 minutes period for (A) Holman's and Ca^{2+}-free Holman's buffer and (B) Bar graph of all data, regardless of time, confirmed this result. n denotes the number of tests examined. AU stands for arbitrary units.

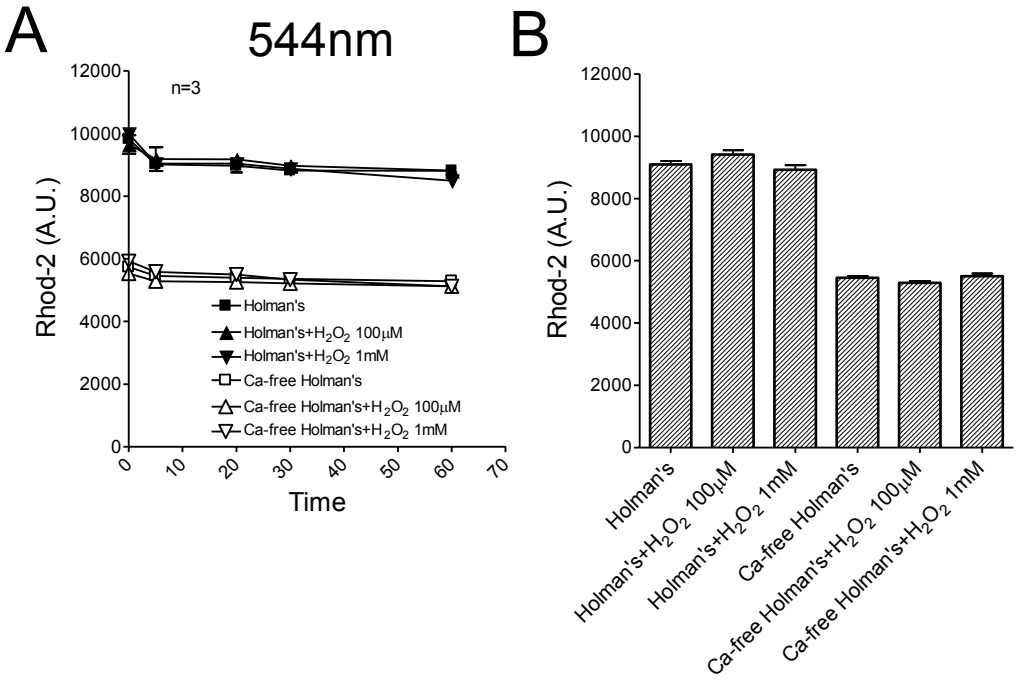

Figure 5.3 Effect of H_2O_2 on dye responsiveness test for Rhod-2 at 544nm. 100 μM and 1 mM H_2O_2 has no effect on Rhod-2 fluorescence over a 60 minutes period for (A) Holman's and Ca^{2+}-free Holman's buffer and (B) Bar graph of all data regardless of time confirmed this result. n denotes the number of tests examined. AU stands for arbitrary units.

5.3.4 Effect of H_2O_2 on Fura-2 responses to calcium

With excitation at 340 nm, over a 60 minutes period, H_2O_2 100 μM or 1 mM did not affect Fura-2 fluorescence in Holman's buffer, Ca^{2+}-free Holman's buffer, HEPES buffer ($CaCl_2$ 1 mM), or Ca^{2+}-free HEPES buffer (without $CaCl_2$). The average fluorescence intensity was approximately 26000 A.U. in Holman's buffer and HEPES buffer and was approximately 15000 A.U. in Ca^{2+}-free Holman's buffer and Ca^{2+}-free HEPES buffer (Figure 5.4).

With excitation at 380nm, over a 60 minutes period, the Fura-2 fluorescence was not altered with the addition of H_2O_2 (100 μM or 1 mM) in Holman's buffer, Ca^{2+}-free Holman's buffer, HEPES buffer or Ca^{2+}-free HEPES buffer. The average fluorescence intensity was approximately 3500 A.U. in Holman's buffer and HEPES buffer and was approximately 17000 A.U. in Ca^{2+}-free Holman's buffer and Ca^{2+}-free HEPES buffer (Figure 5.5).

With excitation at 355 nm, over a 60 minutes period, H_2O_2 100 μM or 1 mM had no effect on Fura-2 fluorescence in Holman's buffer, Ca^{2+}-free Holman's buffer, HEPES buffer or Ca^{2+}-free HEPES buffer. The average fluorescence intensity was approximately 24000 A.U. in Holman's buffer and HEPES buffer and was approximately 19000 A.U. in Ca^{2+}-free Holman's buffer and Ca^{2+}-free HEPES buffer (Figure 5.6).

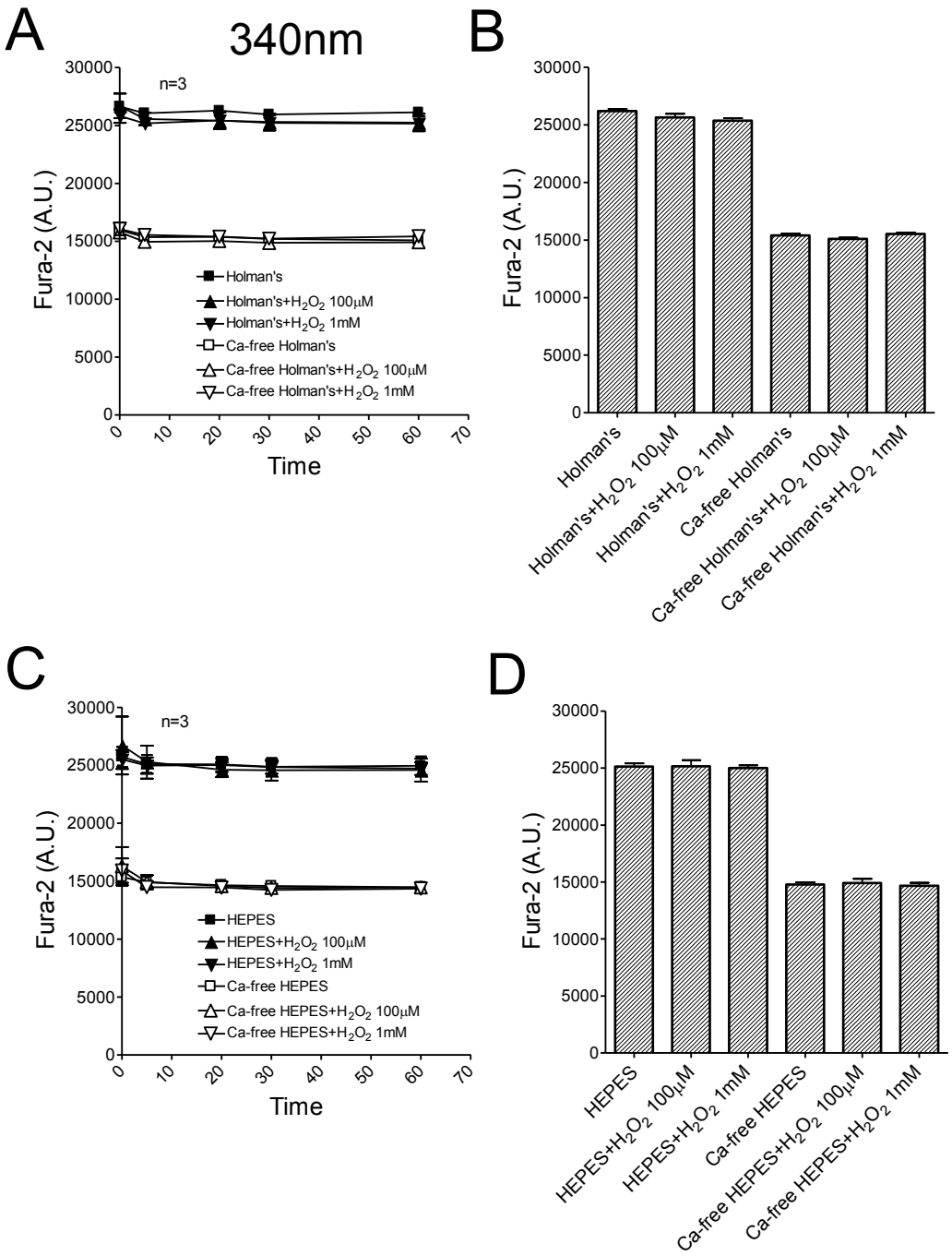

Figure 5.4 Effect of H_2O_2 on dye responsiveness test for Fura-2 at 340nm. 100 μM and 1 mM H_2O_2 has no effect on fura-2 fluorescence at 340nm over a 60 minutes period for (A) Holman's and Ca^{2+}-free Holman's buffer and (B) Bar graph of all data regardless of time confirmed this result. (C and D), similar for HEPES and Ca^{2+}-free HEPES buffer, H_2O_2 did not cause any change in fura-2 fluorescence. n denotes the number of tests examined. AU stands for arbitrary units.

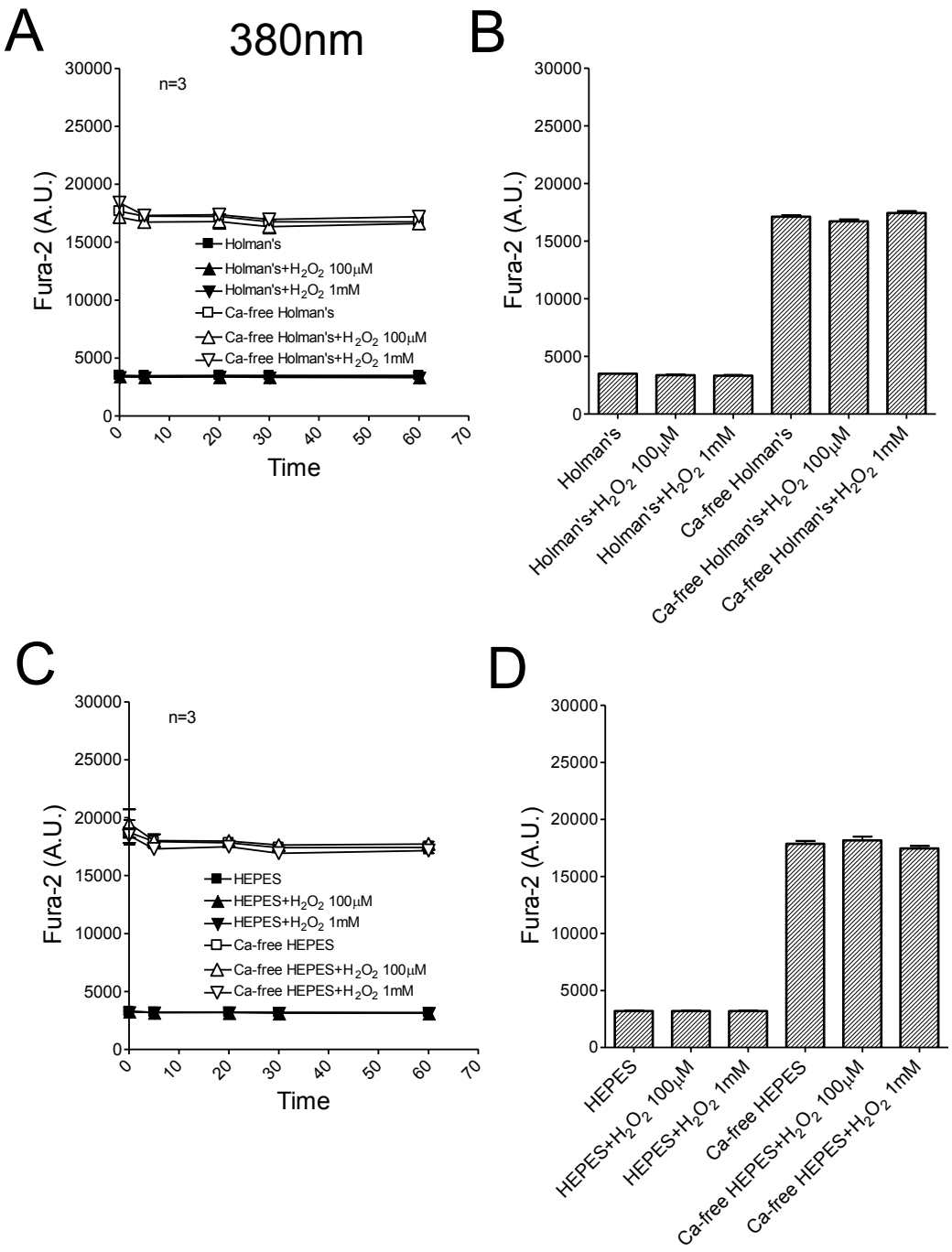

Figure 5.5 Effect of H_2O_2 on dye responsiveness test for Fura-2 at 380nm. 100 μM and 1 mM H_2O_2 has no effect on fura-2 fluorescence at 380nm over a 60 minutes period for (A) Holman's and Ca^{2+}-free Holman's buffer and (B) Bar graph of all data regardless of time confirmed this result. (C and D), similar for HEPES and Ca^{2+}-free HEPES buffer, H_2O_2 did not cause any change in fura-2 fluorescence. n denotes the number of tests examined. AU stands for arbitrary units.

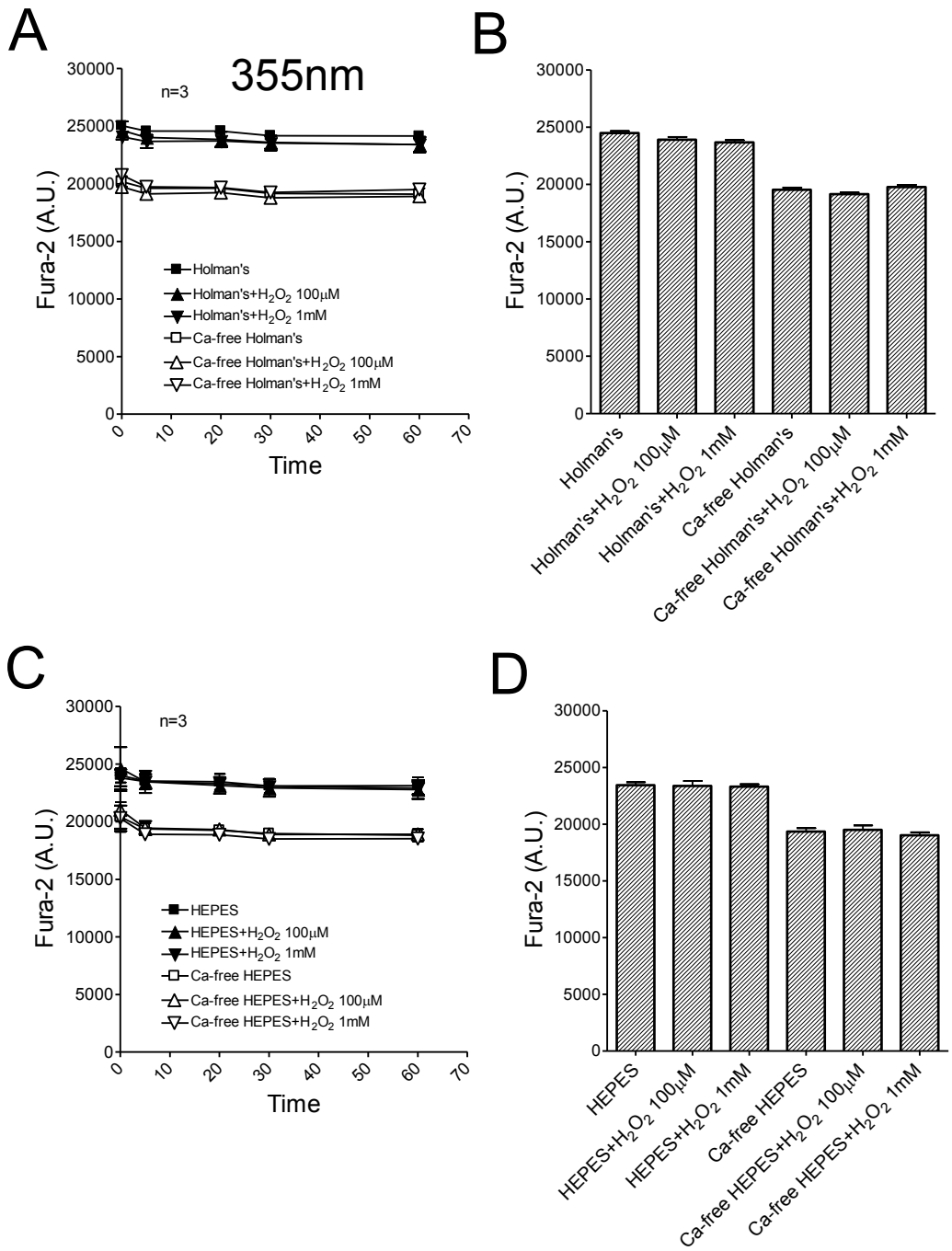

Figure 5.6 Effect of H_2O_2 on dye responsiveness test for Fura-2 at 355nm. 100 μM and 1 mM H_2O_2 has no effect on fura-2 fluorescence at 355nm over a 60 minutes period for (A) Holman's and Ca^{2+}-free Holman's buffer and (B) Bar graph of all data regardless of time confirmed this result. (C and D), similar for HEPES and Ca^{2+}-free HEPES buffer, H_2O_2 did not cause any change in fura-2 fluorescence. n denotes the number of tests examined. AU stands for arbitrary units.

5.3.5 Confocal laser-scanning microscopy imaging using the intracellular Ca^{2+} indicators

Fluo-4 fluorescence was equally distributed inside the cell for both rabbit aortic valve leaflets and EA.hy926 cells incubated with Ca^{2+}-free Holman's buffer (Figure 5.7).

Mag-fluo-4 fluorescence was seen at all parts of the cell except the site of the nuclei in both rabbit aortic valve leaflets and EA.hy926 cells incubated with Holman's buffer. Upon treatment with 30 μM CPA, a decrease in Mag-fluo-4 fluorescence was observed in both tissue (Figure 5.8). It was noted that after CPA treatment, a "dot" of condensed residual Mag-fluo-4 fluorescence was observed at site close to the cell nuclei in the rabbit aortic valve leaflets. This residual fluorescence was persistent after 100 μM TPEN and 20 mM EGTA treatment (Figure 5.9).

In aortic valve leaflets incubated with Holman's buffer, identical loading distribution was seen with co-localization of fluorescent loading by Rhod-2 and mitochondrion-selective MTG (Figure 5.10 A). In comparison, in EA.hy926 cells, the Rhod-2 fluorescence was minimal (Figure 5.10 B).

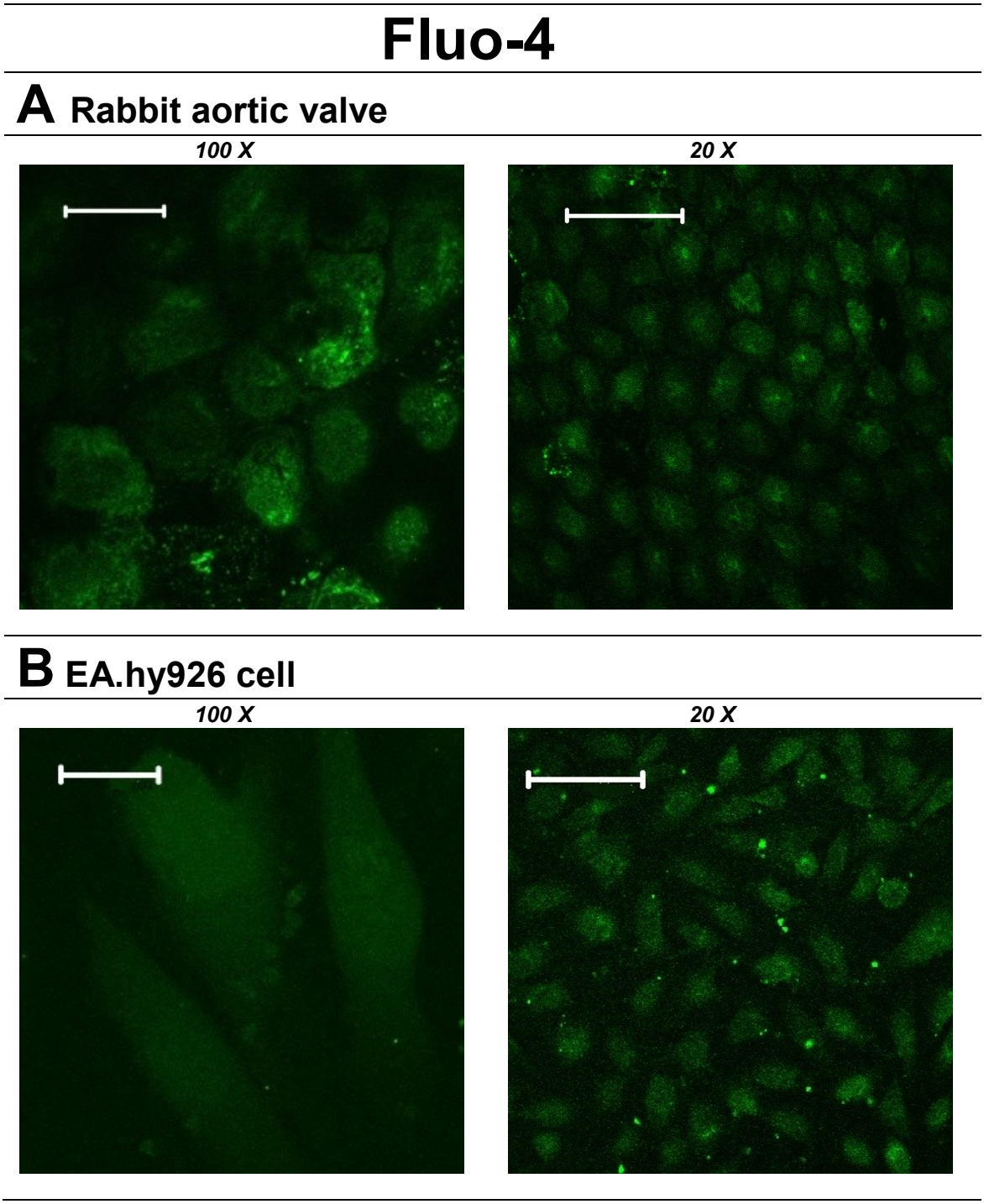

Figure 5.7 Fluo-4 loading in (A) rabbit aortic valve leaflets and (B) EA.hy926 cells. Bar represents 20 μm at 100X or 100 μm at 20X magnification.

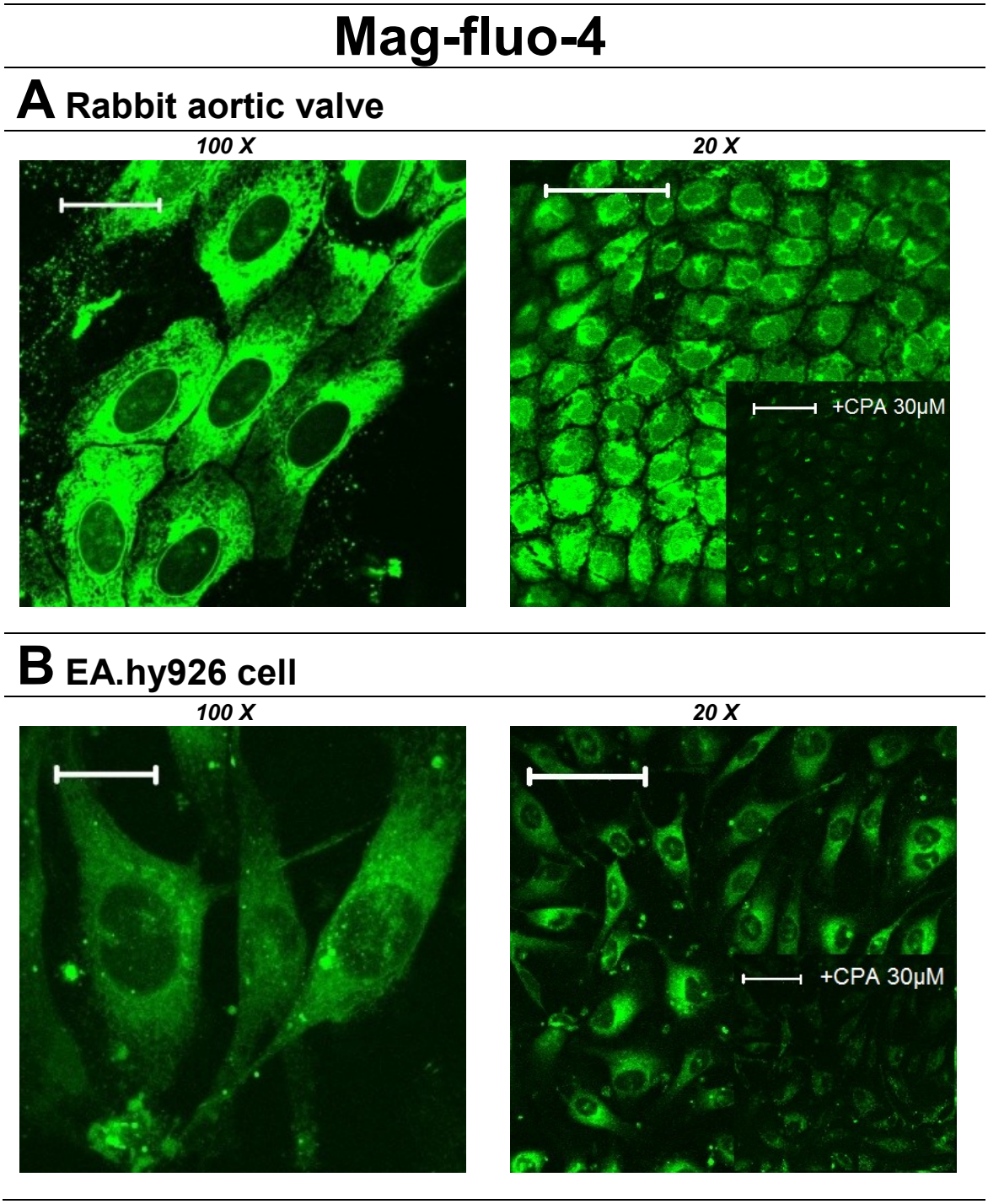

Figure 5.8 Mag-fluo-4 loading in (A) rabbit aortic valve leaflets and (B) EA.hy926 cells. Bar represents 20 μm at 100X or 100 μm at 20X magnification.

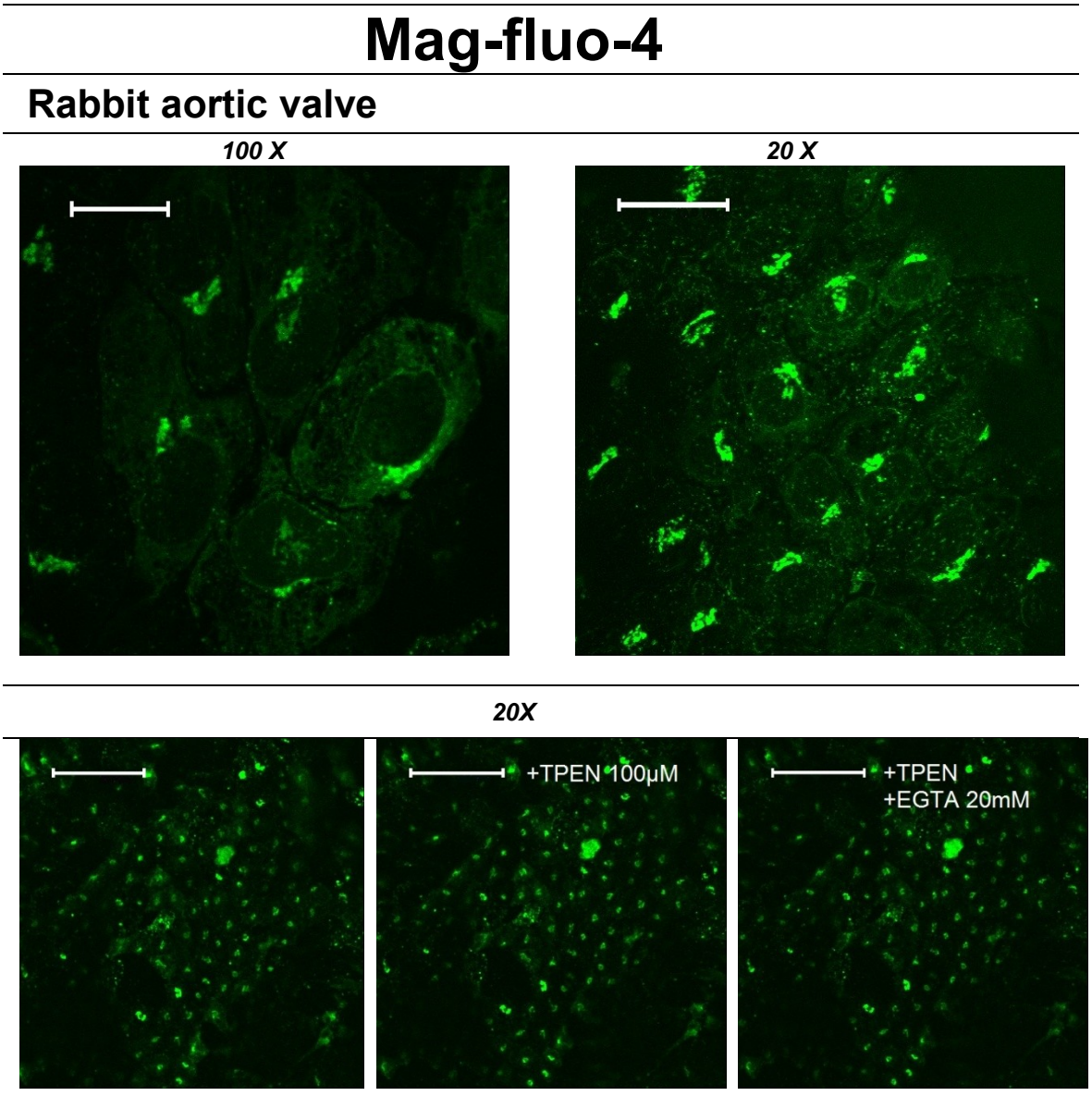

Figure 5.9 Effect of 100 µM TPEN and 20mM EGTA on residual Mag-fluo-4 fluorescence observed in rabbit aortic valve leaflets. Bar represents 20 µm at 100X or 100 µm at 20X magnification.

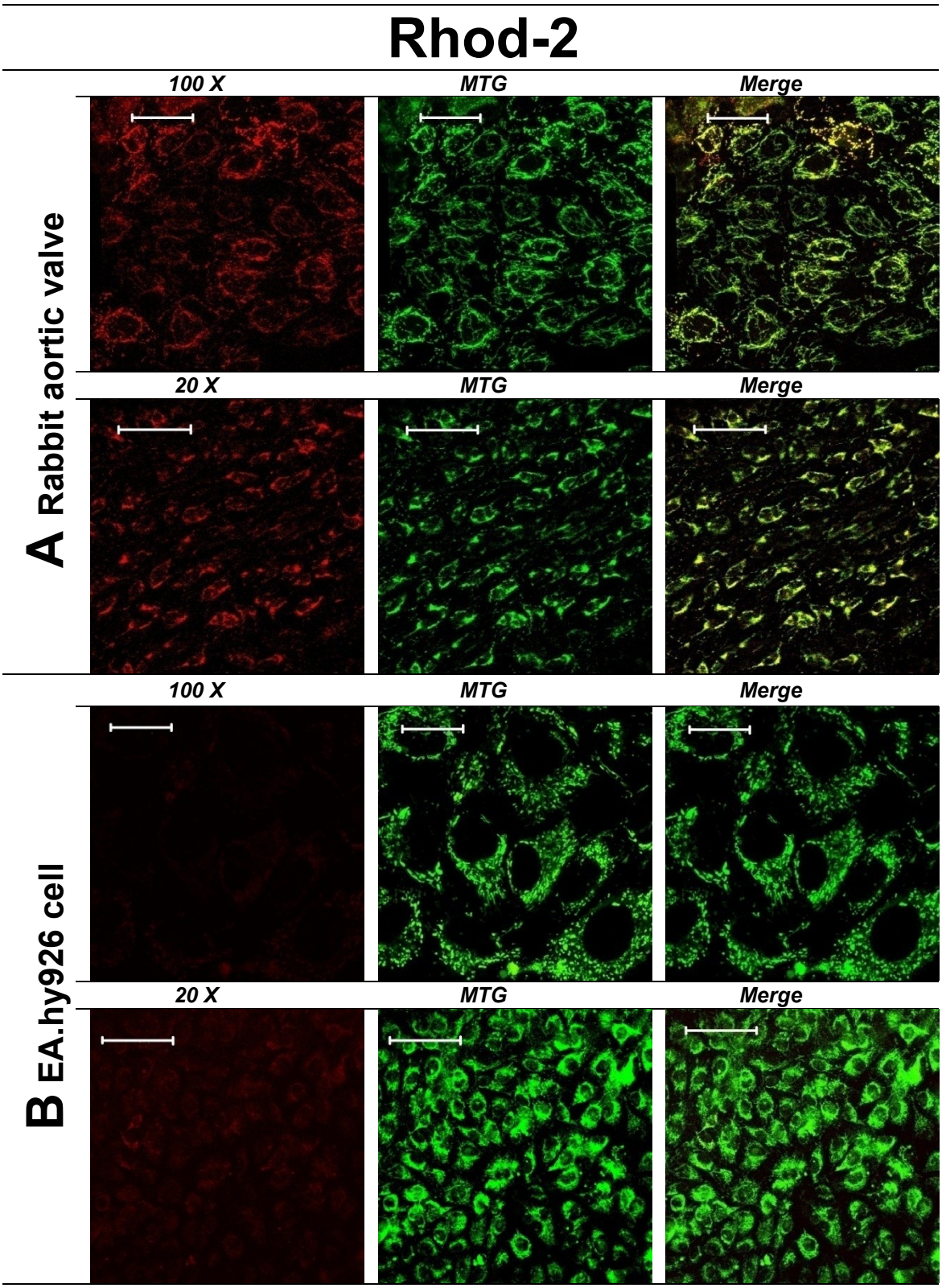

Figure 5.10 Rhod-2 loading in (A) rabbit aortic valve leaflets and (B) EA.hy926 cells. Bar represents 20 µm at 100X or 100 µm at 20X magnification. MTG represents dual loading with MitoTracker Green.

5.4 DISCUSSION

The main findings of the present chapter: (i) the strong oxidant H_2O_2 has no direct effect on response of fluorescence probes Fluo-4, Mag-fluo-4, Rhod-2 and Fura-2 to calcium; (ii) for probe Fluo-4 and Mag-fluo-4, the distribution of fluorescence inside the cells was similar for rabbit aortic valve leaflets and EA.hy926 cells and (iii) the Rhod-2 fluorescence distribution observed in rabbit aortic valve leaflets and EA.hy926 cells were identical to mitochondrion-selective MTG.

In the dye responsiveness test for fluorescence probe Fluo-4, Mag-fluo-4 and Rhod-2, the fluorescence intensity was shifted 1.6 fold, 12 fold and 1.8 fold respectively between Ca^{2+}-rich Holman's buffer and Ca^{2+}-free Holman's buffer. The addition of 100 μM or 1 mM H_2O_2 had no effect on the responses of the probes to calcium. For the ratiometric fluorescence probe Fura-2, three excitation wavelengths were examined in the responsiveness test. At 340 nm and 355 nm, the difference in fluorescence intensity was 1.7 fold and 1.2 fold between Ca^{2+}-rich buffer and Ca^{2+}-free buffer respectively. At 380 nm, the difference in fluorescence intensity was 4.9 fold between Ca^{2+}-free buffer and Ca^{2+}-rich buffer. 100 μM or 1 mM H_2O_2 did not affect Fura-2 responses to calcium. These findings suggested that H_2O_2, as an oxidant, does not chemically alter the fluorescence spectrum of these probes.

Following the procedures and concentrations suggested by supplier Invitrogen, these fluorescence probes were loaded into the rabbit aortic valve leaflets and EA.hy926 cells for comparison. In Ca^{2+}-free Holman's buffer, weak Fluo-4 fluorescence was observed and the intensity was equally distributed across the cell for both aortic valve leaflets and EA.hy926 cells, this demonstrated a low level of cytosolic free Ca^{2+} concentration under Ca^{2+}-free condition. Under high definition (100X) confocal imaging, it was found that in both rabbit aortic valve leaflets and EA.hy926 cells, the Mag-fluo-4 fluorescence was seen at all parts of the cell except the site of the nuclei, indicating a high level of Ca^{2+} concentration in the intracellular stores and a low level of resting

cytosolic free Ca^{2+} concentration in the cytosol. Similar findings have been reported in other type of cells (Park *et al.*, 2000; Petersen *et al.*, 2001; Edwards *et al.*, 2008), thus confirming the success of this dye loading technique.

Interestingly, after CPA treatment, a "dot" of condensed residual Mag-fluo-4 fluorescence was observed in each cell of the rabbit aortic valve leaflets that it is located at site close to the cell nuclei. It was suggested that this may be caused by heavy metal such as zinc ion (Zn^{2+}) that binds to the Mag-fluo-4 molecule (Prof. Karl Swann personal communication). However, neither the intracellular Zn^{2+} chelator TPEN nor the subsequent addition of Ca^{2+} chelator EGTA had any effect on these dots. Due to the fact that the site of these dots was close to the cell nuclei, it was also suggested that they might be the golgi apparatus that plays a role in storing Ca^{2+} that is released from the ER upon CPA treatment (Prof. Karl Swann personal communication). However, it was not feasible to test this hypothesis in the present study due to the absence of a suitable antibody.

The dual loading of Rhod-2 and mitochondria specific MTG in rabbit aortic valve had an identical fluorescence distribution, therefore suggesting that Rhod-2 was indeed loaded inside the mitochondria. It should be noted that the intensity of fluorescence observed in EA.hy926 cells was much lower compared with rabbit aortic valve, a possible explanation is that the mitochondria Ca^{2+} store in the intact tissue has a higher capacity for Ca^{2+} than those in cultured cells.

5.5 CHAPTER SUMMARY

1. H_2O_2 does not interfere with the ability of fluorescence probes Fluo-4, Mag-fluo-4, Rhod-2 and Fura-2 on Ca^{2+} detection in cell-free condition.

2. The distributions of Fluo-4, Mag-fluo-4, Rhod-2 and Fura-2 fluorescence are identical in rabbit aortic valve leaflets and EA.hy926 cells.

Chapter 6

Interactive Roles of Hydrogen Peroxide and Calcium in the Endothelial Signalling Network that Underpins the EDHF Phenomenon

6.1 INTRODUCTION

6.1.1 General backgrounds

The studies reported in Chapter 3 showed that exogenous applied H_2O_2 potentiated electrotonically-mediated EDHF-type relaxation both with receptor-dependent and –independent activation. While in Chapter 4, it was confirmed that the potentiating effect of arsenite on the EDHF-type response was due to the generation of endogenously produced endothelial H_2O_2 by stimulating endothelial NADPH oxidase activity. It has been shown that H_2O_2 contributes to the potentiation of CPA evoked EDHF-type responses by enhancing ER Ca^{2+} release thus elevating endothelial cell $[Ca^{2+}]_i$, thereby activating hyperpolarizing K_{Ca} channels (Edwards *et al.*, 2008). The enhanced elevation of $[Ca^{2+}]_i$ with H_2O_2 was closely mimicked by thimerosal, a thiol reagent known to sensitize the $InsP_3$ receptor, thus suggesting that H_2O_2 may also work by sensitizing the $InsP_3$ receptors on the ER (Edwards *et al.*, 2008). However, the findings of the mechanical studies presented in Chapter 3 suggest that thimerosal did not fully mimic the responses to H_2O_2. Whereas thimerosal promoted the potentiation of both EDHF-

type and NO-mediated responses, H_2O_2 only enhanced the EDHF-type response. These differences in the mechanisms of action of H_2O_2 and thimerosal raise the question, so how does H_2O_2 elevate the intracellular Ca^{2+}? Does H_2O_2 work by modulating intracellular Ca^{2+} release through $InsP_3$ receptors, have an effect on ryanodine-gated channels or SERCA pumps? Ca^{2+} influx via SOCE is triggered secondary to the emptying of ER Ca^{2+} stores, which is also influenced by modulation of these channels, so it is important to understand the role H_2O_2 plays in SOCE.

In Chapter 5, a number of fluorescence probes were validated to use in rabbit preparations, and they will be used to identify key Ca^{2+} signaling interactions. In order to have better spatial resolution, confocal microscopy and confocal friendly probes such as Fluo-4, Mag-fluo-4 and Rhod-2 will be employed in the present study. To monitor extracellular Ca^{2+} influx through non-selective cation channels (Lin *et al.*, 2007), a Mn^{2+} quench technique will be used, this technique also advances as the use of Mn^{2+} ions avoided the selective Ca^{2+} extrusion pathways such as Sodium-Calcium exchanger (NCX) and PMCA (Jardin *et al.*, 2009).

In addition, increase in $[Ca^{2+}]_i$ promote mitochondria uptake via the Ca^{2+} uniporter, which lead to elevated $[Ca^{2+}]_m$ that increase $O_2^{\bullet-}/H_2O_2$ production (Brookes *et al.*, 2004; Zhang and Gutterman, 2007). Therefore, the relationship between mitochondrial Ca^{2+} uptake/H_2O_2 production and the elevated $[Ca^{2+}]_i$ results from the ER store depletion through H_2O_2-mediated mechanism will also be investigated. As shown in Chapter 3, ACh at low concentrations causes transient relaxations in the rabbit iliac artery, whereas the responses evoked by CPA are sustained. To allow imaging of a concentration-dependent effect, I will therefore use CPA to indentify the effects of H_2O_2 on $[Ca^{2+}]_i$, $[Ca^{2+}]_{ER}$ and $[Ca^{2+}]_m$.

Most experiments in this chapter will involve imaging in the rabbit aortic valve leaflets. As explained in Chapter 2, this preparation consists of a double layer of endothelial

cells and possesses the major advantage of circumventing the complicating effects of signals transmitted from subjacent smooth muscle cells via myoendothelial gap junctions. In vessels such as rabbit iliac artery, these gap junction channels allow diffusion of Ca^{2+}/$InsP_3$ from smooth muscle cells and/or the electrotonic transmission of changes in smooth muscle membrane potential and may profoundly influence endothelial responses in intact arterial segments (Dora *et al.*, 1997; Murai *et al.*, 1999). Although it has previously been shown that "residual" L-NAME-insensitive NO activity does not contribute to EDHF-type responses in the rabbit iliac artery (Griffith *et al.*, 2005; Edwards *et al.*, 2007), the studies proposed in this chapter will be performed in the presence of L-NAME and indomethacin to inhibit eNOS and COX.

6.1.2 Aim of this chapter

The aim of the present chapter was to investigate the influence of H_2O_2 in the Ca^{2+} mobilization that underpins the EDHF phenomenon. Experiments in this chapter involve confocal and conventional imaging in the rabbit aortic valves with the Ca^{2+} sensitive fluorescent probes Fluo-4, Fura-2, Mag-fluo-4 and Rhod-2. The Ca^{2+} mobilization between: (i) intracellular free Ca^{2+}; (ii) ER Ca^{2+} stores and (iii) mitochondria Ca^{2+} stores via $InsP_3$ receptors, SERCA pumps and Ca^{2+} influx pathways will be examined in this study.

6.2 MATERIALS AND METHODS

6.2.1 Imaging studies with rabbit aortic valve

Fluorescent probes under study were loaded into the rabbit aortic valves as described in Section 2.1.2 and 2.3.4. After loading, the valves were washed 3 times with indicator-free Holman's buffer or HEPES buffer as required before incubating with L-NAME/indomethacin for 30 minutes. Each leaflet was mounted on a customised 35mm glass bottomed culture dish, which has 3 pairs of pins to hold the leaflets in place.

6.2.2 Imaging studies with EA.hy926 cells

The fluorescent probes under study were loaded into the EA.hy926 human endothelial cells as described in Section 2.4.3 and 2.5.1 in 35mm glass bottomed culture dishes 24 hours prior to experiment. After loading, cells were washed 3 times with indicator-free Holman's buffer before incubating with L-NAME/indomethacin for 30 minutes.

6.2.3 Data recording and Statistics

Details of data analysis for confocal imaging and conventional microscopy studies were described in Section 2.3.7, 2.3.8, 2.5.2 and 2.6. Details of statistical analyses used for each figure were indicated in figures descriptions.

6.3 RESULTS

6.3.1 Effect of H_2O_2 on CPA-evoked elevation of $[Ca^{2+}]_i$ in the rabbit aortic valve leaflets.

In Fluo-4 loaded rabbit aortic valve leaflets incubated with Holman's buffer, CPA caused an increase in Fluo-4 fluorescence signal at 30 μM but not at 10 μM. Higher concentrations of CPA at 100 μM or 3 μM 4-Br-A23187 had no additional effect on the response. Subsequent treatment with 15 mM EGTA fully diminished the fluorescence signal (Figure 6.1).

Due to the low sensitivity of Fluo-4 on Ca^{2+} responses evoked by CPA and 4-Br-A23187 compared with results previously obtained in the laboratory with Fura-2, the experiment on $[Ca^{2+}]_i$ was switched to Fura-2. In Fura-2 loaded rabbit aortic valve leaflets incubated with Holman's buffer, CPA caused a concentration-dependent increase in Fura-2 340/380 ratio, with the maximum reached at 30 μM. 100 μM H_2O_2 by itself caused a small rise of $[Ca^{2+}]_i$, however, a significantly synergistic elevation of $[Ca^{2+}]_i$ by H_2O_2 and 1-10 μM CPA was observed, whereas H_2O_2 was ineffective after 30 μM CPA (Figure 6.2).

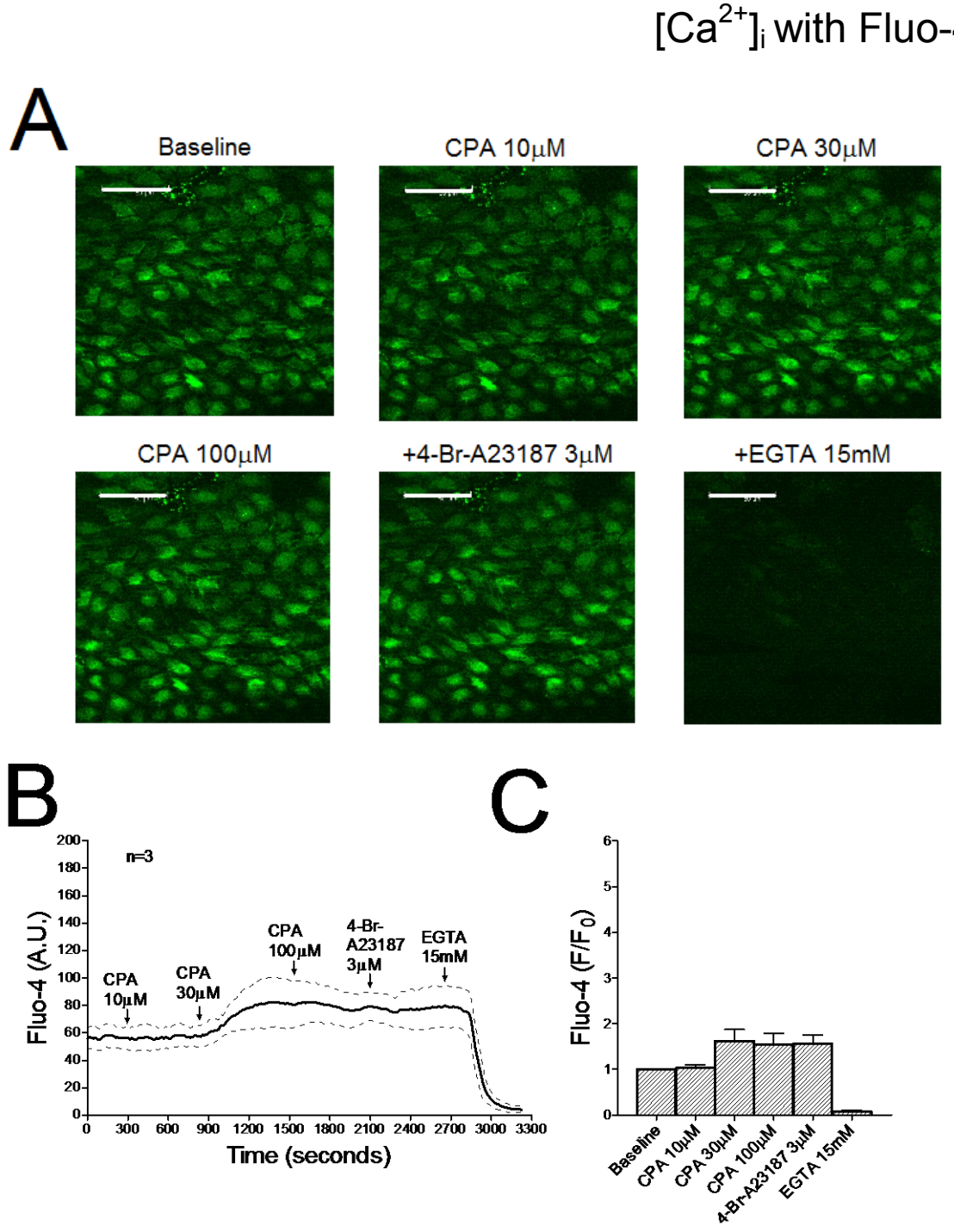

Figure 6.1 CPA-evoked elevation of $[Ca^{2+}]_i$ in Holman's buffer with the rabbit aortic valves. (A) Representative images showing effect of CPA, 4-Br-A23187 and EGTA on Fluo-4 fluorescence. (B) Summary traces showing concentration-dependent elevation of $[Ca^{2+}]_i$ by CPA, whereas 3 μM 4-Br-A23187 was having no additional effect. Subsequent treatment with EGTA caused a strong reduction in fluorescence which was likely to be the result of the chelation of free intracellular calcium. (C) Bar graphs confirming a small increase of $[Ca^{2+}]_i$ by 30 μM CPA. Scalebars denote 50 μm. n denotes the number of animals studied. Error bars were represented by dotted lines.

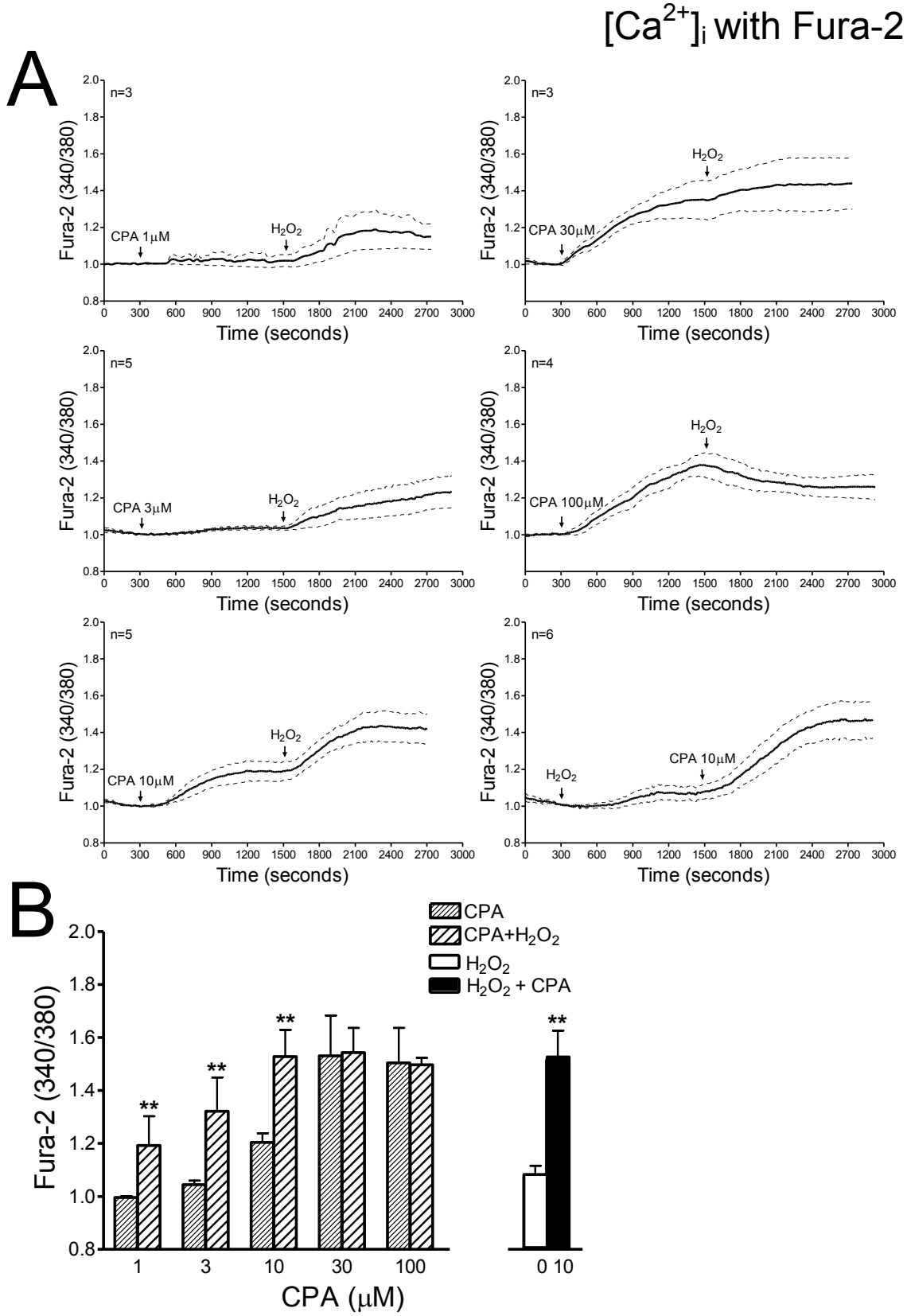

Figure 6.2 Effect of 100 μM H_2O_2 on CPA-evoked elevation of $[Ca^{2+}]_i$ in the rabbit aortic valves. (A) Summary traces showing synergistic elevation of $[Ca^{2+}]_i$ by H_2O_2 and 1-10 μM CPA, whereas H_2O_2 was ineffective after 30 μM CPA. (B) Bar graphs confirming potentiation of $[Ca^{2+}]_i$ by H_2O_2. ** denotes p<0.01 compared with corresponding control in Student's t-test. n denotes the number of animals studied. Error bars were represented by dotted lines.

6.3.2 Effect of thimerosal on CPA-evoked elevation of $[Ca^{2+}]_i$ in the rabbit aortic valve leaflets.

In Fura-2 loaded rabbit aortic valve leaflets incubated with Holman's buffer, thimerosal caused a concentration-dependent increase in Fura-2 340/380 ratio over the concentrations of 30 to 300 μM. Incubation with 10 μM thimerosal by itself did not affect the $[Ca^{2+}]_i$, however, a further significant synergistic elevation of $[Ca^{2+}]_i$ by thimerosal and 1-10 μM CPA was observed. There was no increase in response to 30 μM CPA seen with thimerosal (Figure 6.3).

6.3.3 Effect of H_2O_2 on CPA-evoked depletion of $[Ca^{2+}]_{ER}$ in the rabbit aortic valve leaflets.

In Mag-fluo-4 loaded rabbit aortic valve leaflets incubated with Holman's buffer, CPA caused a concentration-dependent decrease in Mag-fluo-4 fluorescence signal over the range 3 to 30 μM. Incubation with 100 μM H_2O_2 by itself caused a small decrease in $[Ca^{2+}]_{ER}$, however, a further significant synergistic depletion of $[Ca^{2+}]_{ER}$ by H_2O_2 and 10 μM CPA was observed. There was no increase in response to 30 μM CPA seen with H_2O_2 (Figure 6.4).

6.3.4 Effect of thimerosal on CPA-evoked depletion of $[Ca^{2+}]_{ER}$ in the rabbit aortic valve leaflets.

In Mag-fluo-4 loaded rabbit aortic valve leaflets incubated with Holman's buffer, incubation with 10 μM thimerosal by itself did not affect the $[Ca^{2+}]_{ER}$, however, a further significant synergistic depletion of $[Ca^{2+}]_{ER}$ by thimerosal and 3-10 μM CPA was observed. There was no increase in response to 30 μM CPA seen with thimerosal (Figure 6.4).

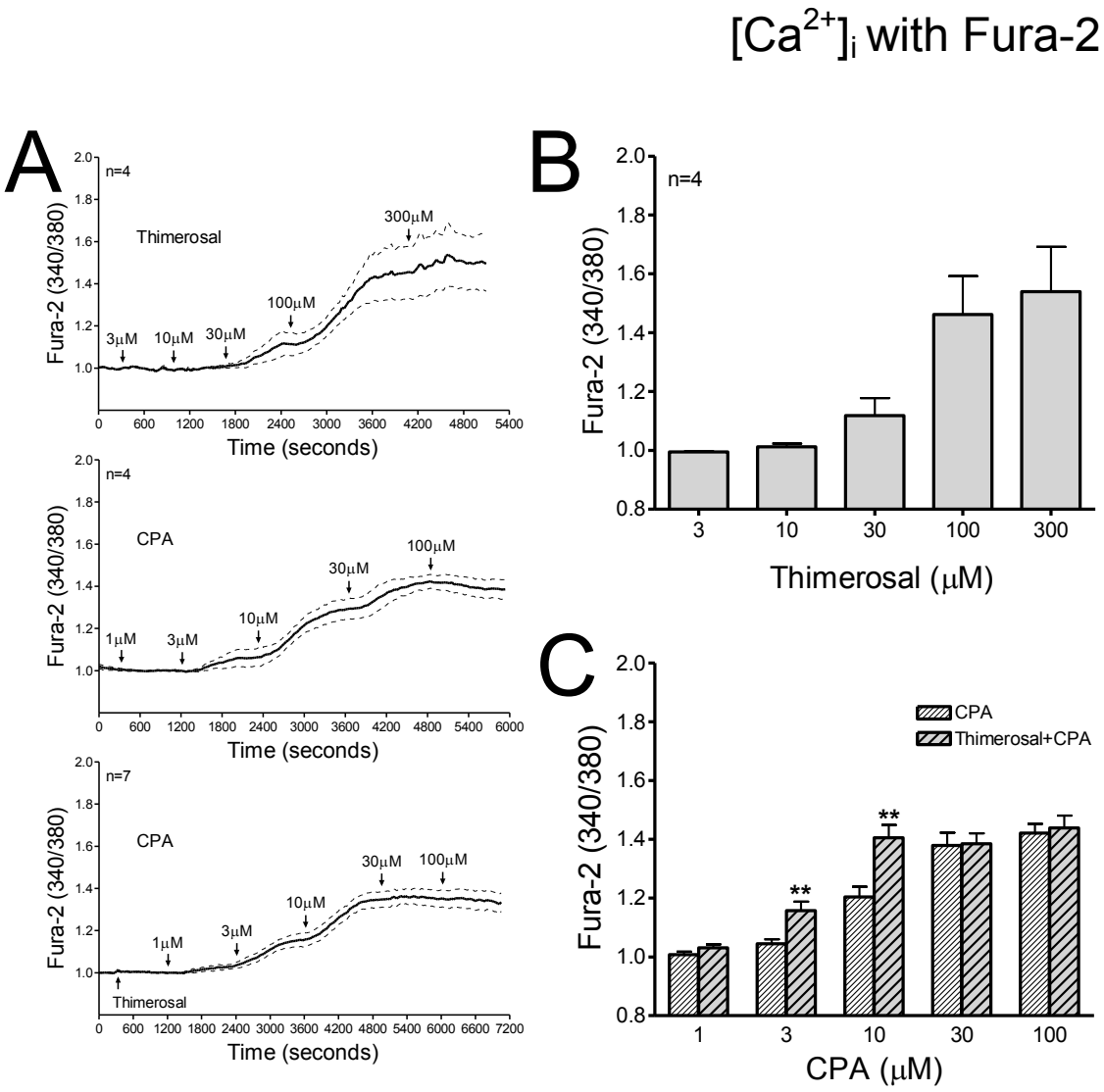

Figure 6.3 Effect of thimerosal on CPA-evoked elevation of $[Ca^{2+}]_i$ in the rabbit aortic valves. (A) Summary traces showing that direct mobilization of Ca^{2+} by thimerosal and concentration-dependent elevation of $[Ca^{2+}]_i$ by CPA in the absence and presence of 10 μM thimerosal. (B) Bar graphs confirming direct mobilization of Ca^{2+} by thimerosal. (C) Bar graphs confirming concentration-dependent elevation of $[Ca^{2+}]_i$ by CPA in the absence and presence of 10 μM thimerosal. ** denotes $p<0.01$ compared with corresponding control in Student's t-test. n denotes the number of animals studied. Error bars were represented by dotted lines.

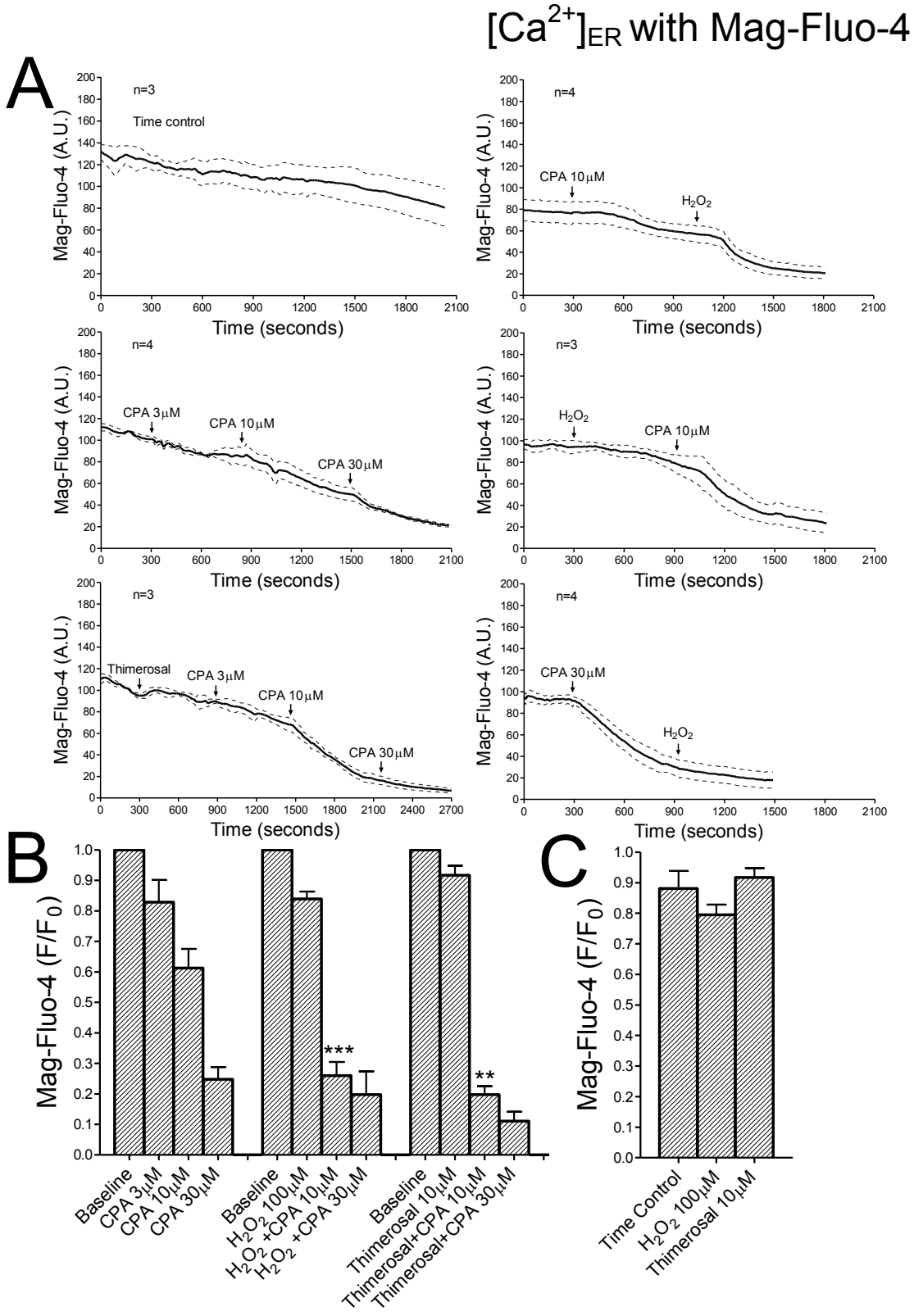

Figure 6.4 Effect of 100 μM H_2O_2 and 10 μM thimerosal on CPA-evoked depletion of ER Ca^{2+} stores in the rabbit aortic valves. (A) Summary traces showing that concentration-dependent depletion of stores by CPA in the absence and presence of H_2O_2 and thimerosal. (B) Bar graphs confirming that store depletion by CPA was potentiated to an equivalent extent by H_2O_2 and thimerosal. (C) Bar graph showing direct effect of H_2O_2 and thimerosal on $[Ca^{2+}]_{ER}$ compared with time control at 900s. ** and ***denote p<0.01 and 0.001 compared with 10 μM CPA alone in Student's t-test. n denotes the number of animals studied. Error bars were represented by dotted lines.

6.3.5 Effect of H_2O_2 on ACh-evoked depletion of $[Ca^{2+}]_{ER}$ in the rabbit aortic valve leaflets.

In Mag-fluo-4 loaded rabbit aortic valve leaflets incubated with Holman's buffer, 1 and 3 μM ACh decreased Mag-fluo-4 fluorescence signal to a similar extent. Incubation with 100 μM H_2O_2 by itself caused a small decrease on $[Ca^{2+}]_{ER}$ (with reference to the time control), however, a further significant potentiated depletion of $[Ca^{2+}]_{ER}$ by H_2O_2 and 1-3 μM ACh was observed (Figure 6.5).

6.3.6 Effect of H_2O_2 on Ca^{2+} re-entry by CPA in the rabbit aortic valve leaflets.

In Fluo-4 loaded rabbit aortic valve leaflets incubated with Ca^{2+}-free Holman's buffer, CPA caused a small transient increase in Fluo-4 fluorescence signal at 10 and 30 μM, the addition of 100 μM H_2O_2 after CPA did not affect the $[Ca^{2+}]_i$. In the presence of H_2O_2, upon addition of Ca^{2+}, the Ca^{2+} re-entry in the presence of 10 μM CPA was significantly increased. There was no increase in response with 30 μM CPA seen with H_2O_2 (Figure 6.6).

6.3.7 Effect of thimerosal on Ca^{2+} re-entry by CPA in the rabbit aortic valve leaflets.

In Fluo-4 loaded rabbit aortic valve leaflets incubated with Ca^{2+}-free Holman's buffer, CPA caused an small transient increase in Fluo-4 fluorescence signal at 10 and 30 μM, the addition of 10 μM thimerosal after the CPA did not affect the $[Ca^{2+}]_i$. In the presence of thimerosal, the Ca^{2+} re-entry by 10 μM CPA was significantly increased. There was no increase in response to 30 μM CPA seen with thimerosal (Figure 6.7).

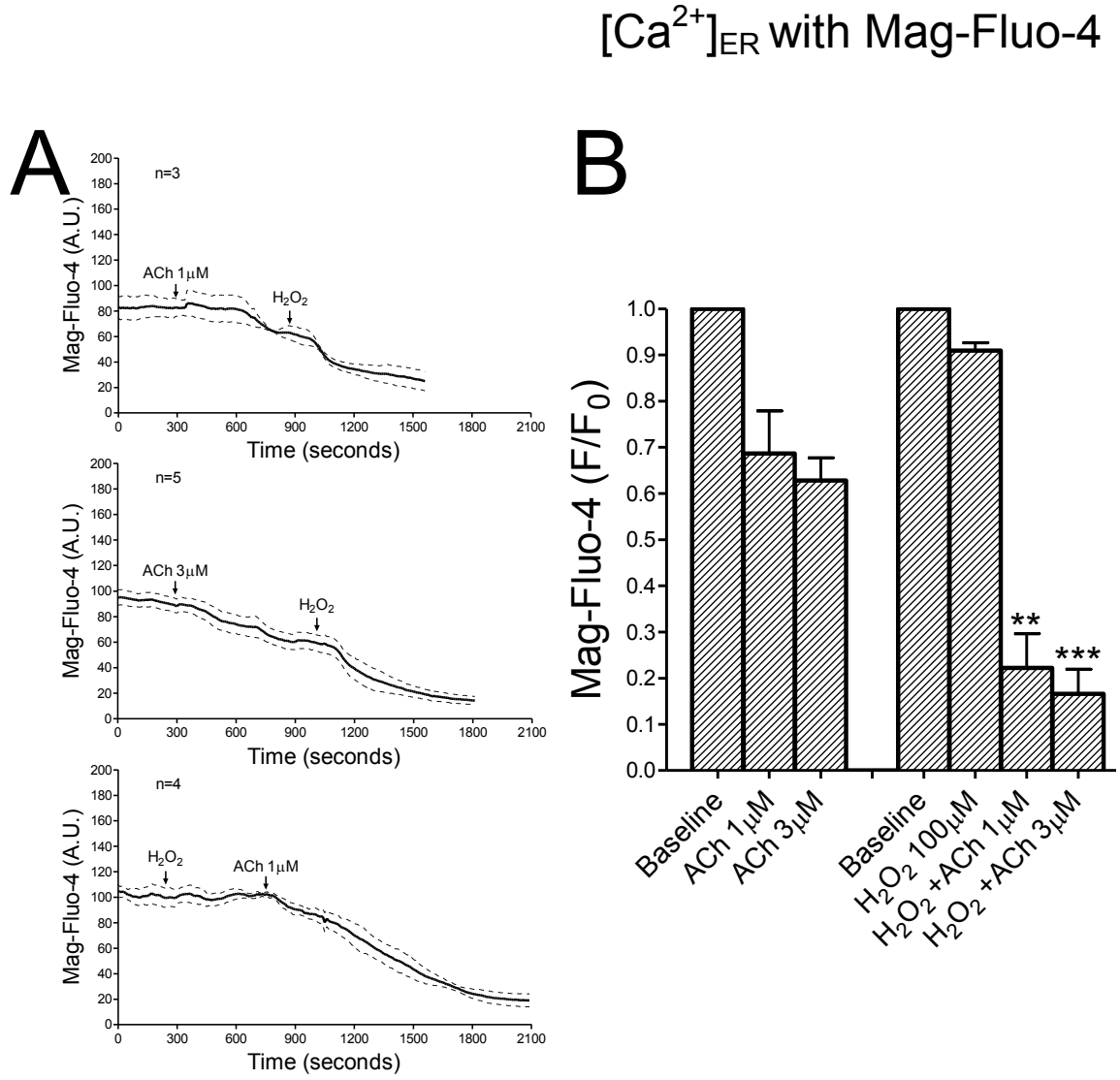

Figure 6.5 Effect of 100 μM H_2O_2 on ACh-evoked depletion of ER Ca^{2+} stores in the rabbit aortic valves. (A) Summary traces showing that concentration-dependent depletion of stores by ACh in the absence and presence of H_2O_2. (B) Bar graphs confirming that store depletion by ACh was potentiated by H_2O_2. ** and ***denote p<0.01 and 0.001 compared with corresponding control in Student's t-test. n denotes the number of animals studied. Error bars were represented by dotted lines.

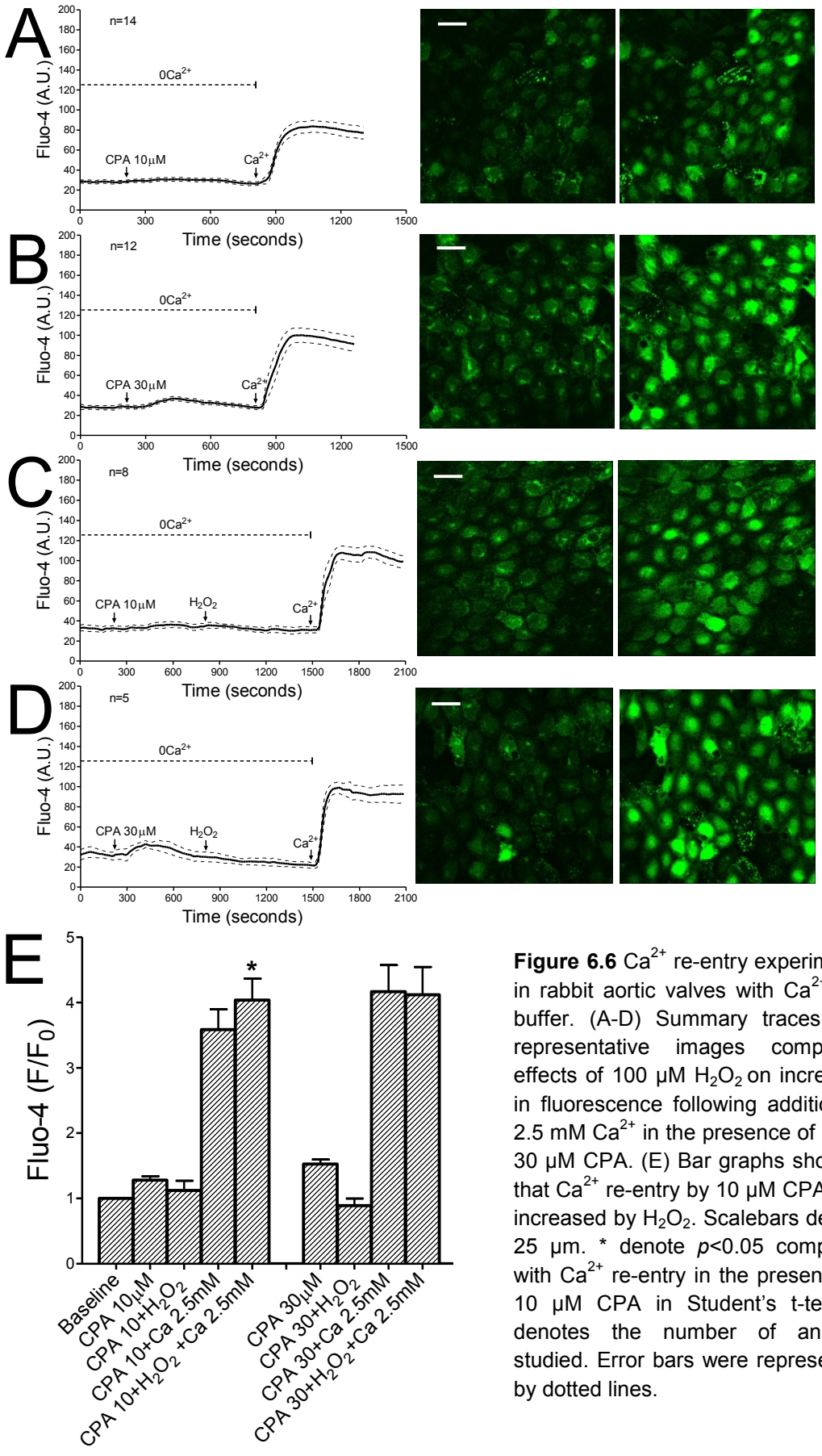

Figure 6.6 Ca^{2+} re-entry experiments in rabbit aortic valves with Ca^{2+}-free buffer. (A-D) Summary traces and representative images comparing effects of 100 μM H_2O_2 on increases in fluorescence following addition of 2.5 mM Ca^{2+} in the presence of 10 or 30 μM CPA. (E) Bar graphs showing that Ca^{2+} re-entry by 10 μM CPA was increased by H_2O_2. Scalebars denote 25 μm. * denote p<0.05 compared with Ca^{2+} re-entry in the presence of 10 μM CPA in Student's t-test. n denotes the number of animals studied. Error bars were represented by dotted lines.

$[Ca^{2+}]_i$ with Fluo-4

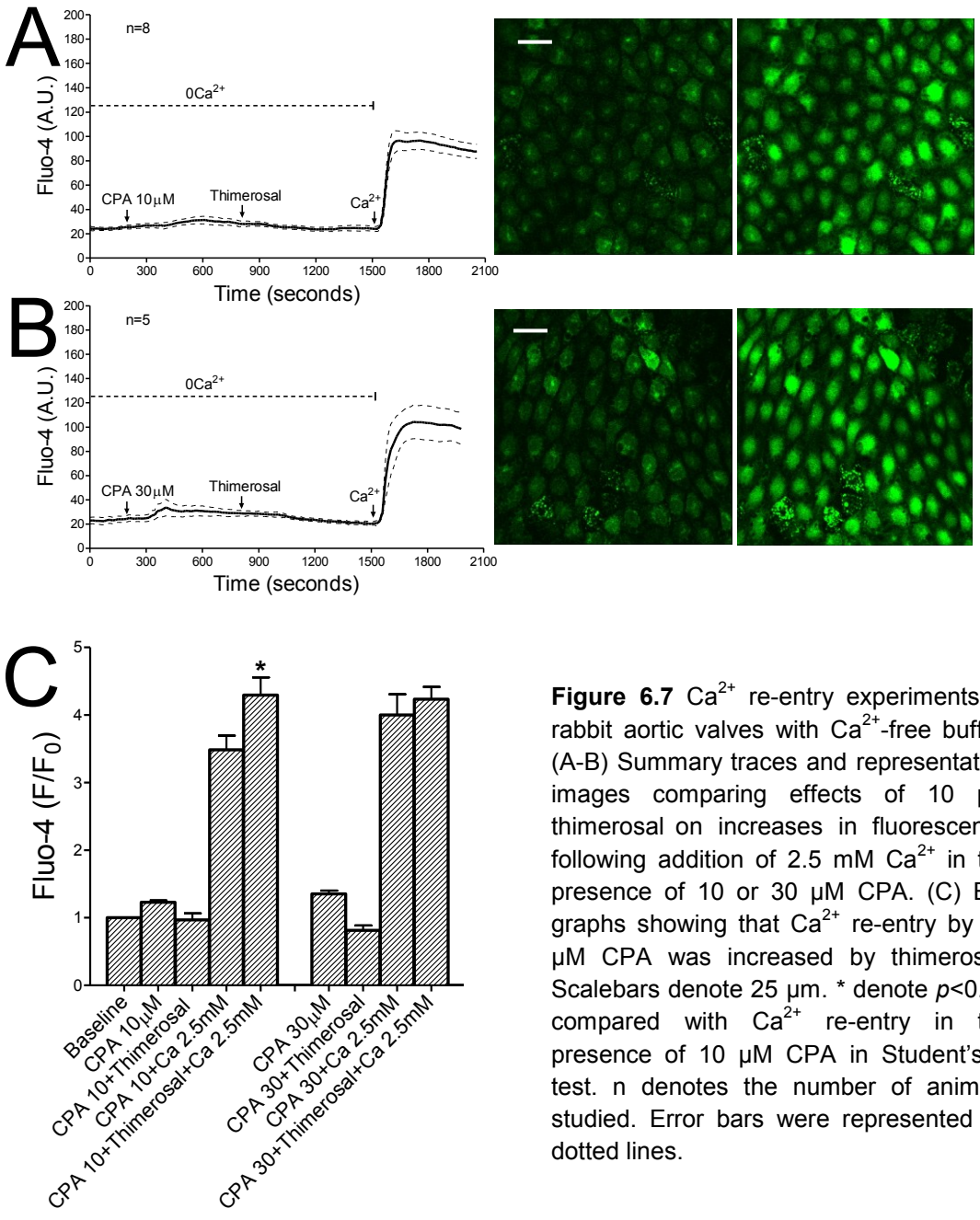

Figure 6.7 Ca^{2+} re-entry experiments in rabbit aortic valves with Ca^{2+}-free buffer. (A-B) Summary traces and representative images comparing effects of 10 μM thimerosal on increases in fluorescence following addition of 2.5 mM Ca^{2+} in the presence of 10 or 30 μM CPA. (C) Bar graphs showing that Ca^{2+} re-entry by 10 μM CPA was increased by thimerosal. Scalebars denote 25 μm. * denote $p<0.05$ compared with Ca^{2+} re-entry in the presence of 10 μM CPA in Student's t-test. n denotes the number of animals studied. Error bars were represented by dotted lines.

6.3.8 Effect of CPA on non-selective divalent cation entry in the rabbit aortic valve leaflets.

In Fura-2 loaded rabbit aortic valve leaflets incubated with HEPES buffer, application of 250 μM Mn^{2+} induced a slow quenching of Fura-2 355nm fluorescence, however, it was without effect on $[Ca^{2+}]_i$ represented by Fura-2 355/380 ratio. Depletion of ER stores with 3 to 30 μM CPA caused a concentration-dependent increase in the rate of Mn^{2+}-induced quenching of Fura-2 355nm fluorescence (Figure 6.8B) with an increase on Fura-2 355/380 ratio.

6.3.9 Effect of H_2O_2 and CPA on non-selective divalent cation entry in the rabbit aortic valve leaflets.

In Fura-2 loaded rabbit aortic valve leaflets incubated with HEPES buffer, incubation with 100 μM H_2O_2 by itself did not affect the rate of Mn^{2+}-induced quenching of Fura-2 355nm fluorescence or $[Ca^{2+}]_i$ as indicated by Fura-2 355/380 ratio. However, the presence of H_2O_2 amplified the effect of 10 μM CPA on increasing the rate of Mn^{2+}-induced Fura-2 355nm quenching. This amplifying effect of H_2O_2 on 10 μM CPA was not apparent with 30 μM CPA (Figure 6.9).

6.3.10 Effect of thimerosal and CPA on non-selective divalent cation entry in the rabbit aortic valve leaflets.

In Fura-2 loaded rabbit aortic valve leaflets incubated with HEPES buffer, incubation with 10 μM thimerosal by itself did not affect the rate of Mn^{2+}-induced quenching of Fura-2 355nm fluorescence or $[Ca^{2+}]_i$ as indicated by Fura-2 355/380 ratio. However, the presence of thimerosal decreased the rate of Mn^{2+} quenching induced by 10 and 30 μM CPA (Figure 6.10).

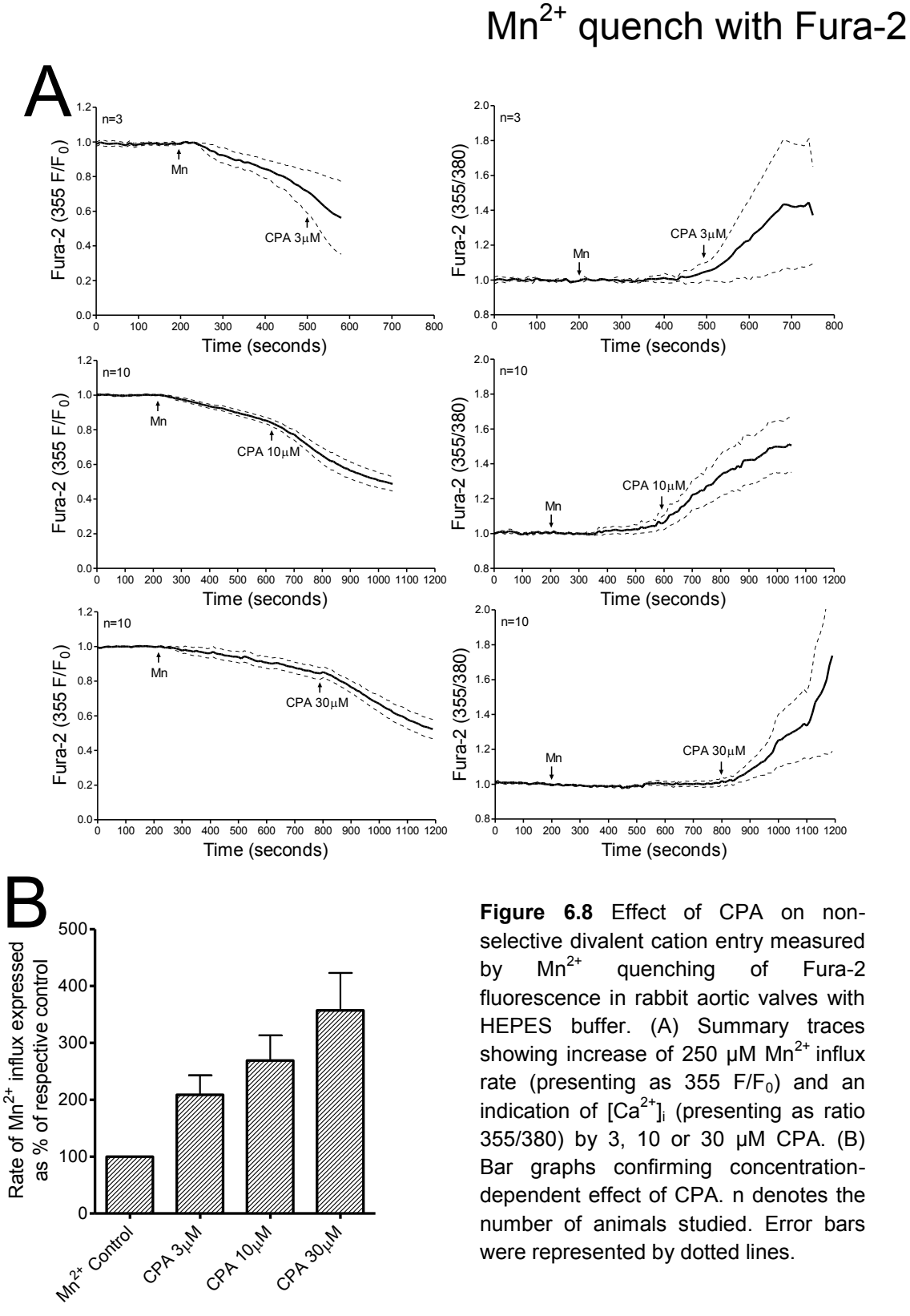

Figure 6.8 Effect of CPA on non-selective divalent cation entry measured by Mn^{2+} quenching of Fura-2 fluorescence in rabbit aortic valves with HEPES buffer. (A) Summary traces showing increase of 250 μM Mn^{2+} influx rate (presenting as 355 F/F_0) and an indication of $[Ca^{2+}]_i$ (presenting as ratio 355/380) by 3, 10 or 30 μM CPA. (B) Bar graphs confirming concentration-dependent effect of CPA. n denotes the number of animals studied. Error bars were represented by dotted lines.

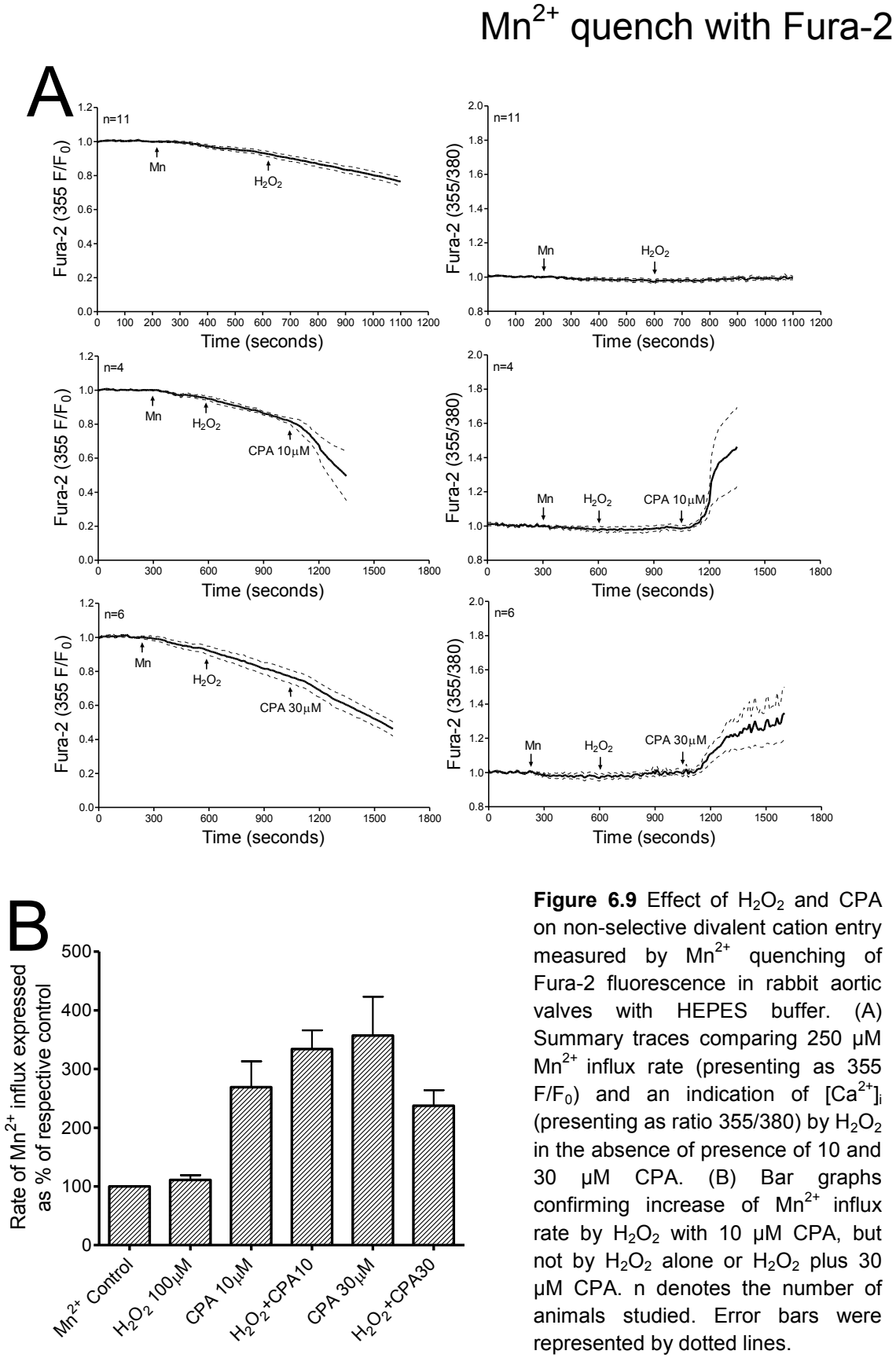

Figure 6.9 Effect of H_2O_2 and CPA on non-selective divalent cation entry measured by Mn^{2+} quenching of Fura-2 fluorescence in rabbit aortic valves with HEPES buffer. (A) Summary traces comparing 250 μM Mn^{2+} influx rate (presenting as 355 F/F_0) and an indication of $[Ca^{2+}]_i$ (presenting as ratio 355/380) by H_2O_2 in the absence of presence of 10 and 30 μM CPA. (B) Bar graphs confirming increase of Mn^{2+} influx rate by H_2O_2 with 10 μM CPA, but not by H_2O_2 alone or H_2O_2 plus 30 μM CPA. n denotes the number of animals studied. Error bars were represented by dotted lines.

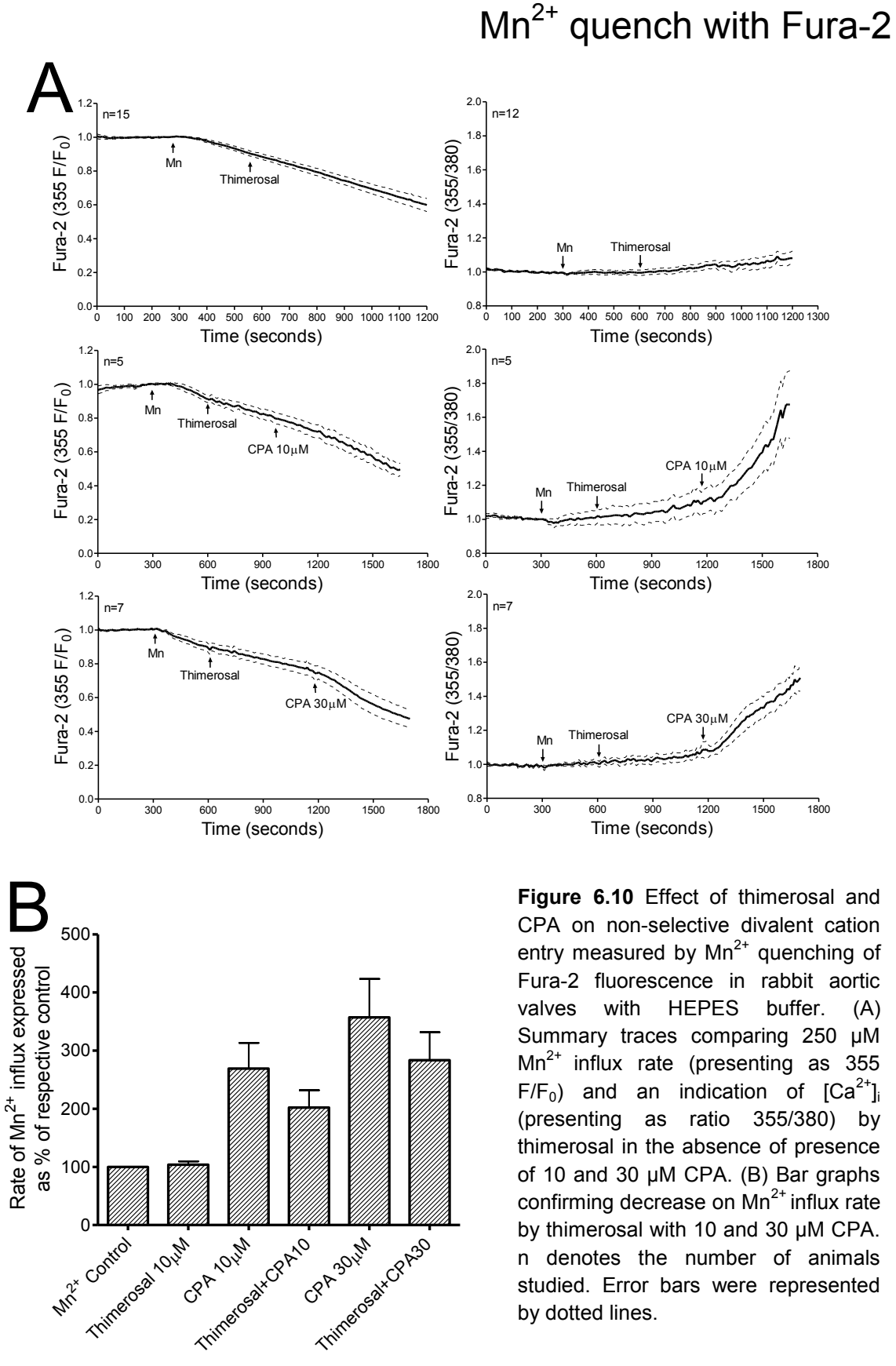

Figure 6.10 Effect of thimerosal and CPA on non-selective divalent cation entry measured by Mn^{2+} quenching of Fura-2 fluorescence in rabbit aortic valves with HEPES buffer. (A) Summary traces comparing 250 μM Mn^{2+} influx rate (presenting as 355 F/F_0) and an indication of $[Ca^{2+}]_i$ (presenting as ratio 355/380) by thimerosal in the absence of presence of 10 and 30 μM CPA. (B) Bar graphs confirming decrease on Mn^{2+} influx rate by thimerosal with 10 and 30 μM CPA. n denotes the number of animals studied. Error bars were represented by dotted lines.

6.3.11 Effect of H_2O_2 and thimerosal on depletion and refilling of $[Ca^{2+}]_{ER}$ in the rabbit aortic valve leaflets.

In Mag-fluo-4 loaded rabbit aortic valve leaflets incubated with Ca^{2+}-free Holman's buffer, the Mag-fluo-4 fluorescence signal was slowly reduced over the time, the ER store was refilled by the addition of 2.5 mM Ca^{2+}, as a small but significant increase on Mag-fluo-4 fluorescence was observed (Figure 6.11A, 6.11F).

In Ca^{2+}-free condition, 100 μM H_2O_2 caused a significant increase on the rate of ER store depletion (with reference to the respective control), however, the ER store was not refilled by the addition of 2.5 mM Ca^{2+} after the H_2O_2 treatment (Figure 6.11B, 6.11F). The increase on the rate of store depletion caused by H_2O_2 was not prevented by 10 μM Xestospongin C (XesC) (Figure 6.11C, 6.11F).

In Ca^{2+}-free condition, 10 μM thimerosal caused a significant increase on the rate of ER store depletion (with reference to the respective control and the ER store was refilled by the addition of 2.5 mM Ca^{2+} after the thimerosal treatment (Figure 6.11D, 6.11F). The increase on the rate of store depletion caused by thimerosal was fully prevented by 10 μM XesC (Figure 6.11E, 6.11F).

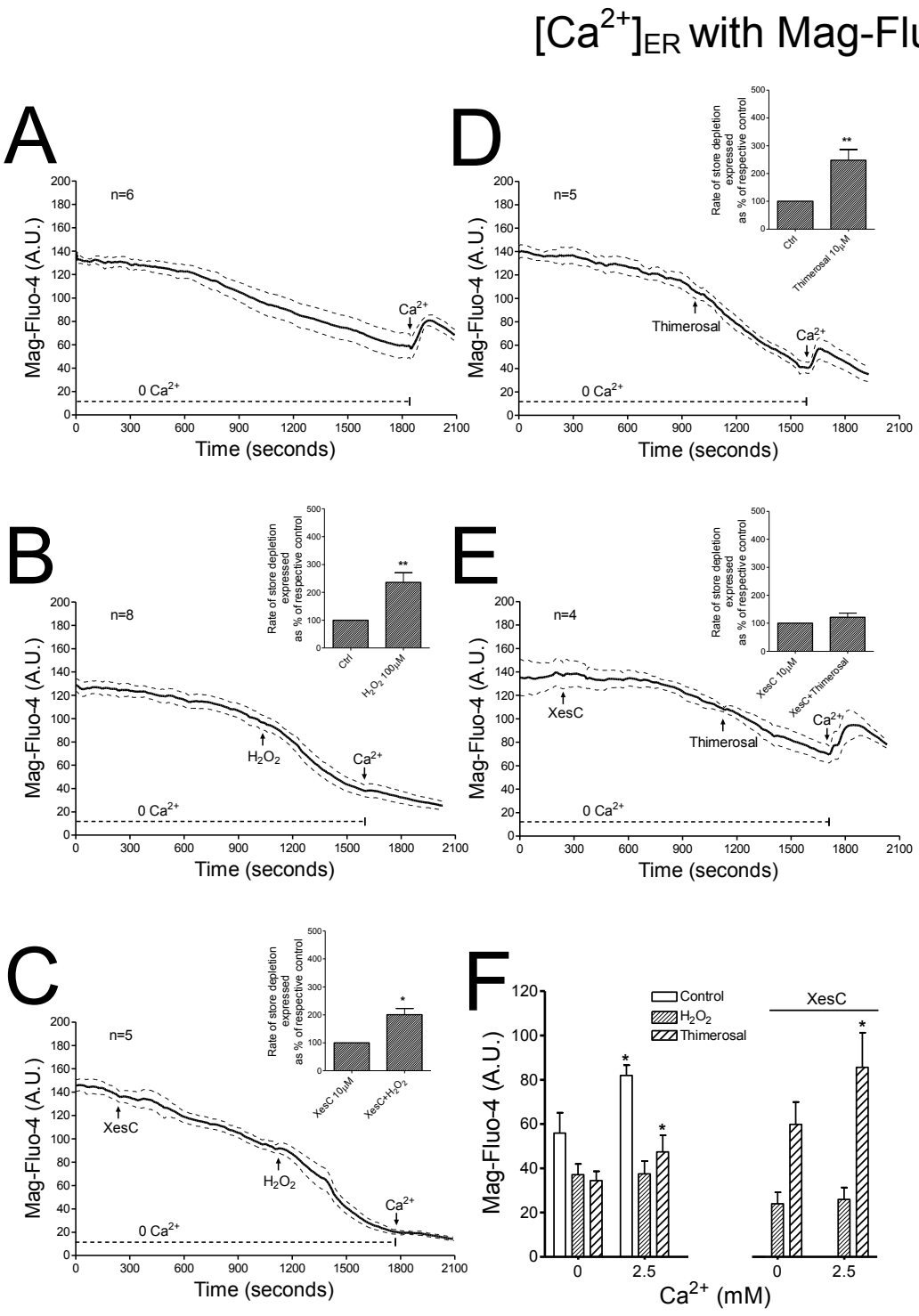

Figure 6.11 Effect of 100 μM H_2O_2 and 10 μM thimerosal on depletion and refilling of ER Ca^{2+} store in rabbit aortic valves with Ca^{2+}-free buffer. (A-E) Summary traces and bar graphs comparing effects of H_2O_2 and thimerosal on depletion of ER Ca^{2+} store, and on increases in fluorescence following addition of 2.5 mM Ca^{2+}, in the absence and presence of 10 μM XesC. (F) Bar graphs confirming Ca^{2+} refilling following addition of 2.5 mM Ca^{2+}, however, the refilling was blocked in the presence of H_2O_2, * and ** denote p<0.05 and 0.01 compared with corresponding control in Student's t-test. n denotes the number of animals studied. Error bars were represented by dotted lines.

6.3.12 Effect of ryanodine on non-selective divalent cation entry and depletion/refilling of $[Ca^{2+}]_{ER}$ in the rabbit aortic valve leaflets.

In Fura-2 loaded rabbit aortic valve leaflets incubated with HEPES buffer, incubation with 100 μM ryanodine by itself did not affect the rate of Mn^{2+}-induced quenching of Fura-2 355mm fluorescence or Fura-2 355/380 ratio. Presence of ryanodine did not influence the effect of 30 μM CPA on increasing the rate of Mn^{2+}-induced quenching (Figure 6.12A).

In Mag-fluo-4 loaded rabbit aortic valve leaflets incubated with Holman's buffer, ryanodine slowly but fully depleted the ER store (with reference to the time control). 100 μM H_2O_2 did not affect the rate of store depletion induced by ryanodine, vice versa, ryanodine did not affect the rate of store depletion induced by H_2O_2 (Figure 6.12B).

In Ca^{2+}-free condition, 100 μM ryanodine caused a significant increase on the rate of ER store depletion (with reference to the respective control) and the ER store was refilled by the addition of 2.5 mM Ca^{2+} after the ryanodine treatment (Figure 6.12C).

6.3.13 Effect of CPA, ACh and A-Br-23187 on $[Ca^{2+}]_m$ in the rabbit aortic valve leaflets.

In Rhod-2 loaded rabbit aortic valve leaflets incubated with Holman's buffer, incubation with 30 μM CPA, 3 μM ACh or 3 μM A-Br-23187 was without effect on Rhod-2 fluorescence signal (Figure 6.13A, 6.13B). In Ca^{2+}-free condition, incubation with 30 μM CPA and subsequent 3 μM 4-Br-A23187 did not affect Rhod-2 fluorescence signal (Figure 6.13C).

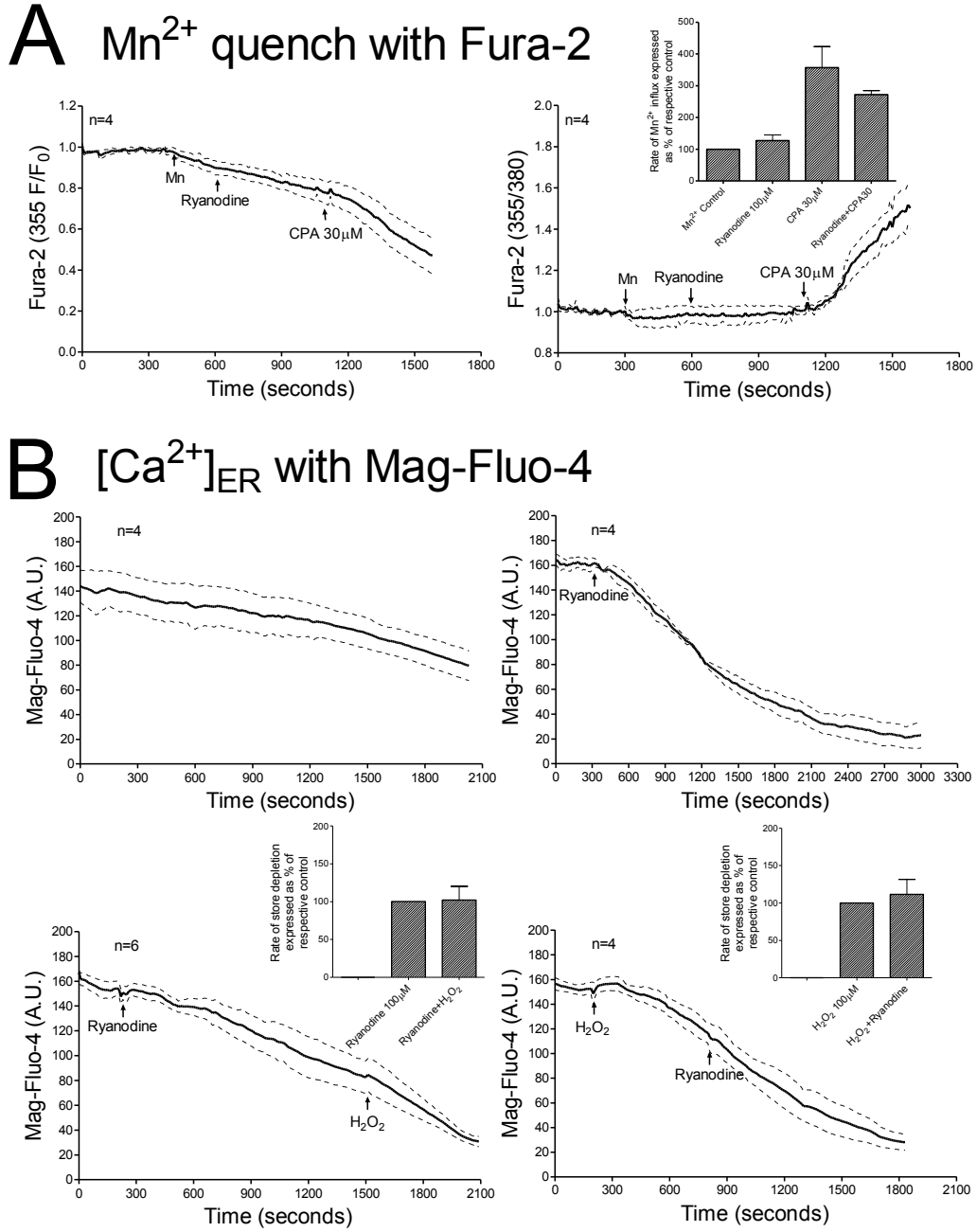

Figure 6.12 Effect of 100 μM ryanodine on Mn^{2+} quenching and depletion of ER Ca^{2+} stores in rabbit aortic valves. (A) Summary traces comparing Mn^{2+} influx rate and $[Ca^{2+}]_i$ by ryanodine and 30 μM CPA. (B) Summary traces and bar graphs showing competitive effect of ryanodine and H_2O_2 on depletion of ER Ca^{2+} stores. (C) Summary traces and bar graphs confirming Ca^{2+} refilling following addition of 2.5 mM Ca^{2+} in the presence of ryanodine. * denotes $p<0.05$ compared with corresponding control in Student's t-test. n denotes the number of animals studied. Error bars were represented by dotted lines.

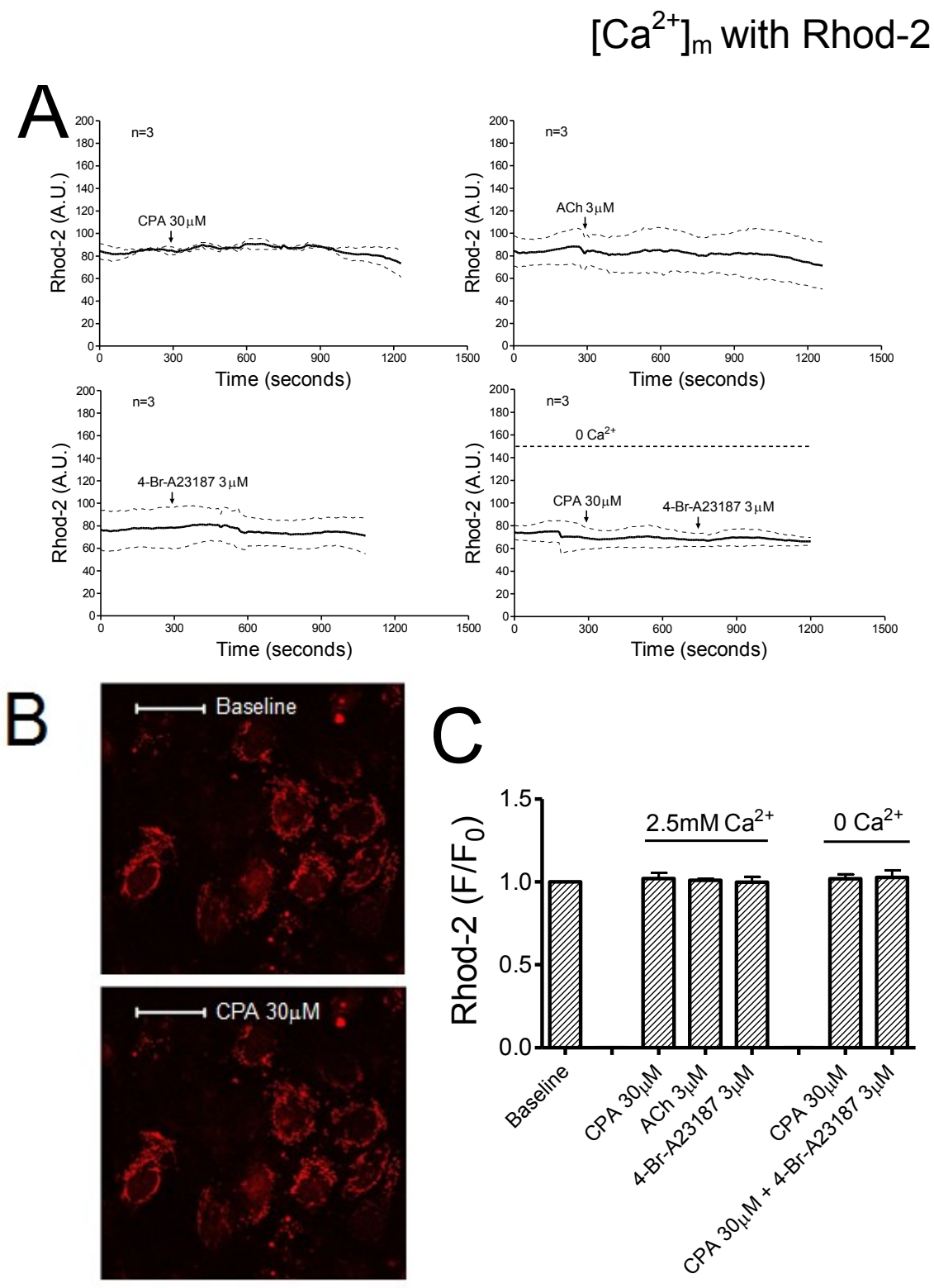

Figure 6.13 Effect of CPA, ACh and 4-Br-A23187 on $[Ca^{2+}]_m$ in the rabbit aortic valves. (A) Summary traces showing 30 μM CPA, 3 μM ACh and 3 μM 4-Br-A23187 was having no effect on $[Ca^{2+}]_m$ in normal or Ca^{2+}-free Holman's buffer. (B) Representative images showing no change on Rhod-2 fluorescence with 30 μM CPA in normal Holman's buffer. (C) Bar graphs confirming the above findings. Scalebars denotes 25 μm. n denotes the number of animals studied. Error bars were represented by dotted lines.

6.3.14 Effect of H_2O_2 and CPA on $[Ca^{2+}]_m$ in EA.hy926 cells.

In Rhod-2 loaded EA.hy926 cells incubated with Holman's buffer, CPA caused a concentration-dependent increase in Rhod-2 fluorescence signal, with maximum reached at 3 μM. Incubation with 100 μM H_2O_2 by itself caused a small raise of $[Ca^{2+}]_m$, however, it synergistically elevated $[Ca^{2+}]_m$ with 1 μM CPA. There was no increase in response to 3 μM CPA seen with H_2O_2 (Figure 6.14).

6.3.15 Effect of thimerosal on CPA-evoked elevation of $[Ca^{2+}]_m$ in EA.hy926 cells.

In Rhod-2 loaded EA.hy926 cells incubated with Holman's buffer, incubation with 10 μM thimerosal by itself caused a small raise of $[Ca^{2+}]_m$. In the presence of thimerosal, the elevation of $[Ca^{2+}]_m$ by 10 or 30 μM CPA was not affected (Figure 6.15).

6.3.16 Effect of H_2O_2 and CPA on $[Ca^{2+}]_{ER}$ in EA.hy926 cells.

In Mag-fluo-4 loaded EA.hy926 cells incubated with Holman's buffer, CPA caused a concentration-dependent decrease in Mag-fluo-4 fluorescence signal, with maximum reached at 30 μM. Incubation with 100 μM H_2O_2 by itself caused a small decrease of $[Ca^{2+}]_{ER}$, however, a further significant synergistic depletion of $[Ca^{2+}]_{ER}$ by H_2O_2 and 1-10 μM CPA was observed. There was no significant increase in response to 30 μM CPA seen with H_2O_2 (Figure 6.16).

6.3.17 Effect of thimerosal on CPA-evoked depletion of $[Ca^{2+}]_{ER}$ in EA.hy926 cells.

In Mag-fluo-4 loaded EA.hy926 cells incubated with Holman's buffer, incubation with 10 μM thimerosal by itself caused a small decrease of $[Ca^{2+}]_{ER}$, however, a further significant synergistic depletion of $[Ca^{2+}]_{ER}$ by thimerosal and 10 μM CPA was observed. There was no significant increase in response to 30 μM CPA seen with thimerosal (Figure 6.17).

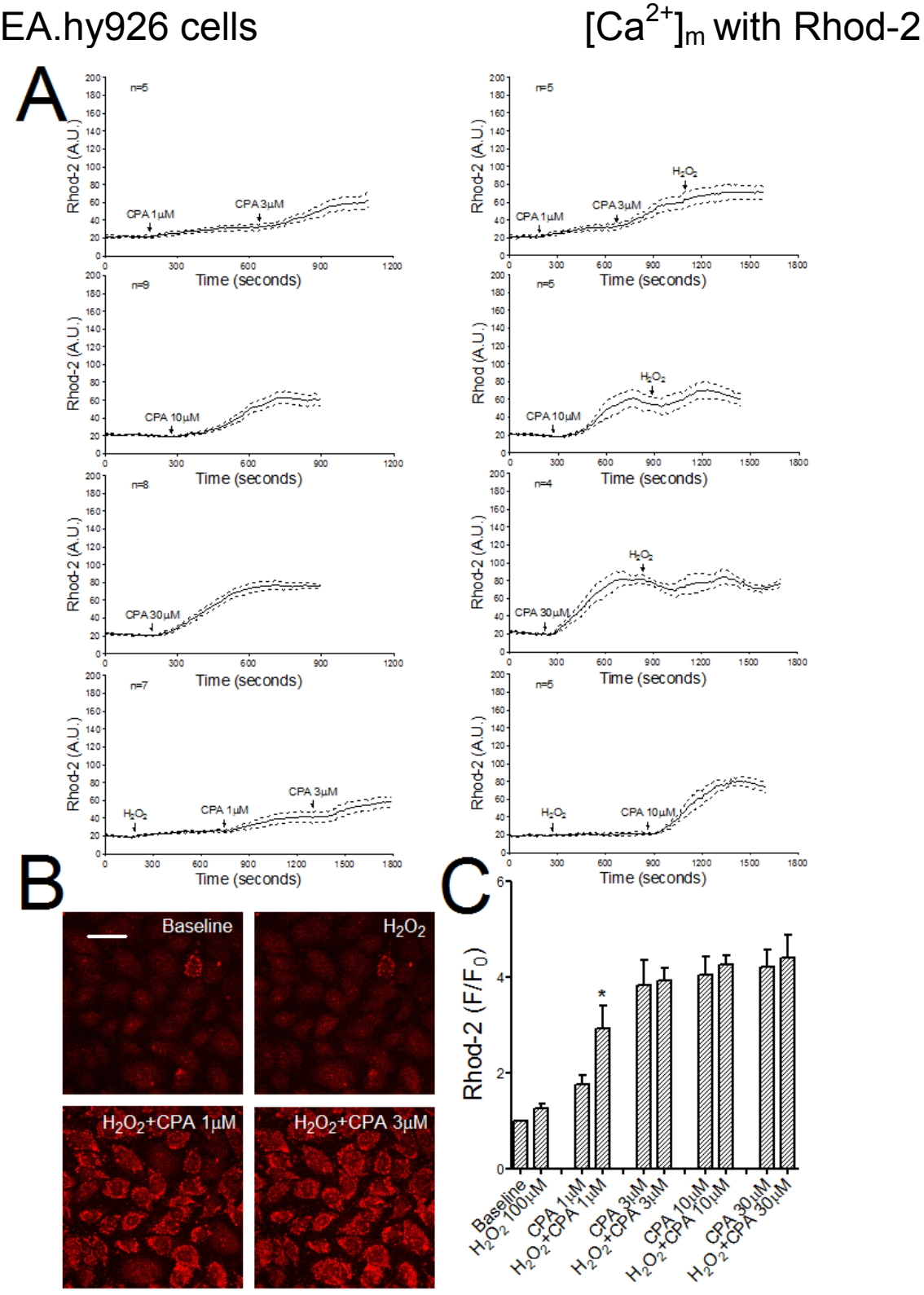

Figure 6.14 Effect of 100 μM H_2O_2 on CPA-evoked elevation of $[Ca^{2+}]_m$ in the EA.hy926 cells. (A) Summary traces showing synergistic elevation of $[Ca^{2+}]_m$ by H_2O_2 and 1 μM CPA, whereas H_2O_2 was ineffective after 3 μM CPA. (B) Representative images showing H_2O_2 caused minimal effect on $[Ca^{2+}]_m$ but facilitated elevation in the presence of 1 μM CPA. (C) Bar graphs confirming the above findings. Scalebars denotes 25 μm. * denotes p<0.05 compared with 1 μM CPA alone in Student's t-test. n denotes the number of experiments studied. Error bars were represented by dotted lines.

EA.hy926 cells $[Ca^{2+}]_m$ with Rhod-2

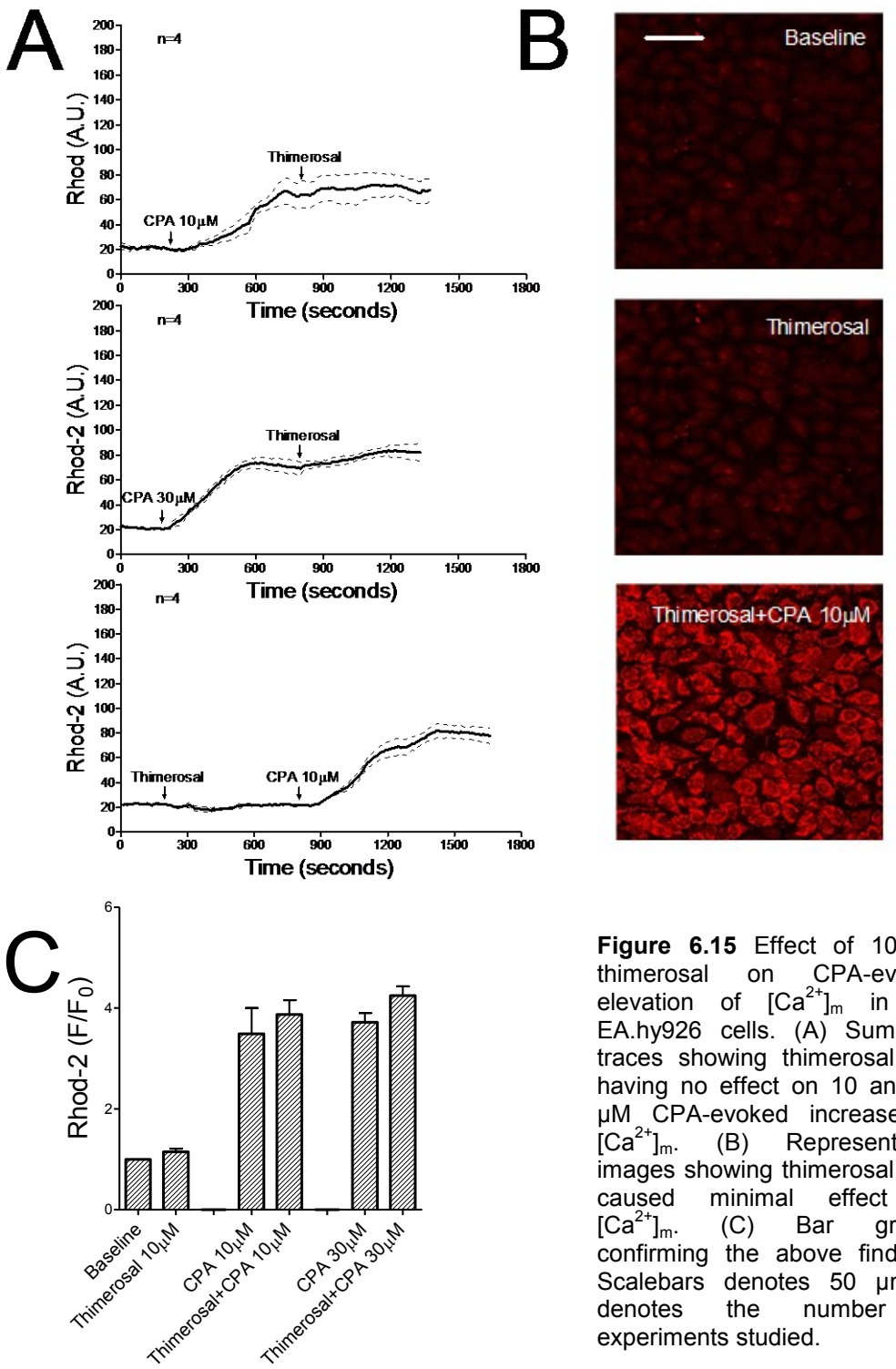

Figure 6.15 Effect of 10 μM thimerosal on CPA-evoked elevation of $[Ca^{2+}]_m$ in the EA.hy926 cells. (A) Summary traces showing thimerosal was having no effect on 10 and 30 μM CPA-evoked increase on $[Ca^{2+}]_m$. (B) Representative images showing thimerosal itself caused minimal effect on $[Ca^{2+}]_m$. (C) Bar graphs confirming the above findings. Scalebars denotes 50 μm. n denotes the number of experiments studied.

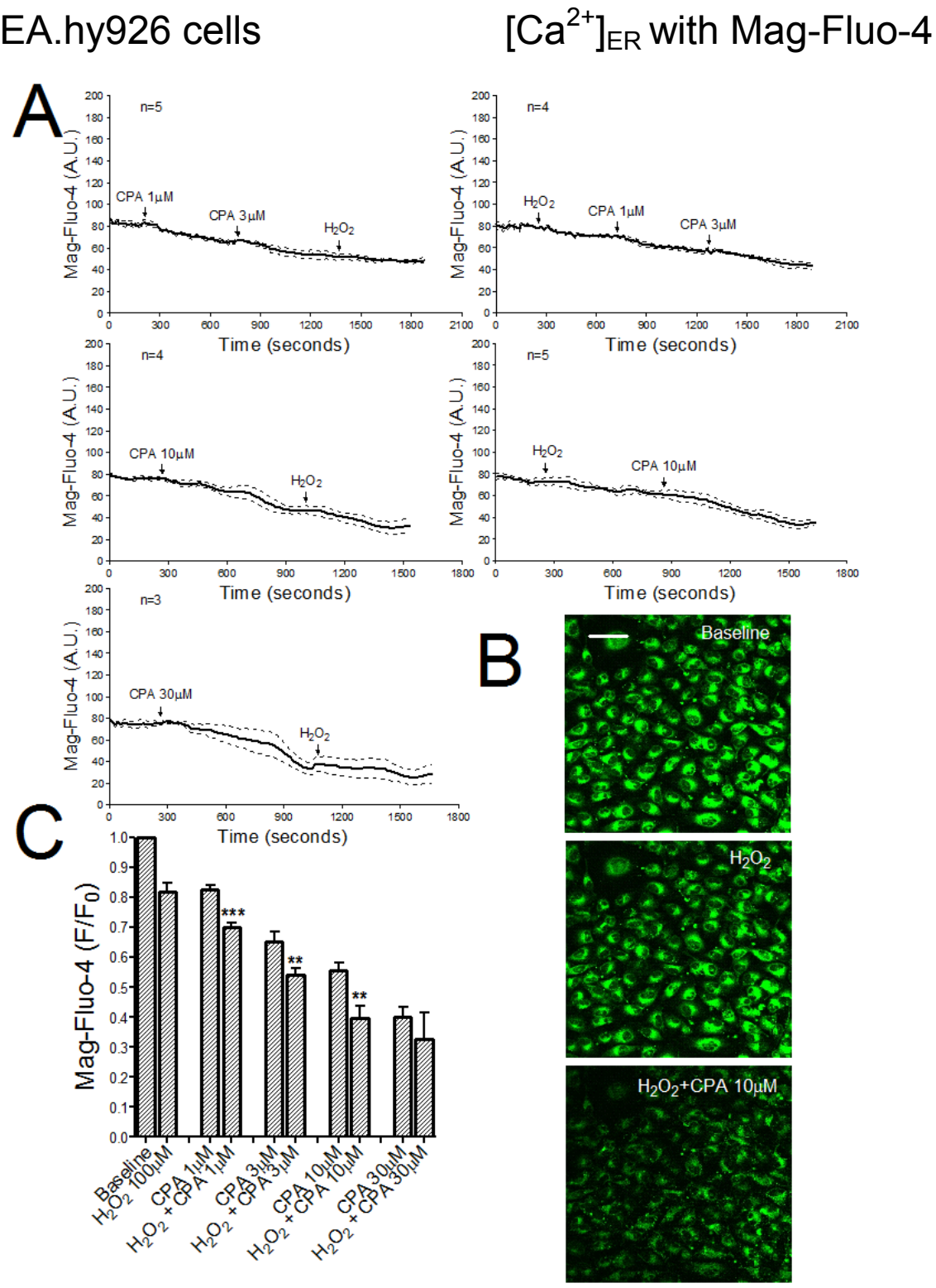

Figure 6.16 Effect of 100 μM H_2O_2 on CPA-evoked depletion of ER Ca^{2+} stores in the EA.hy926 cells. (A) Summary traces showing concentration-dependent depletion of stores by CPA in the absence and presence of H_2O_2. (B) Representative images showing H_2O_2 itself caused minimal effect on $[Ca^{2+}]_{ER}$ but facilitated depletion of stores in the presence of 10 μM CPA. (C) Bar graphs confirming store depletion by CPA was potentiated by H_2O_2. Scalebars denotes 50 μm. ** and *** denote p<0.01 and 0.001 compared with corresponding controlin Student's t-test. n denotes the number of experiments studied. Error bars were represented by dotted lines.

EA.hy926 cells $[Ca^{2+}]_{ER}$ with Mag-Fluo-4

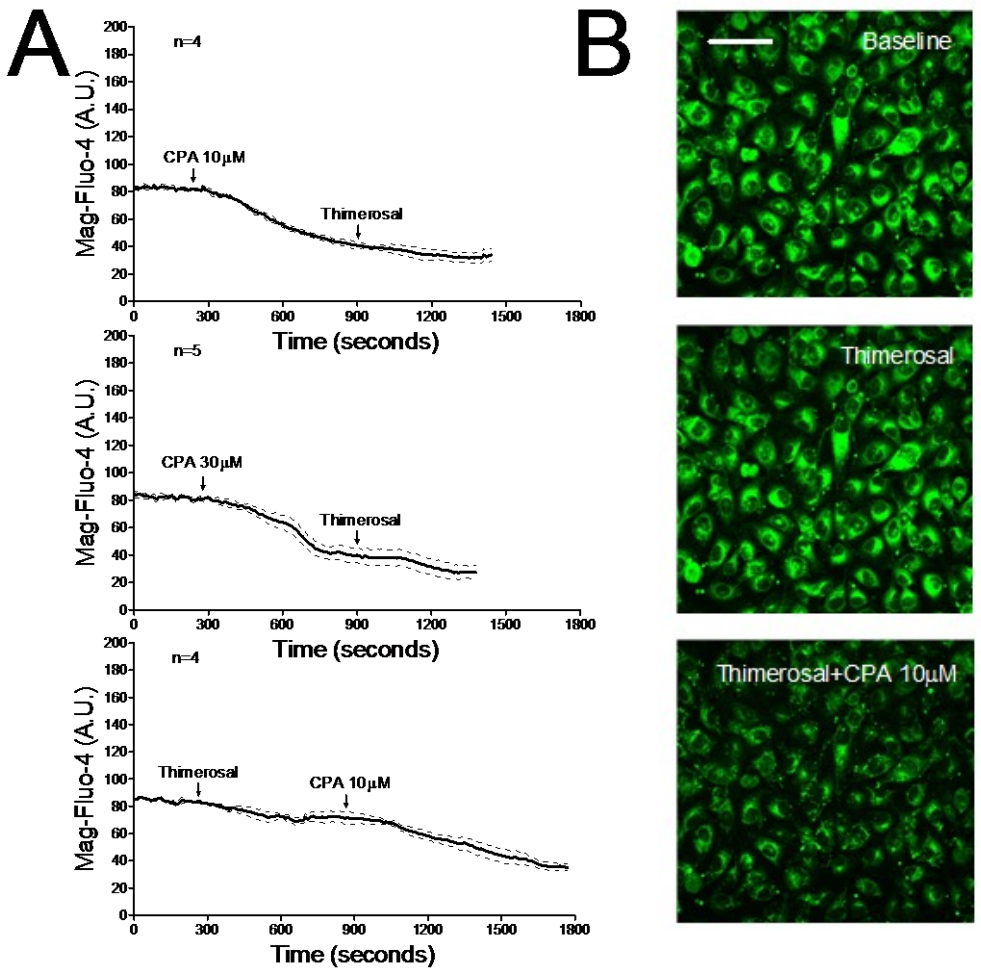

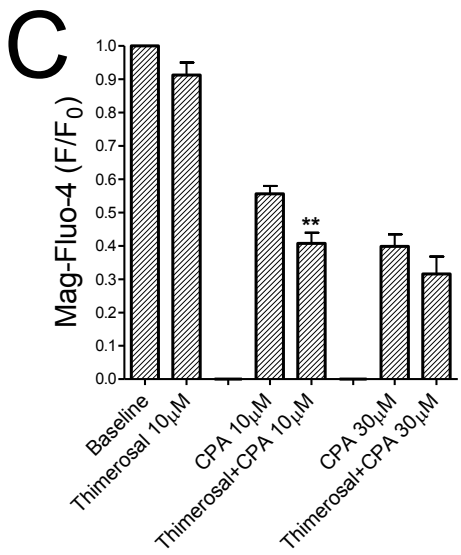

Figure 6.17 Effect of 10 μM thimerosal on CPA-evoked depletion of ER Ca^{2+} stores in the EA.hy926 cells. (A) Summary traces showing concentration-dependent depletion of stores by CPA in the absence and presence of thimerosal. (B) Representative images showing thimerosal itself caused minimal effect on $[Ca^{2+}]_{ER}$ but facilitated depletion of stores in the presence of 10 μM CPA. (C) Bar graphs confirming store depletion by 10 μM CPA was potentiated by thimerosal. Scalebars denotes 50 μm. ** denotes p<0.01 compared with 10 μM CPA alone in Student's t-test. n denotes the number of experiments studied. Error bars were represented by dotted lines.

6.3.18 Effect of H_2O_2 and CPA on $[Ca^{2+}]_i$ in EA.hy926 cells.

In Fluo-4 loaded EA.hy926 cells incubated with Holman's buffer, CPA caused a concentration-dependent increase in Fluo-4 fluorescence signal, with maximum reached at 30 μM. Incubation with 100 μM H_2O_2 by itself caused a small raise of $[Ca^{2+}]_i$, however, a further significant synergistic elevation of $[Ca^{2+}]_i$ by H_2O_2 and 1-10 μM CPA was observed. There was no significant increase in response to 30 μM CPA seen with H_2O_2 (Figure 6.18).

6.3.19 Effect of thimerosal on CPA-evoked elevation of $[Ca^{2+}]_i$ in EA.hy926cells.

In Fluo-4 loaded EA.hy926 cells incubated with Holman's buffer, incubation with 10 μM thimerosal by itself caused a small increase of $[Ca^{2+}]_i$, however, a further significant synergistic elevation of $[Ca^{2+}]_i$ by thimerosal and 10 μM CPA was observed. There was no increase in response to 30 μM CPA seen with thimerosal (Figure 6.19).

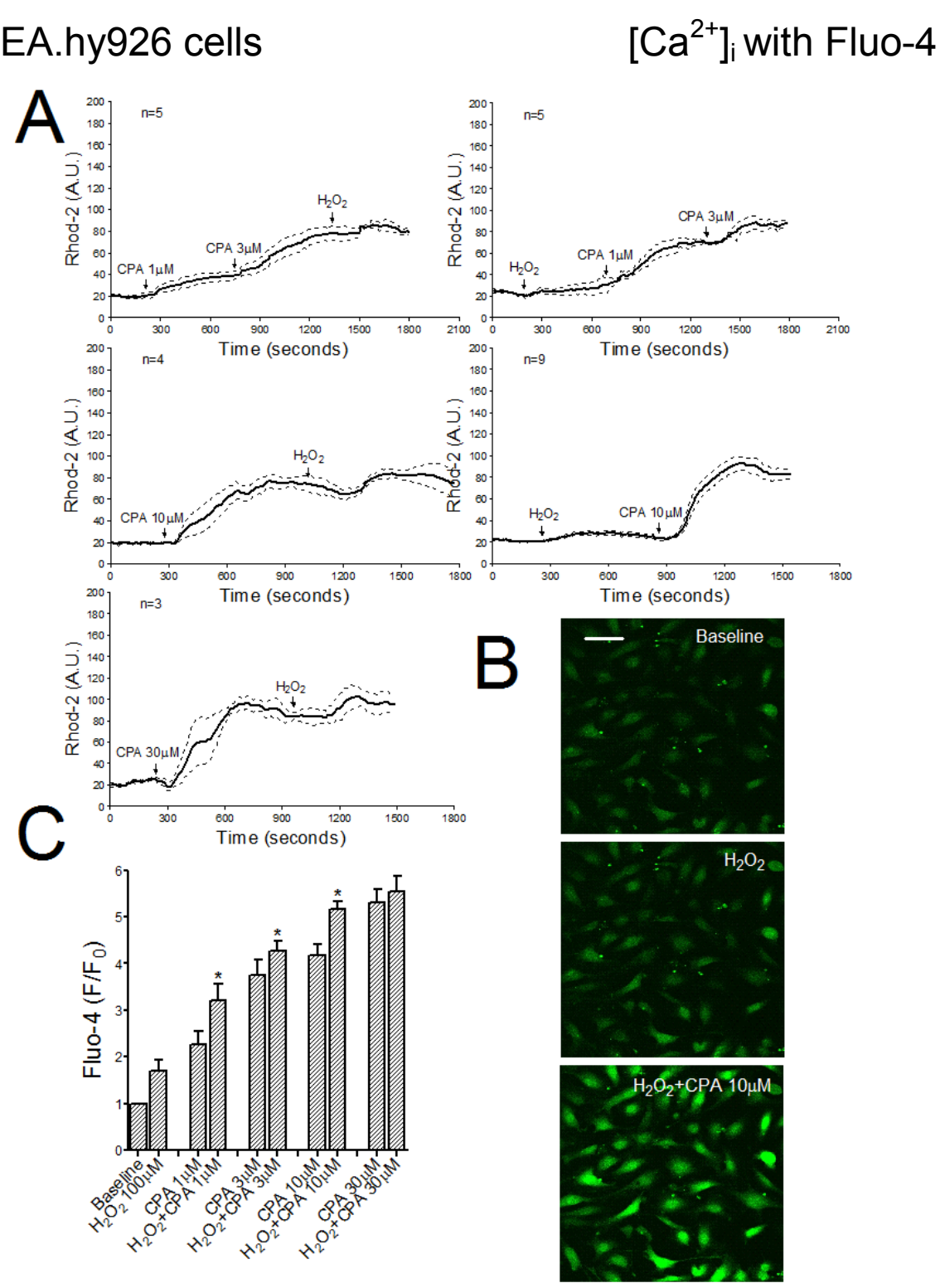

Figure 6.18 Effect of 100 μM H_2O_2 on CPA-evoked elevation of $[Ca^{2+}]_i$ in the EA.hy926 cells. (A) Summary traces showing concentration-dependent elevation of $[Ca^{2+}]_i$ by CPA in the absence and presence of H_2O_2. (B) Representative images showing H_2O_2 itself caused minimal effect on $[Ca^{2+}]_i$ but facilitated elevation of $[Ca^{2+}]_i$ in the presence of 10 μM CPA. (C) Bar graphs confirming elevation of $[Ca^{2+}]_i$ by CPA was potentiated by H_2O_2. Scalebars denotes 50 μm. * denotes p<0.05 compared with corresponding control in Student's t-test. n denotes the number of experiments studied. Error bars were represented by dotted lines.

EA.hy926 cells $[Ca^{2+}]_i$ with Fluo-4

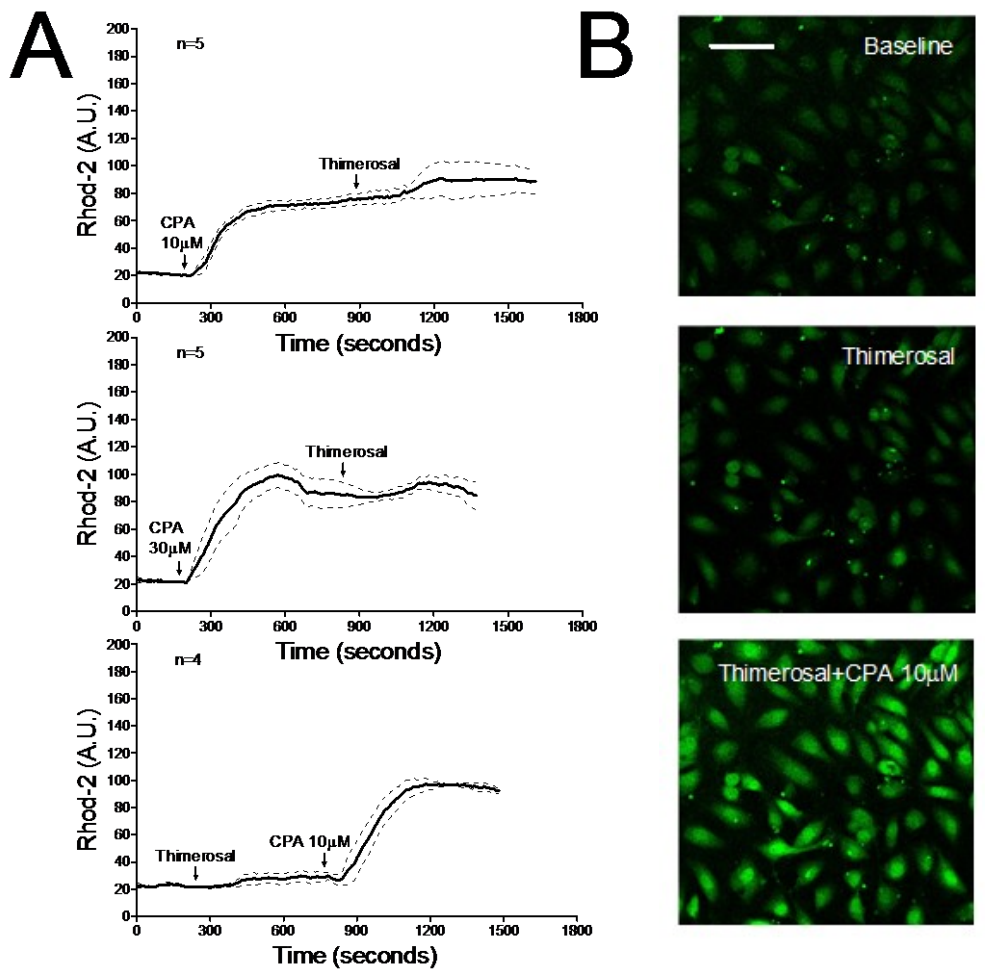

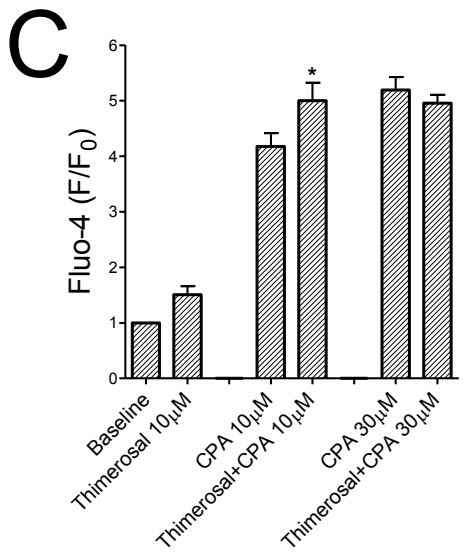

Figure 6.19 Effect of 10 μM thimerosal on CPA-evoked elevation of $[Ca^{2+}]_i$ in the EA.hy926 cells. (A) Summary traces showing concentration-dependent elevation of $[Ca^{2+}]_i$ by CPA in the absence and presence of thimerosal. (B) Representative images showing thimerosal itself caused minimal effect on $[Ca^{2+}]_i$ but facilitated elevation of $[Ca^{2+}]_i$ in the presence of 10 μM CPA. (C) Bar graphs confirming elevation of $[Ca^{2+}]_i$ by 10 μM CPA was potentiated by thimerosal. Scalebars denotes 50 μm. * denotes $p<0.05$ compared with 10 μM CPA alone in Student's t-test. n denotes the number of experiments studied. Error bars were represented by dotted lines.

6.4 DISCUSSION

In the studies presented in Chapters 3 and 4, H_2O_2 has been shown to potentiate the EDHF-type responses but not NO-mediated responses in the rabbit iliac and aorta artery. The present chapter has extended the previous observations and provided new evidence that H_2O_2 may contribute to such potentiation by promoting the elevation of $[Ca^{2+}]_i$, possibly through inhibition of SERCA activity and depletion of ryanodine-sensitive Ca^{2+} stores.

6.4.1 Current investigations

To summarize the main findings of the current chapter: (i) H_2O_2 has a minimal effect on $[Ca^{2+}]_i$ but synergistically elevates $[Ca^{2+}]_i$ with CPA; (ii) H_2O_2 has a minimal effect $[Ca^{2+}]_{ER}$ but synergistically depletes ER Ca^{2+} stores with CPA and ACh; (iii) Ca^{2+} re-entry in the presence of CPA is synergistically increased by H_2O_2; (iv) Non-selective divalent cation entry rate is not affected by H_2O_2 alone, increased by CPA and enhanced by H_2O_2 plus CPA; (v) In Ca^{2+}-free buffer, H_2O_2 depletes the ER Ca^{2+} stores and prevents the store refilling; (vi) XesC is unable to reverse the store depletion by H_2O_2; (vii) H_2O_2 depletes the ER Ca^{2+} store through a ryanodine-sensitive pathway; (viii) H_2O_2 synergistically elevates $[Ca^{2+}]_m$ with CPA in cultured endothelial cells.

100 μM H_2O_2 itself has a minimal effect on $[Ca^{2+}]_i$ in rabbit aortic valve leaflets, however, pre-incubation with H_2O_2 significantly potentiated the elevation of $[Ca^{2+}]_i$ evoked by 1-10 μM CPA. This $[Ca^{2+}]_i$ was maximized at 30 μM CPA at which point there was no further increase by H_2O_2. Thimerosal has been shown to mimic the responses of H_2O_2 in the EDHF-type relaxations in the previous Chapter 3, at concentrations ≥ 30 μM, thimerosal itself caused an increase in basal $[Ca^{2+}]_i$. Pre-incubation with a sub-threshold concentration of 10 μM thimerosal caused a synergistic response with 1-10 μM CPA. This was similar to that observed with H_2O_2, and again $[Ca^{2+}]_i$ was maximized at 30 μM CPA. These experiments measuring $[Ca^{2+}]_i$ in the

rabbit aortic valve were carried out with Fura-2, as the preferred confocal microscopy friendly probe Fluo-4 failed to give a sensitive measure on $[Ca^{2+}]_i$ in Holman's buffer. It is known that the extracellular Ca^{2+} concentration is >1 mM, whereas the $[Ca^{2+}]_i$ is ~100 nM at the resting state (Roy and Hajnoczky, 2008). In rabbit aortic valve, upon treatment, the $[Ca^{2+}]_i$ can be raised to ~600 nM (Edwards *et al.*, 2008), however, Fluo-4 only has a K_d value of ~ 345 nM.

Two principal mechanisms are thought to contribute to the elevation in $[Ca^{2+}]_i$ that underpin the endothelium-dependent responses to agonists: (i) transient Ca^{2+} release from the ER secondary to the formation of $InsP_3$ following activation of PLC and (ii) sustained influx of extracellular Ca^{2+} secondary to depletion of the ER Ca^{2+} store. To test the effect of H_2O_2 on ER Ca^{2+} store, the rabbit aortic valve was first loaded with an ER-specific Ca^{2+} indicator Mag-fluo-4. Pre-incubation with 100 μM H_2O_2 significantly amplified the ER Ca^{2+} store depletion evoked by 10 μM CPA, whereas H_2O_2 itself has minimal effect on $[Ca^{2+}]_{ER}$. Similarly, 10 μM thimerosal minimally affected $[Ca^{2+}]_{ER}$, but pre-incubation with thimerosal amplified the store depletion evoked by 3-10 μM CPA. In the presence of H_2O_2 or thimerosal, no further decrease in $[Ca^{2+}]_{ER}$ evoked by CPA at concentrations ≥ 30 μM was observed. These findings thus matching the range over which H_2O_2 and CPA elevate $[Ca^{2+}]_i$. To test whether this effect of H_2O_2 is a universal phenomenon, the store depletion evoked by ACh was also examined, pre-incubation with 100 μM H_2O_2 significantly potentiated the ER Ca^{2+} store depletion evoked by 1 and 3 μM ACh.

A well-tested Ca^{2+} re-entry protocol (Fernandez-Rodriguez *et al.*, 2009) and Mn^{2+} quench technique (Chen and van Breemen, 1993; Li and van Breemen, 1996) was used to investigate the effect of H_2O_2 on influx of extracellular Ca^{2+} in rabbit aortic valve leaflets. Mn^{2+} ions were often used as a substitute for Ca^{2+} in defining extracellular Ca^{2+} influx, because they share common entry pathways with Ca^{2+} across the plasma membrane, but will not be taken up by ER or SR, and therefore are a good indicator for

non-selective divalent cation entry (Gomes da Costa and Madeira, 1986; Merritt *et al.*, 1989; Missiaen *et al.*, 1990). The SERCA inhibitor CPA was used to deplete stores, as in this way, the potential confounding effects of H_2O_2 on receptor-coupled pathways mediated via PLC was avoided (Hong *et al.*, 2006). In the presence of 100 μM H_2O_2, the Ca^{2+} re-entry evoked by 10 μM CPA was significantly increased, whereas no further increase in Ca^{2+} re-entry evoked by 30 μM CPA was observed. Again, these findings matched the range over which H_2O_2 and CPA elevate $[Ca^{2+}]_i$. Similarly, 10 μM thimerosal increased the Ca^{2+} re-entry evoked by 10 μM but not 30 μM CPA.

At a wavelength of 355 nm, (the isosbestic wavelength for Fura-2 as suggested by Prof. Karl Swann), where the Fura-2 fluorescence intensity is not influenced by $[Ca^{2+}]_i$ changes (Hallam *et al.*, 1988; Chen and van Breemen, 1993; Li and van Breemen, 1996), the application of Mn^{2+} caused a steady quench in Fura-2 fluorescence. Fura-2 ratio 355/380 was also calculated as an indication for $[Ca^{2+}]_i$ levels. Addition of 3 to 30 μM CPA induced a concentration-dependent increase in Mn^{2+} quench rate, and corresponding concentration-dependent elevations in $[Ca^{2+}]_i$ were observed. In the presence of 100 μM H_2O_2 the Mn^{2+} quench rate evoked by 10 μM CPA was significantly increased, whereas no further increase was evoked by 30 μM CPA but a drop in Mn^{2+} quench rate was observed. Again, these findings matched the range over which H_2O_2 and CPA elevate $[Ca^{2+}]_i$. In contrast, 10 μM thimerosal decreased the Mn^{2+} quench rate evoked by both 10 μM and 30 μM CPA. These findings on Ca^{2+} re-entry and Mn^{2+} quench experiments thus suggest that H_2O_2 and CPA synergistically elevate the $[Ca^{2+}]_i$ by depletion of ER store, and consequently increase Ca^{2+} influx via the SOCE. High level of $[Ca^{2+}]_i$ may in fact inhibit the Ca^{2+} influx through NSCCs.

There are three pathways that regulate the ER Ca^{2+} store, Ca^{2+} accumulates via SERCA and Ca^{2+} is released through RyRs and $InsP_3Rs$ (Laude and Simpson, 2009). The synergism of H_2O_2 and thimerosal with CPA and ACh in $[Ca^{2+}]_i$, $[Ca^{2+}]_{ER}$ and Ca^{2+} influx therefore suggests that H_2O_2 may inhibit SERCA activity, sensitize the $InsP_3$

receptor and/or RyRs. Direct evidence that H_2O_2 sensitizes the $InsP_3$ receptor in endothelial cells is suggested by finding that the $InsP_3$ receptor inhibitor heparin abolishes H_2O_2-evoked Ca^{2+} release from ER stores in permeabilized ECV304 cells (Zheng and Shen, 2005). However, the cellline ECV304 is genetically confirmed not to be of HUVEC origin and is therefore an inappropriate cellline to study endothelial cell biology (Brown *et al.*, 2000). H_2O_2 has been shown to cause a decrease on the activities of SERCA pumps in rat ventricular myocytes (Greensmith *et al.*, 2010; Kuster *et al.*, 2010) and increase the sensitivity of HAECs to thapsigargin (Lock *et al.*, 2012). Although there is evidence that RyR blockade with ryanodine inhibits H_2O_2-induced increase in $[Ca^{2+}]_i$ in cultured pulmonary arterial smooth muscle cells (PASMCs) (Lin *et al.*, 2007), no report on the effect of H_2O_2 on RyR is published in endothelial cells. Therefore, a series of experiments were performed to study the role H_2O_2 played in these three mechanisms.

In order to separate the ER store depletion and extracellular Ca^{2+} influx, $[Ca^{2+}]_{ER}$ was examined in Ca^{2+}-free buffer. In Ca^{2+}-free conditions, Ca^{2+} slowly leaks out of the ER and the store then refills upon addition of 2.5 mM extracellular Ca^{2+}. 100 μM H_2O_2 significantly increased the rate of store depletion in comparison with time-control, however, application of $InsP_3$ receptors antagonist XesC was unable to reverse this accelerated depletion evoked by H_2O_2. By contrast, 10 μM thimerosal also significantly increased the rate of store depletion in comparison with time-control, but this accelerated depletion was fully blocked by XesC. Interestingly, H_2O_2 but not thimerosal abolished the store refilling following addition of 2.5 mM extracellular Ca^{2+}, thus suggesting that H_2O_2 promotes CPA-evoked elevation in $[Ca^{2+}]_i$ through decreased activity of SERCA pumps rather than $InsP_3$ receptors.

Besides SERCA and $InsP_3$ receptors, RyRs are also localized in the ER membrane, and play a role in mediating SOCE (Paltauf-Doburzynska *et al.*, 1998). Several studies have confirmed the presence of functional RyRs in rabbit aortic endothelial cells

(Ziegelstein *et al.*, 1994; Wang *et al.*, 1995). At low concentrations, e.g., 1 μM, ryanodine acts as a RyR agonist, however, at higher concentrations, e.g.,100 μM, ryanodine initially opens RyR and subsequently locks it in a low-conductance or closed state and Ca^{2+} release is inhibited (Fill and Copello, 2002; Liang *et al.*, 2004). In the present studies, 100 μM ryanodine itself did not increase Mn^{2+} quench rate or $[Ca^{2+}]_i$, and no further increase but a drop in Mn^{2+} quench rate evoked by 30 μM CPA was observed. Compared to time matched controls, ryanodine induced a slow depletion of ER stores, and the rate of store depletion evoked by ryanodine was not affected by 100 μM H_2O_2, and vice versa, the rate of rate of store depletion evoked by H_2O_2 was not affected by ryanodine. In Ca^{2+}-free conditions, ryanodine also significantly increased the rate of store depletion in comparison with respective control, and the store is refilled following addition of 2.5 mM extracellular Ca^{2+}. These finding suggests that H_2O_2 also promotes CPA-evoked elevation in $[Ca^{2+}]_i$ through ryanodine-gated channels, because they competitively accelerated the rate of store depletion. Interestingly, it has been proposed that SERCA and RyR are components of the same pathway, because the RyR-mediated Ca^{2+} extrusion is effectively blocked once SERCA is inhibited (Liang *et al.*, 2004).

In addition to their role as the main energy-producing organelles, mitochondria are considered as storage site for Ca^{2+} in addition to the ER. Their role in Ca^{2+} mobilization is revealed by their close localization to ER $InsP_3$ receptors and the plasma membrane. And indeed, much recent work has established that mitochondria function in concert with the ER to take up Ca^{2+} that has been released from intracellular stores by the opening of either $InsP_3$ or ryanodine-sensitive Ca^{2+} channels rapidly following stimulation and then subsequently sequester/release this Ca^{2+} slowly back into the cytosol (Rizzuto *et al.*, 1993b; Jouaville *et al.*, 1995; Hajnoczky *et al.*, 1999; Tinel *et al.*, 1999; Glitsch *et al.*, 2002; Montero *et al.*, 2002). However, in rabbit aortic valve leaflets loaded with $[Ca^{2+}]_m$ indicator Rhod-2, the application of intracellular Ca^{2+} stimulator

CPA, ACh or non-fluorescent A23187 analogue 4-Br-A23187 failed to give any elevation in Rhod-2 fluorescence. It was thought the K_d value of Rhod-2 was the cause of this result, but in Ca^{2+}-free condition, CPA and 4-Br-A23187 also failed to give any rise in Rhod-2 fluorescence.

By contrast, in EA.hy926 cells, used as a positive control, a concentration-dependent elevation of $[Ca^{2+}]_m$ was observed with 1 to 3 μM CPA. Pre-incubation of 100 μM H_2O_2 significantly potentiated the elevation of $[Ca^{2+}]_m$ evoked by 1 μM CPA, whereas, no further increase in Rhod-2 fluorescence signal after 3 μM CPA was observed. When imaged using the same parameters, it was noted that rabbit aortic valve leaflets have a much higher basal level of Rhod-2 fluorescence compared with cultured EA.hy926 cells in normal physiological buffer. This might indicate that, in intact tissue like aortic valve, the mitochondria store a large amount of residual Ca^{2+} and are unable to take up any more Ca^{2+} that is released by store depletion. Nevertheless, because of the uncertainty of the loading and de-esterification of Rhod-2 in these two different preparations, this need to be further investigated using a different $[Ca^{2+}]_m$ indicator.

To test the Ca^{2+} mobilization in EA.hy926 cells, the experiments were repeated as in rabbit aortic valves. Pre-incubation with 100 μM H_2O_2 significantly amplified the ER Ca^{2+} store depletion evoked by 1 to 10 μM CPA, whereas H_2O_2 itself has minimal effect on $[Ca^{2+}]_{ER}$ in these cultured cells. Similarly, 10 μM thimerosal minimally affect the $[Ca^{2+}]_{ER}$, but pre-incubation with thimerosal amplified the store depletion evoked by 10 μM CPA. In the presence of H_2O_2 or thimerosal, no further decrease in $[Ca^{2+}]_{ER}$ evoked by CPA at concentrations ≥ 30 μM was observed.

Furthermore, 100 μM H_2O_2 itself has minimal effect on $[Ca^{2+}]_i$ in EA.hy926 cells, however, pre-incubation with H_2O_2 significantly potentiated the elevation of $[Ca^{2+}]_i$ evoked by 1-10 μM CPA. Similarly, pre-incubation with 10 μM thimerosal, a synergism was observed with thimerosal and 10 μM CPA. When $[Ca^{2+}]_i$ was maximized at 30 μM

CPA, no further elevation in $[Ca^{2+}]_i$ was found in the presence of H_2O_2 or thimerosal. These findings thus match the range over which H_2O_2 and CPA depleting the $[Ca^{2+}]_{ER}$.

6.4.2 Conclusions and further studies

The principal finding of the present chapter is that H_2O_2 may contribute to the potentiation of EDHF-type relaxations observed in the rabbit iliac artery by promoting the elevation of intracellular Ca^{2+} level, through inhibition of SERCA activity and the depletion of ryanodine-sensitive Ca^{2+} stores, and therefore increases extracellular Ca^{2+} influx. However, due to the limited responses of the fluorescence indicator Rhod-2 to agonists (ACh, CPA and 4-Br-A23187) treatment, it was unclear whether mitochondria played a role in regulating the Ca^{2+} that has been release by internal stores in rabbit aortic valves. Further investigations will be needed in search for an appropriate indicator.

6.5 CHAPTER SUMMARY

1. H_2O_2 may contribute to potentiated EDHF-type response by promoting the elevation of endothelial $[Ca^{2+}]_i$ and extracellular Ca^{2+} influx.
2. The effect of H_2O_2 on Ca^{2+} mobilization may be affected through inhibition of SERCA and activation of ryanodine-sensitive Ca^{2+} stores.
3. In cultured EA.hy926 human endothelial cells, mitochondria play a role in Ca^{2+} mobilization.

Chapter 7

Summary and Discussion

7.1 OVERVIEW

In cardiovascular diseases such as hypertension, atherosclerosis and diabetes, a decreased NO bioavailability, characteristic of endothelial dysfunction is often observed, and it has now been widely proposed that the EDHF pathway can play a compensatory role for the depressed NO bioavailability (Feletou, 2011b). Although the true identity of EDHF is still questionable, there is growing evidence to suggest that gap junctional communication has an important role in the transduction of this electronic event (Griffith, 2004; Griffith *et al.*, 2004). Indeed, in rabbit arteries of different sizes, a reciprocal relationship between NO- and gap junction-dependent relaxation has been reported (Berman *et al.*, 2002). Decreased NO bioavailability is often associated with excessive generation of ROS, which were regarded as toxic by-products of cell metabolism that contributed to the disrupted endogenous defence mechanisms underlying endothelial dysfunction (Perez-Vizcaino *et al.*, 2010). Nevertheless, in recent years, opinion on the role of ROS in the vascular modulation has changed, in that they have also been shown to act as putative mediators in signalling pathways (Cai, 2005; Schroder and Eaton, 2008). EDHF-mediated vasodilatation is believed to be less sensitive to oxidative stress than NO, and can persist and may compensate for the loss of other vasodilator pathways in disease state (Bagi, 2009). Indeed, H_2O_2 itself induces vasodilatation in many vessel types and was even suggested to be an EDHF (Matoba *et al.*, 2000; Matoba *et al.*, 2002). In rabbit iliac artery, although H_2O_2 did not induce the level of hyperpolarization seen with an authentic EDHF-type response, it

has been shown to enhance Ca^{2+} release from the ER therefore potentiating the EDHF-type relaxation, an action that was mimicked by the thiol oxidant and $InsP_3$ receptor sensitizing agent thimerosal (Chaytor *et al.*, 2003; Edwards *et al.*, 2008). To characterize the interactive roles of H_2O_2 and Ca^{2+} homeostasis in the EDHF phenomenon, this thesis had two aims.

The first aim of this thesis was to elucidate further the role H_2O_2 played in the EDHF-type relaxations in rabbit iliac artery, and also elucidate the interaction between H_2O_2 and NO in this signalling network. To achieve this goal, the receptor-dependent agent ACh and the receptor-independent agent CPA were employed in order to stimulate vascular dilatation by different pathways to assess contribution of H_2O_2 to EDHF-type and NO-mediated relaxation. The direct interaction between H_2O_2 and NO was investigated with L-NAME and the NO donor MAHMA NONOate, distinguishing between the endogenous produced NO and exogenous NO. There is evidence that an inverse relationship was found between NO and EDHF-type responses in the rabbit arteries (Berman *et al.*, 2002), by identifying the role of H_2O_2 in this signalling network will clarify the cellular interactions observed in association gap junction-dependent relaxation and may suggest new therapeutic strategies in the many disease states where NO bioavailability is decreased and EDHF dominates.

The second aim of this thesis was to identify the principal interactions that interlink Ca^{2+} mobilization, influx and H_2O_2 in the endothelial signaling network. To achieve this goal, investigations were carried out with endothelium in order to indentify the effect of H_2O_2 on CPA-evoked increase in $[Ca^{2+}]_i$, ER store depletion, store-operated Ca^{2+} entry, non-selective divalent cation entry and $[Ca^{2+}]_m$. There is evidence that endothelial cells of different species express functional ryanodine receptors (Lesh *et al.*, 1993; Ziegelstein *et al.*, 1994; Wang *et al.*, 1995), however, their role in native tissue has yet to be confirmed and it is important to know the effect of H_2O_2 on this signalling mechansim. The use of rabbit aortic valve leaflets in this part of the study gave great advantage

over the complicating effects of signals such as Ca^{2+}/$InsP_3$ transmitted from subjacent smooth muscle cells via myoendothelial gap junctions. For some experiments, EA.hy926 cells had to be used because of technical problems with the Ca^{2+}-sensitive probes in native tissue.

The results of the investigations carried out in this thesis demonstrated that:

4. *In the rabbit iliac artery, vascular K_{Ca} channels participate in an interactive manner in the EDHF phenomenon.* This finding was supported by data showing that SK_{Ca}, IK_{Ca} and BK_{Ca} synergistically contribute to (i) the EDHF-type hyperpolarizing response evoked by ACh; (ii) the basal tone and (iii) the phenylephrine-induced contraction (Chapter 3, Figure 3.1 and 3.2).

5. *In the rabbit iliac artery, H_2O_2 can amplify EDHF-type relaxations evoked by various modes of stimulation.* This finding was supported by data showing that exogenous H_2O_2 potentiates receptor dependent EDHF-type responses evoked by the receptor-dependent agonist ACh, extending previous findings with receptor-independent stimulus CPA (Chapter 3, Figure 3.3 and 3.4). Both CPA and ACh evoke EDHF-type responses through the elevation of endothelial $[Ca^{2+}]_i$, therefore the findings gave further evidence that H_2O_2 is likely to potentiate the EDHF-type responses by facilitating this increase in $[Ca^{2+}]_i$

6. *H_2O_2 exerts inhibitory effects on NO-mediated endothelium-dependent relaxations.* The finding was supported by data showing that in rabbit iliac artery, H_2O_2 had no effect on relaxations to CPA or ACh in the absence of L-NAME/indomethacin or to the NO donor MAHMA NONOate, whereas in rabbit aorta, H_2O_2 exerted a concentration-dependent and endothelium-dependent inhibitory effect on NO-dependent relaxations evoked by CPA and ACh (Chapter 3, Figure 3.11, 3.12, 3.14 and 3.15). These results demonstrated that

in large arteries such as aorta, exogenous H_2O_2 might directly interact with the endogenous generation of NO, as it can partially impair NO-dependent relaxations in response to both ACh and CPA in rabbit aorta, whereas in smaller arteries such as iliac, EDHF may compensate for the loss of NO.

7. *Arsenite potentiates EDHF-type responses through the elevation of the endogenous endothelial-produced H_2O_2 that is secondary to the activation of NADPH oxidase.* This finding was supported by data showing that arsenite induced potentiation in EDHF-type relaxation in the rabbit iliac artery was prevented by catalase, the catalase/SOD mimetic MnTMPyP and NADPH oxidase inhibitor apocynin, and that the arsenite-induced increases in DHE fluorescence were prevented with the NADPH oxidase inhibitor apocynin in endothelium (Chapter 4, Figure 4.3 and 4.4).

8. *H_2O_2 may contribute to potentiated EDHF-type response by promoting the elevation of endothelial $[Ca^{2+}]_i$ and extracellular Ca^{2+} influx.* This finding was supported by data showing that H_2O_2 by itself has minimal effect on $[Ca^{2+}]_i$, however in combination with 10 μM CPA (but not 30 μM CPA), they synergistically (i) elevated $[Ca^{2+}]_i$ (Chapter 6, Figure 6.2); (ii) depleted $[Ca^{2+}]_{ER}$ (Chapter 6, Figure 6.4); (iii) increased the Ca^{2+} re-entry (Chapter 6, Figure 6.6); and (iv) increased the rate of non-selective divalent cation entry (Chapter 6, Figure 6.9).

9. *The effect of H_2O_2 on Ca^{2+} mobilization may be affected through inhibition of SERCA and activation of ryanodine-sensitive Ca^{2+} stores.* This finding was supported by data showing that (i) In Ca^{2+}-free buffer, H_2O_2 by itself depleted $[Ca^{2+}]_{ER}$ and prevented the ER store refilling (Chapter 6, Figure 6.11B); (ii) the $InsP_3$ receptor antagonist XesC is unable to reverse the depletion of $[Ca^{2+}]_{ER}$ by

H_2O_2 (Chapter 6, Figure 6.11C and 6.11F); and (iii) H_2O_2 and ryanodine competitively depleted $[Ca^{2+}]_{ER}$ (Chapter 6, Figure 6.12).

10. *In cultured EA.hy926 human endothelial cells, mitochondria play a role in Ca^{2+} mobilization.* This finding was supported by data showing that (i) H_2O_2 synergistically elevated the $[Ca^{2+}]_m$ with 10 μM CPA (Chapter 6, Figure 6.14);. and (ii) H_2O_2 synergistically depleted the $[Ca^{2+}]_{ER}$ and elevates the $[Ca^{2+}]_i$ with 1-10 μM CPA (Chapter 6, Figure 6.16 and 6.18).

The principal findings of this study led to the conclusion that H_2O_2 contributes to the potentiation of both receptor-dependent and –independent EDHF-type relaxations observed in the rabbit iliac artery by promoting the elevation of intracellular Ca^{2+} level, through inhibition of SERCA activity and the activation of ryanodine-sensitive Ca^{2+} stores, and therefore the sustained extracellular Ca^{2+} influx required to activate K_{Ca} channels on the endothelium. The inhibitory effect of H_2O_2 on SERCA pump activity is perhaps one of the major findings of this thesis, since it added another possibility by which H_2O_2 plays a role in the endothelial Ca^{2+} homeostasis. Indeed, it was thought that sensitization of the $InsP_3$ receptor underlies the H_2O_2-induced potentiation (Redondo *et al.*, 2004; Zheng and Shen, 2005; Edwards *et al.*, 2008), however, in this study the $InsP_3$ receptor antagonist XesC failed to reverse H_2O_2-evoked depletion of the $[Ca^{2+}]_{ER}$. Instead, H_2O_2 attenuated Ca^{2+} refilling of the ER stores in experiments following re-addition of extracellular Ca^{2+}. The ability of H_2O_2 to promote Ca^{2+} release was attributed to its oxidative function on sulphydryl groups that are present in many Ca^{2+} channels such as the $InsP_3$ receptor and the SERCA pump. It has been shown that, in human platelet, Ca^{2+} release from agonist-sensitive stores by H_2O_2 is mediated by both, $InsP_3$ receptor sensitisation and inactivation of SERCA (Redondo *et al.*, 2004). However, it has also been shown that, in muscle cells, the inhibitory effect of H_2O_2 on the activity of SERCA was independent of sulphydryl group oxidation (Moreau *et al.*,

1998). In addition, this study provides direct evidence for the presence of a functional ryanodine-sensitive Ca^{2+} store in the intact endothelium of rabbit aortic valve leaflets (Figure 7.1).

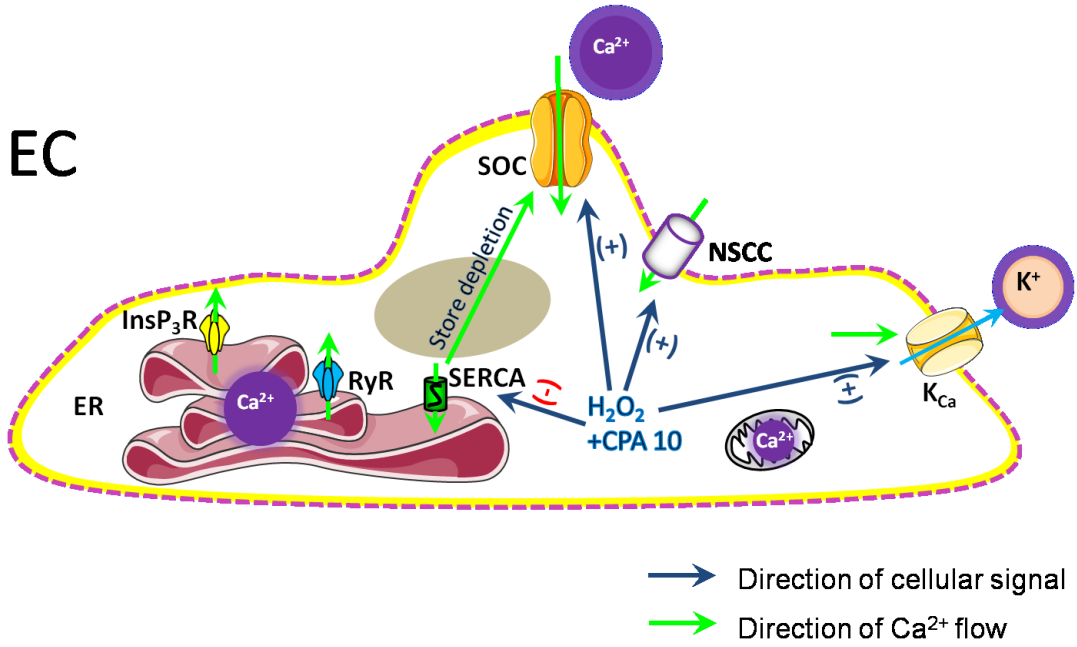

Figure 7.1 Schematic presentations of the complex effects of H_2O_2 and CPA on endothelial Ca^{2+} mobilization. EC: endothelial cell; ER: endoplasmic reticulum; $InsP_3R$: $InsP_3$ receptor; RyR: ryanodine receptor; SERCA: sarcoplasmic-endoplasmic reticulum Ca^{2+}-ATPase; SOC: store-operated Ca^{2+} channel; NSCC: non-selective Ca^{2+} channel; K_{Ca}: Ca^{2+}-activated potassium channel;

There are a number of limitations of the current study that should be considered. As introduced in Chapter 1, the dynamic role of mitochondria in physiological Ca^{2+} signalling is reflected by their close proximity to ER $InsP_3$ receptors and the plasma membrane, a spatial relationship that allows them to function in concert with the ER to sequester/release cytosolic Ca^{2+} and supply the immediate ATP requirement for the removal of Ca^{2+} from the cytosol by the SERCA and PMCA pump (Malli *et al.*, 2003; Camello-Almaraz *et al.*, 2006; Zhang and Gutterman, 2007). However, due to limitation on fluorescence indicator Rhod-2 in that the probe was saturated due to high basal

$[Ca^{2+}]_m$ in the native tissue, it was impossible to determine whether mitochondria played a role in regulation of the Ca^{2+} that has been release by internal stores in rabbit aortic valves. Further investigations are needed to find for an appropriate indicator, and there are newer probes (e.g.) Rhod-FF, X-rhod-1 and X-rhod-5F coming on the market.

In addition, endothelial $[H_2O_2]_i$ was not able to be measured to correlate the findings with Ca^{2+} homeostasis. Cytosolic Ca^{2+} plays an important role in regulating mitochondrial H_2O_2 production, since increases in $[Ca^{2+}]_i$ promote mitochondrial Ca^{2+} uptake via the Ca^{2+} uniporter leading to elevated $[Ca^{2+}]_m$ that increase $O_2^{\bullet-}/H_2O_2$ production (e.g.) by stimulating multiple Ca^{2+}-regulated dehydrogenases in the Krebs cycle and thereby enhancing substrate production and electron flow into the respiratory chain and electron leak to molecular O_2 (Brookes *et al.*, 2004; Zhang and Gutterman, 2007). Indeed, in Chapter 4, it was demonstrated that the endogenous endothelial-produced H_2O_2 from activated NADPH oxidase underlies the arsenite-induced potentiates of EDHF-type responses. However, there was no reliable endogenous H_2O_2 indicator for use in this present study: (i) DCF was unable to detect fluorescence changes upon treatment with 10 or 30 μM CPA or 100 μM H_2O_2 in the rabbit aortic valve leaflets and its specificity to H_2O_2 was questioned as it can also be oxidized by other ROS (Crow, 1997; Wang and Joseph, 1999); (ii) DHE is reported to detect both $O_2^{\bullet-}$ and H_2O_2 (Fernandes *et al.*, 2007; Ray *et al.*, 2011), (iii) Amplex Red assay was not for real time measure of $[H_2O_2]_i$; and (iv) PG1 and PC1 had low sensitivity and long reaction time to $[H_2O_2]$. A genetically encoded fluorescent sensor HyPer has shown a promising result in the cultured EA.hy926 cells, nevertheless, further studies will be needed to investigate the use of HyPer in intact tissue (see Appendix for details).

The findings of the present study suggest a number of possibilities for further research into the role of H_2O_2 plays in the EDH phenomenon that compensates for the decreased NO availability/activity in endothelial dysfunction underlying cardiovascular disease. The present study has provided evidence that exogenous H_2O_2 can potentiate

the EDHF phenomenon, as well as partially impair NO-dependent relaxations in response to both ACh and CPA in rabbit aorta. Further investigations could be carried out to determine if exogenous H_2O_2 also impairs the endogenous NO production and if exogenous NO has any effect in cytosolic [H_2O_2], mitochondrial [$O_2^{\bullet-}$] and $[Ca^{2+}]_m$ in the rabbit aortic valve leaflets or EA.hy926 cells. In detail, the effects of graded concentrations of H_2O_2 on endogenous NO production could be assessed using diaminofluoresceins (DAF) imaging [a group of fluorescent NO-sensitive dyes that were developed by Kojima and colleagues, which can be used routinely to directly measure low-output NO, detection limit: 3–10 nM NO, (Kojima *et al.*, 1998a; Kojima *et al.*, 1998b; Kojima *et al.*, 1998c; Kojima *et al.*, 1999)]. In parallel, the effects of endogenous NO production and exogenous NO (e.g. generated by administering spermine NONOate in the presence of L-NAME) on changes in cytosolic [H_2O_2] (imaging with HyPer), mitochondrial [$O_2^{\bullet-}$] (imaging with MitoSox Red), $[Ca^{2+}]_m$ (imaging with Mag-fluo-4) and membrane potential ($\Delta\psi_m$, imaging with JC-1) could also be assessed in the endothelial cells induced by ACh and CPA. Such experiments would be performed over a range of ambient O_2 tensions because there is evidence that O_2 availability affects the ability of NO to modulate mitochondria activity (Quintero *et al.*, 2006; Erusalimsky and Moncada, 2007). Protocols employing the *s*GC inhibitor ODQ, and a cell permeant cGMP analogue (8-Br-cGMP) would allow distinct effects of NO and cGMP to be dissociated, and findings could be correlated with corresponding measurements of cell membrane potential, $[Ca^{2+}]_i$ and $[Ca^{2+}]_{ER}$ which are themselves regulated by NO/cGMP, as introduced in Section 1.2.4. Use of the agents ACh and CPA would differentially affect specific components of the intracellular signalling network [e.g. CPA will oppose stimulatory effects of NO on the SERCA pump (Adachi *et al.*, 2004)] allowing a composite picture of the effects of NO to be assembled. In HEK cells an analogous approach has shown that NO depolarizes mitochondria and suppresses mitochondrial Ca^{2+} uptake through a cGMP-independent mechanism, with the resulting elevation in

$[Ca^{2+}]_i$ directly inhibiting the SOCC channel (Thyagarajan *et al.*, 2002). Whether similar mechanisms operate in endothelial cells remains to be established.

Furthermore, electrophysiological and mechanical studies with connexin-mimetic peptides have revealed the essentially electrotonic nature of the EDHF phenomenon in the rabbit iliac artery (Griffith *et al.*, 2002; Chaytor *et al.*, 2005). H_2O_2 has been variously reported to inhibit (Upham *et al.*, 1997) or enhance gap junctional communication (Rouach *et al.*, 2004). While the ability of H_2O_2 to potentiate NO-independent, CPA and ACh-evoked relaxation in the rabbit iliac artery suggests that H_2O_2 does not significantly impair electrotonic signalling via vascular gap junctions, its effects on direct intercellular communication in the arterial wall have yet to be investigated formally. It is also theoretically possible that H_2O_2 modulates the functionality of connexin hemichannels present in the endothelial cell membrane which there is evidence that hemichannels opening is enhanced by H_2O_2 (Ramachandran *et al.*, 2007). In addition, there is also evidence that open hemichannels can also facilitate the influx of extracellular Ca^{2+} ions (Li *et al.*, 2001). Whether hemichannels contribute to the ability of H_2O_2 to elevate $[Ca^{2+}]_i$ in native endothelial cells following stimulation in normal $[Ca^{2+}]$ buffer, and thereby enhance relaxation, remains to be explored. In detail, the possible modulatory role of H_2O_2 on gap junctional communication in this vessel could be investigated using a previously validated strategy (i.e.) dye transfer with calcein AM (Griffith *et al.*, 2002), that the inhibitory/stimulatory effects of H_2O_2 on dye transfer in the rabbit iliac artery would be quantified. The presence of hemichannels in the rabbit aortic valve endothelium would also be tested using the established protocol of promoting the opening of such channels by incubation in low Ca^{2+} buffer (Li *et al.*, 2001) and then assessing uptake of tracers such as calcein, and their efflux from preloaded cells (e.g.) after incubation with calcein AM. If evidence for functional hemichannels is forthcoming, connexin-mimetic peptides and glycyrrhetinic acid derivatives, which are both known to block hemichannels, could be used to investigate

their ability to mediate Ca^{2+} influx in Ca^{2+} re-entry experiments. The correct choice of peptide(s) would be determined by identifying the expression of Cxs 37, 40 and 43 in the rabbit aortic valve by immunostaining with specific antibodies, as previously described (Chaytor *et al.*, 2005).

7.2 CONCLUDING REMARKS

This thesis provides evidence that contributes to the notion that H_2O_2 is a physiologically-important signalling molecule that is already known to play a crucial role in arterial function through oxygen sensing, cell growth and proliferation and apoptosis. Data from mechanical and imaging studies confirms a role for H_2O_2 in the Ca^{2+} homeostasis of the endothelial cells, whereby this ROS may compensate for the decreased NO bioavailability by modulating the EDH phenomenon. The finding of the present investigations also gives further insights into the mechanism underlying the compensatory role of the EDH phenomenon to compromised NO-mediated response that are observed in many vessels. Considering that the EDH phenomenon dominate in many small arteries, the modulation of its action are of critical importance for the regulation of blood flow, vascular resistance and blood pressure, and an identification of vessel-specific nature of the EDH phenomenon, its modulation of biological activity by selective activators or inhibitors might have a significant impact to the understanding of vascular maintenance in health and disease, and provide basis for new therapeutic strategies.

Appendix

Limitation and Potential Methods of Direct Imaging of Intracellular Hydrogen Peroxide Concentration

A.1 INTRODUCTION

Although this group is interested in the mechanisms by which reactive oxygen species H_2O_2 functions in endothelial cells, it has yet establish a reliable and sensitive way of sensing and imaging intracellular H_2O_2. In this Appendix, both the unsuccessful and promising investigations performed in this group by author of this thesis and colleagues in the search for a reliable H_2O_2 sensor will be discussed. Mechanisms for sensing H_2O_2 in intact tissues and cultured cells included 2',7'-dichlorodihydrofluorescein diacetate (H_2DCFDA or DCF), DHE, Amplex Red, PG1, PC1 and a protein based sensor HyPer.

A.2 RESULTS AND DISCUSSION

A.2.1 DCF

H_2DCFDA or DCF is a fluorescent probe that has been widely used for imaging $[H_2O_2]_i$. To assess $[H_2O_2]_i$ in endothelial cells, rabbit aortic valve leaflets were incubated with DCF (5 μM) at room temperature in oxygenated Holman's buffer for 30 minutes. After loading of the dye, the valves were briefly rinsed with indicator-free buffer. As shown in Figure A1, DCF was unable to detect fluorescence changes upon treatment with 10 or

30 µM CPA or 100 µM exogenous applied H_2O_2 in the rabbit aortic valve leaflets, whereas increased DCF fluorescence was observed at 1 mM H_2O_2. Indeed, the specificity of this compound to H_2O_2 has been questioned, and several reports have demonstrated that DCF can be oxidized by other ROS, such as $HO^{\bullet}$, and by reactive nitrogen species, such as nitric oxide (•NO) and $ONOO^-$ (Crow, 1997; Wang and Joseph, 1999). Therefore, this probe should be considered as a marker of cellular oxidative stress rather than an indicator of $[H_2O_2]_i$ (Jakubowski and Bartosz, 2000; Tarpey *et al.*, 2004).

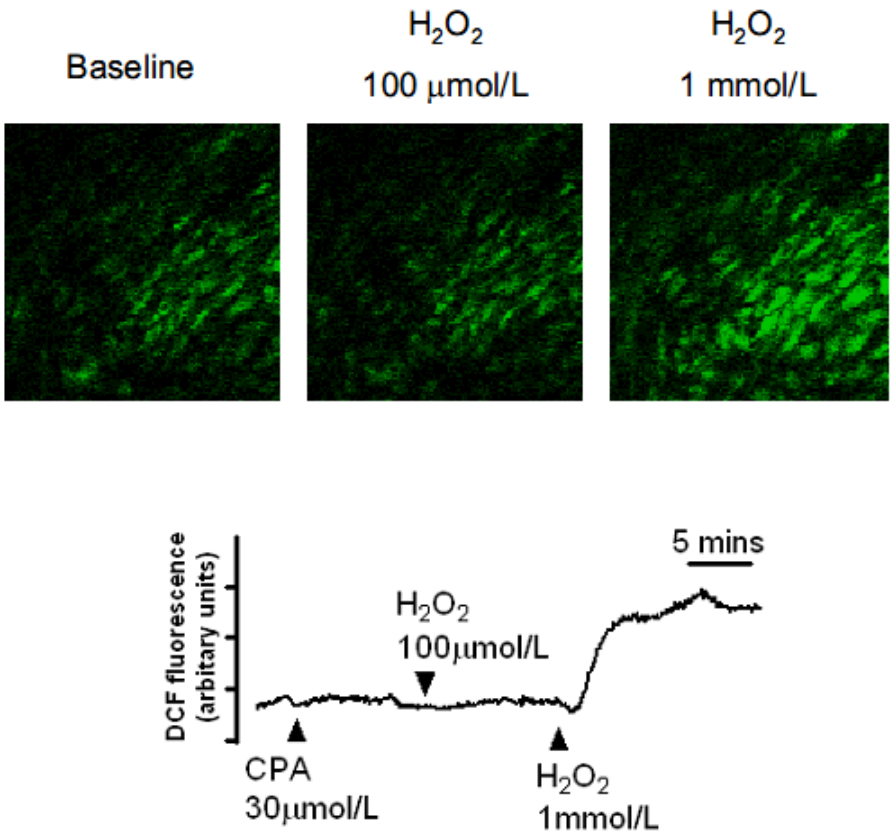

Figure A1 Effects of 30 µM CPA and 100 µM H_2O_2 in rabbit aortic valves loaded with 10 µM DCF for 30 min at room temperature. Confocal imaging demonstrated that 1 mM H_2O_2 were required to increase fluorescence. Figure taken from (Edwards *et al.*, 2008)

A.2.2 DHE

DHE is a fluorescent probe that is used for detecting $O_2^{\bullet-}$, due to its relative specificity for this ROS (Bindokas *et al.*, 1996; Benov *et al.*, 1998). When DHE is oxidized by $O_2^{\bullet-}$, it produces two products, ethidium and 2-hydroxyethidium, these compounds possess overlapping emission spectra and their fluorescence is enhanced by binding to DNA (Zielonka and Kalyanaraman, 2010). However, ethidium can also be oxidized by H_2O_2 via non-specific peroxidase (horseradish peroxidase and myeloperoxidase) catalysis or haem proteins, forming fluorescent oxidation products (Munzel *et al.*, 2002). Therefore, the increased fluorescence in DHE-loaded vascular smooth muscle/ endothelial cells may reflect production of both $O_2^{\bullet-}$ and H_2O_2 (Fernandes *et al.*, 2007; Ray *et al.*, 2011). Indeed, the findings in Chapter 4 have shown an elevated DHE fluorescence upon treatment with arsenite, which increase the endogenous endothelial-produced H_2O_2 secondary to the activation of NADPH oxidase.

A.2.3 Amplex Red

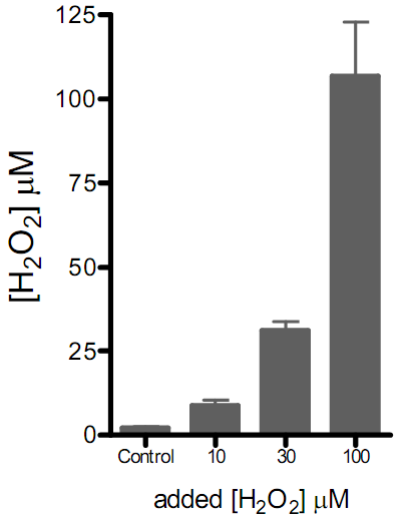

Figure A2 Bar graph showing buffer $[H_2O_2]$ was unchanged at the conclusion of the tension myograph experiments. Figure taken from (Garry *et al.*, 2009)

N-Acetyl-3,7-dihydroxyphenoxazine (Amplex Red) is itself a non-fluorescent molecule, however, when oxidized by H_2O_2 in presence of horseradish peroxidase, it produces the highly fluorescent product resorufin (Mohanty *et al.*, 1997; Zhou *et al.*, 1997).

Samples of buffer (300 µl) were collected at the beginning and end of relaxation protocols in experiments with ACh into a 96-well plate. Amplex Red (10 µM) and horseradish peroxidase (0.6 U/mL) were added into each sample and incubated in the dark at room temperature for 15 minutes. Fluorescence was read at 560 nm using a Fluostar optima spectrophotometer and the corresponding H_2O_2 concentrations were derived from a standard curve. Experiments to obtain the standard curves were performed in the absence of arterial rings with oxygenated buffer maintained at 37^{o}C to match the relaxation protocols. As shown in Figure A2, Amplex Red assay can be used for detecting [H_2O_2] in the buffer system. However, due to the nature of this probe, i.e. needing to be mixed with horseradish peroxidase, the real time measure of intracellular [H_2O_2] is not possible.

A.2.4 PG1 and PC1

Peroxy Green 1 (PG1) and Peroxy Crimson 1 (PC1) are two newly developed fluorescent dyes that are reported to have high selectivity for H_2O_2 (Miller *et al.*, 2007). They are designed to be activated by a single boronate deprotection (i.e. deprotection is the removal of a protecting group which represents a chemically modified functional group, deprotection is used to obtain chemoselectivity in the subsequential chemical reaction) and these H_2O_2-mediated boronate deprotections of PG1 and PC1, in theory, should generate two fluorescent products, 2-methyl-4-O-methyl Tokyo Green and resorufin, respectively. The dyes are a gift from Dr Miller. Rabbit aortic valve leaflets were incubated with PG1 or PC1 (5 µM) at room temperature in oxygenated HEPES buffer for 15 minutes. After loading of the dye, the valves were briefly washed with indicator-free buffer.

In PG1 and PC1 loaded rabbit aortic valve leaflets, PG1 fluorescence was increased by addition of H_2O_2 at concentrations ≥10 mM, whereas PC1 fluorescence was elevated by addition of H_2O_2 at concentrations ≥100 µM (Figure A3, A and B). In spectroscopic

and sensitivity experiments, H_2O_2 caused a concentration and time-dependent increase in both PG1 and PC1 fluorescence (Figure A4, C-E).

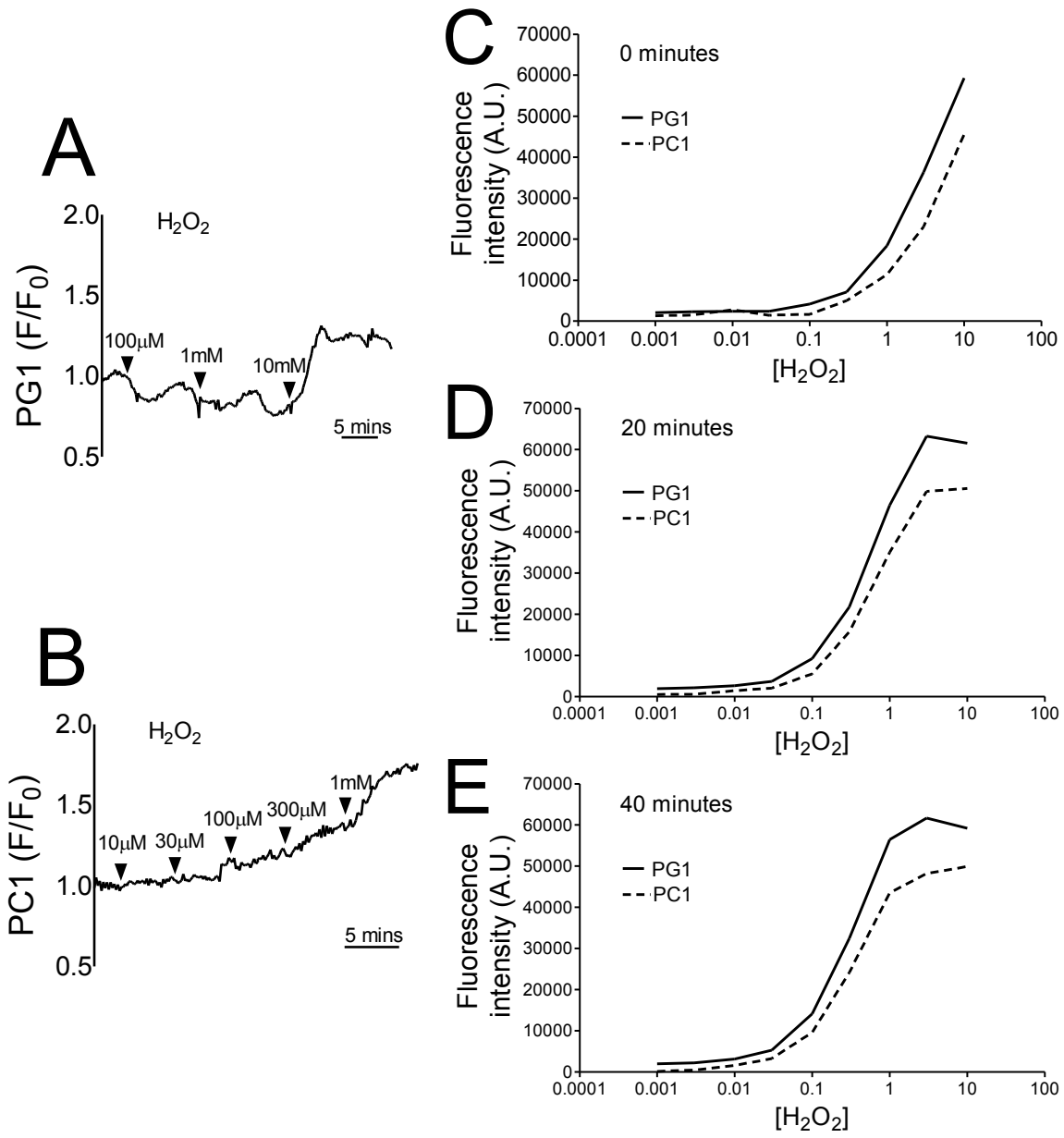

Figure A3 Effect of H_2O_2 on PG1 and PC1 fluorescence. (A) Traces illustrating the concentration-dependent increase in PG1 fluorescence by H_2O_2 in the rabbit aortic valve leaflets. (B) Traces illustrating the concentration-dependent increase in PC1 fluorescence by H_2O_2 in the rabbit aortic valve leaflets. (C-E) Traces illustrating the concentration-dependent increase in PG1 and PC1 fluorescence by H_2O_2 at 0, 20 and 40 minutes after incubation measured by Fluostar spectrophotometer.

The real time confocal microscopy imaging of rabbit aortic valve leaflets loaded with PG1 and PC1 was disappointing. As shown in Figure A3, PG1 fluorescence was only elevated when exogenous applied H_2O_2 at concentrations ≥10 mM. H_2O_2 caused a concentration-dependent increase on PC1 fluorescence at concentrations ≥100 µM. In test-tube experiments with the aid of a spectrophotometer, both dyes were able to detect H_2O_2 in a concentration and time-dependent manner. However, in order to observe nM or µM levels of H_2O_2, a reaction time of 40 minutes or longer was required. Therefore, due to their low sensitivity and long reaction time, PG1 and PC1 may not be the preferred fluorescent probes for real time imaging of intracellular H_2O_2 in tissue culture.

A.2.5 HyPer

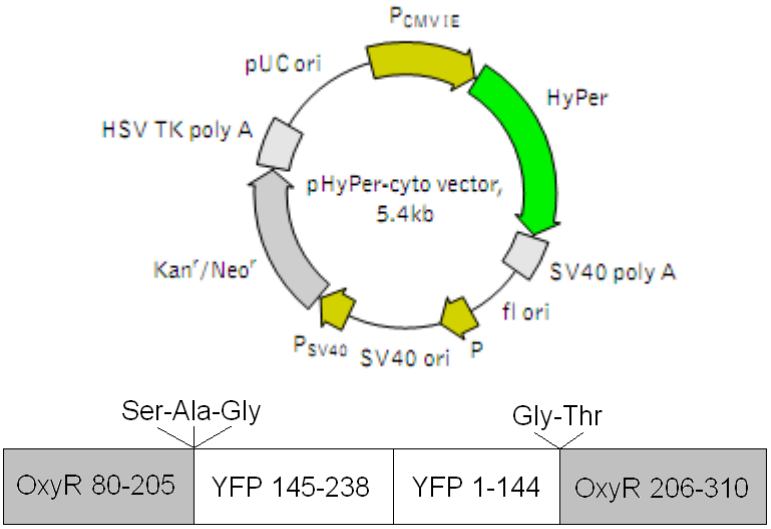

Figure A4. pHyPer-cyto vector design and HyPer construct design

pHyPer-cyto vector was obtained from Evrogen and transformed into competent TOP10 (E. coli) cells using heat shock. The bacterial colonies were collected and subsequently scaled up using the Qiagen Maxi Prep Kit (large scale plamid isolation kit). The result DNA concentration was 2.3µg/µl. This procedure was kindly performed by collaborator Dr Raul Gonzalez-Garcia under the supervision of Prof Karl Swann.

Figure taken from http://evrogen.com

HyPer is a genetically encoded fluorescent sensor capable of detecting intracellular hydrogen peroxide. It was designed by inserting the circularly permuted yellow fluorescent protein into the regulatory domain of *Escherichia.coli* (*E.coli*) protein OxyR (OxyR-RD) (see Figure A4 for information on HyPer vector) (Belousov *et al.*, 2006). The *E.coli* OxyR transcription factor senses hydrogen peroxide and is activated through the formation of an intramolecular disulfide bond (Choi *et al.*, 2001). HyPer allows ratiometric measurement of hydrogen peroxide as it has two excitation peaks, with maximum at 420nm and 500nm, while having one emission peak with maximum at 516nm. When HyPer is exposed to hydrogen peroxide, the excitation peak of 420nm decreases proportionally to the rise in intensity at the excitation peak of 500nm. The oxidized HyPer is capable of reducing inside cells like wild-type OxyR (Evrogen, 2010).

EA.hy926 (2 ml) cells were seeded in 35mm glass bottomed culture dishes in their corresponding complete growth medium at the concentration of $1.5x10^5$ cell/ml for 24 hours, and reached 80-90% confluency at the time of transfection. Plasmid DNA (8 µg) was dissolved in serum/antibiotics free medium to a total volume of 250 µl. Lipofectamine™ 2000 (10 µl) was also dissolved with the same medium to 250 µl. Both mixtures were incubated at room temperature for 5 minutes. The lipid and DNA mixtures were then combined (drop wise over a period of 30 seconds) for a further 20 minutes at room temperature to allow the formation of the DNA-Carrier complexes. During this time, the cells were washed twice with 0.9% w/v saline solution before addition of 2 ml serum/antibiotics free medium containing the transfection complexes, followed by 6 hours incubation at 37°C in a 5% CO_2 in air atmosphere. The complete growth medium was given to the cells after removal of the transfection reagents, and the cells were kept in a cell incubator for 24-48 hours prior to testing for transgene expression.

Experiments with HyPer were carried out with an inverted epifluorescence microscope and visualized with an oil immersion 40X lens. HEPES buffer was used for all

experiments. The successfully transfected EA.hy926 cells (strong and evenly distributed fluorescence appearing across the whole cell) were selected and the intensity was calculated after subtracteion of background. Data were recorded and analysed with Excel/Graphpad Prism 4 software.

In HyPer transfected EA.hy926 cells, 100 μM H_2O_2 caused a ~3 fold increase on HyPer 490/420 ratio, with maximum reached ~1 minute. As shown in Chapter 4, arsenite stimulates intracellular H_2O_2 production, and 100 μM arsenite caused a ~3 fold increase on HyPer 490/420 ratio, with the maximum fluorescence achieved in ~90 minutes. The addition of 100 μM H_2O_2 on top of arsenite, caused a further increase (~5 fold) in the HyPer 490/420 ratio, with maximum reached in ~1 minute (Figure A5).

These findings matched the time over which arsenite potentiates the CPA-evoked EDHF-type responses (30 minutes pre-incubation, 15 minutes PE constriction and ~45 minutes CPA-evoked relaxations) and matched the time over which exposure to 100 μM arsenite (90 minutes) significantly enhanced endothelial nuclear fluorescence in the rabbit aortic valve leaflets loaded with DHE.

A.2.6 CONCLUSIONS AND FURTHER STUDIES

The preliminary data with HyPer transfected endothelial cells showed promising sensitivity to exogenous applied H_2O_2. Further studies will be needed to verify the sensitivity of Hyper to H_2O_2 at lower concentrations. It would be beneficial to test for transfecting of HyPer vector into the rabbit aortic valve leaflets, thus the $[H_2O_2]_i$ can be correlated with effects of exogenous applied H_2O_2 on the Ca^{2+} mobilization in the tissue, as discussed in Chapter 6.

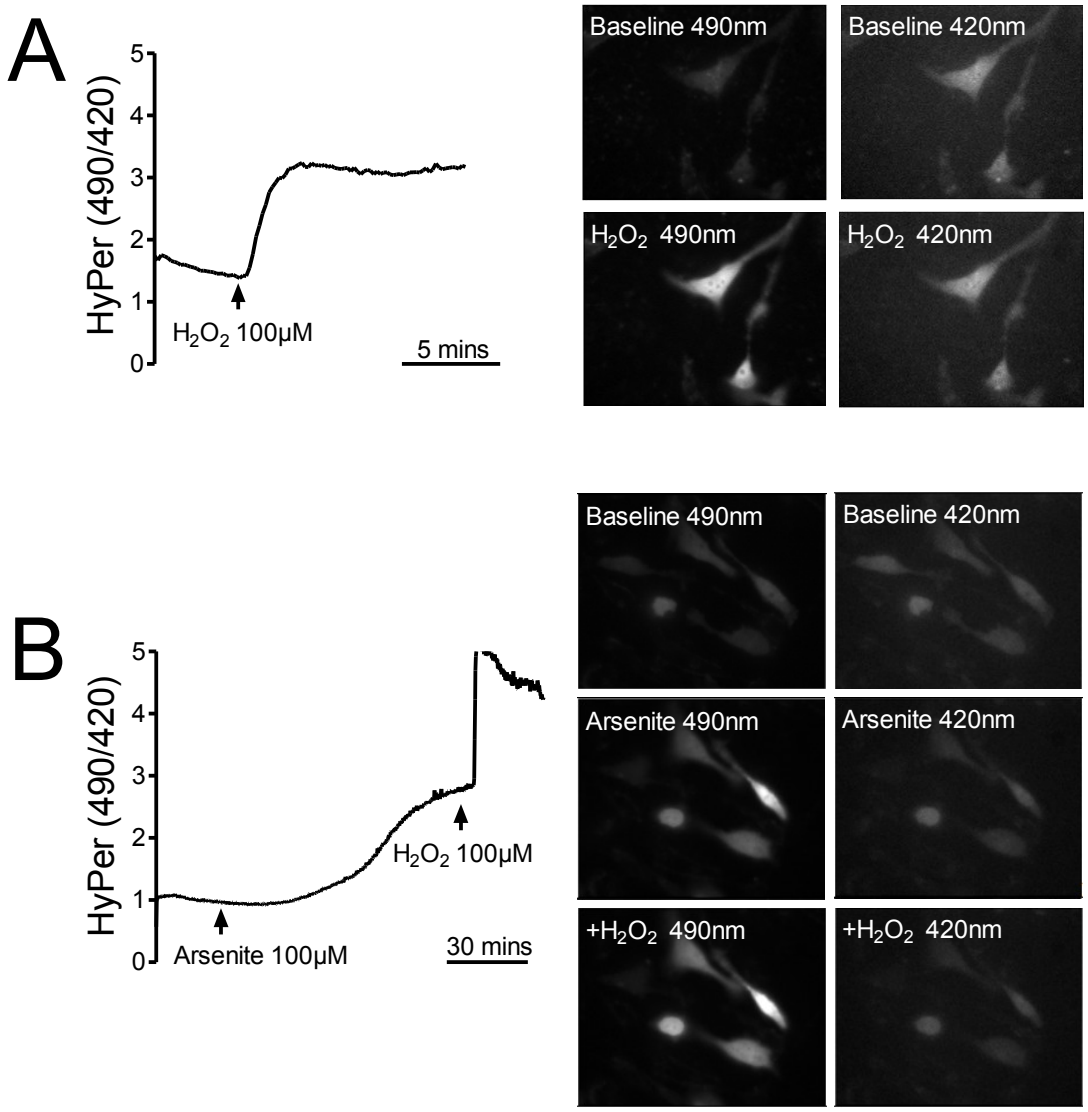

Figure A5 Transfected EA.hy926cells expressing HyPer. (A) Traces and images illustrating the increased fluorescence following addition of 100 µM H_2O_2. (B) Traces and images illustrating the increased fluorescence following addition of 100 µM arsenite and 100 µM H_2O_2.

List of publications

Published scientific abstracts:

Li Y, Edwards DH, Griffith TM. H_2O_2 potentiates the EDHF phenomenon by promoting endothelial Ca^{2+} mobilization. Journal of Vascular Research. 2009;46(Suppl.1):36

Peer reviewed publications:

1. Edwards DH, Li Y, Griffith TM. H_2O_2 potentiates the EDHF phenomenon by promoting endothelial Ca^{2+} mobilization. Arteriosclerosis, Thrombosis, and Vascular Biology. 2008;28(10):1774-81. (Also see Editorial in same issue of the Journal: Graier WF, Hecker M. Endothelial H_2O_2: a bad guy turning good? Arteriosclerosis, Thrombosis, and Vascular Biology. 2008;28(10):1691-3)

2. Edwards DH, Li Y, Ellinsworth DC, Griffith TM. Potentiation of the EDHF phenomenon by inorganic arsenic: role of NADPH oxidase and hydrogen peroxide. Toxicology. Submitted.

Awards

Young Investigator Award (June, 2009). 10th International Symposium on Mechanisms of Vasodilatation, Japan

REFERENCES

Abdullaev IF, Bisaillon JM, Potier M, Gonzalez JC, Motiani RK, Trebak M (2008). Stim1 and Orai1 mediate CRAC currents and store-operated calcium entry important for endothelial cell proliferation. *Circ Res* **103**(11)**:** 1289-1299.

Abran D, Hardy P, Varma DR, Chemtob S (1995). Mechanisms of the biphasic effects of peroxides on the retinal vasculature of newborn and adult pigs. *Exp Eye Res* **61**(3)**:** 285-292.

Absi M, Burnham MP, Weston AH, Harno E, Rogers M, Edwards G (2007). Effects of methyl beta-cyclodextrin on EDHF responses in pig and rat arteries; association between SK(Ca) channels and caveolin-rich domains. *Br J Pharmacol* **151**(3)**:** 332-340.

Adachi T, Weisbrod RM, Pimentel DR, Ying J, Sharov VS, Schoneich C, Cohen RA (2004). S-Glutathiolation by peroxynitrite activates SERCA during arterial relaxation by nitric oxide. *Nat Med* **10**(11)**:** 1200-1207.

Ago T, Kitazono T, Ooboshi H, Iyama T, Han YH, Takada J, Wakisaka M, Ibayashi S, Utsumi H, Iida M (2004). Nox4 as the major catalytic component of an endothelial NAD(P)H oxidase. *Circulation* **109**(2)**:** 227-233.

Aird WC (2007). Phenotypic heterogeneity of the endothelium: I. Structure, function, and mechanisms. *Circ Res* **100**(2)**:** 158-173.

Alonso MT, Barrero MJ, Michelena P, Carnicero E, Cuchillo I, Garcia AG, Garcia-Sancho J, Montero M, Alvarez J (1999). Ca2+-induced Ca2+ release in chromaffin cells seen from inside the ER with targeted aequorin. *J Cell Biol* **144**(2)**:** 241-254.

Andonegui G, Zhou H, Bullard D, Kelly MM, Mullaly SC, McDonald B, Long EM, Robbins SM, Kubes P (2009). Mice that exclusively express TLR4 on endothelial cells can efficiently clear a lethal systemic Gram-negative bacterial infection. *J Clin Invest* **119**(7)**:** 1921-1930.

Andreozzi F, Laratta E, Sciacqua A, Perticone F, Sesti G (2004). Angiotensin II impairs the insulin signaling pathway promoting production of nitric oxide by inducing phosphorylation of insulin receptor substrate-1 on Ser312 and Ser616 in human umbilical vein endothelial cells. *Circ Res* **94**(9)**:** 1211-1218.

Anger M, Samuel JL, Marotte F, Wuytack F, Rappaport L, Lompre AM (1993). The sarco(endo)plasmic reticulum Ca(2+)-ATPase mRNA isoform, SERCA 3, is expressed in endothelial and epithelial cells in various organs. *FEBS Lett* **334**(1)**:** 45-48.

Ardanaz N, Beierwaltes WH, Pagano PJ (2008). Distinct hydrogen peroxide-induced constriction in multiple mouse arteries: potential influence of vascular polarization. *Pharmacol Rep* **60**(1)**:** 61-67.

Arehart E, Stitham J, Asselbergs FW, Douville K, MacKenzie T, Fetalvero KM, Gleim S, Kasza Z, Rao Y, Martel L, Segel S, Robb J, Kaplan A, Simons M, Powell RJ, Moore JH, Rimm EB, Martin KA, Hwa J (2008). Acceleration of cardiovascular disease by a dysfunctional prostacyclin receptor mutation: potential implications for cyclooxygenase-2 inhibition. *Circ Res* **102**(8)**:** 986-993.

Arroyo CM, Carmichael AJ, Bouscarel B, Liang JH, Weglicki WB (1990). Endothelial cells as a source of oxygen-free radicals. An ESR study. *Free Radic Res Commun* **9**(3-6)**:** 287-296.

Babior BM, Lambeth JD, Nauseef W (2002). The neutrophil NADPH oxidase. *Arch Biochem Biophys* **397**(2)**:** 342-344.

Bagi Z (2009). Mechanisms of coronary microvascular adaptation to obesity. *Am J Physiol Regul Integr Comp Physiol* **297**(3)**:** R556-567.

Balakumar P, Kaur J (2009). Arsenic exposure and cardiovascular disorders: an overview. *Cardiovasc Toxicol* **9**(4)**:** 169-176.

Barbato JE, Tzeng E (2004). Nitric oxide and arterial disease. *J Vasc Surg* **40**(1)**:** 187-193.

Barchowsky A, Klei LR, Dudek EJ, Swartz HM, James PE (1999). Stimulation of reactive oxygen, but not reactive nitrogen species, in vascular endothelial cells exposed to low levels of arsenite. *Free Radic Biol Med* **27**(11-12)**:** 1405-1412.

Barlow RS, El-Mowafy AM, White RE (2000). H(2)O(2) opens BK(Ca) channels via the PLA(2)-arachidonic acid signaling cascade in coronary artery smooth muscle. *Am J Physiol Heart Circ Physiol* **279**(2)**:** H475-483.

Barlow RS, White RE (1998). Hydrogen peroxide relaxes porcine coronary arteries by stimulating BKCa channel activity. *Am J Physiol* **275**(4 Pt 2)**:** H1283-1289.

Bauersachs J, Popp R, Hecker M, Sauer E, Fleming I, Busse R (1996). Nitric oxide attenuates the release of endothelium-derived hyperpolarizing factor. *Circulation* **94**(12)**:** 3341-3347.

Belousov VV, Fradkov AF, Lukyanov KA, Staroverov DB, Shakhbazov KS, Terskikh AV, Lukyanov S (2006). Genetically encoded fluorescent indicator for intracellular hydrogen peroxide. *Nat Methods* **3**(4)**:** 281-286.

Bendall JK, Rinze R, Adlam D, Tatham AL, de Bono J, Wilson N, Volpi E, Channon KM (2007). Endothelial Nox2 overexpression potentiates vascular oxidative stress and hemodynamic response to angiotensin II: studies in endothelial-targeted Nox2 transgenic mice. *Circ Res* **100**(7)**:** 1016-1025.

Benov L, Sztejnberg L, Fridovich I (1998). Critical evaluation of the use of hydroethidine as a measure of superoxide anion radical. *Free Radic Biol Med* **25**(7)**:** 826-831.

Beny JL (1990). Thimerosal hyperpolarizes arterial smooth muscles in an endothelium-dependent manner. *Eur J Pharmacol* **185**(2-3)**:** 235-238.

Berman RS, Martin PE, Evans WH, Griffith TM (2002). Relative contributions of NO and gap junctional communication to endothelium-dependent relaxations of rabbit resistance arteries vary with vessel size. *Microvasc Res* **63**(1)**:** 115-128.

Beutner G, Sharma VK, Giovannucci DR, Yule DI, Sheu SS (2001). Identification of a ryanodine receptor in rat heart mitochondria. *J Biol Chem* **276**(24)**:** 21482-21488.

Beutner G, Sharma VK, Lin L, Ryu SY, Dirksen RT, Sheu SS (2005). Type 1 ryanodine receptor in cardiac mitochondria: transducer of excitation-metabolism coupling. *Biochim Biophys Acta* **1717**(1)**:** 1-10.

Bindokas VP, Jordan J, Lee CC, Miller RJ (1996). Superoxide production in rat hippocampal neurons: selective imaging with hydroethidine. *J Neurosci* **16**(4)**:** 1324-1336.

Borda ES, Sterin-Borda L, Gimeno MF, Lazzari MA, Gimeno AL (1983). The stimulatory effect of prostacyclin (PGI2) on isolated rabbit and rat aorta is probably associated to the generation of a thromboxane A2 (TXA2) "like-material". *Arch Int Pharmacodyn Ther* **261**(1)**:** 79-89.

Bossu JL, Elhamdani A, Feltz A (1992a). Voltage-dependent calcium entry in confluent bovine capillary endothelial cells. *FEBS Lett* **299**(3)**:** 239-242.

Bossu JL, Elhamdani A, Feltz A, Tanzi F, Aunis D, Thierse D (1992b). Voltage-gated Ca entry in isolated bovine capillary endothelial cells: evidence of a new type of BAY K 8644-sensitive channel. *Pflugers Arch* **420**(2)**:** 200-207.

Bossu JL, Feltz A, Rodeau JL, Tanzi F (1989). Voltage-dependent transient calcium currents in freshly dissociated capillary endothelial cells. *FEBS Lett* **255**(2)**:** 377-380.

Brading AF, Sneddon P (1980). Evidence for multiple sources of calcium for activation of the contractile mechanism of guinea-pig taenia coli on stimulation with carbachol. *Br J Pharmacol* **70**(2)**:** 229-240.

Brakemeier S, Eichler I, Knorr A, Fassheber T, Kohler R, Hoyer J (2003). Modulation of Ca2+-activated K+ channel in renal artery endothelium in situ by nitric oxide and reactive oxygen species. *Kidney Int* **64**(1)**:** 199-207.

Brandes RP, Barton M, Philippens KM, Schweitzer G, Mugge A (1997). Endothelial-derived superoxide anions in pig coronary arteries: evidence from lucigenin chemiluminescence and histochemical techniques. *J Physiol* **500 (Pt 2):** 331-342.

Brandes RP, Schmitz-Winnenthal FH, Feletou M, Godecke A, Huang PL, Vanhoutte PM, Fleming I, Busse R (2000). An endothelium-derived hyperpolarizing factor distinct from NO and prostacyclin is a major endothelium-dependent vasodilator in resistance vessels of wild-type and endothelial NO synthase knockout mice. *Proc Natl Acad Sci U S A* **97**(17)**:** 9747-9752.

Brandes RP, Schroder K (2008). Composition and functions of vascular nicotinamide adenine dinucleotide phosphate oxidases. *Trends Cardiovasc Med* **18**(1)**:** 15-19.

Brandl CJ, deLeon S, Martin DR, MacLennan DH (1987). Adult forms of the Ca2+ATPase of sarcoplasmic reticulum. Expression in developing skeletal muscle. *J Biol Chem* **262**(8)**:** 3768-3774.

Brandl CJ, Green NM, Korczak B, MacLennan DH (1986). Two Ca2+ ATPase genes: homologies and mechanistic implications of deduced amino acid sequences. *Cell* **44**(4)**:** 597-607.

Brauneis U, Gatmaitan Z, Arias IM (1992). Serotonin stimulates a Ca2+ permeant nonspecific cation channel in hepatic endothelial cells. *Biochem Biophys Res Commun* **186**(3)**:** 1560-1566.

Bredt DS, Snyder SH (1990). Isolation of nitric oxide synthetase, a calmodulin-requiring enzyme. *Proc Natl Acad Sci U S A* **87**(2)**:** 682-685.

Brookes PS, Yoon Y, Robotham JL, Anders MW, Sheu SS (2004). Calcium, ATP, and ROS: a mitochondrial love-hate triangle. *Am J Physiol Cell Physiol* **287**(4)**:** C817-833.

Brown BJ, Hilfiker H, DeMarco SJ, Zacharias DA, Greenwood TM, Guerini D, Strehler EE (1996). Primary structure of human plasma membrane Ca(2+)-ATPase isoform 3. *Biochim Biophys Acta* **1283**(1)**:** 10-13.

Brown J, Reading SJ, Jones S, Fitchett CJ, Howl J, Martin A, Longland CL, Michelangeli F, Dubrova YE, Brown CA (2000). Critical evaluation of ECV304 as a human endothelial cell model defined by genetic analysis and functional responses: a comparison with the human bladder cancer derived epithelial cell line T24/83. *Lab Invest* **80**(1)**:** 37-45.

Bruce JI, Elliott AC (2007). Oxidant-impaired intracellular Ca2+ signaling in pancreatic acinar cells: role of the plasma membrane Ca2+-ATPase. *Am J Physiol Cell Physiol* **293**(3)**:** C938-950.

Budel S, Schuster A, Stergiopoulos N, Meister JJ, Beny JL (2001). Role of smooth muscle cells on endothelial cell cytosolic free calcium in porcine coronary arteries. *Am J Physiol Heart Circ Physiol* **281**(3)**:** H1156-1162.

Burk SE, Lytton J, MacLennan DH, Shull GE (1989). cDNA cloning, functional expression, and mRNA tissue distribution of a third organellar Ca2+ pump. *J Biol Chem* **264**(31)**:** 18561-18568.

Burke-Wolin T, Abate CJ, Wolin MS, Gurtner GH (1991). Hydrogen peroxide-induced pulmonary vasodilation: role of guanosine 3',5'-cyclic monophosphate. *Am J Physiol* **261**(6 Pt 1)**:** L393-398.

Burke TM, Wolin MS (1987). Hydrogen peroxide elicits pulmonary arterial relaxation and guanylate cyclase activation. *Am J Physiol* **252**(4 Pt 2)**:** H721-732.

Burnham MP, Bychkov R, Feletou M, Richards GR, Vanhoutte PM, Weston AH, Edwards G (2002). Characterization of an apamin-sensitive small-conductance Ca(2+)-activated K(+) channel in porcine coronary artery endothelium: relevance to EDHF. *Br J Pharmacol* **135**(5)**:** 1133-1143.

Burnham MP, Johnson IT, Weston AH (2006). Impaired small-conductance Ca2+-activated K+ channel-dependent EDHF responses in Type II diabetic ZDF rats. *Br J Pharmacol* **148**(4)**:** 434-441.

Busse R, Edwards G, Feletou M, Fleming I, Vanhoutte PM, Weston AH (2002). EDHF: bringing the concepts together. *Trends Pharmacol Sci* **23**(8)**:** 374-380.

Bychkov R, Burnham MP, Richards GR, Edwards G, Weston AH, Feletou M, Vanhoutte PM (2002). Characterization of a charybdotoxin-sensitive intermediate conductance Ca2+-activated K+ channel in porcine coronary endothelium: relevance to EDHF. *Br J Pharmacol* **137**(8)**:** 1346-1354.

Bychkov R, Pieper K, Ried C, Milosheva M, Bychkov E, Luft FC, Haller H (1999). Hydrogen peroxide, potassium currents, and membrane potential in human endothelial cells. *Circulation* **99**(13)**:** 1719-1725.

Cai H (2005). Hydrogen peroxide regulation of endothelial function: origins, mechanisms, and consequences. *Cardiovasc Res* **68**(1)**:** 26-36.

Cai S, Sauve R (1997). Effects of thiol-modifying agents on a K(Ca2+) channel of intermediate conductance in bovine aortic endothelial cells. *J Membr Biol* **158**(2)**:** 147-158.

Camello-Almaraz C, Gomez-Pinilla PJ, Pozo MJ, Camello PJ (2006). Mitochondrial reactive oxygen species and Ca2+ signaling. *Am J Physiol Cell Physiol* **291**(5)**:** C1082-1088.

Campbell WB, Gebremedhin D, Pratt PF, Harder DR (1996). Identification of epoxyeicosatrienoic acids as endothelium-derived hyperpolarizing factors. *Circ Res* **78**(3)**:** 415-423.

Carafoli E, James P, Strehler EE (1990). Structure-function relationships in the calcium pump of plasma membranes. *Prog Clin Biol Res* **332:** 181-193.

Cartwright EJ, Oceandy D, Austin C, Neyses L (2011). Ca2+ signalling in cardiovascular disease: the role of the plasma membrane calcium pumps. *Sci China Life Sci* **54**(8)**:** 691-698.

Casteels R, Droogmans G (1981). Exchange characteristics of the noradrenaline-sensitive calcium store in vascular smooth muscle cells or rabbit ear artery. *J Physiol* **317:** 263-279.

Chadha PS, Liu L, Rikard-Bell M, Senadheera S, Howitt L, Bertrand RL, Grayson TH, Murphy TV, Sandow SL (2011). Endothelium-dependent vasodilation in human mesenteric artery is primarily mediated by myoendothelial gap junctions intermediate conductance calcium-activated K+ channel and nitric oxide. *J Pharmacol Exp Ther* **336**(3)**:** 701-708.

Chandra S, Kable EP, Morrison GH, Webb WW (1991). Calcium sequestration in the Golgi apparatus of cultured mammalian cells revealed by laser scanning confocal microscopy and ion microscopy. *J Cell Sci* **100** (Pt 4): 747-752.

Chauhan SD, Nilsson H, Ahluwalia A, Hobbs AJ (2003). Release of C-type natriuretic peptide accounts for the biological activity of endothelium-derived hyperpolarizing factor. *Proc Natl Acad Sci U S A* **100**(3)**:** 1426-1431.

Chaytor AT, Bakker LM, Edwards DH, Griffith TM (2005). Connexin-mimetic peptides dissociate electrotonic EDHF-type signalling via myoendothelial and smooth muscle gap junctions in the rabbit iliac artery. *Br J Pharmacol* **144**(1)**:** 108-114.

Chaytor AT, Edwards DH, Bakker LM, Griffith TM (2003). Distinct hyperpolarizing and relaxant roles for gap junctions and endothelium-derived H2O2 in NO-independent relaxations of rabbit arteries. *Proc Natl Acad Sci U S A* **100**(25)**:** 15212-15217.

Chaytor AT, Evans WH, Griffith TM (1998). Central role of heterocellular gap junctional communication in endothelium-dependent relaxations of rabbit arteries. *J Physiol* **508 (Pt 2):** 561-573.

Chaytor AT, Marsh WL, Hutcheson IR, Griffith TM (2000). Comparison of glycyrrhetinic acid isoforms and carbenoxolone as inhibitors of EDHF-type relaxations mediated via gap junctions. *Endothelium* **7**(4)**:** 265-278.

Chaytor AT, Martin PE, Edwards DH, Griffith TM (2001). Gap junctional communication underpins EDHF-type relaxations evoked by ACh in the rat hepatic artery. *Am J Physiol Heart Circ Physiol* **280**(6)**:** H2441-2450.

Chaytor AT, Martin PE, Evans WH, Randall MD, Griffith TM (1999). The endothelial component of cannabinoid-induced relaxation in rabbit mesenteric artery depends on gap junctional communication. *J Physiol* **520** (Pt 2): 539-550.

Chen K, Kirber MT, Xiao H, Yang Y, Keaney JF, Jr. (2008). Regulation of ROS signal transduction by NADPH oxidase 4 localization. *J Cell Biol* **181**(7)**:** 1129-1139.

Chen Q, van Breemen C (1993). The superficial buffer barrier in venous smooth muscle: sarcoplasmic reticulum refilling and unloading. *Br J Pharmacol* **109**(2)**:** 336-343.

Chin LC, Achike FI, Mustafa MR (2007). Hydrogen peroxide modulates angiotensin II-induced contraction of mesenteric arteries from streptozotocin-induced diabetic rats. *Vascul Pharmacol* **46**(3)**:** 223-228.

Choi H, Kim S, Mukhopadhyay P, Cho S, Woo J, Storz G, Ryu SE (2001). Structural basis of the redox switch in the OxyR transcription factor. *Cell* **105**(1)**:** 103-113.

Cifuentes F, Gonzalez CE, Fiordelisio T, Guerrero G, Lai FA, Hernandez-Cruz A (2001). A ryanodine fluorescent derivative reveals the presence of high-affinity ryanodine binding sites in the Golgi complex of rat sympathetic neurons, with possible functional roles in intracellular Ca(2+) signaling. *Cell Signal* **13**(5)**:** 353-362.

Clapp LH, Turcato S, Hall S, Baloch M (1998). Evidence that Ca2+-activated K+ channels play a major role in mediating the vascular effects of iloprost and cicaprost. *Eur J Pharmacol* **356**(2-3)**:** 215-224.

Colden-Stanfield M, Schilling WP, Possani LD, Kunze DL (1990). Bradykinin-induced potassium current in cultured bovine aortic endothelial cells. *J Membr Biol* **116**(3)**:** 227-238.

Cooper T, Napolitano L, Fitzgerald M, Moore K, Daggett W, Willman V, Sonnenblick E, Hanlon C (1966). Structural basis of cardiac valvar function. *Archives of Surgery* **93**(5)**:** 767.

Corriu C, Feletou M, Canet E, Vanhoutte PM (1996). Endothelium-derived factors and hyperpolarization of the carotid artery of the guinea-pig. *Br J Pharmacol* **119**(5)**:** 959-964.

Corriu C, Feletou M, Edwards G, Weston AH, Vanhoutte PM (2001). Differential effects of prostacyclin and iloprost in the isolated carotid artery of the guinea-pig. *Eur J Pharmacol* **426**(1-2)**:** 89-94.

Cosentino F, Patton S, d'Uscio LV, Werner ER, Werner-Felmayer G, Moreau P, Malinski T, Luscher TF (1998). Tetrahydrobiopterin alters superoxide and nitric oxide release in prehypertensive rats. *J Clin Invest* **101**(7)**:** 1530-1537.

Crane GJ, Gallagher N, Dora KA, Garland CJ (2003). Small- and intermediate-conductance calcium-activated K+ channels provide different facets of endothelium-dependent hyperpolarization in rat mesenteric artery. *J Physiol* **553**(Pt 1)**:** 183-189.

Crow JP (1997). Dichlorodihydrofluorescein and dihydrorhodamine 123 are sensitive indicators of peroxynitrite in vitro: implications for intracellular measurement of reactive nitrogen and oxygen species. *Nitric Oxide* **1**(2)**:** 145-157.

Cseko C, Bagi Z, Koller A (2004). Biphasic effect of hydrogen peroxide on skeletal muscle arteriolar tone via activation of endothelial and smooth muscle signaling pathways. *J Appl Physiol* **97**(3)**:** 1130-1137.

Csordas G, Thomas AP, Hajnoczky G (1999). Quasi-synaptic calcium signal transmission between endoplasmic reticulum and mitochondria. *Embo J* **18**(1)**:** 96-108.

de la Bastie D, Levitsky D, Rappaport L, Mercadier JJ, Marotte F, Wisnewsky C, Brovkovich V, Schwartz K, Lompre AM (1990). Function of the sarcoplasmic reticulum and expression of its Ca2(+)-ATPase gene in pressure overload-induced cardiac hypertrophy in the rat. *Circ Res* **66**(2)**:** 554-564.

De Smedt H, Missiaen L, Parys JB, Bootman MD, Mertens L, Van Den Bosch L, Casteels R (1994). Determination of relative amounts of inositol trisphosphate receptor mRNA isoforms by ratio polymerase chain reaction. *J Biol Chem* **269**(34)**:** 21691-21698.

de Wit C, Griffith TM (2010). Connexins and gap junctions in the EDHF phenomenon and conducted vasomotor responses. *Pflugers Arch* **459**(6)**:** 897-914.

Dedkova EN, Blatter LA (2002). Nitric oxide inhibits capacitative Ca2+ entry and enhances endoplasmic reticulum Ca2+ uptake in bovine vascular endothelial cells. *J Physiol* **539**(Pt 1)**:** 77-91.

DeHaven WI, Smyth JT, Boyles RR, Putney JW, Jr. (2007). Calcium inhibition and calcium potentiation of Orai1, Orai2, and Orai3 calcium release-activated calcium channels. *J Biol Chem* **282**(24)**:** 17548-17556.

Dietrich A, Kalwa H, Gudermann T (2010). TRPC channels in vascular cell function. *Thromb Haemost* **103**(2)**:** 262-270.

Dikalov SI, Dikalova AE, Bikineyeva AT, Schmidt HH, Harrison DG, Griendling KK (2008). Distinct roles of Nox1 and Nox4 in basal and angiotensin II-stimulated superoxide and hydrogen peroxide production. *Free Radic Biol Med* **45**(9)**:** 1340-1351.

Dolman NJ, Gerasimenko JV, Gerasimenko OV, Voronina SG, Petersen OH, Tepikin AV (2005). Stable Golgi-mitochondria complexes and formation of Golgi Ca(2+) gradients in pancreatic acinar cells. *J Biol Chem* **280**(16)**:** 15794-15799.

Dora KA, Doyle MP, Duling BR (1997). Elevation of intracellular calcium in smooth muscle causes endothelial cell generation of NO in arterioles. *Proc Natl Acad Sci U S A* **94**(12)**:** 6529-6534.

Dora KA, Gallagher NT, McNeish A, Garland CJ (2008). Modulation of endothelial cell KCa3.1 channels during endothelium-derived hyperpolarizing factor signaling in mesenteric resistance arteries. *Circ Res* **102**(10)**:** 1247-1255.

Dora KA, Hinton JM, Walker SD, Garland CJ (2000). An indirect influence of phenylephrine on the release of endothelium-derived vasodilators in rat small mesenteric artery. *Br J Pharmacol* **129**(2)**:** 381-387.

Dora KA, Martin PE, Chaytor AT, Evans WH, Garland CJ, Griffith TM (1999). Role of heterocellular Gap junctional communication in endothelium-dependent smooth muscle hyperpolarization: inhibition by a connexin-mimetic peptide. *Biochem Biophys Res Commun* **254**(1)**:** 27-31.

Dora KA, Sandow SL, Gallagher NT, Takano H, Rummery NM, Hill CE, Garland CJ (2003). Myoendothelial gap junctions may provide the pathway for EDHF in mouse mesenteric artery. *J Vasc Res* **40**(5)**:** 480-490.

Doughty JM, Boyle JP, Langton PD (2000). Potassium does not mimic EDHF in rat mesenteric arteries. *Br J Pharmacol* **130**(5)**:** 1174-1182.

Doughty JM, Plane F, Langton PD (1999). Charybdotoxin and apamin block EDHF in rat mesenteric artery if selectively applied to the endothelium. *Am J Physiol* **276**(3 Pt 2)**:** H1107-1112.

Drummond GR, Cai H, Davis ME, Ramasamy S, Harrison DG (2000). Transcriptional and posttranscriptional regulation of endothelial nitric oxide synthase expression by hydrogen peroxide. *Circ Res* **86**(3)**:** 347-354.

Dumollard R, Marangos P, Fitzharris G, Swann K, Duchen M, Carroll J (2004). Sperm-triggered [Ca2+] oscillations and Ca2+ homeostasis in the mouse egg have an absolute requirement for mitochondrial ATP production. *Development* **131**(13)**:** 3057-3067.

Edgell CJ, Haizlip JE, Bagnell CR, Packenham JP, Harrison P, Wilbourn B, Madden VJ (1990). Endothelium specific Weibel-Palade bodies in a continuous human cell line, EA.hy926. *In vitro cellular & developmental biology : journal of the Tissue Culture Association* **26**(12)**:** 1167-1172.

Edgell CJ, McDonald CC, Graham JB (1983). Permanent cell line expressing human factor VIII-related antigen established by hybridization. *Proceedings of the National Academy of Sciences of the United States of America* **80**(12)**:** 3734-3737.

Edwards DH, Chaytor AT, Bakker LM, Griffith TM (2007). Modulation of gap-junction-dependent arterial relaxation by ascorbic acid. *J Vasc Res* **44**(5)**:** 410-422.

Edwards DH, Li Y, Griffith TM (2008). Hydrogen peroxide potentiates the EDHF phenomenon by promoting endothelial Ca2+ mobilization. *Arterioscler Thromb Vasc Biol* **28**(10)**:** 1774-1781.

Edwards G, Dora KA, Gardener MJ, Garland CJ, Weston AH (1998). K+ is an endothelium-derived hyperpolarizing factor in rat arteries. *Nature* **396**(6708)**:** 269-272.

Edwards G, Feletou M, Gardener MJ, Glen CD, Richards GR, Vanhoutte PM, Weston AH (2001). Further investigations into the endothelium-dependent hyperpolarizing effects of bradykinin and substance P in porcine coronary artery. *Br J Pharmacol* **133**(7)**:** 1145-1153.

Edwards G, Feletou M, Gardener MJ, Thollon C, Vanhoutte PM, Weston AH (1999). Role of gap junctions in the responses to EDHF in rat and guinea-pig small arteries. *Br J Pharmacol* **128**(8)**:** 1788-1794.

Edwards G, Thollon C, Gardener MJ, Feletou M, Vilaine J, Vanhoutte PM, Weston AH (2000). Role of gap junctions and EETs in endothelium-dependent hyperpolarization of porcine coronary artery. *Br J Pharmacol* **129**(6)**:** 1145-1154.

Egan K, FitzGerald GA (2006). Eicosanoids and the vascular endothelium. *Handb Exp Pharmacol*(176 Pt 1)**:** 189-211.

Ellinsworth DC Modulation of endothelium-dependent arterial relaxation by inorganic arsenic and glucoseThesis (PhD) - Cardiff University, 2010.

Erusalimsky JD, Moncada S (2007). Nitric oxide and mitochondrial signaling: from physiology to pathophysiology. *Arterioscler Thromb Vasc Biol* **27**(12)**:** 2524-2531.

Evrogen (2010). Hydrogen peroxide sensor HyPer. http://www.evrogen.com/products/HyPer/HyPer_Detailed_description.shtml

Falchetto R, Vorherr T, Carafoli E (1992). The calmodulin-binding site of the plasma membrane Ca2+ pump interacts with the transduction domain of the enzyme. *Protein Sci* **1**(12)**:** 1613-1621.

Fanger CM, Ghanshani S, Logsdon NJ, Rauer H, Kalman K, Zhou J, Beckingham K, Chandy KG, Cahalan MD, Aiyar J (1999). Calmodulin mediates calcium-dependent activation of the intermediate conductance KCa channel, IKCa1. *J Biol Chem* **274**(9)**:** 5746-5754.

Fasolato C, Nilius B (1998). Store depletion triggers the calcium release-activated calcium current (ICRAC) in macrovascular endothelial cells: a comparison with Jurkat and embryonic kidney cell lines. *Pflugers Arch* **436**(1)**:** 69-74.

Favero TG, Zable AC, Abramson JJ (1995). Hydrogen peroxide stimulates the Ca2+ release channel from skeletal muscle sarcoplasmic reticulum. *J Biol Chem* **270**(43)**:** 25557-25563.

Feletou M (2011a). *The Endothelium: Part 1: Multiple Functions of the Endothelial Cells-Focus on Endothelium-Derived Vasoactive Mediators*. edn. San Rafael (CA): Morgan & Claypool Life Sciences.

Feletou M (2011b). *The Endothelium: Part 2: EDHF-Mediated Responses-The Classical Pathway*. edn. San Rafael (CA): Morgan & Claypool Life Sciences.

Fernandes DC, Wosniak J, Jr., Pescatore LA, Bertoline MA, Liberman M, Laurindo FR, Santos CX (2007). Analysis of DHE-derived oxidation products by HPLC in the assessment of superoxide production and NADPH oxidase activity in vascular systems. *Am J Physiol Cell Physiol* **292**(1)**:** C413-422.

Fernandez-Rodriguez S, Edwards DH, Newton B, Griffith TM (2009). Attenuated store-operated Ca2+ entry underpins the dual inhibition of nitric oxide and EDHF-type relaxations by iodinated contrast media. *Cardiovasc Res* **84**(3)**:** 470-478.

Ficarella R, Di Leva F, Bortolozzi M, Ortolano S, Donaudy F, Petrillo M, Melchionda S, Lelli A, Domi T, Fedrizzi L, Lim D, Shull GE, Gasparini P, Brini M, Mammano F, Carafoli E (2007). A functional study of plasma-membrane calcium-pump isoform 2 mutants causing digenic deafness. *Proc Natl Acad Sci U S A* **104**(5)**:** 1516-1521.

Fierro L, Lund PE, Parekh AB (2000). Comparison of the activation of the Ca2+ release-activated Ca2+ current ICRAC to InsP3 in Jurkat T-lymphocytes, pulmonary artery endothelia and RBL-1 cells. *Pflugers Arch* **440**(4)**:** 580-587.

Fill M, Copello JA (2002). Ryanodine receptor calcium release channels. *Physiol Rev* **82**(4)**:** 893-922.

Fleming I, Fisslthaler B, Busse R (1996). Interdependence of calcium signaling and protein tyrosine phosphorylation in human endothelial cells. *J Biol Chem* **271**(18)**:** 11009-11015.

Forstermann U, Burgwitz K, Frolich JC (1986a). Thimerosal induces endothelium-dependent vascular smooth muscle relaxations by interacting with thiol groups. Relaxations are likely to be mediated by endothelium-derived relaxing factor (EDRF). *Naunyn Schmiedebergs Arch Pharmacol* **334**(4)**:** 501-507.

Forstermann U, Goppelt-Strube M, Frolich JC, Busse R (1986b). Inhibitors of acyl-coenzyme A:lysolecithin acyltransferase activate the production of endothelium-derived vascular relaxing factor. *J Pharmacol Exp Ther* **238**(1)**:** 352-359.

Forstermann U, Pollock JS, Schmidt HH, Heller M, Murad F (1991). Calmodulin-dependent endothelium-derived relaxing factor/nitric oxide synthase activity is present in the particulate and cytosolic fractions of bovine aortic endothelial cells. *Proc Natl Acad Sci U S A* **88**(5)**:** 1788-1792.

Foskett JK, White C, Cheung KH, Mak DO (2007). Inositol trisphosphate receptor Ca2+ release channels. *Physiol Rev* **87**(2)**:** 593-658.

Freeman K (2009). Nutrient protection against arsenic toxicity: folate, cysteine support methylation in children. *Environ Health Perspect* **117**(5)**:** A211.

Fujimoto S, Asano T, Sakai M, Sakurai K, Takagi D, Yoshimoto N, Itoh T (2001). Mechanisms of hydrogen peroxide-induced relaxation in rabbit mesenteric small artery. *Eur J Pharmacol* **412**(3)**:** 291-300.

Fujimoto S, Mori M, Tsushima H (2003). Mechanisms underlying the hydrogen peroxide-induced, endothelium-independent relaxation of the norepinephrine-contraction in guinea-pig aorta. *Eur J Pharmacol* **459**(1)**:** 65-73.

Fujino I, Yamada N, Miyawaki A, Hasegawa M, Furuichi T, Mikoshiba K (1995). Differential expression of type 2 and type 3 inositol 1,4,5-trisphosphate receptor mRNAs in various mouse tissues: in situ hybridization study. *Cell Tissue Res* **280**(2)**:** 201-210.

Fukao M, Hattori Y, Kanno M, Sakuma I, Kitabatake A (1997). Sources of Ca2+ in relation to generation of acetylcholine-induced endothelium-dependent hyperpolarization in rat mesenteric artery. *Br J Pharmacol* **120**(7)**:** 1328-1334.

Fulton D, McGiff JC, Wolin MS, Kaminski P, Quilley J (1997). Evidence against a cytochrome P450-derived reactive oxygen species as the mediator of the nitric oxide-independent vasodilator effect of bradykinin in the perfused heart of the rat. *J Pharmacol Exp Ther* **280**(2)**:** 702-709.

Furchgott RF, Zawadzki JV (1980). The obligatory role of endothelial cells in the relaxation of arterial smooth muscle by acetylcholine. *Nature* **288**(5789)**:** 373-376.

Furfine ES, Carbine K, Bunker S, Tanoury G, Harmon M, Laubach V, Sherman P (1997). Potent inhibition of human neuronal nitric oxide synthase by N(G)-nitro-L-arginine methyl ester results from contaminating N(G)-nitro-L-arginine. *Life Sci* **60**(20)**:** 1803-1809.

Furuichi T, Kohda K, Miyawaki A, Mikoshiba K (1994). Intracellular channels. *Curr Opin Neurobiol* **4**(3)**:** 294-303.

Furuichi T, Simon-Chazottes D, Fujino I, Yamada N, Hasegawa M, Miyawaki A, Yoshikawa S, Guenet JL, Mikoshiba K (1993). Widespread expression of inositol 1,4,5-trisphosphate receptor type 1 gene (Insp3r1) in the mouse central nervous system. *Receptors Channels* **1**(1)**:** 11-24.

Furuichi T, Yoshikawa S, Miyawaki A, Wada K, Maeda N, Mikoshiba K (1989). Primary structure and functional expression of the inositol 1,4,5-trisphosphate-binding protein P400. *Nature* **342**(6245)**:** 32-38.

Gao YJ, Hirota S, Zhang DW, Janssen LJ, Lee RM (2003). Mechanisms of hydrogen-peroxide-induced biphasic response in rat mesenteric artery. *Br J Pharmacol* **138**(6)**:** 1085-1092.

Gao YJ, Lee RM (2001). Hydrogen peroxide induces a greater contraction in mesenteric arteries of spontaneously hypertensive rats through thromboxane A(2) production. *Br J Pharmacol* **134**(8)**:** 1639-1646.

Garcia-Cardena G, Oh P, Liu J, Schnitzer JE, Sessa WC (1996). Targeting of nitric oxide synthase to endothelial cell caveolae via palmitoylation: implications for nitric oxide signaling. *Proc Natl Acad Sci U S A* **93**(13)**:** 6448-6453.

Garland JG, McPherson GA (1992). Evidence that nitric oxide does not mediate the hyperpolarization and relaxation to acetylcholine in the rat small mesenteric artery. *Br J Pharmacol* **105**(2)**:** 429-435.

Garry A, Edwards DH, Fallis IF, Jenkins RL, Griffith TM (2009). Ascorbic acid and tetrahydrobiopterin potentiate the EDHF phenomenon by generating hydrogen peroxide. *Cardiovasc Res* **84**(2)**:** 218-226.

Gerasimenko OV, Gerasimenko JV, Belan PV, Petersen OH (1996). Inositol trisphosphate and cyclic ADP-ribose-mediated release of Ca2+ from single isolated pancreatic zymogen granules. *Cell* **84**(3)**:** 473-480.

Gericke M, Droogmans G, Nilius B (1993). Thapsigargin discharges intracellular calcium stores and induces transmembrane currents in human endothelial cells. *Pflugers Arch* **422**(6)**:** 552-557.

Glitsch MD, Bakowski D, Parekh AB (2002). Store-operated Ca2+ entry depends on mitochondrial Ca2+ uptake. *Embo J* **21**(24)**:** 6744-6754.

Gluais P, Edwards G, Weston AH, Vanhoutte PM, Feletou M (2005). Hydrogen peroxide and endothelium-dependent hyperpolarization in the guinea-pig carotid artery. *Eur J Pharmacol* **513**(3)**:** 219-224.

Gomes da Costa A, Madeira VM (1986). Magnesium and manganese ions modulate Ca2+ uptake and its energetic coupling in sarcoplasmic reticulum. *Arch Biochem Biophys* **249**(1)**:** 199-206.

Greeb J, Shull GE (1989). Molecular cloning of a third isoform of the calmodulin-sensitive plasma membrane Ca2+-transporting ATPase that is expressed predominantly in brain and skeletal muscle. *J Biol Chem* **264**(31)**:** 18569-18576.

Greensmith DJ, Eisner DA, Nirmalan M (2010). The effects of hydrogen peroxide on intracellular calcium handling and contractility in the rat ventricular myocyte. *Cell Calcium* **48**(6)**:** 341-351.

Griffith TM (2004). Endothelium-dependent smooth muscle hyperpolarization: do gap junctions provide a unifying hypothesis? *Br J Pharmacol* **141**(6)**:** 881-903.

Griffith TM, Chaytor AT, Bakker LM, Edwards DH (2005). 5-Methyltetrahydrofolate and tetrahydrobiopterin can modulate electrotonically mediated endothelium-dependent vascular relaxation. *Proc Natl Acad Sci U S A* **102**(19)**:** 7008-7013.

Griffith TM, Chaytor AT, Edwards DH (2004). The obligatory link: role of gap junctional communication in endothelium-dependent smooth muscle hyperpolarization. *Pharmacol Res* **49**(6)**:** 551-564.

Griffith TM, Chaytor AT, Taylor HJ, Giddings BD, Edwards DH (2002). cAMP facilitates EDHF-type relaxations in conduit arteries by enhancing electrotonic conduction via gap junctions. *Proc Natl Acad Sci U S A* **99**(9)**:** 6392-6397.

Griffith TM, Edwards DH, Lewis MJ, Newby AC, Henderson AH (1984). The nature of endothelium-derived vascular relaxant factor. *Nature* **308**(5960)**:** 645-647.

Groschner K, Graier WF, Kukovetz WR (1994). Histamine induces K+, Ca2+, and Cl- currents in human vascular endothelial cells. Role of ionic currents in stimulation of nitric oxide biosynthesis. *Circ Res* **75**(2)**:** 304-314.

Grover AK, Samson SE (1997). Peroxide resistance of ER Ca2+ pump in endothelium: implications to coronary artery function. *Am J Physiol* **273**(4 Pt 1)**:** C1250-1258.

Grynkiewicz G, Poenie M, Tsien RY (1985). A new generation of Ca2+ indicators with greatly improved fluorescence properties. *J Biol Chem* **260**(6)**:** 3440-3450.

Gunteski-Hamblin AM, Greeb J, Shull GE (1988). A novel Ca2+ pump expressed in brain, kidney, and stomach is encoded by an alternative transcript of the slow-twitch muscle sarcoplasmic reticulum Ca-ATPase gene. Identification of cDNAs encoding Ca2+ and other cation-transporting ATPases using an oligonucleotide probe derived from the ATP-binding site. *J Biol Chem* **263**(29)**:** 15032-15040.

Haddock RE, Grayson TH, Brackenbury TD, Meaney KR, Neylon CB, Sandow SL, Hill CE (2006). Endothelial coordination of cerebral vasomotion via myoendothelial gap junctions containing connexins 37 and 40. *Am J Physiol Heart Circ Physiol* **291**(5)**:** H2047-2056.

Hajnoczky G, Hager R, Thomas AP (1999). Mitochondria suppress local feedback activation of inositol 1,4, 5-trisphosphate receptors by Ca2+. *J Biol Chem* **274**(20)**:** 14157-14162.

Hakamata Y, Nakai J, Takeshima H, Imoto K (1992). Primary structure and distribution of a novel ryanodine receptor/calcium release channel from rabbit brain. *FEBS Lett* **312**(2-3)**:** 229-235.

Hakim CH, Jackson WF, Segal SS (2008). Connexin isoform expression in smooth muscle cells and endothelial cells of hamster cheek pouch arterioles and retractor feed arteries. *Microcirculation* **15**(6)**:** 503-514.

Hall-Craggs ECB, Abeloff D (1995). *Anatomy as a basis for clinical medicine*. 3rd ed. edn. Williams & Wilkins: London.

Hall MN, Liu X, Slavkovich V, Ilievski V, Pilsner JR, Alam S, Factor-Litvak P, Graziano JH, Gamble MV (2009). Folate, Cobalamin, Cysteine, Homocysteine, and Arsenic Metabolism among Children in Bangladesh. *Environ Health Perspect* **117**(5)**:** 825-831.

Hallam TJ, Jacob R, Merritt JE (1988). Evidence that agonists stimulate bivalent-cation influx into human endothelial cells. *Biochem J* **255**(1)**:** 179-184.

Halliwell B (1993). The role of oxygen radicals in human disease, with particular reference to the vascular system. *Haemostasis* **23** (Suppl 1): 118-126.

Hamilton CA, McPhaden AR, Berg G, Pathi V, Dominiczak AF (2001). Is hydrogen peroxide an EDHF in human radial arteries? *Am J Physiol Heart Circ Physiol* **280**(6)**:** H2451-2455.

Hanson GT, Hanson BJ (2008). Fluorescent probes for cellular assays. *Comb Chem High Throughput Screen* **11**(7)**:** 505-513.

Hattori T, Kajikuri J, Katsuya H, Itoh T (2003). Effects of H2O2 on membrane potential of smooth muscle cells in rabbit mesenteric resistance artery. *Eur J Pharmacol* **464**(2-3)**:** 101-109.

Hayabuchi Y, Nakaya Y, Matsuoka S, Kuroda Y (1998). Hydrogen peroxide-induced vascular relaxation in porcine coronary arteries is mediated by Ca2+-activated K+ channels. *Heart Vessels* **13**(1)**:** 9-17.

He GW (1997). Hyperkalemia exposure impairs EDHF-mediated endothelial function in the human coronary artery. *Ann Thorac Surg* **63**(1)**:** 84-87.

Heinzel B, John M, Klatt P, Bohme E, Mayer B (1992). Ca2+/calmodulin-dependent formation of hydrogen peroxide by brain nitric oxide synthase. *Biochem J* **281 (Pt 3):** 627-630.

Heumuller S, Wind S, Barbosa-Sicard E, Schmidt HH, Busse R, Schroder K, Brandes RP (2008). Apocynin is not an inhibitor of vascular NADPH oxidases but an antioxidant. *Hypertension* **51**(2)**:** 211-217.

Hewavitharana T, Deng X, Soboloff J, Gill DL (2007). Role of STIM and Orai proteins in the store-operated calcium signaling pathway. *Cell Calcium* **42**(2)**:** 173-182.

Hilgers RH, Todd J, Jr., Webb RC (2006). Regional heterogeneity in acetylcholine-induced relaxation in rat vascular bed: role of calcium-activated K+ channels. *Am J Physiol Heart Circ Physiol* **291**(1)**:** H216-222.

Himmel HM, Whorton AR, Strauss HC (1993). Intracellular calcium, currents, and stimulus-response coupling in endothelial cells. *Hypertension* **21**(1)**:** 112-127.

Hirai T, Tsuru H, Tanimitsu N, Takumida M, Watanabe H, Yajin K, Sasa M (2000). Effect of hydrogen peroxide on guinea pig nasal mucosa vasculature. *Jpn J Pharmacol* **84**(4)**:** 470-473.

Hohn J, Pataricza J, Toth GK, Balogh A, Papp JG (1996). Nitric oxide activates an iberiotoxin-sensitive potassium channel in human saphenous vein. *Acta Physiol Hung* **84**(3)**:** 293-294.

Hong JH, Moon SJ, Byun HM, Kim MS, Jo H, Bae YS, Lee SI, Bootman MD, Roderick HL, Shin DM, Seo JT (2006). Critical role of phospholipase Cgamma1 in the generation of H2O2-evoked [Ca2+]i oscillations in cultured rat cortical astrocytes. *J Biol Chem* **281**(19)**:** 13057-13067.

Hong T, Hill CE (1998). Restricted expression of the gap junctional protein connexin 43 in the arterial system of the rat. *J Anat* **192** (Pt 4): 583-593.

Hoth M, Penner R (1992). Depletion of intracellular calcium stores activates a calcium current in mast cells. *Nature* **355**(6358)**:** 353-356.

Hu Q, Corda S, Zweier JL, Capogrossi MC, Ziegelstein RC (1998). Hydrogen peroxide induces intracellular calcium oscillations in human aortic endothelial cells. *Circulation* **97**(3)**:** 268-275.

Hu Q, Zheng G, Zweier JL, Deshpande S, Irani K, Ziegelstein RC (2000). NADPH oxidase activation increases the sensitivity of intracellular Ca2+ stores to inositol 1,4,5-trisphosphate in human endothelial cells. *J Biol Chem* **275**(21)**:** 15749-15757.

Huang A, Sun D, Carroll MA, Jiang H, Smith CJ, Connetta JA, Falck JR, Shesely EG, Koller A, Kaley G (2001). EDHF mediates flow-induced dilation in skeletal muscle

arterioles of female eNOS-KO mice. *Am J Physiol Heart Circ Physiol* **280**(6)**:** H2462-2469.

Huang PL, Huang Z, Mashimo H, Bloch KD, Moskowitz MA, Bevan JA, Fishman MC (1995). Hypertension in mice lacking the gene for endothelial nitric oxide synthase. *Nature* **377**(6546)**:** 239-242.

Hutcheson IR, Chaytor AT, Evans WH, Griffith TM (1999). Nitric oxide-independent relaxations to acetylcholine and A23187 involve different routes of heterocellular communication. Role of Gap junctions and phospholipase A2. *Circ Res* **84**(1)**:** 53-63.

Ignarro LJ, Buga GM, Wood KS, Byrns RE, Chaudhuri G (1987). Endothelium-derived relaxing factor produced and released from artery and vein is nitric oxide. *Proc Natl Acad Sci U S A* **84**(24)**:** 9265-9269.

Ignarro LJ, Burke TM, Wood KS, Wolin MS, Kadowitz PJ (1984). Association between cyclic GMP accumulation and acetylcholine-elicited relaxation of bovine intrapulmonary artery. *J Pharmacol Exp Ther* **228**(3)**:** 682-690.

Iida Y, Katusic ZS (2000). Mechanisms of cerebral arterial relaxations to hydrogen peroxide. *Stroke* **31**(9)**:** 2224-2230.

Irvine RF (1982). How is the level of free arachidonic acid controlled in mammalian cells? *Biochem J* **204**(1)**:** 3-16.

Itoh T, Kajikuri J, Hattori T, Kusama N, Yamamoto T (2003). Involvement of H2O2 in superoxide-dismutase-induced enhancement of endothelium-dependent relaxation in rabbit mesenteric resistance artery. *Br J Pharmacol* **139**(2)**:** 444-456.

Jaimes EA, Sweeney C, Raij L (2001). Effects of the reactive oxygen species hydrogen peroxide and hypochlorite on endothelial nitric oxide production. *Hypertension* **38**(4)**:** 877-883.

Jakubowski W, Bartosz G (2000). 2,7-dichlorofluorescin oxidation and reactive oxygen species: what does it measure? *Cell Biol Int* **24**(10)**:** 757-760.

Jardin I, Lopez JJ, Redondo PC, Salido GM, Rosado JA (2009). Store-operated Ca2+ entry is sensitive to the extracellular Ca2+ concentration through plasma membrane STIM1. *Biochim Biophys Acta* **1793**(10)**:** 1614-1622.

Jin N, Rhoades RA (1997). Activation of tyrosine kinases in H2O2-induced contraction in pulmonary artery. *Am J Physiol* **272**(6 Pt 2)**:** H2686-2692.

Jing Y, Dai J, Chalmers-Redman RM, Tatton WG, Waxman S (1999). Arsenic trioxide selectively induces acute promyelocytic leukemia cell apoptosis via a hydrogen peroxide-dependent pathway. *Blood* **94**(6)**:** 2102-2111.

Johnson I, Spence MTZ (2010). *Molecular Probes Handbook, A Guide to Fluorescent Probes and Labeling Technologies, 11th Edition*. 11 edn. Invitrogen.

Jouaville LS, Ichas F, Holmuhamedov EL, Camacho P, Lechleiter JD (1995). Synchronization of calcium waves by mitochondrial substrates in Xenopus laevis oocytes. *Nature* **377**(6548)**:** 438-441.

Kagota S, Yamaguchi Y, Nakamura K, Kunitomo M (1999). Characterization of nitric oxide- and prostaglandin-independent relaxation in response to acetylcholine in rabbit renal artery. *Clin Exp Pharmacol Physiol* **26**(10)**:** 790-796.

Kamagate A, Herchuelz A, Bollen A, Van Eylen F (2000). Expression of multiple plasma membrane Ca(2+)-ATPases in rat pancreatic islet cells. *Cell Calcium* **27**(4)**:** 231-246.

Karasu C (2000). Time course of changes in endothelium-dependent and -independent relaxation of chronically diabetic aorta: role of reactive oxygen species. *Eur J Pharmacol* **392**(3)**:** 163-173.

Katusic ZS (2002). Back to the salt mines-- endothelial dysfunction in hypertension and compensatory role of endothelium-derived hyperpolarizing factor (EDHF). *J Physiol* **543**(Pt 1)**:** 1.

Katusic ZS, Schugel J, Cosentino F, Vanhoutte PM (1993). Endothelium-dependent contractions to oxygen-derived free radicals in the canine basilar artery. *Am J Physiol* **264**(3 Pt 2)**:** H859-864.

Katz SD, Krum H (2001). Acetylcholine-mediated vasodilation in the forearm circulation of patients with heart failure: indirect evidence for the role of endothelium-derived hyperpolarizing factor. *Am J Cardiol* **87**(9)**:** 1089-1092.

Kerkar S, Speyer C, Tyburski J, Steffes C (2001). Reactive oxygen metabolites induce a biphasic contractile response in microvascular lung pericytes. *J Trauma* **51**(3)**:** 440-445.

Kimlicka L, Van Petegem F (2011). The structural biology of ryanodine receptors. *Sci China Life Sci* **54**(8)**:** 712-724.

Kinnula VL, Everitt JI, Whorton AR, Crapo JD (1991). Hydrogen peroxide production by alveolar type II cells, alveolar macrophages, and endothelial cells. *Am J Physiol* **261**(2 Pt 1)**:** L84-91.

Knowles RG, Palacios M, Palmer RM, Moncada S (1989). Formation of nitric oxide from L-arginine in the central nervous system: a transduction mechanism for stimulation of the soluble guanylate cyclase. *Proc Natl Acad Sci U S A* **86**(13)**:** 5159-5162.

Kobayashi T, Tahara Y, Matsumoto M, Iguchi M, Sano H, Murayama T, Arai H, Oida H, Yurugi-Kobayashi T, Yamashita JK, Katagiri H, Majima M, Yokode M, Kita T, Narumiya S (2004). Roles of thromboxane A(2) and prostacyclin in the development of atherosclerosis in apoE-deficient mice. *J Clin Invest* **114**(6)**:** 784-794.

Kohler R, Degenhardt C, Kuhn M, Runkel N, Paul M, Hoyer J (2000). Expression and function of endothelial Ca(2+)-activated K(+) channels in human mesenteric artery: A single-cell reverse transcriptase-polymerase chain reaction and electrophysiological study in situ. *Circ Res* **87**(6)**:** 496-503.

Kojima H, Nakatsubo N, Kikuchi K, Kawahara S, Kirino Y, Nagoshi H, Hirata Y, Nagano T (1998a). Detection and imaging of nitric oxide with novel fluorescent indicators: diaminofluoresceins. *Anal Chem* **70**(13)**:** 2446-2453.

Kojima H, Nakatsubo N, Kikuchi K, Urano Y, Higuchi T, Tanaka J, Kudo Y, Nagano T (1998b). Direct evidence of NO production in rat hippocampus and cortex using a new fluorescent indicator: DAF-2 DA. *Neuroreport* **9**(15)**:** 3345-3348.

Kojima H, Sakurai K, Kikuchi K, Kawahara S, Kirino Y, Nagoshi H, Hirata Y, Nagano T (1998c). Development of a fluorescent indicator for nitric oxide based on the fluorescein chromophore. *Chem Pharm Bull (Tokyo)* **46**(2)**:** 373-375.

Kojima H, Urano Y, Kikuchi K, Higuchi T, Hirata Y, Nagano T (1999). Fluorescent Indicators for Imaging Nitric Oxide Production. *Angew Chem Int Ed Engl* **38**(21)**:** 3209-3212.

Kong ID, Koh SD, Bayguinov O, Sanders KM (2000). Small conductance Ca2+-activated K+ channels are regulated by Ca2+-calmodulin-dependent protein kinase II in murine colonic myocytes. *J Physiol* **524** (Pt 2): 331-337.

Kruger O, Plum A, Kim JS, Winterhager E, Maxeiner S, Hallas G, Kirchhoff S, Traub O, Lamers WH, Willecke K (2000). Defective vascular development in connexin 45-deficient mice. *Development* **127**(19)**:** 4179-4193.

Ku DD, Nelson JM, Caulfield JB, Winn MJ (1990). Release of endothelium-derived relaxing factors from canine cardiac valves. *J Cardiovasc Pharmacol* **16**(2)**:** 212-218.

Kuster GM, Lancel S, Zhang J, Communal C, Trucillo MP, Lim CC, Pfister O, Weinberg EO, Cohen RA, Liao R, Siwik DA, Colucci WS (2010). Redox-mediated reciprocal regulation of SERCA and Na+-Ca2+ exchanger contributes to sarcoplasmic reticulum Ca2+ depletion in cardiac myocytes. *Free Radic Biol Med* **48**(9)**:** 1182-1187.

Kwan HY, Huang Y, Yao X (2000). Store-operated calcium entry in vascular endothelial cells is inhibited by cGMP via a protein kinase G-dependent mechanism. *J Biol Chem* **275**(10)**:** 6758-6763.

Lacza Z, Puskar M, Kis B, Perciaccante JV, Miller AW, Busija DW (2002). Hydrogen peroxide acts as an EDHF in the piglet pial vasculature in response to bradykinin. *Am J Physiol Heart Circ Physiol* **283**(1)**:** H406-411.

Lai FA, Dent M, Wickenden C, Xu L, Kumari G, Misra M, Lee HB, Sar M, Meissner G (1992). Expression of a cardiac Ca(2+)-release channel isoform in mammalian brain. *Biochem J* **288** (Pt 2): 553-564.

Landmesser U, Dikalov S, Price SR, McCann L, Fukai T, Holland SM, Mitch WE, Harrison DG (2003). Oxidation of tetrahydrobiopterin leads to uncoupling of endothelial cell nitric oxide synthase in hypertension. *J Clin Invest* **111**(8)**:** 1201-1209.

Lang NN, Luksha L, Newby DE, Kublickiene K (2007). Connexin 43 mediates endothelium-derived hyperpolarizing factor-induced vasodilatation in subcutaneous resistance arteries from healthy pregnant women. *Am J Physiol Heart Circ Physiol* **292**(2)**:** H1026-1032.

Lanner JT, Georgiou DK, Joshi AD, Hamilton SL (2010). Ryanodine receptors: structure, expression, molecular details, and function in calcium release. *Cold Spring Harb Perspect Biol* **2**(11)**:** a003996.

Larsen BT, Bubolz AH, Mendoza SA, Pritchard KA, Jr., Gutterman DD (2009). Bradykinin-induced dilation of human coronary arterioles requires NADPH oxidase-derived reactive oxygen species. *Arterioscler Thromb Vasc Biol* **29**(5)**:** 739-745.

Larsen BT, Gutterman DD, Sato A, Toyama K, Campbell WB, Zeldin DC, Manthati VL, Falck JR, Miura H (2008). Hydrogen peroxide inhibits cytochrome p450 epoxygenases: interaction between two endothelium-derived hyperpolarizing factors. *Circ Res* **102**(1)**:** 59-67.

Lassegue B, Griendling KK (2010). NADPH oxidases: functions and pathologies in the vasculature. *Arterioscler Thromb Vasc Biol* **30**(4)**:** 653-661.

Lassegue B, Sorescu D, Szocs K, Yin Q, Akers M, Zhang Y, Grant SL, Lambeth JD, Griendling KK (2001). Novel gp91(phox) homologues in vascular smooth muscle cells : nox1 mediates angiotensin II-induced superoxide formation and redox-sensitive signaling pathways. *Circ Res* **88**(9)**:** 888-894.

Laude AJ, Simpson AW (2009). Compartmentalized signalling: Ca2+ compartments, microdomains and the many facets of Ca2+ signalling. *Febs J* **276**(7)**:** 1800-1816.

Ledoux J, Taylor MS, Bonev AD, Hannah RM, Solodushko V, Shui B, Tallini Y, Kotlikoff MI, Nelson MT (2008). Functional architecture of inositol 1,4,5-trisphosphate signaling in restricted spaces of myoendothelial projections. *Proc Natl Acad Sci U S A* **105**(28)**:** 9627-9632.

Lee MY, Jung BI, Chung SM, Bae ON, Lee JY, Park JD, Yang JS, Lee H, Chung JH (2003). Arsenic-induced dysfunction in relaxation of blood vessels. *Environ Health Perspect* **111**(4)**:** 513-517.

Leffler CW, Busija DW, Armstead WM, Mirro R (1990). H2O2 effects on cerebral prostanoids and pial arteriolar diameter in piglets. *Am J Physiol* **258**(5 Pt 2)**:** H1382-1387.

Lesh RE, Marks AR, Somlyo AV, Fleischer S, Somlyo AP (1993). Anti-ryanodine receptor antibody binding sites in vascular and endocardial endothelium. *Circ Res* **72**(2)**:** 481-488.

Leung PC, Cheng KT, Liu C, Cheung WT, Kwan HY, Lau KL, Huang Y, Yao X (2006). Mechanism of non-capacitative Ca2+ influx in response to bradykinin in vascular endothelial cells. *J Vasc Res* **43**(4): 367-376.

Levick JR (2010). *An introduction to cardiovascular physiology*. 5th ed. edn. Hodder Arnold: London.

Li F, Sugishita K, Su Z, Ueda I, Barry WH (2001). Activation of connexin-43 hemichannels can elevate [Ca(2+)]i and [Na(+)]i in rabbit ventricular myocytes during metabolic inhibition. *J Mol Cell Cardiol* **33**(12)**:** 2145-2155.

Li JM, Shah AM (2002). Intracellular localization and preassembly of the NADPH oxidase complex in cultured endothelial cells. *J Biol Chem* **277**(22)**:** 19952-19960.

Li L, van Breemen C (1996). Agonist- and CPA-induced elevation of cytoplasmic free Ca2+ in intact valvular endothelium from rabbits. *Am J Physiol* **270**(3 Pt 2)**:** H837-848.

Li M, Fukagawa NK (2010). Age-related changes in redox signaling and VSMC function. *Antioxid Redox Signal* **12**(5)**:** 641-655.

Liang W, Buluc M, van Breemen C, Wang X (2004). Vectorial Ca2+ release via ryanodine receptors contributes to Ca2+ extrusion from freshly isolated rabbit aortic endothelial cells. *Cell Calcium* **36**(5)**:** 431-443.

Lin MJ, Yang XR, Cao YN, Sham JS (2007). Hydrogen peroxide-induced Ca2+ mobilization in pulmonary arterial smooth muscle cells. *Am J Physiol Lung Cell Mol Physiol* **292**(6)**:** L1598-1608.

Liou J, Kim ML, Heo WD, Jones JT, Myers JW, Ferrell JE, Jr., Meyer T (2005). STIM is a Ca2+ sensor essential for Ca2+-store-depletion-triggered Ca2+ influx. *Curr Biol* **15**(13)**:** 1235-1241.

Liu BF, Xu X, Fridman R, Muallem S, Kuo TH (1996). Consequences of functional expression of the plasma membrane Ca2+ pump isoform 1a. *J Biol Chem* **271**(10)**:** 5536-5544.

Liu C, Ngai CY, Huang Y, Ko WH, Wu M, He GW, Garland CJ, Dora KA, Yao X (2006). Depletion of intracellular Ca2+ stores enhances flow-induced vascular dilatation in rat small mesenteric artery. *Br J Pharmacol* **147**(5)**:** 506-515.

Liu LH, Paul RJ, Sutliff RL, Miller ML, Lorenz JN, Pun RY, Duffy JJ, Doetschman T, Kimura Y, MacLennan DH, Hoying JB, Shull GE (1997). Defective endothelium-dependent relaxation of vascular smooth muscle and endothelial cell Ca2+ signaling in mice lacking sarco(endo)plasmic reticulum Ca2+-ATPase isoform 3. *J Biol Chem* **272**(48)**:** 30538-30545.

Liu Y, Bubolz AH, Mendoza S, Zhang DX, Gutterman DD (2011). H2O2 is the transferrable factor mediating flow-induced dilation in human coronary arterioles. *Circ Res* **108**(5)**:** 566-573.

Lock JT, Sinkins WG, Schilling WP (2012). Protein S-Glutathionylation enhances Ca2+-induced Ca2+ release via the IP3 Receptor in Cultured Aortic Endothelial Cells. *J Physiol*.

Lockwich TP, Liu X, Singh BB, Jadlowiec J, Weiland S, Ambudkar IS (2000). Assembly of Trp1 in a signaling complex associated with caveolin-scaffolding lipid raft domains. *J Biol Chem* **275**(16)**:** 11934-11942.

Looft-Wilson RC, Payne GW, Segal SS (2004). Connexin expression and conducted vasodilation along arteriolar endothelium in mouse skeletal muscle. *J Appl Physiol* **97**(3)**:** 1152-1158.

Loot AE, Schreiber JG, Fisslthaler B, Fleming I (2009). Angiotensin II impairs endothelial function via tyrosine phosphorylation of the endothelial nitric oxide synthase. *J Exp Med* **206**(13)**:** 2889-2896.

Luckhoff A, Busse R (1990). Calcium influx into endothelial cells and formation of endothelium-derived relaxing factor is controlled by the membrane potential. *Pflugers Arch* **416**(3)**:** 305-311.

Lytton J, MacLennan DH (1988). Molecular cloning of cDNAs from human kidney coding for two alternatively spliced products of the cardiac Ca2+-ATPase gene. *J Biol Chem* **263**(29)**:** 15024-15031.

MacLennan DH, Brandl CJ, Korczak B, Green NM (1985). Amino-acid sequence of a Ca2+ + Mg2+-dependent ATPase from rabbit muscle sarcoplasmic reticulum, deduced from its complementary DNA sequence. *Nature* **316**(6030)**:** 696-700.

Malli R, Frieden M, Osibow K, Zoratti C, Mayer M, Demaurex N, Graier WF (2003). Sustained Ca2+ transfer across mitochondria is Essential for mitochondrial Ca2+ buffering, sore-operated Ca2+ entry, and Ca2+ store refilling. *J Biol Chem* **278**(45)**:** 44769-44779.

Malli R, Frieden M, Trenker M, Graier WF (2005). The role of mitochondria for Ca2+ refilling of the endoplasmic reticulum. *J Biol Chem* **280**(13)**:** 12114-12122.

Marchenko SM, Sage SO (1996). Calcium-activated potassium channels in the endothelium of intact rat aorta. *J Physiol* **492** (Pt 1): 53-60.

Marrelli SP (2002). Altered endothelial Ca2+ regulation after ischemia/reperfusion produces potentiated endothelium-derived hyperpolarizing factor-mediated dilations. *Stroke* **33**(9)**:** 2285-2291.

Martin PE, Wall C, Griffith TM (2005). Effects of connexin-mimetic peptides on gap junction functionality and connexin expression in cultured vascular cells. *Br J Pharmacol* **144**(5)**:** 617-627.

Martin W, Villani GM, Jothianandan D, Furchgott RF (1985). Selective blockade of endothelium-dependent and glyceryl trinitrate-induced relaxation by hemoglobin and by methylene blue in the rabbit aorta. *J Pharmacol Exp Ther* **232**(3)**:** 708-716.

Matchkov VV, Rahman A, Bakker LM, Griffith TM, Nilsson H, Aalkjaer C (2006). Analysis of effects of connexin-mimetic peptides in rat mesenteric small arteries. *Am J Physiol Heart Circ Physiol* **291**(1)**:** H357-367.

Mathias RS, Zhang SJ, Wilson E, Gardner P, Ives HE (1997). Non-capacitative calcium entry in Chinese hamster ovary cells expressing the platelet-derived growth factor receptor. *J Biol Chem* **272**(46)**:** 29076-29082.

Matoba T, Shimokawa H (2003). Hydrogen peroxide is an endothelium-derived hyperpolarizing factor in animals and humans. *J Pharmacol Sci* **92**(1)**:** 1-6.

Matoba T, Shimokawa H, Kubota H, Morikawa K, Fujiki T, Kunihiro I, Mukai Y, Hirakawa Y, Takeshita A (2002). Hydrogen peroxide is an endothelium-derived hyperpolarizing factor in human mesenteric arteries. *Biochem Biophys Res Commun* **290**(3)**:** 909-913.

Matoba T, Shimokawa H, Morikawa K, Kubota H, Kunihiro I, Urakami-Harasawa L, Mukai Y, Hirakawa Y, Akaike T, Takeshita A (2003). Electron spin resonance detection of hydrogen peroxide as an endothelium-derived hyperpolarizing factor in porcine coronary microvessels. *Arterioscler Thromb Vasc Biol* **23**(7)**:** 1224-1230.

Matoba T, Shimokawa H, Nakashima M, Hirakawa Y, Mukai Y, Hirano K, Kanaide H, Takeshita A (2000). Hydrogen peroxide is an endothelium-derived hyperpolarizing factor in mice. *J Clin Invest* **106**(12)**:** 1521-1530.

Maxwell AJ (2002). Mechanisms of dysfunction of the nitric oxide pathway in vascular diseases. *Nitric Oxide* **6**(2)**:** 101-124.

McCulloch AI, Bottrill FE, Randall MD, Hiley CR (1997). Characterization and modulation of EDHF-mediated relaxations in the rat isolated superior mesenteric arterial bed. *Br J Pharmacol* **120**(8)**:** 1431-1438.

Meera P, Wallner M, Song M, Toro L (1997). Large conductance voltage- and calcium-dependent K+ channel, a distinct member of voltage-dependent ion channels with seven N-terminal transmembrane segments (S0-S6), an extracellular N terminus, and an intracellular (S9-S10) C terminus. *Proc Natl Acad Sci U S A* **94**(25)**:** 14066-14071.

Meldolesi J (2004). The development of Ca2+ indicators: a breakthrough in pharmacological research. *Trends Pharmacol Sci* **25**(4)**:** 172-174.

Mendis S, Puska P, Norrving B (2011). *Global atlas on cardiovascular disease prevention and control*. edn. World Health Organization in collaboration with the World Heart Federation and the World Stroke Organization: Geneva.

Merritt JE, Jacob R, Hallam TJ (1989). Use of manganese to discriminate between calcium influx and mobilization from internal stores in stimulated human neutrophils. *J Biol Chem* **264**(3)**:** 1522-1527.

Mian KB, Martin W (1995). The inhibitory effect of 3-amino-1,2,4-triazole on relaxation induced by hydroxylamine and sodium azide but not hydrogen peroxide or glyceryl trinitrate in rat aorta. *Br J Pharmacol* **116**(8)**:** 3302-3308.

Mignery GA, Sudhof TC, Takei K, De Camilli P (1989). Putative receptor for inositol 1,4,5-trisphosphate similar to ryanodine receptor. *Nature* **342**(6246)**:** 192-195.

Miller EW, Tulyathan O, Isacoff EY, Chang CJ (2007). Molecular imaging of hydrogen peroxide produced for cell signaling. *Nat Chem Biol* **3**(5)**:** 263-267.

Minta A, Kao JP, Tsien RY (1989). Fluorescent indicators for cytosolic calcium based on rhodamine and fluorescein chromophores. *J Biol Chem* **264**(14)**:** 8171-8178.

Missiaen L, Declerck I, Droogmans G, Plessers L, De Smedt H, Raeymaekers L, Casteels R (1990). Agonist-dependent Ca2+ and Mn2+ entry dependent on state of filling of Ca2+ stores in aortic smooth muscle cells of the rat. *J Physiol* **427:** 171-186.

Missiaen L, Van Acker K, Van Baelen K, Raeymaekers L, Wuytack F, Parys JB, De Smedt H, Vanoevelen J, Dode L, Rizzuto R, Callewaert G (2004). Calcium release from the Golgi apparatus and the endoplasmic reticulum in HeLa cells stably expressing targeted aequorin to these compartments. *Cell Calcium* **36**(6)**:** 479-487.

Miura H, Bosnjak JJ, Ning G, Saito T, Miura M, Gutterman DD (2003). Role for hydrogen peroxide in flow-induced dilation of human coronary arterioles. *Circ Res* **92**(2)**:** e31-40.

Mohanty JG, Jaffe JS, Schulman ES, Raible DG (1997). A highly sensitive fluorescent micro-assay of H2O2 release from activated human leukocytes using a dihydroxyphenoxazine derivative. *J Immunol Methods* **202**(2)**:** 133-141.

Moncada S, Gryglewski R, Bunting S, Vane JR (1976). An enzyme isolated from arteries transforms prostaglandin endoperoxides to an unstable substance that inhibits platelet aggregation. *Nature* **263**(5579)**:** 663-665.

Moncada S, Herman AG, Higgs EA, Vane JR (1977). Differential formation of prostacyclin (PGX or PGI2) by layers of the arterial wall. An explanation for the anti-thrombotic properties of vascular endothelium. *Thromb Res* **11**(3)**:** 323-344.

Moneer Z, Dyer JL, Taylor CW (2003). Nitric oxide co-ordinates the activities of the capacitative and non-capacitative Ca2+-entry pathways regulated by vasopressin. *Biochem J* **370**(Pt 2)**:** 439-448.

Montero M, Alonso MT, Albillos A, Cuchillo-Ibanez I, Olivares R, Villalobos C, Alvarez J (2002). Effect of inositol 1,4,5-trisphosphate receptor stimulation on mitochondrial [Ca2+] and secretion in chromaffin cells. *Biochem J* **365**(Pt 2)**:** 451-459.

Montezano AC, Burger D, Ceravolo GS, Yusuf H, Montero M, Touyz RM (2011). Novel Nox homologues in the vasculature: focusing on Nox4 and Nox5. *Clin Sci (Lond)* **120**(4)**:** 131-141.

Moreau VH, Castilho RF, Ferreira ST, Carvalho-Alves PC (1998). Oxidative damage to sarcoplasmic reticulum Ca2+-ATPase AT submicromolar iron concentrations: evidence for metal-catalyzed oxidation. *Free Radic Biol Med* **25**(4-5)**:** 554-560.

Morgado M, Cairrao E, Santos-Silva AJ, Verde I (2012). Cyclic nucleotide-dependent relaxation pathways in vascular smooth muscle. *Cell Mol Life Sci* **69**(2)**:** 247-266.

Mottola A, Antoniotti S, Lovisolo D, Munaron L (2005). Regulation of noncapacitative calcium entry by arachidonic acid and nitric oxide in endothelial cells. *Faseb J* **19**(14)**:** 2075-2077.

Mulvany MJ, Halpern W (1976). Mechanical properties of vascular smooth muscle cells in situ. *Nature* **260**(5552)**:** 617-619.

Munzel T, Afanas'ev IB, Kleschyov AL, Harrison DG (2002). Detection of superoxide in vascular tissue. *Arterioscler Thromb Vasc Biol* **22**(11)**:** 1761-1768.

Murai T, Muraki K, Imaizumi Y, Watanabe M (1999). Levcromakalim causes indirect endothelial hyperpolarization via a myo-endothelial pathway. *Br J Pharmacol* **128**(7)**:** 1491-1496.

Murphy ME, Brayden JE (1995a). Apamin-sensitive K+ channels mediate an endothelium-dependent hyperpolarization in rabbit mesenteric arteries. *J Physiol* **489** (Pt 3): 723-734.

Murphy ME, Brayden JE (1995b). Nitric oxide hyperpolarizes rabbit mesenteric arteries via ATP-sensitive potassium channels. *J Physiol* **486 (Pt 1):** 47-58.

Nakai J, Imagawa T, Hakamat Y, Shigekawa M, Takeshima H, Numa S (1990). Primary structure and functional expression from cDNA of the cardiac ryanodine receptor/calcium release channel. *FEBS Lett* **271**(1-2)**:** 169-177.

Nakanishi S, Kuwajima G, Mikoshiba K (1992). Immunohistochemical localization of ryanodine receptors in mouse central nervous system. *Neurosci Res* **15**(1-2)**:** 130-142.

Nakayama T, Soma M, Watanabe Y, Hasimu B, Sato M, Aoi N, Kosuge K, Kanmatsuse K, Kokubun S, Marrow JD, Oates JA (2002). Splicing mutation of the prostacyclin synthase gene in a family associated with hypertension. *Biochem Biophys Res Commun* **297**(5)**:** 1135-1139.

Neylon CB, Richards SM, Larsen MA, Agrotis A, Bobik A (1995). Multiple types of ryanodine receptor/Ca2+ release channels are expressed in vascular smooth muscle. *Biochem Biophys Res Commun* **215**(3)**:** 814-821.

Ng KF, Leung SW, Man RY, Vanhoutte PM (2008). Endothelium-derived hyperpolarizing factor mediated relaxations in pig coronary arteries do not involve Gi/o proteins. *Acta Pharmacol Sin* **29**(12)**:** 1419-1424.

Orio P, Rojas P, Ferreira G, Latorre R (2002). New disguises for an old channel: MaxiK channel beta-subunits. *News Physiol Sci* **17:** 156-161.

Otsu K, Willard HF, Khanna VK, Zorzato F, Green NM, MacLennan DH (1990). Molecular cloning of cDNA encoding the Ca2+ release channel (ryanodine receptor) of rabbit cardiac muscle sarcoplasmic reticulum. *J Biol Chem* **265**(23)**:** 13472-13483.

Pagano PJ, Clark JK, Cifuentes-Pagano ME, Clark SM, Callis GM, Quinn MT (1997). Localization of a constitutively active, phagocyte-like NADPH oxidase in rabbit aortic adventitia: enhancement by angiotensin II. *Proc Natl Acad Sci U S A* **94**(26)**:** 14483-14488.

Palmer RM, Ashton DS, Moncada S (1988). Vascular endothelial cells synthesize nitric oxide from L-arginine. *Nature* **333**(6174)**:** 664-666.

Palmer RM, Ferrige AG, Moncada S (1987). Nitric oxide release accounts for the biological activity of endothelium-derived relaxing factor. *Nature* **327**(6122)**:** 524-526.

Paltauf-Doburzynska J, Posch K, Paltauf G, Graier WF (1998). Stealth ryanodine-sensitive Ca2+ release contributes to activity of capacitative Ca2+ entry and nitric oxide synthase in bovine endothelial cells. *J Physiol* **513 (Pt 2):** 369-379.

Papassotiriou J, Kohler R, Prenen J, Krause H, Akbar M, Eggermont J, Paul M, Distler A, Nilius B, Hoyer J (2000). Endothelial K(+) channel lacks the Ca(2+) sensitivity-regulating beta subunit. *Faseb J* **14**(7)**:** 885-894.

Park MK, Petersen OH, Tepikin AV (2000). The endoplasmic reticulum as one continuous Ca(2+) pool: visualization of rapid Ca(2+) movements and equilibration. *Embo J* **19**(21)**:** 5729-5739.

Parkington HC, Tare M, Tonta MA, Coleman HA (1993). Stretch revealed three components in the hyperpolarization of guinea-pig coronary artery in response to acetylcholine. *J Physiol* **465:** 459-476.

Pasyk E, Inazu M, Daniel EE (1995). CPA enhances Ca2+ entry in cultured bovine pulmonary arterial endothelial cells in an IP3-independent manner. *Am J Physiol* **268**(1 Pt 2)**:** H138-146.

Pelaez NJ, Braun TR, Paul RJ, Meiss RA, Packer CS (2000a). H(2)O(2) mediates Ca(2+)- and MLC(20) phosphorylation-independent contraction in intact and permeabilized vascular muscle. *Am J Physiol Heart Circ Physiol* **279**(3)**:** H1185-1193.

Pelaez NJ, Osterhaus SL, Mak AS, Zhao Y, Davis HW, Packer CS (2000b). MAPK and PKC activity are not required for H(2)O(2)-induced arterial muscle contraction. *Am J Physiol Heart Circ Physiol* **279**(3)**:** H1194-1200.

Pendergrass W, Wolf N, Poot M (2004). Efficacy of MitoTracker Green and CMXrosamine to measure changes in mitochondrial membrane potentials in living cells and tissues. *Cytometry A* **61**(2)**:** 162-169.

Penna A, Demuro A, Yeromin AV, Zhang SL, Safrina O, Parker I, Cahalan MD (2008). The CRAC channel consists of a tetramer formed by Stim-induced dimerization of Orai dimers. *Nature* **456**(7218)**:** 116-120.

Perez-Vizcaino F, Cogolludo A, Moreno L (2010). Reactive oxygen species signaling in pulmonary vascular smooth muscle. *Respir Physiol Neurobiol* **174**(3)**:** 212-220.

Periasamy M, Kalyanasundaram A (2007). SERCA pump isoforms: their role in calcium transport and disease. *Muscle Nerve* **35**(4)**:** 430-442.

Petersen OH (1996). Can Ca2+ be released from secretory granules or synaptic vesicles? *Trends Neurosci* **19**(10)**:** 411-413.

Petersen OH, Tepikin A, Park MK (2001). The endoplasmic reticulum: one continuous or several separate Ca(2+) stores? *Trends Neurosci* **24**(5)**:** 271-276.

Petersson J, Zygmunt PM, Hogestatt ED (1997). Characterization of the potassium channels involved in EDHF-mediated relaxation in cerebral arteries. *Br J Pharmacol* **120**(7)**:** 1344-1350.

Pfeifer A, Klatt P, Massberg S, Ny L, Sausbier M, Hirneiss C, Wang GX, Korth M, Aszodi A, Andersson KE, Krombach F, Mayerhofer A, Ruth P, Fassler R, Hofmann F

(1998). Defective smooth muscle regulation in cGMP kinase I-deficient mice. *Embo J* **17**(11)**:** 3045-3051.

Phillips SA, Hatoum OA, Gutterman DD (2007). The mechanism of flow-induced dilation in human adipose arterioles involves hydrogen peroxide during CAD. *Am J Physiol Heart Circ Physiol* **292**(1)**:** H93-100.

Pinton P, Pozzan T, Rizzuto R (1998). The Golgi apparatus is an inositol 1,4,5-trisphosphate-sensitive Ca2+ store, with functional properties distinct from those of the endoplasmic reticulum. *Embo J* **17**(18)**:** 5298-5308.

Plane F, Pearson T, Garland CJ (1995). Multiple pathways underlying endothelium-dependent relaxation in the rabbit isolated femoral artery. *Br J Pharmacol* **115**(1)**:** 31-38.

Pomerantz K, Sintetos A, Ramwell P (1978). The effect of prostacyclin on the human umbilical artery. *Prostaglandins* **15**(6)**:** 1035-1044.

Pomposiello S, Rhaleb NE, Alva M, Carretero OA (1999). Reactive oxygen species: role in the relaxation induced by bradykinin or arachidonic acid via EDHF in isolated porcine coronary arteries. *J Cardiovasc Pharmacol* **34**(4)**:** 567-574.

Poot M, Zhang YZ, Kramer JA, Wells KS, Jones LJ, Hanzel DK, Lugade AG, Singer VL, Haugland RP (1996). Analysis of mitochondrial morphology and function with novel fixable fluorescent stains. *J Histochem Cytochem* **44**(12)**:** 1363-1372.

Popp R, Gogelein H (1992). A calcium and ATP sensitive nonselective cation channel in the antiluminal membrane of rat cerebral capillary endothelial cells. *Biochim Biophys Acta* **1108**(1)**:** 59-66.

Prakriya M, Feske S, Gwack Y, Srikanth S, Rao A, Hogan PG (2006). Orai1 is an essential pore subunit of the CRAC channel. *Nature* **443**(7108)**:** 230-233.

Presley AD, Fuller KM, Arriaga EA (2003). MitoTracker Green labeling of mitochondrial proteins and their subsequent analysis by capillary electrophoresis with laser-induced fluorescence detection. *J Chromatogr B Analyt Technol Biomed Life Sci* **793**(1)**:** 141-150.

Putney JW, Jr. (1986). A model for receptor-regulated calcium entry. *Cell Calcium* **7**(1)**:** 1-12.

Putney JW, Jr. (1990). Receptor-regulated calcium entry. *Pharmacol Ther* **48**(3)**:** 427-434.

Qian Y, Liu KJ, Chen Y, Flynn DC, Castranova V, Shi X (2005). Cdc42 regulates arsenic-induced NADPH oxidase activation and cell migration through actin filament reorganization. *J Biol Chem* **280**(5)**:** 3875-3884.

Quignard JF, Feletou M, Thollon C, Vilaine JP, Duhault J, Vanhoutte PM (1999). Potassium ions and endothelium-derived hyperpolarizing factor in guinea-pig carotid and porcine coronary arteries. *Br J Pharmacol* **127**(1)**:** 27-34.

Quintero M, Colombo SL, Godfrey A, Moncada S (2006). Mitochondria as signaling organelles in the vascular endothelium. *Proc Natl Acad Sci U S A* **103**(14)**:** 5379-5384.

Quirk JC, Reinhart PH (2001). Identification of a novel tetramerization domain in large conductance K(ca) channels. *Neuron* **32**(1)**:** 13-23.

Ramachandran S, Xie LH, John SA, Subramaniam S, Lal R (2007). A novel role for connexin hemichannel in oxidative stress and smoking-induced cell injury. *PLoS One* **2**(8)**:** e712.

Randall MD, Alexander SP, Bennett T, Boyd EA, Fry JR, Gardiner SM, Kemp PA, McCulloch AI, Kendall DA (1996). An endogenous cannabinoid as an endothelium-derived vasorelaxant. *Biochem Biophys Res Commun* **229**(1)**:** 114-120.

Randall MD, Kendall DA (1997). Involvement of a cannabinoid in endothelium-derived hyperpolarizing factor-mediated coronary vasorelaxation. *Eur J Pharmacol* **335**(2-3)**:** 205-209.

Rapoport RM, Murad F (1983). Agonist-induced endothelium-dependent relaxation in rat thoracic aorta may be mediated through cGMP. *Circ Res* **52**(3)**:** 352-357.

Ray R, Murdoch CE, Wang M, Santos CX, Zhang M, Alom-Ruiz S, Anilkumar N, Ouattara A, Cave AC, Walker SJ, Grieve DJ, Charles RL, Eaton P, Brewer AC, Shah AM (2011). Endothelial Nox4 NADPH oxidase enhances vasodilatation and reduces blood pressure in vivo. *Arterioscler Thromb Vasc Biol* **31**(6)**:** 1368-1376.

Ray R, Shah AM (2005). NADPH oxidase and endothelial cell function. *Clin Sci (Lond)* **109**(3)**:** 217-226.

Redondo PC, Salido GM, Rosado JA, Pariente JA (2004). Effect of hydrogen peroxide on Ca2+ mobilisation in human platelets through sulphydryl oxidation dependent and independent mechanisms. *Biochem Pharmacol* **67**(3)**:** 491-502.

Rees DD, Palmer RM, Hodson HF, Moncada S (1989). A specific inhibitor of nitric oxide formation from L-arginine attenuates endothelium-dependent relaxation. *Br J Pharmacol* **96**(2)**:** 418-424.

Reinhardt TA, Filoteo AG, Penniston JT, Horst RL (2000). Ca(2+)-ATPase protein expression in mammary tissue. *Am J Physiol Cell Physiol* **279**(5)**:** C1595-1602.

Rhoades RA, Packer CS, Roepke DA, Jin N, Meiss RA (1990). Reactive oxygen species alter contractile properties of pulmonary arterial smooth muscle. *Can J Physiol Pharmacol* **68**(12)**:** 1581-1589.

Rizzuto R, Brini M, Murgia M, Pozzan T (1993a). Microdomains with high Ca2+ close to IP3-sensitive channels that are sensed by neighboring mitochondria. *Science* **262**(5134)**:** 744-747.

Rizzuto R, Brini M, Pozzan T (1993b). Intracellular targeting of the photoprotein aequorin: A new approach for measuring, in living cells, Ca(2+) concentrations in defined cellular compartments. *Cytotechnology* **11**(Suppl 1)**:** S44-46.

Rizzuto R, Pinton P, Carrington W, Fay FS, Fogarty KE, Lifshitz LM, Tuft RA, Pozzan T (1998). Close contacts with the endoplasmic reticulum as determinants of mitochondrial Ca2+ responses. *Science* **280**(5370)**:** 1763-1766.

Rodriguez-Martinez MA, Garcia-Cohen EC, Baena AB, Gonzalez R, Salaices M, Marin J (1998). Contractile responses elicited by hydrogen peroxide in aorta from normotensive and hypertensive rats. Endothelial modulation and mechanism involved. *Br J Pharmacol* **125**(6)**:** 1329-1335.

Rogers PA, Dick GM, Knudson JD, Focardi M, Bratz IN, Swafford AN, Jr., Saitoh S, Tune JD, Chilian WM (2006). H2O2-induced redox-sensitive coronary vasodilation is

mediated by 4-aminopyridine-sensitive K+ channels. *Am J Physiol Heart Circ Physiol* **291**(5)**:** H2473-2482.

Roos J, DiGregorio PJ, Yeromin AV, Ohlsen K, Lioudyno M, Zhang S, Safrina O, Kozak JA, Wagner SL, Cahalan MD, Velicelebi G, Stauderman KA (2005). STIM1, an essential and conserved component of store-operated Ca2+ channel function. *J Cell Biol* **169**(3)**:** 435-445.

Rouach N, Calvo CF, Duquennoy H, Glowinski J, Giaume C (2004). Hydrogen peroxide increases gap junctional communication and induces astrocyte toxicity: regulation by brain macrophages. *Glia* **45**(1)**:** 28-38.

Roy SS, Hajnoczky G (2008). Calcium, mitochondria and apoptosis studied by fluorescence measurements. *Methods* **46**(3)**:** 213-223.

Rubanyi GM, Lorenz RR, Vanhoutte PM (1985). Bioassay of endothelium-derived relaxing factor(s): inactivation by catecholamines. *Am J Physiol* **249**(1 Pt 2)**:** H95-101.

Rubanyi GM, Vanhoutte PM (1986). Superoxide anions and hyperoxia inactivate endothelium-derived relaxing factor. *Am J Physiol* **250**(5 Pt 2)**:** H822-827.

Ruiz E, Lorente R, Tejerina T (1997). Effects of calcium dobesilate on the synthesis of endothelium-dependent relaxing factors in rabbit isolated aorta. *Br J Pharmacol* **121**(4)**:** 711-716.

Rusko J, Tanzi F, van Breemen C, Adams DJ (1992). Calcium-activated potassium channels in native endothelial cells from rabbit aorta: conductance, Ca2+ sensitivity and block. *J Physiol* **455:** 601-621.

Sandow SL (2004). Factors, fiction and endothelium-derived hyperpolarizing factor. *Clin Exp Pharmacol Physiol* **31**(9)**:** 563-570.

Sandow SL, Haddock RE, Hill CE, Chadha PS, Kerr PM, Welsh DG, Plane F (2009). What's where and why at a vascular myoendothelial microdomain signalling complex. *Clin Exp Pharmacol Physiol* **36**(1)**:** 67-76.

Sandow SL, Neylon CB, Chen MX, Garland CJ (2006). Spatial separation of endothelial small- and intermediate-conductance calcium-activated potassium channels (K(Ca)) and connexins: possible relationship to vasodilator function? *J Anat* **209**(5)**:** 689-698.

Sandow SL, Tare M, Coleman HA, Hill CE, Parkington HC (2002). Involvement of myoendothelial gap junctions in the actions of endothelium-derived hyperpolarizing factor. *Circ Res* **90**(10)**:** 1108-1113.

Sato A, Sakuma I, Gutterman DD (2003). Mechanism of dilation to reactive oxygen species in human coronary arterioles. *Am J Physiol Heart Circ Physiol* **285**(6)**:** H2345-2354.

Schachinger V, Zeiher AM (2000). Atherosclerosis-associated endothelial dysfunction. *Z Kardiol* **89 (**Suppl 9): IX/70-74.

Schreiber M, Yuan A, Salkoff L (1999). Transplantable sites confer calcium sensitivity to BK channels. *Nat Neurosci* **2**(5)**:** 416-421.

Schroder E, Eaton P (2008). Hydrogen peroxide as an endogenous mediator and exogenous tool in cardiovascular research: issues and considerations. *Curr Opin Pharmacol* **8**(2)**:** 153-159.

Schror K, Verheggen R (1986). Prostacyclins are only weak antagonists of coronary vasospasm induced by authentic thromboxane A2 and serotonin. *J Cardiovasc Pharmacol* **8**(3)**:** 607-613.

Schubert R, Serebryakov VN, Engel H, Hopp HH (1996). Iloprost activates KCa channels of vascular smooth muscle cells: role of cAMP-dependent protein kinase. *Am J Physiol* **271**(4 Pt 1)**:** C1203-1211.

Scotland RS, Chauhan S, Vallance PJ, Ahluwalia A (2001). An endothelium-derived hyperpolarizing factor-like factor moderates myogenic constriction of mesenteric resistance arteries in the absence of endothelial nitric oxide synthase-derived nitric oxide. *Hypertension* **38**(4)**:** 833-839.

Shaul PW, Smart EJ, Robinson LJ, German Z, Yuhanna IS, Ying Y, Anderson RG, Michel T (1996). Acylation targets emdothelial nitric-oxide synthase to plasmalemmal caveolae. *J Biol Chem* **271**(11)**:** 6518-6522.

Sheehan DW, Giese EC, Gugino SF, Russell JA (1993). Characterization and mechanisms of H2O2-induced contractions of pulmonary arteries. *Am J Physiol* **264**(5 Pt 2)**:** H1542-1547.

Shen KZ, Lagrutta A, Davies NW, Standen NB, Adelman JP, North RA (1994). Tetraethylammonium block of Slowpoke calcium-activated potassium channels expressed in Xenopus oocytes: evidence for tetrameric channel formation. *Pflugers Arch* **426**(5)**:** 440-445.

Shimokawa H, Matoba T (2004). Hydrogen peroxide as an endothelium-derived hyperpolarizing factor. *Pharmacol Res* **49**(6)**:** 543-549.

Shimokawa H, Morikawa K (2005). Hydrogen peroxide is an endothelium-derived hyperpolarizing factor in animals and humans. *J Mol Cell Cardiol* **39**(5)**:** 725-732.

Shmigol AV, Eisner DA, Wray S (2001). Simultaneous measurements of changes in sarcoplasmic reticulum and cytosolic. *J Physiol* **531**(Pt 3)**:** 707-713.

Shuttleworth TJ (1996). Arachidonic acid activates the noncapacitative entry of Ca2+ during [Ca2+]i oscillations. *J Biol Chem* **271**(36)**:** 21720-21725.

Shuttleworth TJ, Thompson JL (1996). Evidence for a non-capacitative Ca2+ entry during [Ca2+] oscillations. *Biochem J* **316** (Pt 3): 819-824.

Shuttleworth TJ, Thompson JL (1998). Muscarinic receptor activation of arachidonate-mediated Ca2+ entry in HEK293 cells is independent of phospholipase C. *J Biol Chem* **273**(49)**:** 32636-32643.

Shuttleworth TJ, Thompson JL, Mignen O (2004). ARC channels: a novel pathway for receptor-activated calcium entry. *Physiology (Bethesda)* **19:** 355-361.

Simon AM, McWhorter AR (2002). Vascular abnormalities in mice lacking the endothelial gap junction proteins connexin37 and connexin40. *Dev Biol* **251**(2)**:** 206-220.

Simon AM, McWhorter AR (2003). Role of connexin37 and connexin40 in vascular development. *Cell Commun Adhes* **10**(4-6)**:** 379-385.

Smith C, Mitchinson MJ, Aruoma OI, Halliwell B (1992). Stimulation of lipid peroxidation and hydroxyl-radical generation by the contents of human atherosclerotic lesions. *Biochem J* **286** (Pt 3): 901-905.

Smith KR, Klei LR, Barchowsky A (2001). Arsenite stimulates plasma membrane NADPH oxidase in vascular endothelial cells. *Am J Physiol Lung Cell Mol Physiol* **280**(3)**:** L442-449.

Sokoya EM, Burns AR, Setiawan CT, Coleman HA, Parkington HC, Tare M (2006). Evidence for the involvement of myoendothelial gap junctions in EDHF-mediated relaxation in the rat middle cerebral artery. *Am J Physiol Heart Circ Physiol* **291**(1)**:** H385-393.

Sotnikova R (1998). Investigation of the mechanisms underlying H2O2-evoked contraction in the isolated rat aorta. *Gen Pharmacol* **31**(1)**:** 115-119.

Stahl WL, Eakin TJ, Owens JW, Jr., Breininger JF, Filuk PE, Anderson WR (1992). Plasma membrane Ca(2+)-ATPase isoforms: distribution of mRNAs in rat brain by in situ hybridization. *Brain Res Mol Brain Res* **16**(3-4)**:** 223-231.

States JC, Srivastava S, Chen Y, Barchowsky A (2009). Arsenic and cardiovascular disease. *Toxicol Sci* **107**(2)**:** 312-323.

Stauffer TP, Guerini D, Carafoli E (1995). Tissue distribution of the four gene products of the plasma membrane Ca2+ pump. A study using specific antibodies. *J Biol Chem* **270**(20)**:** 12184-12190.

Stauffer TP, Hilfiker H, Carafoli E, Strehler EE (1993). Quantitative analysis of alternative splicing options of human plasma membrane calcium pump genes. *J Biol Chem* **268**(34)**:** 25993-26003.

Stefanska J, Pawliczak R (2008). Apocynin: molecular aptitudes. *Mediators Inflamm* **2008:** 106507.

Straub AC, Clark KA, Ross MA, Chandra AG, Li S, Gao X, Pagano PJ, Stolz DB, Barchowsky A (2008). Arsenic-stimulated liver sinusoidal capillarization in mice requires NADPH oxidase-generated superoxide. *J Clin Invest* **118**(12)**:** 3980-3989.

Streb H, Irvine RF, Berridge MJ, Schulz I (1983). Release of Ca2+ from a nonmitochondrial intracellular store in pancreatic acinar cells by inositol-1,4,5-trisphosphate. *Nature* **306**(5938)**:** 67-69.

Sumi D, Taguchi K, Sun Y, Shinkai Y, Kumagai Y (2005). Monomethylarsonous acid inhibits endothelial nitric oxide synthase activity. *Journal of Health Science* **51:** 728-730.

Sundqvist T (1991). Bovine aortic endothelial cells release hydrogen peroxide. *J Cell Physiol* **148**(1)**:** 152-156.

Surroca A, Wolff D (2000). Inositol 1,4,5-trisphosphate but not ryanodine-receptor agonists induces calcium release from rat liver Golgi apparatus membrane vesicles. *J Membr Biol* **177**(3)**:** 243-249.

Szewczyk MM, Davis KA, Samson SE, Simpson F, Rangachari PK, Grover AK (2007). Ca2+-pumps and Na2+-Ca2+-exchangers in coronary artery endothelium versus smooth muscle. *J Cell Mol Med* **11**(1)**:** 129-138.

Szewczyk MM, Pande J, Akolkar G, Grover AK (2010). Caloxin 1b3: a novel plasma membrane Ca(2+)-pump isoform 1 selective inhibitor that increases cytosolic Ca(2+) in endothelial cells. *Cell Calcium* **48**(6)**:** 352-357.

Tabet F, Savoia C, Schiffrin EL, Touyz RM (2004). Differential calcium regulation by hydrogen peroxide and superoxide in vascular smooth muscle cells from spontaneously hypertensive rats. *J Cardiovasc Pharmacol* **44**(2)**:** 200-208.

Takac I, Schroder K, Brandes RP (2012). The Nox family of NADPH oxidases: friend or foe of the vascular system? *Curr Hypertens Rep* **14**(1)**:** 70-78.

Takeshima H, Nishimura S, Matsumoto T, Ishida H, Kangawa K, Minamino N, Matsuo H, Ueda M, Hanaoka M, Hirose T, et al. (1989). Primary structure and expression from complementary DNA of skeletal muscle ryanodine receptor. *Nature* **339**(6224)**:** 439-445.

Tanaka M, Kanatsuka H, Ong BH, Tanikawa T, Uruno A, Komaru T, Koshida R, Shirato K (2003). Cytochrome P-450 metabolites but not NO, PGI2, and H2O2 contribute to ACh-induced hyperpolarization of pressurized canine coronary microvessels. *Am J Physiol Heart Circ Physiol* **285**(5)**:** H1939-1948.

Tang EH, Vanhoutte PM (2008). Gene expression changes of prostanoid synthases in endothelial cells and prostanoid receptors in vascular smooth muscle cells caused by aging and hypertension. *Physiol Genomics* **32**(3)**:** 409-418.

Tarpey MM, Wink DA, Grisham MB (2004). Methods for detection of reactive metabolites of oxygen and nitrogen: in vitro and in vivo considerations. *Am J Physiol Regul Integr Comp Physiol* **286**(3)**:** R431-444.

Tate RM, Repine JE (1983). Hydrogen peroxide causes permeability edema and hypertension in isolated salt-perfused rabbit lungs. *Chest* **83**(5 Suppl)**:** 48S-50S.

Taylor HJ, Chaytor AT, Edwards DH, Griffith TM (2001). Gap junction-dependent increases in smooth muscle cAMP underpin the EDHF phenomenon in rabbit arteries. *Biochem Biophys Res Commun* **283**(3)**:** 583-589.

Taylor HJ, Chaytor AT, Evans WH, Griffith TM (1998). Inhibition of the gap junctional component of endothelium-dependent relaxations in rabbit iliac artery by 18-alpha glycyrrhetinic acid. *Br J Pharmacol* **125**(1)**:** 1-3.

Thebaud B, Michelakis E, Wu XC, Harry G, Hashimoto K, Archer SL (2002). Sildenafil reverses O2 constriction of the rabbit ductus arteriosus by inhibiting type 5 phosphodiesterase and activating BK(Ca) channels. *Pediatr Res* **52**(1)**:** 19-24.

Thengchaisri N, Kuo L (2003). Hydrogen peroxide induces endothelium-dependent and -independent coronary arteriolar dilation: role of cyclooxygenase and potassium channels. *Am J Physiol Heart Circ Physiol* **285**(6)**:** H2255-2263.

Thomas SR, Schulz E, Keaney JF, Jr. (2006). Hydrogen peroxide restrains endothelium-derived nitric oxide bioactivity -- role for iron-dependent oxidative stress. *Free Radic Biol Med* **41**(4)**:** 681-688.

Thyagarajan B, Malli R, Schmidt K, Graier WF, Groschner K (2002). Nitric oxide inhibits capacitative Ca2+ entry by suppression of mitochondrial Ca2+ handling. *Br J Pharmacol* **137**(6)**:** 821-830.

Tinel H, Cancela JM, Mogami H, Gerasimenko JV, Gerasimenko OV, Tepikin AV, Petersen OH (1999). Active mitochondria surrounding the pancreatic acinar granule region prevent spreading of inositol trisphosphate-evoked local cytosolic Ca(2+) signals. *Embo J* **18**(18)**:** 4999-5008.

Tomioka H, Hattori Y, Fukao M, Watanabe H, Akaishi Y, Sato A, Kim TQ, Sakuma I, Kitabatake A, Kanno M (2001). Role of endothelial Ni(2+)-sensitive Ca(2+) entry pathway in regulation of EDHF in porcine coronary artery. *Am J Physiol Heart Circ Physiol* **280**(2)**:** H730-737.

Toro L, Wallner M, Meera P, Tanaka Y (1998). Maxi-K(Ca), a Unique Member of the Voltage-Gated K Channel Superfamily. *News Physiol Sci* **13:** 112-117.

Torrecillas G, Boyano-Adanez MC, Medina J, Parra T, Griera M, Lopez-Ongil S, Arilla E, Rodriguez-Puyol M, Rodriguez-Puyol D (2001). The role of hydrogen peroxide in the contractile response to angiotensin II. *Mol Pharmacol* **59**(1)**:** 104-112.

Touyz RM (2008). Apocynin, NADPH oxidase, and vascular cells: a complex matter. *Hypertension* **51**(2)**:** 172-174.

Tran QK, Watanabe H (2006). Calcium signalling in the endothelium. *Handb Exp Pharmacol*(176 Pt 1)**:** 145-187.

Trebak M, Ginnan R, Singer HA, Jourd'heuil D (2010). Interplay between calcium and reactive oxygen/nitrogen species: an essential paradigm for vascular smooth muscle signaling. *Antioxid Redox Signal* **12**(5)**:** 657-674.

Tsai SH, Hsieh MS, Chen L, Liang YC, Lin JK, Lin SY (2001). Suppression of Fas ligand expression on endothelial cells by arsenite through reactive oxygen species. *Toxicol Lett* **123**(1)**:** 11-19.

Tsien RY (1980). New calcium indicators and buffers with high selectivity against magnesium and protons: design, synthesis, and properties of prototype structures. *Biochemistry* **19**(11)**:** 2396-2404.

Tsien RY (1981). A non-disruptive technique for loading calcium buffers and indicators into cells. *Nature* **290**(5806)**:** 527-528.

Ujiie H, Chaytor AT, Bakker LM, Griffith TM (2003). Essential role of Gap junctions in NO- and prostanoid-independent relaxations evoked by acetylcholine in rabbit intracerebral arteries. *Stroke* **34**(2)**:** 544-550.

Ungvari Z, Csiszar A, Koller A (2002). Increases in endothelial Ca(2+) activate K(Ca) channels and elicit EDHF-type arteriolar dilation via gap junctions. *Am J Physiol Heart Circ Physiol* **282**(5)**:** H1760-1767.

Upham BL, Kang KS, Cho HY, Trosko JE (1997). Hydrogen peroxide inhibits gap junctional intercellular communication in glutathione sufficient but not glutathione deficient cells. *Carcinogenesis* **18**(1)**:** 37-42.

Vahter M (2002). Mechanisms of arsenic biotransformation. *Toxicology* **181-182:** 211-217.

Vanhoutte PM, Feletou M (2005). *EDHF : the complete story*. edn. CRC ; London : Taylor & Francis [distributor]: Boca Raton, Fla.

Vergara C, Latorre R, Marrion NV, Adelman JP (1998). Calcium-activated potassium channels. *Curr Opin Neurobiol* **8**(3)**:** 321-329.

Vermassen E, Parys JB, Mauger JP (2004). Subcellular distribution of the inositol 1,4,5-trisphosphate receptors: functional relevance and molecular determinants. *Biol Cell* **96**(1)**:** 3-17.

Vinet R, Vargas FF (1999). L- and T-type voltage-gated Ca2+ currents in adrenal medulla endothelial cells. *Am J Physiol* **276**(4 Pt 2)**:** H1313-1322.

Wada S, Okabe E (1997). Susceptibility of caffeine- and Ins(1,4,5)P3-induced contractions to oxidants in permeabilized vascular smooth muscle. *Eur J Pharmacol* **320**(1)**:** 51-59.

Wallner M, Meera P, Toro L (1996). Determinant for beta-subunit regulation in high-conductance voltage-activated and Ca(2+)-sensitive K+ channels: an additional transmembrane region at the N terminus. *Proc Natl Acad Sci U S A* **93**(25)**:** 14922-14927.

Wang H, Joseph JA (1999). Quantifying cellular oxidative stress by dichlorofluorescein assay using microplate reader. *Free Radic Biol Med* **27**(5-6)**:** 612-616.

Wang R (2009). Hydrogen sulfide: a new EDRF. *Kidney Int* **76**(7)**:** 700-704.

Wang X, Lau F, Li L, Yoshikawa A, van Breemen C (1995). Acetylcholine-sensitive intracellular Ca2+ store in fresh endothelial cells and evidence for ryanodine receptors. *Circ Res* **77**(1)**:** 37-42.

Wei EP, Kontos HA (1990). H2O2 and endothelium-dependent cerebral arteriolar dilation. Implications for the identity of endothelium-derived relaxing factor generated by acetylcholine. *Hypertension* **16**(2)**:** 162-169.

Weston AH, Absi M, Ward DT, Ohanian J, Dodd RH, Dauban P, Petrel C, Ruat M, Edwards G (2005). Evidence in favor of a calcium-sensing receptor in arterial endothelial cells: studies with calindol and Calhex 231. *Circ Res* **97**(4)**:** 391-398.

Wheal AJ, Alexander SP, Randall MD (2012). Hydrogen peroxide as a mediator of vasorelaxation evoked by N-oleoylethanolamine and anandamide in rat small mesenteric arteries. *Eur J Pharmacol* **674**(2-3)**:** 384-390.

WHO (2012). http://www.who.int/topics/cardiovascular_diseases/en/.

Widmaier EP, Raff H, Strang KT, Vander AJ (2004). *Vander, Sherman, & Luciano's human physiology : the mechanisms of body function*. 9th edn. McGraw-Hill Higher Education: Boston.

Wigg SJ, Tare M, Tonta MA, O'Brien RC, Meredith IT, Parkington HC (2001). Comparison of effects of diabetes mellitus on an EDHF-dependent and an EDHF-independent artery. *Am J Physiol Heart Circ Physiol* **281**(1)**:** H232-240.

Williams SP, Dorn GW, 2nd, Rapoport RM (1994). Prostaglandin I2 mediates contraction and relaxation of vascular smooth muscle. *Am J Physiol* **267**(2 Pt 2)**:** H796-803.

Wood PG, Gillespie JI (1998). Evidence for mitochondrial Ca(2+)-induced Ca2+ release in permeabilised endothelial cells. *Biochem Biophys Res Commun* **246**(2)**:** 543-548.

Wu KK, Liou JY (2005). Cellular and molecular biology of prostacyclin synthase. *Biochem Biophys Res Commun* **338**(1)**:** 45-52.

Wuytack F, Papp B, Verboomen H, Raeymaekers L, Dode L, Bobe R, Enouf J, Bokkala S, Authi KS, Casteels R (1994). A sarco/endoplasmic reticulum Ca(2+)-ATPase 3-type Ca2+ pump is expressed in platelets, in lymphoid cells, and in mast cells. *J Biol Chem* **269**(2)**:** 1410-1416.

Xia XM, Fakler B, Rivard A, Wayman G, Johnson-Pais T, Keen JE, Ishii T, Hirschberg B, Bond CT, Lutsenko S, Maylie J, Adelman JP (1998). Mechanism of calcium gating in small-conductance calcium-activated potassium channels. *Nature* **395**(6701)**:** 503-507.

Xia XM, Zeng X, Lingle CJ (2002). Multiple regulatory sites in large-conductance calcium-activated potassium channels. *Nature* **418**(6900)**:** 880-884.

Xiao CY, Hara A, Yuhki K, Fujino T, Ma H, Okada Y, Takahata O, Yamada T, Murata T, Narumiya S, Ushikubi F (2001). Roles of prostaglandin I(2) and thromboxane A(2) in cardiac ischemia-reperfusion injury: a study using mice lacking their respective receptors. *Circulation* **104**(18)**:** 2210-2215.

Ya J, Erdtsieck-Ernste EB, de Boer PA, van Kempen MJ, Jongsma H, Gros D, Moorman AF, Lamers WH (1998). Heart defects in connexin43-deficient mice. *Circ Res* **82**(3)**:** 360-366.

Yada T, Shimokawa H, Hiramatsu O, Kajita T, Shigeto F, Goto M, Ogasawara Y, Kajiya F (2003). Hydrogen peroxide, an endogenous endothelium-derived hyperpolarizing factor, plays an important role in coronary autoregulation in vivo. *Circulation* **107**(7)**:** 1040-1045.

Yamada N, Makino Y, Clark RA, Pearson DW, Mattei MG, Guenet JL, Ohama E, Fujino I, Miyawaki A, Furuichi T, et al. (1994). Human inositol 1,4,5-trisphosphate type-1 receptor, InsP3R1: structure, function, regulation of expression and chromosomal localization. *Biochem J* **302** (Pt 3): 781-790.

Yamamoto-Hino M, Sugiyama T, Hikichi K, Mattei MG, Hasegawa K, Sekine S, Sakurada K, Miyawaki A, Furuichi T, Hasegawa M, et al. (1994). Cloning and characterization of human type 2 and type 3 inositol 1,4,5-trisphosphate receptors. *Receptors Channels* **2**(1)**:** 9-22.

Yamamoto K, Ando J (2004). [Shear-stress sensing via P2 purinoceptors in vascular endothelial cells]. *Nihon Yakurigaku Zasshi* **124**(5)**:** 319-328.

Yamamoto K, Korenaga R, Kamiya A, Ando J (2000). Fluid shear stress activates Ca(2+) influx into human endothelial cells via P2X4 purinoceptors. *Circ Res* **87**(5)**:** 385-391.

Yamamoto N, Watanabe H, Kakizawa H, Hirano M, Kobayashi A, Ohno R (1995). A study on thapsigargin-induced calcium ion and cation influx pathways in vascular endothelial cells. *Biochim Biophys Acta* **1266**(2)**:** 157-162.

Yamamoto Y, Fukuta H, Nakahira Y, Suzuki H (1998). Blockade by 18beta-glycyrrhetinic acid of intercellular electrical coupling in guinea-pig arterioles. *J Physiol* **511 (Pt 2):** 501-508.

Yang H, Shi M, VanRemmen H, Chen X, Vijg J, Richardson A, Guo Z (2003). Reduction of pressor response to vasoconstrictor agents by overexpression of catalase in mice. *Am J Hypertens* **16**(1)**:** 1-5.

Yang Z, Zhang A, Altura BT, Altura BM (1999a). Hydrogen peroxide-induced endothelium-dependent relaxation of rat aorta involvement of Ca2+ and other cellular metabolites. *Gen Pharmacol* **33**(4)**:** 325-336.

Yang ZW, Zhang A, Altura BT, Altura BM (1998a). Endothelium-dependent relaxation to hydrogen peroxide in canine basilar artery: a potential new cerebral dilator mechanism. *Brain Res Bull* **47**(3)**:** 257-263.

Yang ZW, Zheng T, Wang J, Zhang A, Altura BT, Altura BM (1999b). Hydrogen peroxide induces contraction and raises [Ca2+]i in canine cerebral arterial smooth muscle: participation of cellular signaling pathways. *Naunyn Schmiedebergs Arch Pharmacol* **360**(6)**:** 646-653.

Yang ZW, Zheng T, Zhang A, Altura BT, Altura BM (1998b). Mechanisms of hydrogen peroxide-induced contraction of rat aorta. *Eur J Pharmacol* **344**(2-3)**:** 169-181.

Yashiro Y, Duling BR (2000). Integrated Ca(2+) signaling between smooth muscle and endothelium of resistance vessels. *Circ Res* **87**(11)**:** 1048-1054.

Yeromin AV, Zhang SL, Jiang W, Yu Y, Safrina O, Cahalan MD (2006). Molecular identification of the CRAC channel by altered ion selectivity in a mutant of Orai. *Nature* **443**(7108)**:** 226-229.

Yoshida T, Inoue R, Morii T, Takahashi N, Yamamoto S, Hara Y, Tominaga M, Shimizu S, Sato Y, Mori Y (2006). Nitric oxide activates TRP channels by cysteine S-nitrosylation. *Nat Chem Biol* **2**(11)**:** 596-607.

Yoshimoto A, Nakanishi K, Anzai T, Komine S (1990). Effects of inositol 1,4,5-trisphosphate on calcium release from the endoplasmic reticulum and Golgi apparatus in mouse mammary epithelial cells: a comparison during pregnancy and lactation. *Cell Biochem Funct* **8**(4)**:** 191-198.

Yuan XJ, Tod ML, Rubin LJ, Blaustein MP (1996). NO hyperpolarizes pulmonary artery smooth muscle cells and decreases the intracellular Ca2+ concentration by activating voltage-gated K+ channels. *Proc Natl Acad Sci U S A* **93**(19)**:** 10489-10494.

Yusifov T, Savalli N, Gandhi CS, Ottolia M, Olcese R (2008). The RCK2 domain of the human BKCa channel is a calcium sensor. *Proc Natl Acad Sci U S A* **105**(1)**:** 376-381.

Zafari AM, Ushio-Fukai M, Akers M, Yin Q, Shah A, Harrison DG, Taylor WR, Griendling KK (1998). Role of NADH/NADPH oxidase-derived H2O2 in angiotensin II-induced vascular hypertrophy. *Hypertension* **32**(3)**:** 488-495.

Zarain-Herzberg A, MacLennan DH, Periasamy M (1990). Characterization of rabbit cardiac sarco(endo)plasmic reticulum Ca2(+)-ATPase gene. *J Biol Chem* **265**(8)**:** 4670-4677.

Zembowicz A, Hatchett RJ, Jakubowski AM, Gryglewski RJ (1993). Involvement of nitric oxide in the endothelium-dependent relaxation induced by hydrogen peroxide in the rabbit aorta. *Br J Pharmacol* **110**(1)**:** 151-158.

Zhang BM, Kohli V, Adachi R, Lopez JA, Udden MM, Sullivan R (2001). Calmodulin binding to the C-terminus of the small-conductance Ca2+-activated K+ channel hSK1 is affected by alternative splicing. *Biochemistry* **40**(10)**:** 3189-3195.

Zhang DX, Gutterman DD (2007). Mitochondrial reactive oxygen species-mediated signaling in endothelial cells. *Am J Physiol Heart Circ Physiol* **292**(5)**:** H2023-2031.

Zhang H, Inazu M, Weir B, Buchanan M, Daniel E (1994). Cyclopiazonic acid stimulates Ca2+ influx through non-specific cation channels in endothelial cells. *Eur J Pharmacol* **251**(2-3)**:** 119-125.

Zhao M, Li P, Li X, Zhang L, Winkfein RJ, Chen SR (1999). Molecular identification of the ryanodine receptor pore-forming segment. *J Biol Chem* **274**(37)**:** 25971-25974.

Zheng Y, Shen X (2005). H2O2 directly activates inositol 1,4,5-trisphosphate receptors in endothelial cells. *Redox Rep* **10**(1)**:** 29-36.

Zhou M, Diwu Z, Panchuk-Voloshina N, Haugland RP (1997). A stable nonfluorescent derivative of resorufin for the fluorometric determination of trace hydrogen peroxide: applications in detecting the activity of phagocyte NADPH oxidase and other oxidases. *Anal Biochem* **253**(2)**:** 162-168.

Zhu X, Jiang M, Birnbaumer L (1998). Receptor-activated Ca2+ influx via human Trp3 stably expressed in human embryonic kidney (HEK)293 cells. Evidence for a non-capacitative Ca2+ entry. *J Biol Chem* **273**(1)**:** 133-142.

Ziegelstein RC, Spurgeon HA, Pili R, Passaniti A, Cheng L, Corda S, Lakatta EG, Capogrossi MC (1994). A functional ryanodine-sensitive intracellular Ca2+ store is present in vascular endothelial cells. *Circ Res* **74**(1)**:** 151-156.

Zielonka J, Kalyanaraman B (2010). Hydroethidine- and MitoSOX-derived red fluorescence is not a reliable indicator of intracellular superoxide formation: another inconvenient truth. *Free Radic Biol Med* **48**(8)**:** 983-1001.

Zorzato F, Fujii J, Otsu K, Phillips M, Green NM, Lai FA, Meissner G, MacLennan DH (1990). Molecular cloning of cDNA encoding human and rabbit forms of the Ca2+ release channel (ryanodine receptor) of skeletal muscle sarcoplasmic reticulum. *J Biol Chem* **265**(4)**:** 2244-2256.

Zygmunt PM, Plane F, Paulsson M, Garland CJ, Hogestatt ED (1998). Interactions between endothelium-derived relaxing factors in the rat hepatic artery: focus on regulation of EDHF. *Br J Pharmacol* **124**(5)**:** 992-1000.